






Universitat Autònoma de Barcelona

Nicotinamide effects on adiposity, energy metabolism, inflammation and atherosclerosis in mice

Karen Alejandra Méndez Lara

ADVERTIMENT. L'accés als continguts d'aquesta tesi queda condicionat a l'acceptació de les condicions d'ús establertes per la següent llicència Creative Commons:  http://cat.creativecommons.org/?page_id=184

ADVERTENCIA. El acceso a los contenidos de esta tesis queda condicionado a la aceptación de las condiciones de uso establecidas por la siguiente licencia Creative Commons:  <http://es.creativecommons.org/blog/licencias/>

WARNING. The access to the contents of this doctoral thesis it is limited to the acceptance of the use conditions set by the following Creative Commons license:  <https://creativecommons.org/licenses/?lang=en>

Nicotinamide effects on adiposity, energy
metabolism, inflammation and atherosclerosis in
mice

Karen Alejandra Méndez Lara

Doctoral Program in Biochemistry, Molecular Biology and Biomedicine.
Department of Biochemistry and Molecular Biology.
Institut de Recerca de l'Hospital de la Santa Creu i Sant Pau

Barcelona, September 2019



**Universitat Autònoma
de Barcelona**



Nicotinamide effects on adiposity, energy metabolism, inflammation and atherosclerosis in mice

Karen Alejandra Méndez Lara

Doctoral Program in Biochemistry, Molecular Biology and Biomedicine.
Department of Biochemistry and Molecular Biology.
Institut de Recerca de l'Hospital de la Santa Creu i Sant Pau

Directors:

Josep Julve Gil, PhD.
Institut de Recerca de l'Hospital de la Santa Creu i Sant Pau

Francisco Blanco Vaca, MD, PhD.
Servei de Bioquímica, Hospital de la Santa Creu i Sant Pau.
Departament de Bioquímica i Biologia Molecular. Universitat Autònoma de Barcelona (UAB).

Autonomous University of Barcelona
Department of Biochemistry and Molecular Biology.
Doctoral Program in Biochemistry, Molecular Biology and Biomedicine.

**Nicotinamide effects on adiposity, energy metabolism,
inflammation and atherosclerosis in mice**

Thesis presented by Karen Alejandra Méndez Lara to apply for the degree of Doctor by the Autonomous University of Barcelona in the program of PhD. in Biochemistry, Molecular Biology and Biomedicine.

This thesis has been carried out in the Molecular Bases of Cardiovascular Disease group of the Hospital de Santa Creu i Sant Pau, co-directed by Dr. Josep Julve and Dr. Francisco Blanco-Vaca.

Dr. Josep Julve
Senior Researcher
Institut de Recerca de l'Hospital de
la Santa Creu i Sant Pau

Dr. Francisco Blanco Vaca
P.I. of Molecular Bases of
Cardiovascular Disease group.
Servei de Bioquímica, Hospital de
la Santa Creu i Sant Pau.
Departament de Bioquímica i
Biologia Molecular.
Universitat Autònoma de
Barcelona (UAB).

Karen Alejandra Méndez Lara
Institut de Recerca de l'Hospital de la Santa Creu i Sant Pau

Barcelona, September 2019

• TABLE OF CONTENTS

•	TABLE OF CONTENTS	5
•	TABLE OF FIGURES	11
•	TABLE OF TABLES	17
•	ABBREVIATIONS	19
•	ABSTRACT	21
•	GRAPHICAL ABSTRACT	25
•	1. INTRODUCTION	27
▶	1.1 Mouse models of obesity	30
▶	1.2 Adipose tissue plasticity in physio(patho)logy	32
	1.2.1 General characteristics of adipose tissue	33
	1.2.2 Types of adipose tissue	33
	1.2.3 Functional units of fat pads	38
	1.2.4 Dysfunctional adipose tissue in obesity	42
▶	1.3 Obesity and cardiovascular disease	50
▶	1.4 Anti-obesity strategies	51
	1.4.1 Current emerging therapeutic strategies targeting adipose tissue	51
•	2. HYPOTHESIS	61
•	OBJECTIVES	63
•	3. MATERIALS AND METHODS	65

▶ 3.1 Mice and diets.....	65
3.1.1 Common methods and procedures in different experimental designs.....	65
3.1.2 Evaluation of the safe dose	66
3.1.3 Evaluation of vitamin B3 forms on body weight gain prevention	69
3.1.4 Assessment of anti-atherogenic action by NAM	72
3.1.5 Diets used in this work.....	73
▶ 3.2 Biochemical analyses	74
3.2.1 Plasma analysis of biochemical parameters	74
3.2.2 Cytokine determination in plasma using a multiplex approach ...	83
3.2.3 Isolation of lipoproteins from sequential ultracentrifugation.....	84
3.2.4 ApoE-deficient mice phenotyping	93
3.2.5 Nicotinamide and N-methylnicotinamide determination in plasma	93
▶ 3.3 Tissue analyses.....	96
3.3.1 Tissue collection	96
3.3.2 Histological analysis	96
3.3.2a Adipocytes, BAT and liver droplets quantification	96
3.3.2b Analysis and quantification of arterial lesions	97
3.3.2c ORO Staining	97
3.3.2d F4/80 Immunohistochemical staining	99
3.3.3 Determination of fecal and liver triglycerides.....	100
3.3.4 Determination of energy metabolites	100
3.3.5 Protein abundance and gene expression analyses	103

3.3.5a Western blot analysis.....	103
3.3.5b Gene expression analysis.....	104
▶ 3.4 <i>Functional tests</i>	110
3.4.1 Glucose tolerance test	110
3.4.2 Insulin sensitivity test	111
3.4.3 Susceptibility to lipoprotein oxidation	112
▶ 3.5 <i>In vivo kinetic studies</i>	114
3.5.1 <i>In vivo</i> non-HDL turnover	114
3.5.2 Distribution of intragastrically-administered [3H]-cholesterol in mice.....	118
3.5.3 Assessment of oxygen consumption in mouse by indirect calorimetry.....	119
3.5.4 Magnetic resonance imaging (MRI) analysis	120
3.5.5 Palmitate β -oxidation measurement in isolated mitochondria ...	121
▶ 3.6 <i>In vitro studies</i>	124
3.6.1 NAM-mediated prevention of lipopolysaccharide(LPS)-induced inflammation.....	124
▶ 3.7 <i>Statistical analysis</i>	125
• 4. <i>RESULTS</i>	127
4.1 <i>Evaluating vitamin B₃ forms tolerance</i>	127
4.1.1 Choosing the best dose	127
▶ 4.2 <i>Impact of vitamin B₃ forms on body weight and adiposity in non-obese mice fed a regular diet (RD)</i>	132

4.2.1 Gross parameters and systemic phenotype.....	132
4.2.1a Biochemical parameters	139
4.2.1b Glucose homeostasis	141
▶ 4.3 <i>Impact of vitamin B3 forms on body weight and adiposity in a mouse model of diet-induced obesity (DIO)</i>	144
4.3.1 Gross parameters and systemic phenotype.....	144
4.3.1a Biochemical and molecular parameters	150
4.3.1b Glucose homeostasis	153
▶ 4.4 <i>Impact of different doses of NAM on body weight and adiposity in DIO mice</i>	155
4.4.1 Gross parameters and systemic phenotype.....	155
4.4.1a MRI analysis.....	158
4.4.1b Biochemical parameters	161
4.4.1c Histologic and molecular analysis on fatty liver	165
4.4.1d Glucose homeostasis	169
4.4.2 Energy metabolism	171
4.4.2a Global energy expenditure by indirect calorimetry analysis....	171
4.4.2b Energy metabolites in scWAT	176
4.4.2c Mitochondrial activity and mass surrogates in iBAT	180
4.4.3 Molecular and plasticity analysis on adipose tissue	182
4.4.3a Browning.....	182
4.4.3b Obesity-related inflammation	190
▶ 4.5 <i>Effect of NAM-treated ApoE-deficient mice on chronic inflammation: Atherosclerosis</i>	193

4.5.1 Inflammation analysis <i>in vitro</i>	193
4.5.2 Gross parameters and systemic phenotype.....	194
4.5.2a Biochemical parameters	196
4.5.2b Non-HDL metabolism	198
4.5.2c Anti-oxidative function of lipoproteins	201
4.5.2d Histologic and molecular analysis on fatty liver	206
4.5.3 Atherosclerosis development.....	207
4.5.4 Systemic inflammation markers.....	209
• 5. DISCUSSION.....	215
▶ 5.1 Determination of oral dose of NAM to mice.....	215
▶ 5.2 Anti-obesity mechanisms of NAM	219
▶ 5.3 Effect of NAM on adipose “browning”	220
▶ 5.4 Contribution of NAM-mediated NAD ⁺ boost to adipose phenotype.....	224
▶ 5.5 Effect of NAM on other mechanisms of energy expenditure	226
▶ 5.6 NAM on homeostasis and metabolism of glucose....	227
▶ 5.7 NAM on fatty liver.....	228
▶ 5.8 NAM administration prevented vascular chronic inflammation and atherosclerosis in ApoE-deficient mice ...	229
5.8a Anti-inflammatory effect of NAM	229

5.8b Anti-oxidant effect of NAM.....	232
▶ 5.9 <i>Limitations of the study</i>	235
• 6. <i>CONCLUSIONS</i>	237
• 7. <i>References</i>	239

• TABLE OF FIGURES

Figure 1 Factors that affect obesity development.....	28
Figure 2 Fat depot distribution in humans and mice.	35
Figure 3 Morphological appearance of BAT and WAT.	36
Figure 4 Distribution of major BAT depots in mouse and human.	37
Figure 5 Modulation of immune-metabolism during obesity.....	41
Figure 6 Central nodes for cellular NAD ⁺ metabolism.....	54
Figure 7 Structural formula of nicotinamide	58
Figure 8 Choosing a safe dose of vitamin B3 forms.	67
Figure 9 Mouse testing using higher doses of NAM than 1%.	68
Figure 10 Validation of the maximal safe dose.	68
Figure 11. Impact of vitamin B3 forms on mice phenotype.	69
Figure 12. Impact of vitamin B3 forms on a mouse model of induced obesity.	70
Figure 13. Impact of different doses of NAM on a mouse model of induced obesity.	71
Figure 14. Effect of NAM in the development of atherosclerosis.	72
Figure 15. Serial dilutions of the standard.	77
Figure 16. Serial dilutions of the standard.	80
Figure 17. Radding and Steinberg formula.....	85
Figure 18. Effect of NAM on the production of TNF α by LPS-stimulated macrophages.	125
Figure 19. Effect of vitamin B3 forms on body and liver weight.	127

Figure 20. Effect of vitamin B3 forms on body weight gain.	131
Figure 21. Effect of vitamin B3 forms on body weight gain.	131
Figure 22. Body weight follow-up in mice fed a RD.	132
Figure 23. Relation between body weight and adiposity with adipokines related with obesity.	136
Figure 24. Effect of vitamin B3 forms on gross parameters in mice fed a RD.	137
Figure 25. Relationship between total body and fat pad weights.	137
Figure 26. Effect of vitamin B3 forms on fat cell size from eWAT and scWAT in mice fed a RD.	138
Figure 27. Relationship between total body and fat pad weights and plasma levels of FFA.	140
Figure 28. Functional analysis of glucose metabolism in mice on a RD: GTT.	142
Figure 29. Functional analysis of glucose metabolism in mice on a RD: insulin sensitivity.	143
Figure 30. Effect of vitamin B3 forms on DIO mice.	146
Figure 31. Relation between body weight and adiposity with adipokines involved in obesity in DIO mice.	148
Figure 32. Histological images of epididymal and subcutaneous WAT in DIO mice.	149
Figure 33. Gene expression of molecular targets involved in inflammatory processes in eWAT in DIO mice.	149
Figure 34. Relationship between total body and fat pad weights and plasma levels of FFA in DIO mice.	151
Figure 35. Gene expression of Cd36 in liver in DIO mice.	152
Figure 36. Functional analysis of glucose metabolism in DIO mice: GTT.	154

Figure 37. Functional analysis of glucose metabolism in DIO mice: insulin sensitivity. 154

Figure 38. Effect of different doses on NAM on gross parameters in DIO mice. 157

Figure 39. Relationship between total body and fat pad weights in DIO mice. 158

Figure 40. Representative T1W used to measure total fat pad in DIO mice and treated with different doses of NAM for 3 consecutive months. 159

Figure 41. . Box-plot representing relative values or ROIs showing total fat pad and liver fat in DIO mice and treated with different doses of NAM for 3 consecutive months. 160

Figure 42. Relationship between total body and fat pad weights with liver fat fraction in DIO mice. 161

Figure 43. NAM and its methylated form (me- NAM) displayed a dose-dependent shape in plasma in DIO mice. 162

Figure 44. Relationship between total body and fat pad weights and plasma levels of FFA in DIO mice. 163

Figure 45. Effect of NAM on fatty liver in DIO mice. 165

Figure 46. Impact of NAM over fatty liver-related markers in DIO mice. 167

Figure 47. Gene expression of molecular targets involved in NAM metabolism in liver and adipose tissue in DIO mice. 169

Figure 48. Effect of different doses of NAM on functional analysis of glucose metabolism in DIO mice: glucose tolerance test. 170

Figure 49. Effect of different doses of NAM on functional analysis of glucose metabolism in DIO mice: insulin sensitivity. 170

Figure 50. Analysis of energy expenditure of DIO mice measured in metabolic cages. 172

Figure 51. Analysis of glucose oxidation measured in metabolic cages of DIO mice.....	173
Figure 52. Analysis of lipid oxidation measured in metabolic cages of DIO mice.	174
Figure 53. Relationship between total body and fat pad weights with RER in DIO mice.....	175
Figure 54. Analysis of NADt, NAD+, NADH and NAD+/NADH in scWAT in DIO mice.....	176
Figure 55. Relationship between NAD+ and NADt and Namp1 mRNA in scWAT in DIO mice.....	177
Figure 56. Analysis of [ATP+ ADP+ AMP] and AMP/ATP ratio in scWAT in DIO mice.....	178
Figure 57. Relationship between [ATP+ADP+AMP] and [NAD+ / NADH] ratio in scWAT in DIO mice.....	178
Figure 58. AMPK analysis in scWAT of DIO mice.	179
Figure 59. AMPK activity and its relationship with adenosine phosphate in subcutaneous white adipose tissue.....	180
Figure 60. Analysis of mitochondrial activity in BAT of DIO mice.....	180
Figure 61. Western blot analysis of Complex III and TIM44 protein in iBAT of DIO mice.....	181
Figure 62. Effect NAM over browning on scWAT in DIO mice.....	183
Figure 63. Effect NAM on iBAT in DIO mice.....	183
Figure 64. Analysis of Ucp1 protein in scWAT of DIO mice.....	184
Figure 65. Western blot analysis of Ucp1 protein in BAT of DIO mice.....	185
Figure 66. Relationship mRNA levels of browning and mitochondrial targets with RER in scWAT of DIO mice.	189
Figure 67. Effect NAM over crown-like structures (CLS) on eWAT in DIO mice.	190

Figure 68. Evaluation of plasma cytokines associated with inflammation in DIO mice.....	192
Figure 69. Gene expression of an inflammation target in an in vitro assay...	193
Figure 70. Effect of vitamin B3 forms on gross parameters in ApoE-deficient mice.....	194
Figure 71. NAM and its methylated form (me-NAM) displayed a dose-dependent shape in plasma in ApoE-deficient mice.....	196
Figure 72. Effect of NAM on metabolic fate of non-HDL lipoproteins in plasma in ApoE-deficient mice.....	200
Figure 73. Atheroprotective property of non-HDL particles of ApoE-deficient mice.....	202
Figure 74. Antioxidant activity of LDL particles of human plasma incubated with different concentrations of NAM.....	203
Figure 75. Effect of NAM in liver in ApoE-deficient mice.....	207
Figure 76. Representative images of proximal aorta of ApoE-deficient mice treated with different doses of NAM for 1 month.	208
Figure 77. Relationship between circulating plasma NAM levels and atherosclerosis in ApoE-deficient mice.....	209
Figure 78. Evaluation of plasmatic cytokines associated with inflammation in ApoE-deficient mice.....	210
Figure 79. Gene expression in thoracoabdominal aorta determined by real-time PCR analysis in ApoE-deficient mice.....	211
Figure 80. Representative IHQ of F4/80 or thoracoabdominal aortas of ApoE-deficient mice treated and non-treated with NAM.....	212
Figure 81. Gene expression of molecular targets regulated by LXR in the thoracoabdominal aorta of ApoE-deficient mice.....	213

• TABLE OF TABLES

Table 1. Experimental diet nutrient information.	73
Table 2. Transitions used in QqQ shown by different metabolites.	95
Table 3. List of specific Taqman probes used for gene expression analysis.	108
Table 4. List of primers sequences used for gene expression analysis.	109
Table 5. . Effect of vitamin B3 forms on hepatic transaminases in mice fed a RD.	128
Table 6. Effect of vitamin B3 forms on plasma biochemical parameters in mice fed a RD.	129
Table 7. Effect of vitamin B3 forms on plasma biochemical parameters in mice fed a RD.	130
Table 8. Effect of vitamin B3 forms on gross parameters in mice fed a RD ..	133
Table 9. Effect of vitamin B3 forms on critical hormones involved in adiposity in mice fed a RD.	135
Table 10. Effect of vitamin B3 forms on plasma biochemical parameters in mice fed a RD.	139
Table 11. . Effect of vitamin B3 forms on hepatic and renal parameters in mice fed a RD.	141
Table 12. Effect of vitamin B3 forms on glucose homeostasis in mice fed a RD.	141
Table 13. Effect of vitamin B3 forms on gross parameters in DIO mice.	145
Table 14. Effect of vitamin B3 forms on critical hormones involved in adiposity in DIO mice.	147
Table 15. Effect of vitamin B3 forms on biochemical parameters in DIO mice.	150
Table 16. . Effect of vitamin B3 forms on hepatic and renal parameters in DIO mice.	152

Table 17. Effect of vitamin B3 forms on glucose homeostasis in DIO mice. .	153
Table 18. Effects of different doses of NAM in DIO mice.....	156
Table 19. Effect NAM on plasma biochemical parameters in DIO mice.....	163
Table 20. Effect of NAM on hepatic and renal parameters in DIO mice.....	164
Table 21. Gene expression of molecular targets involved in macrophages infiltration and inflammation in DIO mice	166
Table 22. Gene expression of molecular targets involved in NAM metabolism in liver and adipose tissue in DIO mice.	168
Table 23. Gene expression of molecular targets involved in energy homeostasis and browning of scWAT and iBAT in DIO mice.	187
Table 24. Gene expression of molecular targets involved in macrophages infiltration and inflammation in DIO mice.	191
Table 25. Effect of NAM on gross parameters in ApoE-deficient mice.....	195
Table 26. Effect of NAM on plasma biochemical parameters in ApoE-deficient mice.....	197
Table 27.Effect of NAM on the relative composition of non-HDL particles of ApoE-deficient mice.	198
Table 28. Hepatic gene expression profile of molecular targets involved in non-HDL clearance in ApoE-deficient mice.	201
Table 29. Gene expression of molecular targets involved in oxidation and inflammatory properties in liver, eWAT and aorta of ApoE-deficient mice	204
Table 30. Gene expression of hepatic molecular targets involved in NAM metabolism of ApoE-deficient mice.	205
Table 31. Effect of NAM on hepatic and renal parameters in ApoE-deficient mice.	206

• ABBREVIATIONS

ADP	adenosin diphosphate
AKT	protein kinase B
ALT	alanine aminotransferase
AMP	adenosin monophosphate
AMPK	5' adenosine monophosphate-activated protein kinase
AST	aspartate aminotransferase
ATP	adenosin triphosphate
BAT	brown adipose tissue
cDNA	complementary deoxyribonucleic acid
Cpt1b	carnitine palmitoyltransferase 1b, muscle
DIO	diet induced obesity
DNA	deoxyribonucleic acid
EDTA	Ethylenediamine tetraacetic acid
ELISA	enzyme-linked immunosorbent assay
<i>eNamp1</i>	extracellular nicotinamide phosphoribosyltransferase
FFA	free fatty acid
FOXO	the forkhead box O family
GTT	glucose tolerance test
HDL	high density lipoprotein
HFD	high fat diet
HPLC	high-performance liquid chromatography
IL-4	interleukin 4
IL-6	interleukin 6
IL-10	interleukin 10
<i>iNamp1</i>	intracellular nicotinamide phosphoribosyltransferase
ITT	insulin tolerance test
LDL	low density lipoprotein

LC-MS/MS	liquid chromatography (LC) with mass spectrometry in tandem (MS/MS)
mRNA	Messenger ribonucleic acid
NA	nicotinic acid
NAD⁺	nicotinamide adenine dinucleotide, oxide
NADH	nicotinamide adenine dinucleotide, reduced
NAM	nicotinamide
<i>Nampt</i>	nicotinamide phosphoribosyltransferase
NMN	mononucleotide nicotinamide
NR	riboside nicotinamide
P-AMPK	phosphorylated 5' adenosine monophosphate-activated protein kinase
PCR	polimerase chain reaction
PGC-1a/Ppargc1a	Peroxisome Proliferator–Activated Receptor Gamma Coactivator alpha
Pparg	peroxisome proliferator activated receptor gamma
PGC-1b/Ppargc1b	peroxisome proliferative activated receptor, gamma, coactivator 1 beta
RNA	ribonucleic acid
qPCR	quantitative PCR
ROS	reactive oxygen species
SD	standard deviation
SEM	standard error of the mean
SIRT1	sirtuin 1
TCA	trichloroacetic Acid
Tnfa	tumor necrosis factor'
Ucp1	uncoupling protein 1 (mitochondrial, proton carrier)'
VLDL	very low-density lipoproteins
WAT	white adipose tissue

• ABSTRACT

Background and hypothesis

Adipose tissue dysfunction is a hallmark of obesity and is frequently associated with distorted metabolic homeostasis, cardiovascular and chronic, low-grade inflammatory diseases. Several recent studies point to pharmacological and/or nutritional health initiatives targeting adipose tissue being a promising approach to obesity prevention. In this regard, nicotinamide adenine dinucleotide (NAD)⁺ precursors, such as nicotinamide riboside and mononucleotide nicotinamide has been proven beneficial in increasing energy metabolism and preventing body weight gain *in vivo*. However, neither their favorable anti-obesity impact on disturbed white adipose tissue (WAT) physiology and plasticity nor in alleviating chronic inflammation, which frequently accompanies obesity, was not eventually pursued in any of these studies. In addition to the above-mentioned NAD precursors, nicotinamide (NAM) is also a physiological precursor of NAD⁺. However, its contribution in boosting energy metabolism and body weight gain still remains elusive. Although a growing body of evidences also supports a role for NAM as an anti-oxidant and anti-inflammatory agent both *in vitro* and *in vivo*, its potential contribution in preventing atherosclerosis, which is one of the main mechanisms involved in cardiovascular disease *in vivo*, has not previously been proven yet.

Aims

The aim of this study was twofold: to investigate the effect of NAM supplementation in (1) preventing weight gain and adiposity; (2) improving features of chronic inflammation in appropriate mouse models of obesity (diet-induced obesity -DIO- mice) and atherosclerosis (i.e., ApoE-deficient mice).

Results

NAM administration to mice was provided orally via tap water at libitum. Its administration was shown palatable, safe and well tolerated at doses below 1%.

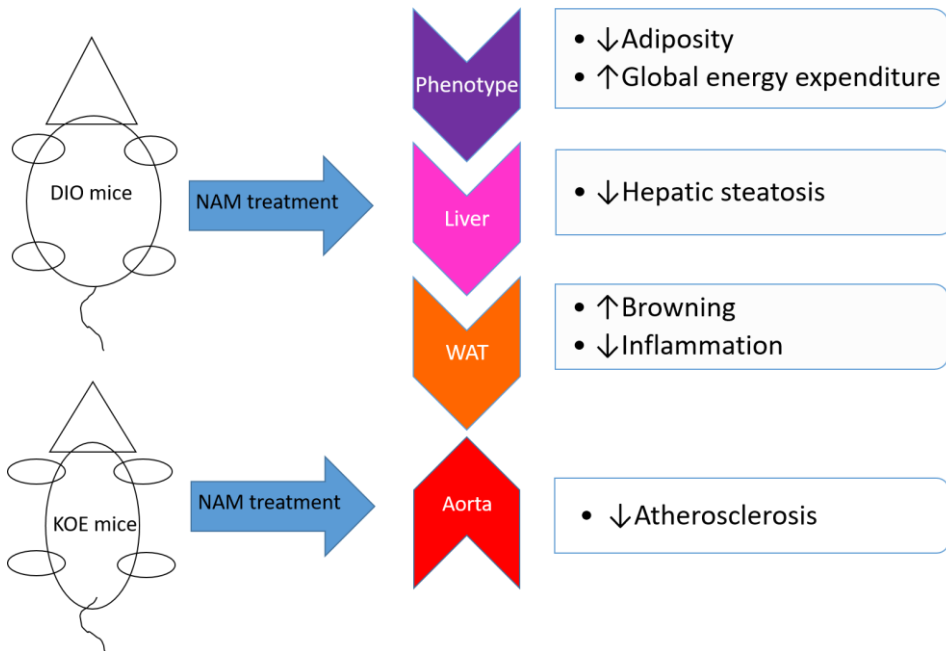
NAM supplementation, at the highest dose used (1%) (NAM HD-treated mice), prevented body weight gain, with the latter being mainly and repeatedly accompanied by reduction in fat accumulation in different regional depots, and hepatic steatosis. Mechanistically, such anti-adiposity effect by NAM was mainly accompanied by an [i] increased global energy expenditure, [ii] enhanced promotion of browning in subcutaneous (sc)WAT, as revealed by elevations in the relative mRNA and protein abundance of the uncoupling protein (Ucp)-1, and [iii] elevation of the de novo synthesis of NAD⁺ and NAD/NADH ratio in scWAT of NAM HD-treated, DIO mice. Notably, the AMP content was significantly elevated in scWAT of NAM HD-treated, DIO mice. Also, the NAD⁺/NADH ratio was directly related to the AMP/ATP ratio. Overall these data suggested a situation of energy demand in scWAT from NAM HD-treated mice. Concomitantly, the protein abundance of the active (phosphorylated) form of AMP-activated kinase was also elevated in this tissue of NAM HD-treated mice.

NAM supplementation also improved the global inflammatory condition and prevented atherosclerosis development in mice. This was revealed by [i] elevations in the circulating concentrations of interleukin (IL)-10 and [ii] up-regulation of relative mRNA of *Il10* in both adipose and aortic tissues, which potentially suggested a switch to anti-inflammatory M2 macrophages. This phenotype was accompanied by a commensurate reduction in atherosclerosis development in NAM-treated, ApoE-deficient mice. In addition to improved inflammation, non-HDL of NAM-treated, ApoE-deficient mice were less prone to oxidation than those from untreated mice, being this effect at least partly provided by the intrinsic anti-oxidant action of NAM.

Conclusions

Dietary supplementation with NAM to mice prevented body weight gain and adiposity by boosting energy expenditure, with this being mainly attributed to induction of browning and energy demand in scWAT. NAM also promoted anti-inflammatory and anti-oxidant actions. Its administration increased gene expression *Ucp1* in target tissues, including aorta, and protected against development of atherosclerosis.

• GRAPHICAL ABSTRACT



In brief:

This work shows that NAM supplementation via tap water prevents whole-body and fat gain in mice by boosting energy metabolism and inducing browning in subcutaneous (sc)WAT of obese mice. Also, in ApoE-deficient mice, NAM treatment promotes anti-inflammatory and anti-oxidant effects, being this associated with atherosclerosis prevention.

• 1. INTRODUCTION

Obesity is a main, yet most neglected, public health concern worldwide [1]. The epidemic of obesity presents a major challenge to chronic disease prevention and health across the lifespan in human beings. Steadily rising prevalence of overweight and obesity have increased in the last years mainly due to an increasingly sedentary lifestyle and nutritional transition consumption to processed and hyper caloric foods [2]. This trend has driven a remarkable increase in our understanding of adipose biology and obesity.

Overweight or obesity is defined as the accumulation of excess fat in the body which usually appears when energy intake (i.e, food consumption) exceeds caloric expenditure (i.e., basal metabolism, which includes biochemical pathways required to maintain global metabolic homeostasis, physical activity and adaptive thermogenesis). Energy expenditure is along with glucose intolerance and insulin resistance a common metabolic alteration in obesity [3].

Obesity has not been considered until relatively recently as a complex chronic disease. In its development, this metabolic condition results from a constant and complex interplay between predisposing genes, socioeconomic, behavioral and environmental stimuli [4] (Figure 1). In this context, genome-wide association studies have discovered genes that affect appetite and adiposity [5]. Over-consumption of hyper caloric foods and sedentary lifestyle are the best characterized environmental factors involved in adipose mass gain. Ageing, gender, ethnicity are other factors that may also influence adiposity [5]. Some drugs, including thiazolidinediones (i.e., a class of PPAR γ agonists), antidepressants and anti-convulsants, glucocorticoids, estrogens, atypical antipsychotics, can contribute to fat accumulation.

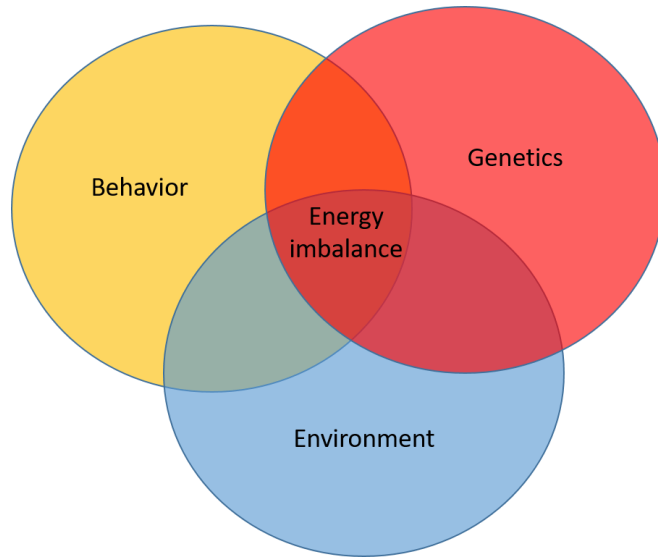


Figure 1 Factors that affect obesity development

Adipose tissue plays an important role in the maintenance of metabolic homeostasis in vivo [6]. The storage of energy as lipids and sequester them from the extracellular environment in intracellular organelles known as lipid droplets is a highly conserved mechanism in mammals. Adipose tissue depots (also called fat pads) are found in different regions but they are also present in close contact with other organs, where they modulate organ remodeling and function.

During obesity, adipose tissue plasticity and expandability underlie tissue dysfunction and are key determinants of obesity-associated metabolic dysregulation [7]. These features frequently appear when adipose tissue fails to appropriately expand to store energy overload, which leads to adverse metabolic problems in ectopic fat accumulation in many other tissues for a long time. This phenotype further results in other health complications and reduces life expectancy [8], thereby increasing rates of morbidity and mortality in obese patients. However, adipose gain may not necessarily be pathogenic [9]. Compelling evidence support the concept that the pathogenic link between fat gain and obesity-related metabolic and cardiovascular co-morbidities may be rather related to fat function and ectopic accumulation.

Obesity is also a largely preventable disease. Current attempts have been moderately effective for the treatment of obesity [10]. Despite having been proved beneficial for treating obesity, the effectiveness of existing pharmacological and dietary approaches fails to be maintained at long term. Thus, a better understanding of the etiology of obesity is required for the development of more successful and personalized prevention and treatment strategies. The latter have been suggested at least partly to be attributed to the fact that such therapies have not been directly addressed to target tissues which become physiologically disrupted. One of the most important representatives is the white adipose tissue. Adipose tissue is a multifactorial organ which becomes severely dysfunctional and fails to appropriately face to excess energy incomes during obesity. Indeed, this tissue has gained substantial interest with regard to its potential to be therapeutically targeted [10].

The rising incidence of obesity and costs to treat its associated diseases rises the need for a better understanding of all aspects of adipocyte (fat cell) biology, to ascertain how increased adiposity leads to disease. To that effect, mouse models have been an essential tool in expanding our understanding of molecular roots of obesity is a pre-requisite to improve both prevention and management of this entity. Studies in rodents and humans have allowed the identification of genes predisposing to obesity and analyzing the effect of targeted treatments using gene manipulation, pharmacological and nutritional approaches. Importantly, the accessibility of target tissues involved in obesity that are not easily attainable from humans also contribute to further dissect the effectiveness of each of these therapies and anticipate to undesirable metabolic side-effects [11].

▶ 1.1 Mouse models of obesity

Obesity involves decades of pathophysiological changes and adaptation. Therefore, it is difficult to ascertain the exact mechanisms for this long-term process in humans. Several surrogate mouse models are the most common experimental approaches to circumvent some of these issues.

Admittedly, the criteria for choosing animal models of obesity are based on altered control of eating and/or body weight. The availability of genetically defined strains as well as widely-developed genetic manipulation techniques allow to test the contribution of genes in the development of obesity [12]. This includes murine gene loss- or gain-of-function strategies, monogenic and polygenic models, and different environmental exposure models [13].

The mouse model of diet-induced obesity (DIO) has become one of the most important approaches for understanding the interplay of high-calorie diets in westernized societies and the development of obesity. The DIO model closely mimics the increasingly availability of nutritionally poor, high-calorie foods commonly consumed over the past decades, and which are main contributors of the obesity trend in human societies. High-fat diets produce increased body weight and increased adiposity in various obesity-prone mouse strains [14]. Obesity-prone and -resistant definition is based on body fat composition data from “Naggett1” in the ‘Mouse Phenome Database’ (MDP) (<https://phenome.jax.org/projects/Naggett1>), whereby body fat composition was measured in up to 39 different mouse strains that were fed a HFD for 8 weeks. Importantly, DIO mice exhibit obesity and metabolic phenotypes that are comparable to humans and can be measured with standardized diagnostic tests. Based on earlier reports [15, 16], the obesity-prone, inbred strain C57BL/6J is commonly selected to study the obesity-promoting effects of a HFD. General advantages of working with mouse models include the low maintenance cost, which is related to its small size and the fact that they reach sexual maturity more rapidly than other mammals. Moreover, mice breeding is easy as they have a shorter gestation period and relatively abundant offspring to conduct studies. More detailed phenotyping, such as direct metabolic measurements and

assessment of body fat content, that are difficult and costly in large numbers of humans are also possible in mice [17-19]. Importantly, environmental factors can be carefully controlled and specifically manipulated in mouse models [20], thereby reducing environmental heterogeneity. Mice also provide obesity-related tissues such as hepatic tissue that are otherwise difficult to obtain in humans [21]. However, mouse models of obesity also show some flaws. For instance, different conclusions may be reached in mouse and humans due to the analysis of different phenotypes. Indeed, body mass index (BMI) measurements are typical in human studies, whereas the direct measurement of percent of body fat or body fat mass is more common in mouse models. Unlike humans, there is no defined threshold for obesity based on BMI in mice. Also, and compared with humans, the secondary complications of obesity substantially depend on the genetic background of the strain [22].

▶ 1.2 Adipose tissue plasticity in physio(patho)logy

Adipose tissue is designed to function as the main long-term, energy-reservoir organ, and actively controls energy homeostasis. Indeed, this tissue stores excess energy in the form of triglycerides in living lipid-laden, parenchymal cells, defined as adipocytes, and is able to mobilize lipid reserves by releasing free fatty acids under conditions of nutritional deprivation or caloric restriction [5].

The classical perception of adipose tissue as an energy store has been replaced over the last decades by the notion that this tissue also plays a central role in lipid and glucose metabolism and also serves as an endocrine organ capable of synthesizing a number of biologically active compounds, including hormones and cytokines, that signal metabolic homeostasis of adipose tissue and also other organs [23, 24]. Particularly, leptin and adiponectin are secreted by adipose tissue and finely modulate feeding behavior and glucose and lipid metabolism, as well as many other physiological processes such as inflammation, angiogenesis or energy homeostasis [23, 25]. As a rule, plasma adipokines rise proportionally with fat mass, except for plasma adiponectin which is frequently decreased in obese patients [23].

Given its lipid buffering capacity and its endocrine function, healthy adipose tissue regulates circulation lipids flux according to energy demands controlling energy intake and expenditure. Thus, adipose tissue of healthy, non-obese individuals is able to maintain energy homeostasis, systemic insulin sensitivity and prevent overfeeding [26], but during obesity, it becomes dysfunctional and fails to confer such beneficial metabolic effects.

In mammals, adipose tissue is also relevant in thermoregulation through its insulator properties and ability to generate heat via non-shivering thermogenesis.

Adipose tissue and inflammation are also closely related in obesity [27]. Indeed, adipose tissue undergoes fibro-inflammation, which further compromises its functionality. During sustained obesity the enlargement (hypertrophy) of adipocytes is frequently accompanied by macrophage/leukocyte infiltration in

both humans and rodent models [28]. Inflammatory cell recruitment in adipose tissue is further linked to systemic inflammation and oxidative stress [29]. Importantly, pro-inflammatory cytokines, but also chemokines and adipokines are then secreted by adipose tissue, either by adipocytes or macrophages/leukocytes. Of note, such obesity-induced inflammation may further contribute to altered insulin and lipid metabolism and atherogenesis in vivo [30].

In addition to its role as central nexus of metabolic communication and control, thermoregulation, and inflammation, this tissue also contributes in the mechanical protection of a series of organs from injury.

In the following sections, anatomical and histological aspects of adipose tissue and relation to physiology, and its relation with dysfunctional adipose during development of obesity will be deeply dissected.

1.2.1 General characteristics of adipose tissue

Adipose tissue can be defined as a type of connective tissue that is mainly composed of adipocytes [5]. Adipocytes are typically found in large aggregates in adipose tissue or “fat” in many organs and different body regions (Figure 2). Adipose tissue is a dynamic organ which can range from 4% to >40% of total body composition in adult humans [31].

1.2.2 Types of adipose tissue

In mammals, there are two main, visually distinct types of adipose tissue, white adipose tissue (WAT) and brown adipose tissue (BAT) [32].

WAT

In mammals, WAT is usually distributed throughout the body in several distinct discrete anatomical fat depots (Figure 2) [33, 34]. WAT appears generally further sub-classified based on its anatomical location in two major depots, defined as intra-abdominal/visceral (visc)WAT and subcutaneous (sc)WAT. In humans, viscWAT include omental, mesenteric, retroperitoneal (perirenal areas), gonadal, and pericardial WAT. However, it is also found around internal organs and specialized tissues, including vasculature. The other fat depot, the scWAT, is located in different body regions under the skin. In humans, clusters of scWAT can be found in upper (deep and superficial abdomen) and lower (gluteofemoral) body regions [35].

In mice, scWAT is generally located beneath the skin and outside the peritoneal cavity, while viscWAT is located in the abdominal cavity [36]. Although mice and humans share most of fat distribution, they also have distinctive fat depots (Figure 2).

The biology of viscWAT is different from that of scWAT [37]. Different locations suggest that adipose tissue characteristics in each fat depot may differ in its function. Indeed, different WAT depots may be metabolically distinct despite sharing relatively conserved morphology. For instance, viscWAT depots are commonly associated with (cardio)metabolic disorders, including obesity and diabetes [38], whereas scWAT confers beneficial effects on metabolism [39]. Differing metabolic functions of these two major fat depots are extensively reviewed elsewhere [40, 41].

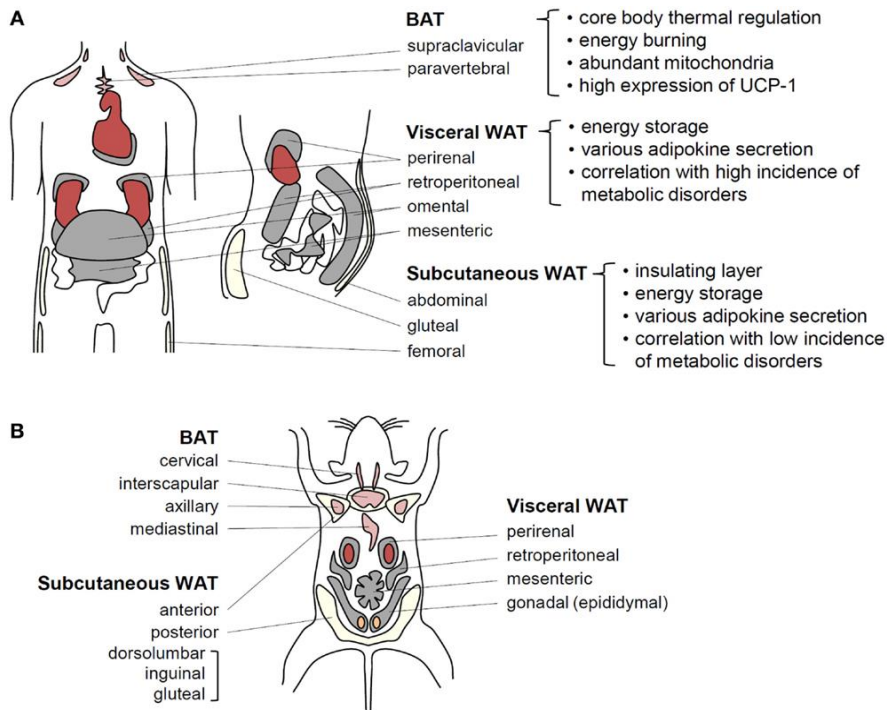


Figure 2 Fat depot distribution in humans and mice.

From [26]

BAT

Histologically, WAT is visually distinct from BAT (Figure 3). In contrast to WAT, BAT is frequently distributed at different locations throughout the body [31]. BAT pads are considerably smaller by volumen and denser than WAT depots, especially in humans, who have lower body surface-to-volume ratio than rodents. Compared with WAT, BAT appears highly vascularized [42].

The largest and most extensively studied BAT depot in rodents, and in most mammals, is located between the shoulder blades (interscapular (i)BAT) and around the kidney (perirenal BAT) as well as in cervical and axillar regions, though it can also be found in other sites such as the para-aortic region, neck and mediastinum [43] (Figure 4). In humans, BAT was thought to be exclusively present in the interscapular region during the perinatal period and adults

chronically exposed to extreme cold; however, recent studies revealed that adult humans have an active BAT [44].

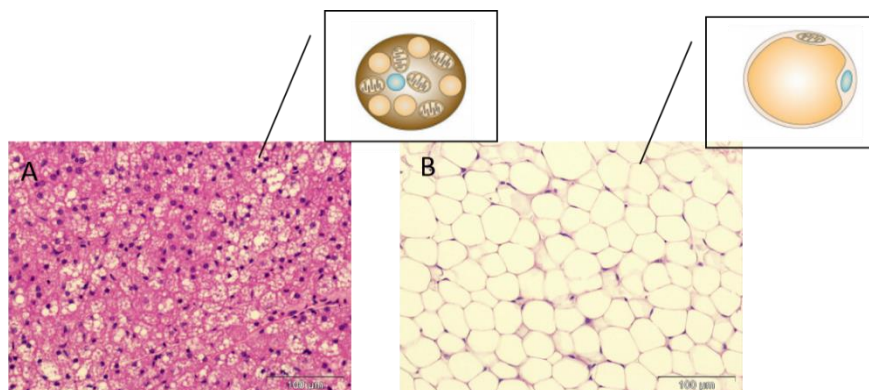


Figure 3 Morphological appearance of BAT and WAT.

Representative mice biopsies of (A) BAT and (B) WAT, fixed with formalin, stained with hematoxylin/eosin and captured at 20X.

The primary main function of BAT is energy dissipation via non-shivering thermoregulation rather than to serve as energy store. Indeed, this tissue uses the triglycerides stored in its numerous lipid droplets as fuel for adaptive, non-shivering thermogenesis [45, 46] and, when fully activated, is able to take up large amounts of fatty acids and glucose from the circulation [46-48].

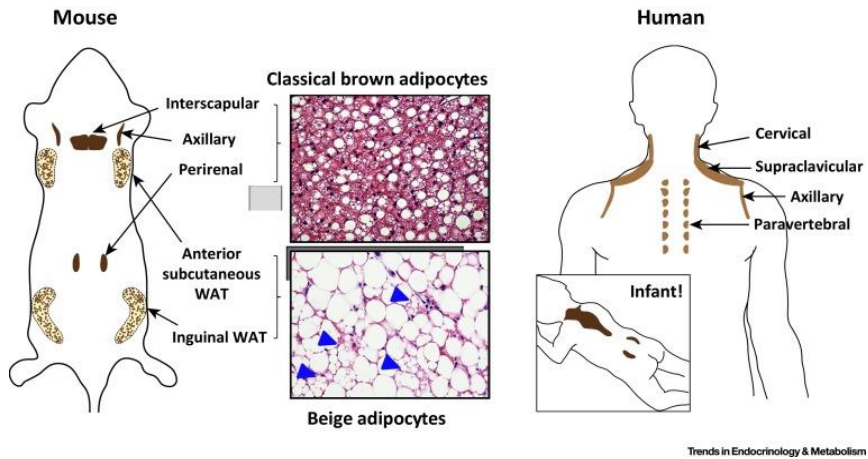


Figure 4 Distribution of major BAT depots in mouse and human.

From [31]

BAT is highly innervated by the sympathetic nervous system which rapidly triggers brown adipocyte activation upon cold stimulation [46, 49]. In addition to this signal originating from the central nervous system, endocrine and paracrine mediators of brown adipocytes have also been identified, including liver-derived bile acids [50, 51], cardiac natriuretic peptides [52], as well as locally released adenosine [53].

Emerging evidence suggests that mammals possess another type of thermogenic adipocyte (i.e., with characteristics of brown adipocytes) in within WAT depots, defined as 'beige' or 'brite' adipocytes [54]. However, it is not still clear whether such different designations refer to the same cell type. Indeed, limited genetic tracing experiments suggest that there may be heterogeneity among cell types that are capable of browning. In contrast to brown adipocytes which are located in precisely dedicated BAT depots, beige adipocytes are an inducible form of thermogenic adipocytes that sporadically reside within WAT depots.

1.2.3 Functional units of fat pads

White adipocytes

The accumulation of lipids is characteristic of many cell types; however, the evolution of specialized fat-storing cells, commonly defined as white adipocytes has provided a safe and specific compartment to that effect. White adipocytes are the main cell type present in WAT and are characterized by the presence of a single, large lipid droplet, only a small amount of cytoplasm, and flattened, non-centrally located nuclei, which appear compressed between the lipid droplet and cell membrane; hence they are also defined as 'unilocular' adipocytes.

The 'classical' function of white adipocytes is to serve as energy store. In conditions of energy excess, free fatty acids released from the hydrolysis of circulating triglycerides, by the action of lipoprotein lipase (LPL), enter adipocytes and are reesterified into triglycerides in a process that involves the sequential action of multiple enzymes, which including glycerol-3-phosphate acyltransferase (G3PAT) and diacylglyceride acyltransferase (DGAT) among others. *De novo* generated triglycerides accumulate within lipid droplets. Conversely, in situations of energy deficiency, triglycerides may be mobilized by the action of hormone-sensitive lipase (HSL), adipose tissue triglyceride lipase (ATGL), and monoglyceride lipase (MGL) which releases free fatty acid into circulation.

In addition to the energy-storing properties of white adipocytes, this cell type also has the ability to produce different molecules, including adipokines (adipocyte-derived cytokines), such as leptin, adiponectin and adipisin, and cytokines, such as tumor necrosis factor alpha (Tnfa). The list of adipokines is growing and the understanding of their physiological role on energy balance, cardiovascular function, immune regulation, and nutrient homeostasis exhibit therapeutic potential. However, the specific mechanisms whereby adipokines act on different target tissues still need to be further elucidated.

Brown adipocytes

Brown adipocytes convert chemical energy into heat [55]. Alike white adipocytes, brown adipocytes have multiple lipid droplets of differing size and are rich in mitochondria [7]; hence BAT adopts a brownish color. Nuclei are round and centrally located. Brown adipocytes express a unique thermogenic and mitochondrial genetic program that promotes mitochondrial biogenesis, energy uncoupling and energy dissipation, which provides heat to the organism [55]. Energy dissipation is provided by an abundance of mitochondria as well as by specialized proteins, including a unique protein to thermogenic adipocytes, uncoupling protein-1 (Ucp1). This protein collapses the electron gradient to generate heat rather than ATP [46].

Activation of brown adipocytes with inducers of the brown fat thermogenic program significantly contribute to systemic metabolism by increasing energy expenditure through heat production. The relevance of BAT is exemplified by the fact that in rodents, BAT and liver take up equal amounts of energy from circulation, a process which is able to normalize glucose and lipid values in insulin resistant and hyperlipidemic mice [56].

Beige or 'brite' adipocytes

Beige adipocytes are another type of thermogenic fat cell [31]. This cell type may also be present in WAT and exerts a key role in the regulation of systemic energy homeostasis in mammals. In WAT, this class of adipocytes have a remarkably capacity to alter metabolic phenotype from typical WAT to those resembling brown adipocytes [31]. This phenomenon has been defined as 'browning' and is readily induced by cold exposure and β -adrenergic stimulation. Although browning has been extensively demonstrated only in small mammals, and the extent to which this occurs in humans is still debated. Typically, browning

involves the appearance of multilocular adipocyte clusters that are dispersed among unilocular white adipocytes [31].

Like brown adipocytes, beige adipocytes display thermogenic properties in addition to sharing common morphological and biochemical properties, including multiple lipid droplets and elevated number of mitochondria. However, compelling evidence also suggests distinct characteristics between both types of thermogenic adipocytes. While some brown adipocyte-like express Ucp1 [57, 58], recent evidences may indicate that Ucp1 is not essential for the chronic thermogenic actions of β 3-adrenergic agonists, or for the appearance of multilocular fat cells in white fat depots [58, 59]. Supporting to this, their role in the metabolism of glucose may also be accounted for by Ucp1-independent mechanisms [60]. Consistently, Ucp1-negative multilocular adipocytes has been reported to show elevated metabolic rates [61] and PPAR- α -dependent up-regulation of fatty acid oxidation [62].

Immune cells

Adipocytes are not the only cell type of WAT. This tissue also contains different types of immune cells [5, 63, 64]. Under healthy conditions, the numbers of immune cells are relatively low; however, upon an inflammatory state, as that induced by experimental obesity, immune cell numbers increase rapidly, thereby contributing to metabolic imbalance.

WAT has its own population of resident macrophages, defined as adipose tissue macrophages [65] (Figure 5). This cell type is commonly identified by immunohistochemistry using specific anti-Cd68 antibodies; and hence produce the majority of cytokines from adipose tissue [66, 67]. These cells affect both the metabolic and endocrine functions of adipose tissue [67-69]. Adipose macrophages is actually an heterogeneous population and may be divided into at least two subtypes [70]. Pro-inflammatory, classically-activated macrophages (i.e., M1 macrophages) are associated with immune defense, whereas anti-inflammatory, classically-activated macrophages (i.e., M2 macrophages) are involved in tissue repair and restoration. The ratio between M1/M2 macrophages

is an indicator of the *in vivo* polarization status of resident macrophages of adipose tissue in response to different stimuli. Pro-inflammatory M1 macrophages accumulate in adipose tissue in obesity [28, 71]. Consistent with this view, macrophages recruited from adipose tissue from diet-induced obesity (DIO) mice have increased inflammatory properties [72]. In contrast, polarization towards anti-inflammatory M2 macrophages preserves insulin sensitivity via PPAR γ -dependent mechanism [73, 74]. More recently, it has been found that M2 macrophages from adipose tissue also secrete catecholamines, which are involved in increased catabolism and maintaining of thermoregulatory functions in response to cold exposure [75].

Additional immune cell types are present in adipose tissue, though few of them are detected in normal homeostatic conditions. Among them, monocyte, T lymphocyte, leukocyte, neutrophil numbers increase rapidly in WAT in obesity and contribute to the metabolic imbalance of this tissue [5, 63, 64].

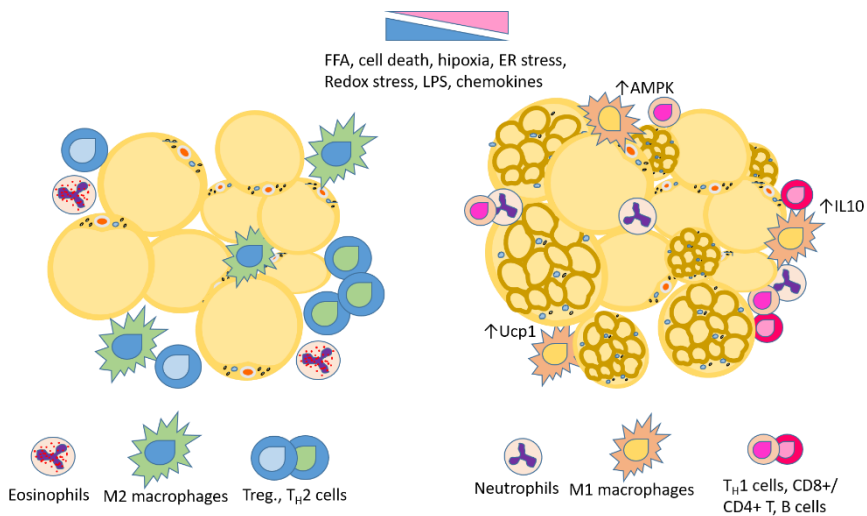


Figure 5 Modulation of immune-metabolism during obesity.

Adapted from [76].

1.2.4 Dysfunctional adipose tissue in obesity

When obesity and inflammation are sustained, adaptive homeostatic mechanisms fail, leading to WAT dysfunction [77, 78]. WAT dysfunction generally involves functional changes in adipocytes and macrophages. The term WAT dysfunction is currently used to define abnormal production of pro-atherogenic, pro-inflammatory and pro-diabetic adipokines, which is generally accompanied by a decreased production of adiponectin.

The potential mechanisms involved in adipose tissue dysfunction are heterogeneous and may act directly or in cascade. These include changes in adipose plasticity, ectopic (mainly visceral) fat accumulation, tissue inflammation, and metabolic inflexibility. In addition, tissue cells have the ability to initiate adaptive responses to dysmetabolic stimuli, by plasticity mechanisms, or modification in energy demands, via altering the number, morphology, or remodeling of mitochondria [79]. Indeed, mitochondrial dysfunction may contribute to pathological changes in human tissues in obese.

Adipose plasticity

As a dynamic tissue, WAT may undergo various cellular and structural remodeling processes in response to excess energy and hence the need of energy storage [65]. Tissue remodeling frequently occurs by modifying adipocyte characteristics (i.e., number, size, metabolism). Thus, when tissue expansion is needed, it generally occurs via coordination of [i] enlargement adipocyte size (hypertrophy) and/or number (hyperplasia), [ii] recruitment of inflammatory cells, and [iii] remodeling of the vasculature and the extracellular matrix to allow adequate extracellular expansion, oxygenation and mobilization of nutrients [27].

Similar to WAT, BAT is present at different body sites and can be increased and decreased by environmental signals.

Although adipocyte cellularity is determined early in life, cell turnover remains active throughout life [65]. Interestingly, adipocyte cell turnover is independent of body mass index, which further supports the notion that the adipocyte population is early established and is relatively static in adulthood [80, 81]. Apart from homeostatic turnover involved in cell renewal, adipocyte progenitors are activated during in response to signals of hyperplastic expansion. Interestingly, these progenitors can participate in catabolic remodeling, or browning of adipose tissue. Differentiated adipocytes can also contribute to adipose tissue plasticity by undergoing a phenotypic switch between anabolic to catabolic states. Anatomic location determines whether adipose tissue expansion occurs by hypertrophic or hyperplastic mechanisms in humans and rodents [65]. Remarkably, adipocytes from WAT retain the ability to convert their metabolic phenotype from typical white adipocytes to those resembling brown adipocytes [82-84].

Ectopic fat accumulation

The accumulation of fat deposition in other tissues that regulate metabolic homeostasis, progressive insulin resistance and increases the risk for type 2 diabetes mellitus is referred to as lipotoxicity [85, 86]. Ectopic fat storage during adipose expansion includes extracellular accumulation of fat in intra-abdominal visceral, omental, pericardial, perirenal, and retroperitoneal depots. However, intracellular accumulation of fat in different cell types in organs (i.e., liver, skeletal muscle, heart, pancreas, and kidney) also constitutes a sign of abnormal adipose tissue expansion. Indeed, ectopic accumulation of lipids in the liver, skeletal muscle and pancreas is tightly related to insulin resistance and related diseases, including atherosclerosis [87-91].

Inflammation

Several of the mechanisms involved in adipose dysfunctionality may, either directly or sequentially, induce inflammation. Indeed, obesity is regarded as an inflammatory disease provided by numerous studies showing a moderate increase in circulating pro-inflammatory cytokines in obese patients and the identification of different immune cell types infiltrating the adipose tissue [92]. Rodent and human adipose tissue especially in obese states is the target of macrophage infiltration [28]. Macrophage infiltration proportionally increases with fat mass accumulation and adipocyte hypertrophy [93]. Infiltration of macrophages rises in response to death of hypertrophied adipocytes and aggregate in the form of 'crown-like structures', which completely surround adipocytes [94].

In addition to macrophages, the accumulation of T-lymphocytes is also increased in epididymal fat of mice made obese with a high-fat diet and occurs before the accumulation of macrophages [95], thereby suggesting that at least in rodent tissue lymphocyte infiltration might be a primary event in adipose tissue inflammation in obesity.

Neutrophils are the first immune cell type to appear to the inflamed site even before monocyte/macrophage infiltration occurs. Thus, it is tempting to suggest that neutrophil infiltration may precede that of macrophages into 'inflamed' adipose tissue. Supporting this view, neutrophils early and transiently infiltrate the parenchyma of intra-abdominal adipose tissue in the course of high-fat feeding in mice [96].

WAT dysfunction is defined by impaired secretion of different adipokines and cytokines [97], thereby contributing to systemic concentrations of pro- and anti-inflammatory cytokines. Indeed, increased numbers of macrophages in human adipose tissue of obese patients are reported to enhance the obesity-related, low-grade chronic inflammation [23]. As secretory cells, resident macrophages may significantly contribute to this phenotype. In WAT dysfunction, the production and secretion of cytokines/adipokines is shifted towards a pro-

inflammatory, atherogenic, and diabetogenic secretion pattern (secreting TNF α and IL-6) in obese (i.e., M1 macrophages). Interestingly, anti-inflammatory mediators, including adiponectin and interleukin (IL)-10, appear reduced in obese states [98], but their systemic levels ameliorate upon excess weight loss interventions (i.e., surgical) [99]. Systemic adiponectin is increased in obese women after body weight reduction in obese women through lifestyle changes is associated with an increase in systemic adiponectin [100]. Conversely, in these conditions systemic IL-10 was not influenced after moderate (diet-induced) weight loss [101].

Metabolic inflexibility

Tissue plasticity was first used as a term to characterize the ability of tissues to respond to a variety of stimuli [102]. Metabolic flexibility is the ability to respond or adapt to changes in metabolic or energy demand. This concept broadly refers to physiological adaptability and it is required to encompass shifts in fuel availability (i.e., glucose and fatty acids) to meet energy demands (i.e., to generate chemical energy and/or key metabolites). Insulin release is a major driver of this shift as it governs metabolic machinery to move from catabolic to anabolic processes to store energy.

Metabolic flexibility appears altered in obesity and type 2 diabetes, when fuel selection fails [102]. In the context of obesity, insulin resistance would be an example of metabolic inflexibility, i.e., dysfunctional response to insulin-mediated stimulation, and can develop in many tissues and organs, including WAT.

Despite the analysis of metabolic flexibility in WAT is poorly explored; several reports suggest that this tissue also plays an active role in the metabolism of glucose and lipids, as well as having the potential to increase thermogenesis (i.e., browning) [103-105]. As previously indicated, WAT buffers circulating free fatty acids for peripheral tissues such as the liver via a fine-tuned system that

allows their uptake, esterification, and release [106]. Importantly, this process also occurs in BAT [107], though metabolic flexibility of BAT involves intracellular triglyceride combustion to obtain energy rather than storage and supply for peripheral tissues, as is the case of WAT.

Excess of WAT (i.e., obesity) is related to metabolic complications. However, the mass of WAT is not itself the only cause to explain obesity-related complications, which highlights the importance of healthy, metabolically adaptable WAT to explain them. In this regard, free fatty acid levels (coming from an inappropriate lipolysis) represent an etiological factor for insulin resistance and type 2 diabetes mellitus [108, 109]. In humans, the only significant site of free fatty acid release is abdominal scWAT [110]. Insulin-induced suppression of triglyceride lipolysis in WAT is disturbed in the type 2 diabetes mellitus [111], which put emphasis in the sensitivity (flexibility) of WAT to insulin in a healthy state and reveals the potential of this tissue, which is prone to blunted insulin responsiveness, as an early aberration in the etiology of whole-body insulin resistance and type 2 diabetes mellitus.

The metabolic adaptability of WAT in obesity to expand and continuously store free fatty acids apparently inertly as its 'classical' function, which is down-regulated in conditions of obesity-driven insulin resistance of basal (fasting) [112, 113] and dietary fat storage [114]. Expandibility of WAT is limiting. Thiazolidinediones (TZDs) markedly improve insulin sensitivity and glucose metabolism by expanding WAT via PPAR γ activation and improving triglyceride metabolism [115].

The potential usefulness of metabolic flexibility as viable targets for preventing or treating obesity and type 2 diabetes mellitus is controversial. The effectiveness of these therapies flounders in conditions whereby fuel selection appears altered, but in the absence of concomitant increases in energy demand, as it occurs in nutrient overload or obesity [116]. Indeed, increasing mitochondrial fatty acid flux and oxidation may [117] or may not [118] improve insulin resistance. Taken together, strategies against metabolic diseases such as obesity will be effective only whether they exert a concomitant increase in energy expenditure or demand (like exercise).

Mitochondrial dysfunction

Mitochondria play a central role in metabolism in adipose tissue [119]. They deeply contribute to lipolysis and lipogenesis pathways in white adipocytes, and weight control is now widely accepted [120].

Mitochondrial dysfunction may result from a decreased mitochondrial biogenesis, reduced mitochondrial content, and/or a decrease in the protein content and activity of oxidative proteins 'per unit of mitochondria' [121]. Although the main tissues affected by mitochondrial dysfunction are those with high energy demand, including skeletal muscle, heart, brain; accumulating evidence targeting mitochondria in adipocytes or adipose tissues strongly suggests that mitochondrial impairment in adipose tissue from obese also contribute to whole-body pathological consequences [120, 122]. However, this is not still clear whether mitochondrial dysfunction plays a causative or adaptive role in various metabolic conditions related to obesity or type 2 diabetes mellitus. Compelling lines of evidence indicate that major factors contributing to mitochondrial defects in adipose tissues are oxidative stress, insulin resistance, genetic factors and sedentary lifestyle without physical activity [123].

- *Oxidative stress*

Oxidative stress has been implicated in the pathogenesis of obesity [124]. Oxidative stress is defined by a disequilibrium between the production of ROS and antioxidant defence [125]. Mitochondria represent the major source of intracellular free radicals. Excess ROS species may damage proteins, lipids, and DNA in cells. Defects in the transfer of electrons across the mitochondrial membrane as results of their accumulation in the respiratory chain complexes, enhances their binding with free oxygen, and hence ROS production [126]. Increases in ROS may be also caused by elevated levels of fatty acids via NADPH oxidase activation in adipocytes [127]. In this scenario, ROS may contribute to abnormal production rates of different adipokynes, including

adiponectin. In obese mice, fat accumulation correlates with systemic oxidative stress and treatment with inhibitors of NADPH oxidase reduces ROS production in adipose tissue, attenuated adipokine dysregulation, and improved diabetes, hyperlipidemia, and hepatic steatosis in humans and mice [127]. Moreover, increases in intracellular ROS levels elicited by mitochondrial dysfunction promotes adipocyte dysfunction in the maintenance of glucose homeostasis through attenuation of insulin signalling, down-regulation of glucose transporter-(Glut)4 expression, and decrease in adiponectin secretion [128].

- *Insulin resistance*

Insulin resistance is a metabolic defect associated with obesity [129], which consists of an dysfunctional action of insulin to produce its effects on glucose, protein and lipid metabolism in target tissues. Decreased insulin response to glucose, dislipidemia, and obesity frequently progress into Type 2 diabetes mellitus with a decline in the β -cell function, sustained hyperglycemia and increased advanced glycation end products (AGE) formation. AGE may in turn contribute to insulin resistance in adipose tissue of obese [130]. The contribution of mitochondria in adipose tissues in the onset and progression of insulin resistance is controversial. Recent data suggest a role for an altered flux of mitochondrial calcium in impairing insulin sensitivity [131] that is associated with impaired mitochondrial biogenesis and decreased expression of mitochondrial proteins in adipose tissue [132, 133]. However, ROS-induced mitochondrial dysfunction may be a valid mechanism in skeletal muscle, but not in adipocytes [134], suggesting that it may be tissue-specific.

- *Genetic factors*

There is a spectrum of genes and/or gene variants linked to mitochondrial function and mass in adipose tissue positively related to obesity or obesity-related phenotypes [135]. Moreover, altered gene expression of molecular

targets controlling mitochondrial activity and biogenesis in adipose tissue may be caused by mutations of both nuclear and mitochondrial genomes [124, 136] as well as defects in the gene expression mitochondria-related genes in adipocytes [132, 137, 138]. In this context, transcriptional activators such as *Pgc1a* and *Pgc1b* play a crucial role in coordinating the gene expression of mitochondrial and nuclear genes related to mitochondrial metabolism in both WAT and BAT [139, 140]. *Pgc1 α* enhances PPAR γ in human WAT toward a transcriptional program linked to energy dissipation through an increased expression of *Ucp1* [141]. Consistent with this view, gene expression of *Pgc1a* is reduced in scWAT of morbidly obese patients [142]. Although it is still pending to elucidate whether decreases in the expression of *Pgc1a* can lead to development of obesity or just a consequence of it, the up-regulation of thermogenic genes in WAT might offer new therapeutic tools for obesity.

- *Changes in human behavior and lifestyle*

Sedentary lifestyle have a dramatic impact on human health [143, 144]. Exercise is a major modulator of mitochondrial function [145, 146]. Indeed, the 'beiging' of WAT concomitant to induced gene expression of *Ucp1* (specific of brown adipocytes) has been shown in WAT in response to exercise training [147]. Supporting to this, elevations in the mRNA levels of *Pgc1a* has been found in WAT of mice subjected an acute exercise training [148].

► 1.3 Obesity and cardiovascular disease

Compelling clinical studies suggest that obesity is an independent risk factor for cardiovascular disease [149]. This co-morbidity is frequently associated with an altered metabolic profile, defined as metabolic syndrome [108, 109]. Besides metabolic syndrome, excess adipose tissue accumulation elicits a spectrum of cardiovascular adaptations in obese patients [150, 151].

Coronary artery disease (CAD) represents one of the main outcomes of cardiovascular disease [152]. Atherosclerosis development is the pathogenic mechanism underlying CAD. Atherosclerosis progression typically begins as results of accumulating cholesterol deposits in monocyte-derived macrophage foam cells in the intima of large arteries (fatty streaks) at early stages of human life [153-155]. Endothelial dysfunction in epicardial vessels and inflammation in the vessel wall are two of the main early events involved in its progression.

Obese patients are at high risk for CAD [152]. Atherosclerosis can be assessed through determining the carotid intimal-medial thickness (IMT), a marker of generalized atherosclerosis. Despite its limitations [156, 157], this carotid IMT has been linked to obesity [158-161].

Adipose tissue synthesizes and releases to circulation a variety of molecules with a role in cardiovascular homeostasis. Indeed, this tissue is a significant source of tumor necrosis factor-alpha (Tnf- α) and interleukin-(IL)6 as well as other adiponectins [162-165]. Particularly, adipose tissue is a main contributor of total circulating IL-6 levels, with around 30% of this cytokine coming from this tissue [166, 167]. Of clinical consideration, this finding is very important since IL-6 modulates hepatic synthesis and release of CRP, a marker of chronic inflammation, which can trigger acute coronary syndrome [168].

On a clinical context, circulating concentrations of PAI-1, C-reactive protein (CRP), fibrinogen, and Tnf- α are all related to body mass index (BMI) [166, 169]. However, other surrogates of body weight, such as waist-to-hip ratio and waist circumference are also good indicators of abdominal obesity, and found to be more closely related to atherosclerosis than BMI [170].

▶ 1.4 Anti-obesity strategies

Attempts to prevent obesity have had limited success thus far. Conventional strategies including dietary and lifestyle modifications can be effective in preventing or treating obesity, but not permanently [10]. A number of pharmacological approaches, which act by suppressing food or caloric intake, inhibiting absorption of fats, or improve insulin function and energy expenditure, have been proven beneficial for treating obesity as a complement to either dietary and lifestyle [10] or surgical interventions [171]. Of note, these approaches have not been exempt of harmful side effects and chances of recurrence with severity or effective at all at long term. Although bariatric surgery is today the most effective long-term therapy for the treatment of obesity [172]; this is not exempt of specific clinical post-surgical problems including adaptations of eating behaviours to new gastro-intestinal physiology status, and the need to face changes in drug pharmacokinetics for the management of obesity-associated complications. Moreover, a long-term follow-up is also recommended to prevent and manage weight regain after bariatric surgery [172].

1.4.1 Current emerging therapeutic strategies targeting adipose tissue

Understanding the molecular and cellular roots of obesity is an important prerequisite to improve both prevention and management of obesity, and thus in the development of novel potential therapeutic interventions [10]. In the last decade, the discovery of novel inter-organ crosstalks and molecular signalings in tissues, which have raised substantial interest in relation to its potential to be therapeutically targeted.

The relevance of adipose tissue in controlling diverse physiological and pathological processes have been underscored for many years [173]. Indeed, unhealthy expansion of WAT has been related to multiple adverse

consequences, including inflammation, fibrosis, hypoxia, dysregulation of adipokine secretion, and disrupted mitochondrial function [10]. However, its management has long been unmet by current anti-obesity pharmacological interventions. In recent years, a range of new potential anti-obesity pharmacotherapies have been developed in parallel to recent findings on adipose tissue biology. Indeed, several anti-obesity treatments are already available, with many other potential therapies are currently under investigation as potential novel anti-obesity therapeutic targets (i.e., adipokine-based therapies, promotion of white fat 'beiging' or 'browning', and modulation of inflammation and fibrosis) (reviewed in [10]).

In this section we will mention two of the multiple adipose targeted strategies currently investigated to improve obesity-associated WAT dysfunction.

BAT activation and WAT browning

The list of experimental candidates that induce BAT and/or beiging/browning of WAT is continuously growing (reviewed in [10]). Mitochondrial energy dissipation through 'chemical uncoupling' has also been considered as a target for obesity treatment. However, many of them have side effects which may compromise their therapeutic use or still are on an experimental stage.

Over recent years, the potential use of molecular candidates known to influence brown and/or beige adipose tissue formation have been considered, including TZDs, as well as developmental regulators such as Fgf21 [174, 175], intestinal agonists of the bile acid sensor farnesoid X receptor [176], and adiponectin [177], among some others are excellently reviewed in [10]. Of note, some of them still are at preclinical stages of development or their effectiveness or mechanisms of action are yet to be determined in human clinical trials (reviewed in [10]). This is the case, for instance, of one of these candidates, the Fgf21, which has recently been shown to involve Ucp1- and beiging-independent anti-obesogenic effects in two recent studies [178, 179], despite it was previously described to promote WAT beiging in mice [174]. Some of them may also exert

favorable effects on adipose tissue mitochondrial dysfunction, such as TZDs, by stimulating mitochondrial biogenesis and oxidative capacity in adipocytes [180].

PPAR γ signaling has evidenced new therapeutic venues by revealing new molecules and down-stream mediators as targets for pharmacological interventions. PPAR γ and sirtuin (Sirt)1, a nuclear NAD⁺-dependent class III histone deacetylase, signalings are tightly connected. Sirt1-mediated deacetylation of PPAR γ leads to up-regulation of BAT-specific genes [181]. In adipose tissue, Sirt1 directly suppress PPAR γ [182]. Adipocyte-specific deficiency of Sirt1 protects against obesity in diet-induced obesity (DIO) mice by decreasing the cyclin-dependent-like kinase 5 (CDK5), which in turn results in a reduced selective phosphorylation of PPAR γ [183].

Adipose tissue inflammation

PPAR γ has potent anti-inflammatory properties [184]. Indeed, its deficiency in macrophages impairs their reprogramming from M1 (pro-inflammatory) to M2 (anti-inflammatory) maturation [74], suggesting that macrophage polarization towards the alternative state might be a useful strategy for treating inflammation in adipose tissue from obese.

On the other hand, Sirt1 reduces pro-inflammatory events in adipose tissue [185]. Its deficiency in WAT activates PPAR γ activity SIRT1 downregulation in adipose tissue may resolve long-term inflammation by activation of PPAR γ [186]. Overall, these findings would target Sirt1 as a promising candidate for therapeutic intervention.

Nicotinamide adenine dinucleotide (NAD⁺) precursors as anti-obesity strategy

NAD⁺ is an important cofactor in all living cells and involved in crucial biological processes by [187, 188]. NAD⁺ is abundantly found in different cellular compartments, including mitochondria, cytoplasm, and nucleus. It is crucial for many cellular metabolism pathways, including glycolysis, fatty acid β -oxidation, tricarboxylic acid cycle. Its reduced form (NADH) is a primary electron donor in the production of adenosine triphosphate (ATP) via anaerobic glycolysis and mitochondrial oxidative phosphorylation (OXPHOS) [189] (**Figure 11**). Furthermore, NAD⁺ can also be used by different protein regulators, including NAD⁺-dependent deacetylases (also named as sirtuins) and poly (ADP-ribose) polymerases (PARPs) which are DNA damage sensors [187, 188, 190-192]. Additionally, other enzymes, such as NAD⁺ glycohydrolases (i.e., CD38 and CD157) also consume NAD⁺ to produce ADP-ribose or cyclic-ADP-ribose [193]. Thus, the role of NAD⁺ has expanded to be simply a key molecule in intermediate metabolism to a crucial regulator of multiple signaling pathways [194].

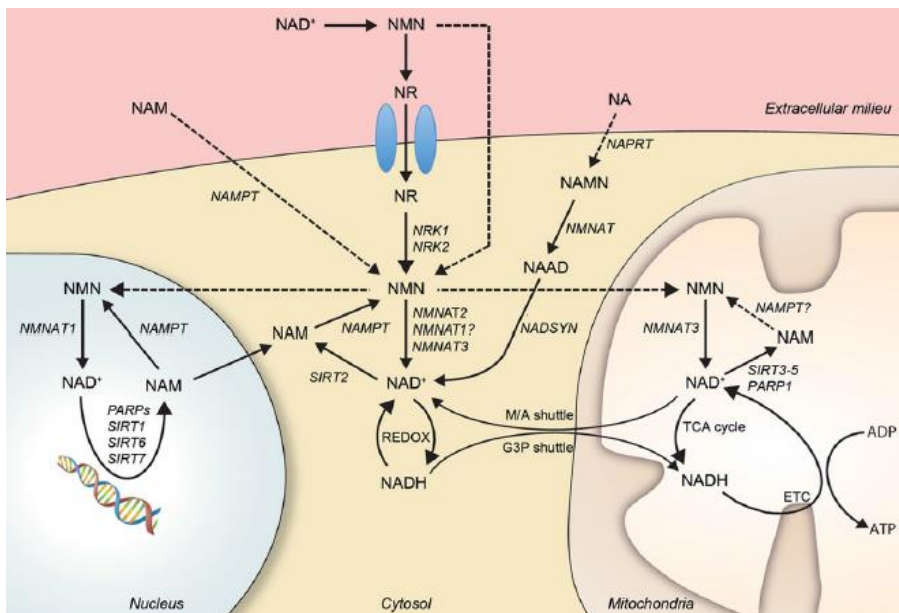


Figure 6 Central nodes for cellular NAD⁺ metabolism

From [187]

Although de novo synthesis of NAD from tryptophan is possible, this process is complex, since it consists of 8 enzymatic reactions, so to produce NAD the use of other precursors, including NAM, nicotinamide ribose (NR), and its phosphorylated form, nicotinamide mononucleotide (NMN) [195], which have a high therapeutic potential [196]. Nicotinamide phosphoribosyltransferase (Nampt), catalyzes the synthesis of NMN from NAM, NR kinase (Nrk) [197], participates in the conversion of NR into NMN and adenylyltransferases (Nmats) [198] catalyze the passage of NMN to NAD⁺. In addition to these enzymes, nicotinamide N-methyltransferase (NNMT) [197] also plays a physiological role in regulating tissue levels of NAM since it is its main substrate. Specifically, this enzyme catalyzes the N-methylation reaction of NAM and other analogous molecules, using S-adenosyl methionine (SAM) as a donor of methyl groups [199], producing N-methyl NAM (me-NAM) and S-adenosylhomocysteine (SAH) [200, 201]. One of the products resulting from its activity, me-NAM, is a physiological inhibitor of NNMT [197]. Although there is no human study in which the impact of treatment with me-NAM on obesity or type 2 diabetes mellitus has been addressed, it shows anti-inflammatory, antioxidant and antidiabetic effects in different experimental models [202-206]. In this same line of argument, a recent study demonstrates the administration of another NAM derivative, isoNAM [207], which has also been reported to protect against the development of diabetes in experimental models. Although it has not been experimentally demonstrated, it is possible that isoNAM could be competing with NAM as a NNMT substrate and at least in part its effect was due to a decrease in NNMT activity.

Altered circulating levels of Nampt, the key limiting regulator of the intracellular NAD⁺ pool, are associated with various metabolic disorders, including obesity, non-alcoholic fatty liver disease (NAFLD) and type 2 diabetes by influencing the oxidative stress response, apoptosis, lipid and glucose metabolism, inflammation and insulin resistance [189].

On the other hand, a key regulator of cellular energy balance throughout the body is the protein kinase activated by AMP (AMPK). This protein is activated under conditions of cellular energy demand, inactivating anabolic pathways, which consume ATP, and activating catabolic pathways, generating ATP. Consistently, AMPK is activated in conditions whereby intracellular concentrations of AMP are increased and ATP concentrations decreased. Consequently, the AMP/ATP ratio increase. AMP/ATP ratio drives the allosteric phosphorylation, and thereby activation of AMPK [208].

AMPK activity levels are reduced in clinical and experimental models of obesity and insulin resistance [209]. Thus, there is an increasing interest in pharmacologically increasing AMPK levels in obesity models through the administration of antidiabetic drugs such as metformin. It is also described that AMPK modulates energy expenditure by regulating the levels of NAD⁺ and with it the activity of SIRT1 [210].

The pharmacological induction of AMPK activity promotes an increase in the activity of Sirt1 and this in turn promotes an increase in mitochondrial β -oxidation, and therefore an increase in the NAD⁺/NADH ratio. In this way AMPK regulates the expression of mitochondrial genes and lipid metabolism through the modulation of the activity of PGC1 α by SIRT1. This interaction could be interchangeable, so activating SIRT1 would promote fatty acid oxidation and indirectly activate AMPK [210].

- *Metabolic effects of NR or NMN*

Intracellular levels of NAD⁺ decrease with age and its deterioration promotes several aging-associated diseases, including metabolic diseases such as obesity and type 2 diabetes mellitus [211]. Up-regulation of NAD⁺ metabolism, including dietary supplementation with NAD⁺ precursors exhibits beneficial effects against aging and aging-associated diseases [212]. As such, NAD⁺ intermediates could also be a new physiological regulator of adipose tissue function and multi-organ insulin sensitivity, providing important mechanistic and

therapeutic insights into obesity-associated metabolic complications [213, 214]. Indeed, recent studies show that the administration of NAD⁺ precursors (i.e., vitamin B3 derivatives) as a strategy to protect against the development of obesity induced by the high-fat diet, contributing to improved oxidative metabolism [215, 216] and improve insulin sensitivity [215, 217] in mice. In these studies, two NAD⁺ intermediates have independently been assessed, such as NR or NMN. Both NR and NMN are physically stable natural compounds that serve as an efficient source of NAD⁺ (Figure 6); however, and dependent of the NAD⁺ intermediate used, the intracellular content of NAD⁺ was coincidentally observed in skeletal muscle of treated mice [215, 216], and other tissues, such as liver [215]. NR [215], but not NMN [216], administration resulted in intracellular elevations of NAD⁺ in BAT. Neither of them produced concomitant elevations of intracellular NAD⁺ in WAT [215, 216].

Administration of NR also reduces plasma concentration of cholesterol in treated mice [215]. Consistently, NMN also favorably reduced systemic cholesterol, but also triglyceride and free fatty acid levels [217].

Reductions in the bioavailability of intracellular NAD⁺ is a hallmark of aging and may underlie a wide-range of age-related diseases, including metabolic disorders such as obesity and diabetes mellitus type 2 [211]. Compelling evidence suggests that elevating NAD⁺ levels by administering NAD⁺ intermediates may be a promising therapeutic strategy to prevent adverse effects of aging. Consistently, administration of NMN raises the bioavailability of NAD⁺ and improves insulin resistance in treated mice [216]. Notably, recent data also show that chronic supplementation of other NAD⁺ intermediate in healthy middle-aged and elderly adults also raises tissue levels of NAD⁺ [218]. Importantly, NR also was well-tolerated in treated humans.

- *Metabolic effects of nicotinamide (NAM)*

Likewise NR and NMN, nicotinamide (NAM, IUPAC name: 3-pyridinecarboxamide) (Figure 7) is another precursor for NAD⁺ synthesis [214, 219].

Studies in experimental models demonstrate that its in vivo administration have anti-diabetic effects [207, 217, 220-246], though such favorable effect may be dependent on the administered dose [247, 248], strain [222], and dietary pattern [249]. The latter is relevant for human studies as it would be suggesting that diet, among other factors, may need to be further controlled.

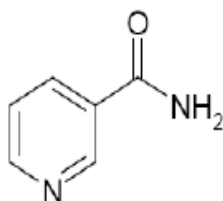


Figure 7 Structural formula of nicotinamide

The favorable influence of NAM over diabetes mellitus led to directly investigate its potential therapeutic use in diabetic patients [250]. Indeed, the administration of NAM has beneficial effects associated with a higher clinical remission rate, improves metabolic control and preserves or increases the function of beta cells [251]. However, and despite the absence of adverse effects, NAM did not prove to be effective at all or yielded contradictory results in different studies [251-271], so the investigation of its potential role as an anti-diabetic agent has been progressively abandoned over the last years. Interestingly, no changes on body weight, adiposity index and plasma lipid concentration in any of these studies, which could be at least in part due to the fact that such trials were conducted in non-obese diabetic patients, and thus they would possibly be unforeseen.

NAM supplementation improves insulin sensitivity in rats made obese with a high-fat diet [231]. Similar results have also been described in obese animals that have been administered with other NAM derivative (i.e., isoNAM) [207].

The potential favorable impact of NAM on body weight in experimental models is rather elusive. The latter has been mostly and likely due to experimental design issues. Indeed, many studies have been made using supraphysiological doses of this vitamin form. Moreover, NAM has been also administered intraperitoneally or oral-gavaged in different studies [231, 272] frequently using high-concentration, single-bolus preparations rather than lower and chronically administered doses.

The oral administration of daily doses of 1% NAM supplemented by either the drinking water or diet in mice has been reported to be safer and not related to significant adverse effects [246]. Importantly, at this dose, palatability signs were not detected as revealed by the fact that treated mice did not drink or eat less than untreated mice. However, and alike the above mentioned NR and NMN, a favorable effect on body weight gain by NAM has not been reported in any study.

Another differential trait compared with other derivatives (i.e., NR and NMN) [215, 217] and another form of vitamin B3 (i.e., NA, IUPAC name: 3-pyridine carboxylic acid) is that its administration does not favorably influence systemic lipid levels nor has it been associated with an improvement in cardiovascular risk [273]. Of them, NA is the most studied and is currently used in clinical practice as a therapy for treating hyperlipidemias, given that has been described having lipid-lowering [274] and vasodilatory effects [275]. However, when given at larger doses, NA administration may cause flushing, itching, hypotension and headaches as main adverse side effects [276], which strongly limits its use as a drug therapy.

The importance of increasing the bioavailability of NAD⁺ in obesity models is due to the fact that it has a fundamental role in energy metabolism, in particular, mitochondrial oxidative metabolism, as well as being used as a substrate by several enzymes such as sirtuins, involved in mitochondrial biogenesis and homeostasis [187]. Like NR and NMN, NAM might also be considered as an intracellular NAD⁺ precursor and stimulate energy metabolism; however it has not previously analyzed.

Anti-inflammatory effects of NAM

Dietary deficiency of vitamin B3 forms has been associated with different inflammatory processes, including dermatitis, irritation and inflammation of mucose membranes [277-280].

NAM administration is used in dermatology for treating different skin affections with inflammatory course, including dermatitis, acne and skin irritations [281-284] and even, it has been reported to have a photoprotection actions [285]. Its administration has also been proven beneficial to prevent intestinal inflammation in patients and in an experimental model [286].

The anti-inflammatory effects of NAM have been in previous studies in vitro in immune cell types involved in chronic inflammatory processes such as atherosclerosis [287-295]. In one of these studies [287], it has been proposed that NAM may promote the differentiation of monocytes to macrophages with restricted inflammatory traits, i.e., with strong reduction of the pro-inflammatory features. However, there is any study directly assessing the anti-atherogenic potential of NAM in vivo. Interestingly, me-NAM has been shown to protect against atherosclerosis [296].

Dietary supplementation of NMN and NR have been previously reported to be involved in vascular protection against oxidative stress [297] and reversing vascular damage [298]. However, such favorable effects were not attributed to changes in the inflammatory status of target tissues. Furthermore, atherosclerosis was not further assessed [297, 298].

Importantly, NA administration shows anti-atherogenic effects in vivo in different animal models of atherosclerosis [299-304]. In contrast with the reported about NA side effects, NAM is not a vasodilator, so does not cause the flushing that occurs with NA, thus having an added potential therapeutic value [305].

• 2. HYPOTHESIS

A growing body of experimental evidences suggests that vitamin B₃ derivatives, such as Nicotinamide Mononucleotide (NMN) and Nicotinamide Riboside (NR), may protect against weight gain and improve obesity-related complications. Also, the amide form of vitamin B₃, Nicotinamide (NAM) displays potent anti-inflammatory properties in different experimental models as well as in patients.

Vitamin B₃ is a main precursor of cellular NAD. Indeed, the above-mentioned NAD intermediates have been reported to enhance energy expenditure *in vivo* due to improved skeletal muscle mitochondrial function through Sirt1 signaling. However, the direct impact of these intermediates on WAT physiology has not been explored yet.

The use of NAM, which is also a potential source of NAD, on energy metabolism, remains poorly explored. In part by its reportedly action as an *in vitro* Sirt1 inhibitor. However, recent evidences show that such anti-Sirt1 signaling effect might not be reproduced *in vivo*.

On the other hand, NAM administration has been proven as anti-inflammatory. In particular, NAM treatment of activated macrophages, a common cell phenotype present in different pro-inflammatory states, reduces the production of inflammatory cytokines *in vitro*.

We therefore tested the hypothesis that NAM treatment might prevent fat accumulation and induce energy expenditure in obese mice. As 'inflamed' adiposity is a common trait in obesity, we also tested the hypothesis that NAM would reduce inflammation in the fat depots of treated obese mice.

Finally, we also tested the hypothesis that NAM administration *in vivo* would prevent the development of atherosclerosis in an appropriate animal model.

• OBJECTIVES

The main focus of this thesis was to assess the impact of NAM supplementation in mouse models of obesity, chronic inflammation and atherosclerosis.

Therefore, the specific goals of this study were:

1. To establish one or more safe and well tolerated dose for oral NAM fortification in mice to assess the beneficial effect, if any, of this form of vitamin B₃ on weight gain without adverse effects.
2. To assess the most effective dose of NAM on body weight gain and adiposity in non-obese mice and in a mouse model of high-fat diet-induced (DIO) obesity.
3. To determine whether the NAM effects were specific by checking the impact of another common form of the vitamin B₃, Nicotinic Acid (NA), on the DIO model.
4. To explore the potential energy metabolism mechanisms related to NAM-mediated effect on adiposity, by analyzing the:
 - a. NAM-derived metabolome (i.e., NAM, me-NAM, NAD⁺/NADH) and metabolites of energy metabolites (adenosine phosphates) in adipose tissue, including the molecular determinants involved in their tissue levels (i.e., Nampt, Ampk).
 - b. Global energy expenditure.

- c. Adipose tissue plasticity and remodeling.
 - d. Glucose homeostasis.
 - e. Liver status.
5. To evaluate the potential role of NAM on systemic and adipose tissue inflammation.
 6. To determine NAM effect on the aortic atherosclerosis in ApoE-deficient mice.

• 3. MATERIALS AND METHODS

▶ 3.1 Mice and diets

In this work different research designs were built to assess the impact of different vitamin B₃ forms on energy metabolism, body weight gain, accumulation of adiposity, inflammation and atherosclerosis in appropriate mouse models.

Specific methods and procedures of each research design are described in subsequent subsections.

All animal procedures were reviewed and approved by the Institutional Animal Care Committee and Use Committee of the Institut de Recerca de l'Hospital de la Santa Creu i Sant Pau (Procedure N^o 126), and the methods were conducted in accordance with the approved guidelines.

3.1.1 Common methods and procedures in different experimental designs

The different groups of mice had an equal distribution of characteristics before starting research studies. Some of the experimental designs were repeated as many times as needed to fulfill each of the programmed analysis. Mice had free access to food and water and were used after a minimum of 7 days acclimatization to the housing conditions. Both NAM (and NA) were administered to mice was administered orally via tap water (1%). The initial range of doses of NAM (and NA) was established according to previous publications [306].

All animals were kept in a temperature-controlled environment (20°C) and humidity (66%) with a 12-hour (h) light/dark cycle. Body weight gain and food and water consumption were weekly monitored during the period of treatment.

At the end of the studies, mice were kept on a 4-h food deprivation, euthanized, and ex-sanguinated by cardiac puncture previously anesthetized with isoflurane vapors (Forane®, Abbott). Blood was collected and either plasma or serum were obtained by centrifugation at 3,000 g for 10 min. Food and water intake were monitored for 2 days before the animals were euthanized. Mice were previously placed individually in regular cages and acclimatized for 24h.

3.1.2 Evaluation of the safe dose

Male wild type mice on a C57BL/6J background were from Jackson Laboratories (Bar Harbor, ME, USA; stock n: 00664. <https://www.jax.org/strain/000664>).

Two-month-old, male mice (i.e., with weights between 22 and 25 g), were randomly distributed into seven groups (n = 8 mice each, n = 56) depending on whether they received tap water supplemented with different doses (i.e., 0.1-0.5- 1%) of two forms of vitamin B₃, NAM or NA, as appropriate, or non-supplemented with any form of vitamin B₃ (untreated mice), for 1 month.

In this first approach, the mice were fed a low-fat diet (regular diet, RD) (Table 3.1) (Teklad Global 14% Protein Rodent Maintenance Diet 4% fat, 2.9 kcal/g) (Figure 8).

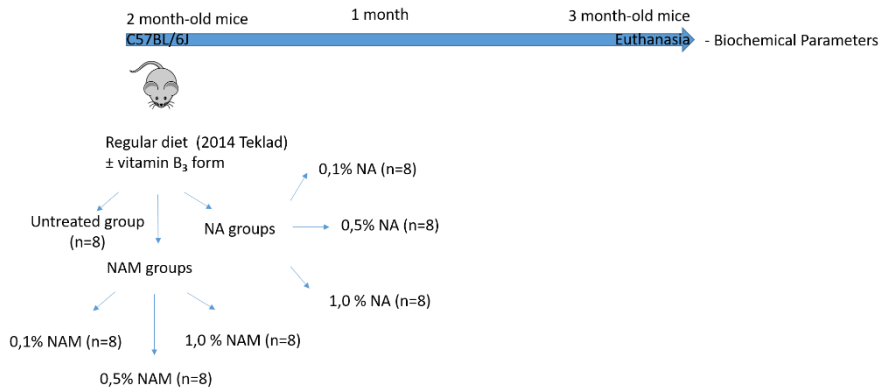


Figure 8 Choosing a safe dose of vitamin B3 forms.

Two-month-old, mice (on a C57BL/6J genetic background) were fed with a regular diet and supplemented with different doses of NAM or NA, and their controls, an untreated group. The analysis of gross and biochemical parameters was performed after 1 month of treatment (n = 8 per group).

On a pilot study, the effect of higher doses (than 1%) of NAM (i.e., 2.5 and 5%) on mice was also assessed to directly assess their impact on mouse physiology at longer term (i.e., 3 months).

Two-month-old, male mice (i.e., with weights ranging from 22 to 25 g) were randomly distributed into three groups (n = 5 mice each, n = 15) depending on whether they were orally dosed with 0% (untreated mice), 2.5%, and 5% of NAM via tap water. At these doses, water palatability was deeply affected as shown by the reduced rates of water consumption. Additionally, food consumption and hence body weight gain also was reduced compared with untreated mice together with signs of altered renal function (see results section for further details). The latter findings made the pilot experiment to be eventually discontinued after 2 months of treatment (Figure 9).

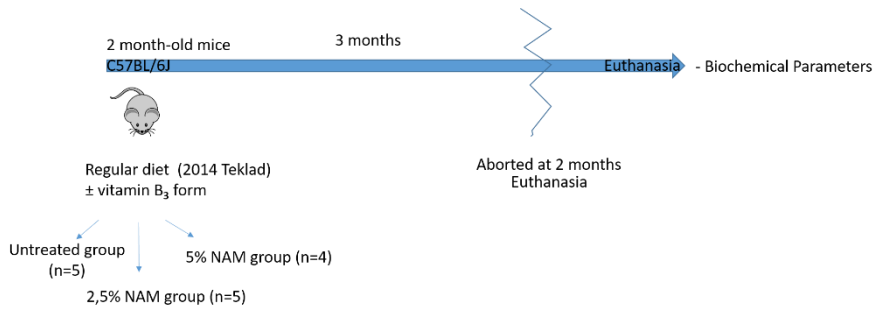


Figure 9 Mouse testing using higher doses of NAM than 1%.

Mice with genetic background C57BL/6J at 2 months of age were fed with a regular diet and supplemented with two different doses of NAM (2.5% and 5%). Mice receiving non-supplemented water were used as the control, untreated group. At these high doses water palatability was highly affected. Indeed, after 2 months of treatment, the experiment had to be discontinued due to adverse problems affecting food consumption. (n = 4-5 per group).

After establishing that 1% of NAM or NA doses were safe in short-term studies (1 month), a pilot experiment was developed to test long-term effects (i.e., 3 months) (Figure 10).

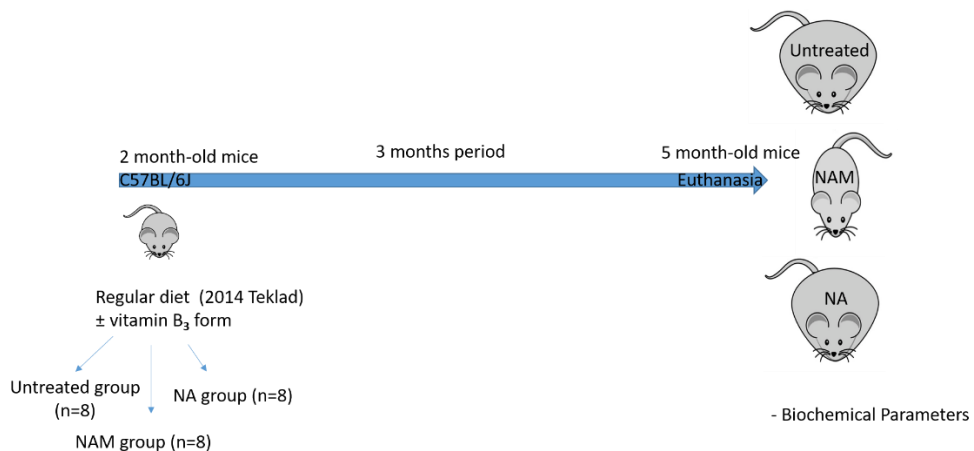


Figure 10 Validation of the maximal safe dose.

Mice with genetic background C57BL/6J at 2 months of age were fed with a regular diet and supplemented with different doses of NAM or NA, and their controls, an untreated group. The analysis of body and biochemical parameters were performed on samples obtained after 3 months of treatment (n = 8 per group).

3.1.3 Evaluation of vitamin B3 forms on body weight gain prevention

The effects of vitamin B₃ forms administration on gross, including body weight and adiposity, and metabolic parameters of non-obese mice the procedures were replicated in the pilot experiment in order to validate preliminary results.

Male wild type mice on a C57BL/6J background were from Jackson Laboratories (Bar Harbor, ME, USA; stock n: 00664. <https://www.jax.org/strain/000664>) were used.

Two-month-old mice, weighing between 22 and 25 g, were randomly distributed into three groups (n = 8 mice each, n = 24) depending on whether they received tap water non-supplemented (untreated mice), or supplemented with two different forms of a single dose (i.e., 1%) of either NAM or NA, as appropriate for 3 months.

Mice were fed a RD (Teklad Global 14% Protein Rodent Maintenance Diet 4% fat, 2.9 kcal/g) (Figure 11). NA was administered to mice to compare the phenotype of NA-treated mice with that shown in NAM-treated mice at the same dose.

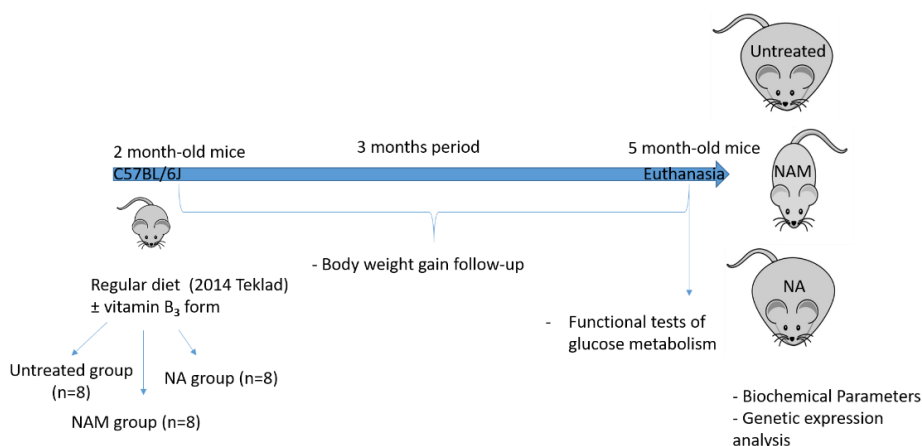


Figure 11. Impact of vitamin B3 forms on mice phenotype.

The study of the different body parameters was carried out, biochemical and histological, as well as the evaluation of the impact of the phenotype in different functional tests in C57BL/6J fed with a regular diet and supplemented with NAM or NA, respectively and their controls, an untreated group. The analysis of body, biochemical and histological tests were performed on samples obtained at 5 months of age. Functional tests related to glucose metabolism were performed at 19 weeks of age (n=8 per group)

The impact of these two different vitamin B₃ forms on gross, including body weight and adiposity, and metabolic parameters was also assessed in mice made obese with a high-fat diet also defined as diet-induced obesity (DIO) mice.

In this independent setting, male wild type mice on a C57BL/6J background were acquired from Jackson Laboratories (Bar Harbor, ME, USA; stock n: 00664. <https://www.jax.org/strain/000664>).

Two-month-old, male mice, weighing between 22 and 25 g, were challenged to a high-fat diet (HFD) (TD.07011, ENVIGO, containing 29% of fat by weight and 23% saturated fat/total fat) and randomly distributed into three groups (n = 8 mice each, n = 24) depending on whether they received tap water non-supplemented (untreated mice), or supplemented with two different forms of vitamin B₃, NAM (or NA) (i.e., 1%), as appropriate, for 3 consecutive months (Figure 12).

In this set of experiments the intended use of NA treatment was included to compare the gross phenotype of NA-treated mice with that of NAM-treated mice.

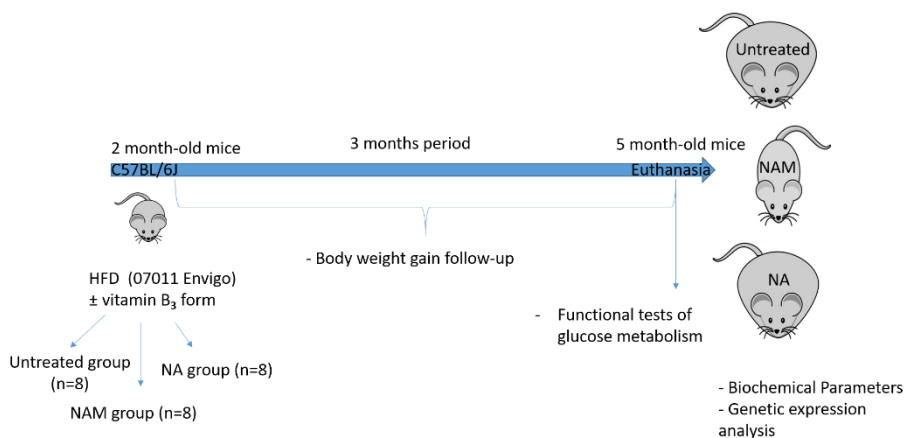


Figure 12. Impact of vitamin B₃ forms on a mouse model of induced obesity.

The study of the different body parameters was carried out, biochemical and histological, as well as the evaluation of the impact of the phenotype in different functional tests in C57BL/6J fed with a HFD and supplemented with NAM or NA, respectively and their controls, an untreated group. The analysis of body, biochemical and histological tests were performed on samples obtained at 5 months of age. Functional tests related to glucose metabolism were performed at 19 weeks of age (n=8 per group).

In an independent setting, the effects of NAM, but not NA, administration on gross phenotype and metabolic characteristics of mice were assessed.

In this case, apart from the tolerable, higher dose of NAM (1%) used, later on defined as high dose (NAM HD), a group of mice receiving a quarter of the highest safe dose tested (i.e., 0.25%), later on defined as low dose (NAM LD) was included to evaluate dose-dependent effects by NAM *in vivo*.

Male wild-type mice on a C57BL/6J background were acquired from Jackson Laboratories (Bar Harbor, ME, USA; stock n: 00664. <https://www.jax.org/strain/000664>).

Two-month-old, male mice, weighing between 22 and 25 g, were challenged to a HFD (TD.07011, ENVIGO, containing 29% of fat by weight and 23% saturated fat/total fat) and randomly distributed into three groups (n = 8 mice each, n = 24) depending on whether they received tap water non-supplemented (untreated mice), or supplemented with two different doses of NAM (i.e., 0.25% NAM, NAM LD; 1% NAM, NAM HD), as appropriate, for 3 consecutive months (Figure 13).

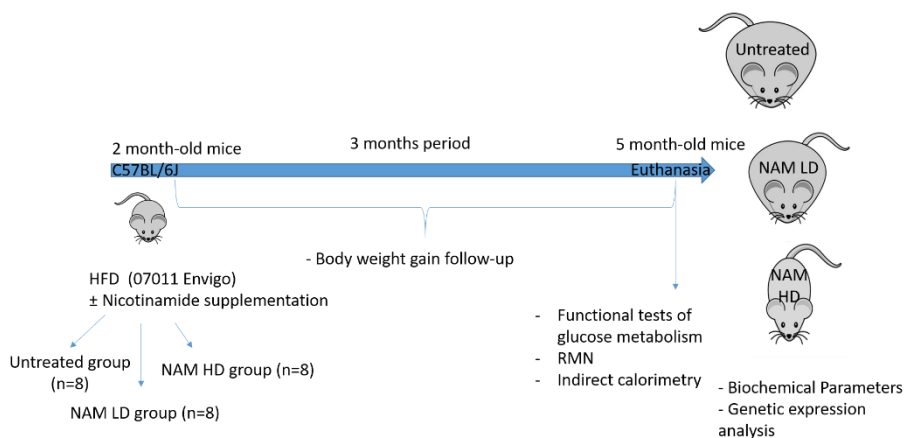


Figure 13. Impact of different doses of NAM on a mouse model of induced obesity.

The study of the different body parameters was carried out, biochemical and histological, as well as the evaluation of the impact of the phenotype in different functional tests in C57BL/6J fed with a HFD and supplemented with two different doses of NAM, respectively and their controls, an untreated group. The analysis of body, biochemical and histological tests were performed on samples obtained at 5 months of age. Functional tests related to glucose metabolism were performed at 19 weeks of age.

3.1.4 Assessment of anti-atherogenic action by NAM

In this final experimental setting, the effect of NAM on chronic inflammation, ApoE-deficient mice were used, which is a mouse model prone to develop massive atherosclerosis when challenged a high-cholesterol, high fat diet.

Male ApoE-deficient mice on a C57BL/6J background were from Jackson Laboratories (Bar Harbor, ME, USA; stock n: 02052. <https://www.jax.org/strain/002052>).

Two-month-old, male mice, weighing 22 to 25 g, were challenged to a high-cholesterol, high fat diet ((western-type diet) TD.88137, ENVIGO, containing 21% of fat by weight, and 27% saturated fat/total fat, and 0.25% cholesterol) and randomly distributed into three groups (n = 8 mice each, n = 24) depending on whether they received tap water non-supplemented (untreated mice), or supplemented with two different doses of NAM (i.e., 0.25 and 1%), as appropriate, for 1 month (Figure 14), timeline long enough for these mice to develop detectable atherosclerosis.

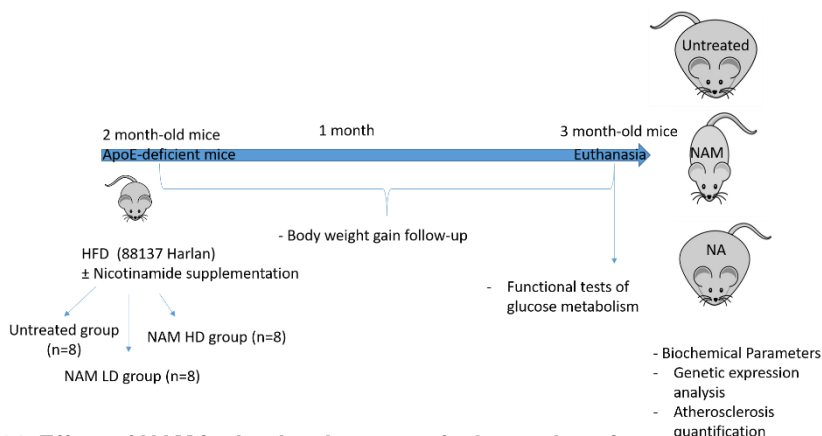


Figure 14. Effect of NAM in the development of atherosclerosis.

The study of the different body parameters was carried out, biochemical and histological, as well as the evaluation of the impact of the phenotype in different functional tests in ApoE-deficient mice fed with a HFD and supplemented with NAM or NA, respectively and their controls, an untreated group. The analysis of body, biochemical and histological tests were performed on samples obtained at 3 months of age. The functional tests in vivo that consisted respectively in the evaluation of metabolism of [³H]-labeled [1 α ,2 α (n)-³H]-cholesterol lipoproteins and postprandial olive oil test were carried out in groups of mice independent. Functional tests related to glucose metabolism were performed at 11 weeks of age. Functional tests of ex vivo non-HDL lipoproteins (ie, function antioxidant) were performed using plasma lipoproteins isolated by ultracentrifugation from pools of 2-3 plasmas of different individuals of each group experimental.

3.1.5 Diets used in this work

	Regular diet (Teklad 2014)	High Fat Diet (Envigo 07011)	High Fat Diet (Harlan 88137)
Protein (%)	20.0	21.0	15.2
Carbohydrate (%)	67.0	24.6	42.7
Fat (%)	13.0	54.4	42.0
Energy density (Kcal/g)	2.9	4.9	4.5

Table 1. Experimental diet nutrient information.

Main gross dietary components are shown as percentage expressed by weight of diet.

▶ 3.2 Biochemical analyses

3.2.1 Plasma analysis of biochemical parameters

Plasma biochemistry was pursued by using either automated or manual approaches, as appropriate. Thus, routine biochemical parameters were analyzed using commercial kits adapted to an autoanalyzer. Circulating levels of specific adipokines (i.e., adiponectin and leptin) were analyzed using specific ELISA kits. Finally, circulating levels of cytokines were determined using a Luminex approach.

Automated analysis of plasma biochemicals

Principle

An automated COBAS analyzer is a medical laboratory instrument designed to rapidly determine different biochemical parameters in a number of biological samples and biofluids, including plasma or urine. These analyses may be useful in the diagnosis of diseased states or to evaluate the reversal of disease states.

Procedure

Blood was extracted directly from heart after anaesthetizing mice with isoflurane. Briefly, blood was immediately centrifuged after collection at 3,000 *g* and 4°C, and the supernatant was collected and stored at –80°C until analysis.

Most plasma chemicals such as cholesterol (cat#3039773190); triglycerides (cat#20767107322); glucose (cat#4404483190); creatinine (cat#04810716190), alanine aminotransferase (ALT, cat#20764949322) and aspartate aminotransferase (AST, cat#20764949322) activities were determined using commercial kits adapted to a COBAS c501 autoanalyzer (Roche Diagnostics, Madrid, Spain). Free cholesterol (cat#435-35801), phospholipids (cat#296-63801), and free fatty acids (FFA, NEFA-HR1: cat#434-91795; NEFA-HR2:

cat#436-91995) were determined using reagents from Wako Diagnostics. Triglyceride determinations were corrected for the free glycerol present in plasma (cat#F6428-40ML; Sigma-Aldrich St. Louis, MO). Quality control testing for each of these assays was done at run-time and all of them fell within the acceptable range defined as 2 times the standard deviation. Precicontrol clin chem Multi 1 (cat# 5117208922, Roche diagnostics) and Precicontrol clin chem Multi 2 (cat# 5117291922, Roche diagnostics) and (cat#410-00102, Wako Chemicals). The calculated coefficient of variation for each assay was ~10%. HDL cholesterol was measured in apolipoprotein (Apo)B-depleted plasma, obtained after precipitation with phosphotungstic acid and magnesium ions (Roche Diagnostics).

Analysis of insulin and adipokines in plasma samples by ELISA approaches

Circulating biochemical molecules involved in glucose metabolism and adipokines were assessed using commercial ELISA kits.

Plasma insulin determination

Principle

Crystal Chem's Ultra Sensitive Mouse Insulin ELISA Kit is based on a sandwich enzyme immunoassay kit. Plasma insulin was determined using the Ultra-Sensitive Mouse Insulin Elisa Kit (Ref. 90080, Crystal Chem Inc., Downers Grove IL, USA).

Procedure

1. Add 95 μ L diluent with 5 μ L sample
2. Incubate at 4°C for 2 h
3. Wash plate twice with wash buffer
4. Add 100 μ L conjugate solution
5. Incubate at room temperature for 30 min

6. Wash plate twice with wash buffer
7. Add 100 μ L substrate solution
8. Incubate for 40 min (low/wide range) or 10 min (high range), as appropriate.
9. Add 100 μ L stop solution
10. Measure optical density at wavelength (λ) = 450/630 nm using a Beckman AD340 spectrophotometer (Beckman)

Adipokine determination in plasma samples

Plasma Leptin determination

Principle

Plasma leptin was determined using the Invitrogen™ Mouse Leptin solid-phase sandwich Enzyme-Linked Immunosorbent Assay (ELISA) Kit (Ref. KMC2281, Invitrogen). This assay is designed to detect and quantify the level of mouse leptin in serum and plasma. The assay recognizes both natural and recombinant mouse leptin.

Procedure

Preparation of samples and standards

1. Dilute serum and plasma samples 1:5 with Standard Diluent Buffer.
2. Reconstitute Ms Leptin Standard to 30,000 pg/mL with Standard Diluent Buffer. Refer to the standard vial label for instructions. Mix gently and allow the contents to sit for 10 min to ensure complete reconstitution. Label as 30,000 pg/mL mouse leptin. Use the standard within 15 min of reconstitution.
3. Add 300 μ L Reconstituted Standard to one tube containing 1.2 mL Standard Diluent Buffer and mix. Label as 6,000 pg/mL mouse leptin.
4. Add 300 μ L Standard Diluent Buffer to each of 7 tubes labeled as follows: 3,000, 1500, 750, 375, 187.5, 93.8, and 0 pg/mL mouse leptin.

- Make serial dilutions of the standard as described below in the dilution diagram. Mix thoroughly between steps. Discard any remaining reconstituted standard.

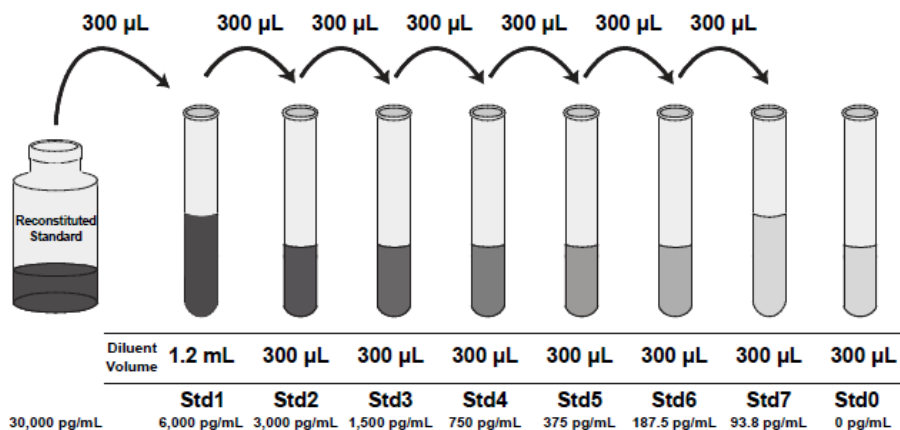


Figure 15. Serial dilutions of the standard.

Preparation of Streptavidin -HRP solution

The Streptavidin-HRP [100x] is in 50% glycerol, which is viscous. To ensure accurate dilution:

- For each 8-well strip used in the assay, pipet 10 µL Streptavidin-HRP (100X) solution, wipe the pipette tip with clean absorbent paper to remove any excess solution, and dispense the solution into a tube containing 1 mL of Streptavidin-HRP Diluent. Mix thoroughly. Streptavidin-HRP [1x] should be prepared within 15 min of usage.
- Return the unused Streptavidin-HRP [100x] solution to the refrigerator.

Performing the ELISA

Bind Antigen

1. Add 100 μ L of standards, controls, or samples to the appropriate wells. Leave the wells for chromogen blanks empty.
2. Cover the plate with a plate cover and incubate for 2 hours at 37°C.
3. Thoroughly aspirate the solution and wash wells 4 times with Wash Buffer [1x].

Add biotin conjugate

1. Add 100 μ L Ms Leptin Biotin Conjugate solution into each well except the chromogen blanks.
2. Cover the plate with plate cover and incubate for 1 h at room temperature.
3. Thoroughly aspirate the solution and wash wells 4 times with Wash Buffer [1x].

Add streptavidin-HRP

1. Add 100 μ L Streptavidin-HRP solution [1x] into each well except the chromogen blanks.
2. Cover the plate with a plate cover and incubate for 30 min at room temperature.
3. Thoroughly aspirate the solution from the wells and wash wells 5 times with Wash Buffer [1x].

Add stabilized chromogen

1. Add 100 μ L Stabilized Chromogen to each well. The substrate solution begins to turn blue.
2. Incubate at room temperature in the dark for 30 min.

Add Stop solution

1. Add 100 μ L Stop Solution to each well. Tap the side of the plate to mix. The solution in the wells changes from blue to yellow.

Read the plate and generate the standard curve

Read the absorbance at $\lambda = 450$ nm. Read the plate within 2 h after adding the Stop Solution. Optimally, the background absorbance may be subtracted from all data points, including standards, unknowns and controls, prior to plotting. Final concentrations for unknown samples and controls were calculated using the appropriate factor to correct for the sample dilution.

Readings were ensued using a Beckman AD340 spectrophotometer (Beckman).

Plasma adiponectin determination

Principle

Plasma adiponectin was determined using the Invitrogen™ Mouse Adiponectin solid-phase sandwich Enzyme-Linked Immunosorbent Assay (ELISA) Kit (Ref. KMP0041, Invitrogen). This assay is designed to detect and quantify the level of mouse adiponectin in serum, plasma. The assay recognizes both natural and recombinant mouse adiponectin.

Procedure

Preparation of samples and standards

Pre-dilute samples

Dilute serum and plasma samples 20,000-fold with ELISA buffer [1x].

Standards

Reconstitute Ms Adiponectin Standard to 16 ng/mL with 1 mL of deionized water. Mix gently and allow the contents to sit for 10 min to ensure complete reconstitution. Label as 16 ng/mL mouse adiponectin. Use the standard within 1 hour of reconstitution.

Add 300 μ L ELISA Buffer [1x] to each of 8 tubes labeled as follows: 8, 4, 2, 1, 0.5, 0.25, 0.125, and 0 ng/mL mouse adiponectin.

Make serial dilutions of the standard as shown in the following dilution diagram. Mix thoroughly between steps. Discard any remaining reconstituted standard.

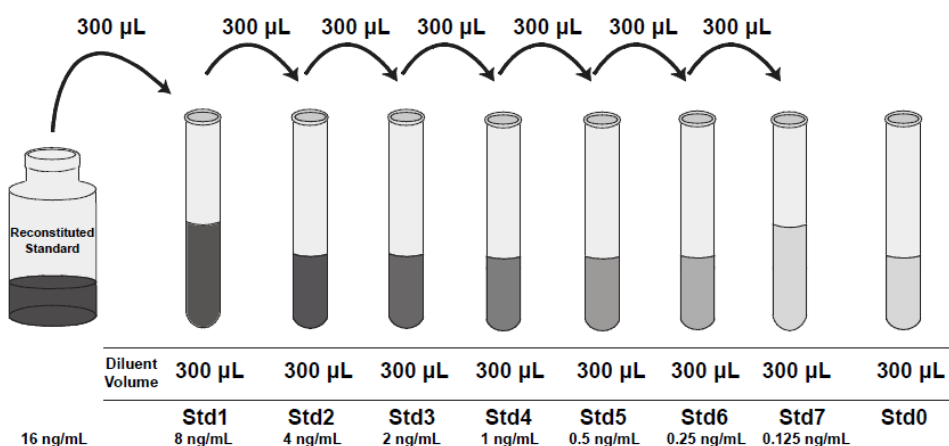


Figure 16. Serial dilutions of the standard.

Preparation of Detection Antibody solution [1x]

Dilute 50 μL of Detection Antibody 200X with 10 mL of 1X ELISA Buffer. Label as Detector Antibody [1x]. Diluted Detection Antibody is not stable and cannot be stored.

Preparation of anti-rabbit IgG HRP solution [1x]

Dilute HRP [100x] 1:100 (v:v) and add 100 μL to 10 mL of ELISA Buffer [1x]. Label this as HRP solution [1x]. This solution is stable within 1 h.

Performing the ELISA

Bind Antigen

1. Add 100 μL of standards, controls, or pre-diluted samples to the appropriate wells. Leave the wells for chromogen blanks empty.
2. Cover the plate with a plate cover and incubate at 37°C for 1 h.
3. Thoroughly aspirate the solution and wash wells 3 times with Wash Buffer [1x].

Add detector antibody

1. Add 100 μL of Ms Adiponectin Detection Antibody solution into each well except the chromogen blanks.
2. Cover the plate with plate cover and incubate at 37°C for 1 h.
3. Thoroughly aspirate the solution and wash wells 3 times with Wash Buffer [1x].

Add IgG-HRP

1. Add 100 μ L Anti-Rabbit IgG HRP into each well except the chromogen blanks.
2. Cover the plate with a plate cover and incubate at 37°C for 1 h.
3. Thoroughly aspirate the solution from the wells and wash wells 5 times with Wash Buffer [1x].

Add TMB Substrate Solution

1. Add 100 μ L TMB Substrate Solution to each well. The substrate solution begins to turn blue.
2. Incubate for 20 min at room temperature in the dark.

Add Stop solution

1. Add 100 μ L Stop Solution to each well. Tap the side of the plate to mix. The solution in the wells typically changes from blue to yellow.

Read the plate and generate the standard curve

Read the absorbance at $\lambda = 450$ nm. Read the plate within 2 h after adding the Stop Solution. Optimally, the background absorbance may be subtracted from all data points, including standards, unknowns and controls, prior to plotting. Final concentrations for unknown samples and controls were calculated using the appropriate factor to correct for the sample dilution.

Readings were ensued using a Beckman AD340 spectrophotometer (Beckman).

3.2.2 Cytokine determination in plasma using a multiplex approach

Principle

The sample is added to a mixture of color-coded beads, pre-coated with analyte-specific capture antibodies. The antibodies bind to the analytes of interest. Biotinylated detection antibodies specific to the analytes of interest are added and form an antibody-antigen sandwich. Phycoerythrin (PE)-conjugated streptavidin is added. It binds to the biotinylated detection antibodies.

Magnetic beads are typically read on a dual-laser flow-based detection instrument, such as the Luminex® 100™, Luminex 200™. One laser classifies the bead and determines the analyte that is being detected. The second laser determines the magnitude of the PE-derived signal, which is in direct proportion to the amount of analyte bound.

Procedure

This analysis was pursued at Mercedes Camacho's lab in the Institut de Recerca de l'Hospital de la Santa Creu i Sant Pau. A magnetic bead-based Milliplex Map Mouse Cytokine/Chemokine Magnetic Bead kit (MCYTOMAG-70K) (Merck-Millipore) was used, designing a 5-plex custom kit containing the specific cytokines, including IL10, IL6, IL4, and TNFa.

The assay was performed following the manufacturer's instructions. Briefly, 25 µL of standard, control, assay buffer (as background) and diluted samples were incubated along with 25 µL of the magnetic bead mix (containing beads for each cytokine) overnight. Beads were washed and incubated with 25 µL of the detection antibodies for 1h. Afterward, without washing or removing the detection antibody, 25 µL of streptavidin-PE (SA-PE) were added for 30 min. After washing, the beads were suspended in 100 µL of drive fluid for analysis. All incubations were performed at room temperature and shaking. Plate analysis was performed in a Luminex Corporation® MAGPIX® instrument with XPONENT® using xMAP® technology (Millipore Corporation, Billerica, MA).

3.2.3 Isolation of lipoproteins from sequential ultracentrifugation

Principle

Ultracentrifugation is an important tool in biochemical research of plasma lipoproteins as it enables their sequential concentration at different densities and to be determined independently. The isolation of lipoproteins may be preparative (i.e., large volumes of plasma are used to obtain maximal quantity of specific lipoprotein classes) or analytical (i.e., small volumes of plasma are needed to characterize the chemical composition of lipoprotein subfractions).

Materials

- Analytical ELIP type tubes (maximal volume 2.5 mL) (polycarbonate plastic).
- Preparative centrifuge tube (maximal volume 20 mL) (polycarbonate plastic)
- Density Solutions used:
 - Preparation of density solution 1.006 g/mL: add chloramphenicol 0.1 g, NaCl: 17.5 g, Ethylenediaminetetraacetic acid (EDTA)-disodium dehydrated (molecular weight, MW: 404.45 g/mol) : 0.81 g, gentamycin: 4 mL (160 mg) and dissolve all components in distilled water in a final volumen of 2 L. Adjust at pH 7.4
 - Preparation of density solution 1.019 g/mL: add kalium Bromide (KBr): 9.5 g to 500 mL of density solution 1.006 g/mL (KBr is just directly added to this volume of 1.006 g/mL solution).
 - Preparation of density solution 1.063 g/mL: add KBr: 8.53 g to 100 mL of density solution 1.006 g/mL (KBr is just directly added to this volume of 1.006 g/mL solution).

- Preparation of density solution 1.340 g/mL: add KBr: 57,40 g to 100 mL of density solution 1.006 g/mL (KBr is just directly added to this volume, reaching 117.9 mL).
- Ultracentrifuge Beckman.
- Analytical fixed-angle rotor (50.3, Beckman Coulter)
- Lab material (pippetes, tips, Eppendorf tubes, ...)

Procedure

The isolation of the different plasma lipoproteins was carried out by sequential ultracentrifugation by a method described by Havel and collaborators [307]. This method is based on the fact that all the lipoproteins can be isolated by flotation at a lower density than that of each type of lipoproteins (very-low-density lipoproteins, i.e., VLDL, $d < 1.006$ g/mL; low-density lipoprotein, i.e., LDL, $1.019 < d < 1.063$ g/mL; and high-density lipoproteins, i.e., HDL, $1.063 < d < 1.210$ g/mL). Currently, the density of plasma/serum is 1.006 g/mL. Final plasma densities were adjusted using the formula of Radding and Steinberg [308] (Figure 17).

$$X = \frac{V * (fd - id)}{1 - (0.312 * fd)}$$

Figure 17. Radding and Steinberg formula.

Where X = g of KBr; V = volume of plasma in mL, fd = final density, id = initial density, and 0.312 = partial specific volume of KBr. The plasma density is approximately 1.006 g/mL. Sequential fractionation of the different plasma lipoprotein fractions by ultracentrifugation is based on adjusting with KBr and in a phased manner the plasma fraction at an appropriate density for each of the plasma lipoprotein species. The calculation of the amount of KBr needed to adjust plasma density was performed using this formula. Final volume is determined by the maximum capacity provided by the ELIP class tube (up to 2.5 mL).

Alike human plasma, mouse plasma lacks a defined LDL fraction and circulating cholesterol is mainly transported in HDL. Indeed, HDL is considered the main circulating lipoprotein fraction in mouse plasma. Therefore, in this work the density range <1.063 g/mL was used to isolate the non-HDL fraction, which includes the triglyceride-rich lipoproteins along that of LDL lipoprotein fraction, whereas the HDL fraction was obtained from non-HDL-free plasma.

The isolation of particular species at a specific flotation density by ultracentrifugation should be made sequentially to avoid contamination of different lipoprotein classes. For instance, isolation of HDL, the lipoproteins of lower density are first removed from plasma after adjusting its density at a final density of 1.063 g/mL, which embraces all non-HDL lipoproteins. After removal of floating non-HDL, the remaining volume of plasma (defined as non-HDL-free plasma) may be then adjusted to a density of 1.210 g/mL, at which HDL will float and may be collected.

Following this procedure, plasma lipoprotein fractions (non-HDL and HDL) (density range <1.063 g/mL) were obtained from independent plasma pools composed of a minimum of 2-3 mice/experimental group, whereas human LDL (LDL, $1.019 < d < 1.063$ g/mL) were obtained from normolipidemic volunteers was isolated from plasma-EDTA were isolated from pooled plasma by sequential ultracentrifugation at $100,000$ g for 24 h in an analytical fixed-angle rotor (50.3, Beckman Coulter). The obtention and use of human plasma samples for this study were approved by the Ethics Committee of the Hospital de la Santa Creu i Sant Pau in Barcelona.

In the present work, the plasma non-HDL fraction (density range <1.063 g/mL) was isolated from mouse plasma to be used for in vivo kinetics studies, whereas LDL used in ex vivo studies to assess the susceptibility to oxidation in the presence of different concentrations of NAM.

Isolation of mouse non-HDL fraction

Radding & Steinberg formula was used to adjust the initial volume of plasma (initial density (id) = 1.006 g/mL) to a final density of 1.063 g/mL to obtain the non-HDL fraction. Calculations were as follows:

$$\text{g KBr} = \frac{V * (fd - id)}{1 - (0.312 * fd)} = \frac{2.5 * (1.063 - 1.006)}{1 - (0.312 * 1.063)} = \frac{0.1425}{0.6683} = 0.213 \text{ g KBr}$$

Once calculated the needed quantity in g of KBr, these were added to the plasma sample using the concentrated density solution 1.340 g/mL:

$$\frac{0.213 \text{ g} * 117.9 \text{ mL}}{57.4 \text{ g}} = 0.437 \text{ mL of density solution } 1.340 \text{ g/mL}$$

The initial volume of plasma was typically ranging between 0.5 to 1 mL. This volume was established to warrant that the sum of plasma and added solution density did not exceed the maximal working volume determined by the capacity of ELIP type tubes (i.e., 2.5 mL).

Thus, the ELIP type tube will contain the initial volume of plasma, the calculated volume of concentrated density solution 1.340 g/mL, and the initial density solution up to a final volume of 2.5 mL. For instance, taking 0.5 mL as an initial volume of plasma, the final volume in the ELIP type tube should be as follows:

0.5 mL initial plasma volume + 0.437 mL of density solution 1.340 g/mL + volume of initial density solution = (up to a maximal of) 2.5 mL;

→ volume of initial density solution = 2.5 mL - (0.5 mL + 0.437 mL) = 1.563 mL of density solution 1.006 g/mL (initial density of plasma)

Isolation of mouse HDL fraction

The remaining volume of non-HDL-depleted plasma (initial density (id) = 1.063 g/mL) was next adjusted to a final density of 1.210 g/mL to obtain the HDL fraction. The volume of non-HDL-depleted plasma was first adjusted to that of the original plasma pool. Calculations used the Radding & Steinberg formula and were as follows:

$$\text{g KBr} = \frac{V * (fd - id)}{1 - (0.312 * fd)} = \frac{2.5 * (1.210 - 1.063)}{1 - (0.312 * 1.210)} = \frac{0.3675}{0.6225} = 0.590 \text{ g KBr}$$

Once calculated the needed quantity in g of KBr, these were added to the plasma sample using the concentrated density solution 1.340 g/mL:

$$\frac{0.590 \text{ g} * 117.9 \text{ mL}}{57.4 \text{ g}} = 1.212 \text{ mL of density solution } 1.340 \text{ g/mL}$$

Again, this volume was established to warrant that the sum of plasma and added solution density did not exceed the maximal working volume determined by the capacity of ELIP type tubes (i.e., 2.5 mL).

Thus, the ELIP type tube will contain the initial volume of plasma, the calculated volume of concentrated density solution 1.340 g/mL, and the initial density solution up to a final volume of 2.5 mL. For instance, taking 0.5 mL as an initial volume of plasma, the final volume in the ELIP type tube should be as follows:

0.5 mL initial plasma volume + 1.212 mL of density solution 1.340 g/mL + volume of initial density solution = (up to a maximal of) 2.5 mL

→ volume of initial density solution = 2.5 mL - (0.5 mL + 1.212 mL) = 0.788 mL of density solution 1.063 g/mL (initial density of non-HDL-depleted plasma)

In the case of kinetics experiments, the volume of plasma pool was up to 5 mL which was distributed in 1-mL aliquots and processed in parallel. Lipoprotein-depleted plasma was discarded.

Isolation of human LDL fraction

Radding & Steinberg formula was used to adjust the initial volume of plasma (initial density (id) = 1.006 g/mL) to a final density of 1.019 g/mL to first remove triglyceride-rich lipoproteins (i.e., VLDL, and intermediate-density lipoproteins, abbreviated as IDL and also defined as VLDL remnants).

In this case, the initial volume of plasma was typically ranging between 50 to 100 mL. To that effect preparative, polycarbonate centrifuge tubes were used. Plasma was distributed in as many tubes as necessary to warrant that the sum of plasma in each tube and added solution density did not exceed the maximal working volume determined by the capacity of this type of centrifuge tube (i.e., 20 mL).

Calculations were as follows (per one tube):

$$\text{g KBr} = \frac{V * (fd - id)}{1 - (0.312 * fd)} = \frac{20 * (1.019 - 1.006)}{1 - (0.312 * 1.019)} = \frac{0.26}{0.6821} = 0.3812 \text{ g KBr}$$

Once calculated the needed quantity in g of KBr, these were added to the plasma sample as many tubes as necessary considering initial volume of the plasma pool. As previously described, the quantity in g of KBr was added using the concentrated density solution 1.340 g/mL:

$$\frac{0.3812 \text{ g} * 117.9 \text{ mL}}{57.4 \text{ g}} = 0.7830 \text{ mL of density solution } 1.340 \text{ g/mL}$$

Thus, the centrifuge tube will contain the initial volume of plasma, the calculated volume of concentrated density solution 1.340 g/mL, and the initial density

solution up to a final volume of 20 mL. For instance, taking 15 mL as an initial volume of plasma in each tube, the final volume of density solution 1.006 g/mL needed was:

15 mL initial plasma volume + 0.7830 mL of density solution 1.340 g/mL + volume of initial density solution = (up to a maximal of) 20 mL;

→ volume of initial density solution = 20 mL - (15 mL + 0.7830 mL) = 4.217 mL of density solution 1.006 g/mL (initial density of plasma)

After removal of floating lipoproteins, i.e., VLDL and IDL, the LDL were next isolated. To that effect the final density of the VLDL- and IDL-depleted plasma was readjusted to a final density of 1.063 g/mL. Before proceeding, the volume of VLDL- and IDL-depleted plasma was readjusted to the original initial volume of plasma with the density solution 1.019 g/mL.

VLDL- and IDL-depleted plasma was distributed in as many tubes as necessary to warrant that the sum of plasma in each tube and added solution density did not exceed the maximal working volume determined by the capacity of this type of centrifuge tube (i.e., 20 mL).

Calculations were as follows (per one tube):

$$\text{g KBr} = \frac{V * (fd - id)}{1 - (0.312 * fd)} = \frac{20 * (1.063 - 1.019)}{1 - (0.312 * 1.063)} = \frac{0.88}{0.6683} = 1.3167 \text{ g KBr}$$

Once calculated the needed quantity in g of KBr, these were added to the VLDL- and IDL-depleted plasma in each of the tubes where the volume was distributed considering initial volume of the plasma pool. As previously described, the quantity in g of KBr was added using the concentrated density solution 1.340 g/mL:

$$\frac{1.3167 \text{ g} * 117.9 \text{ mL}}{57.4 \text{ g}} = 2.705 \text{ mL of density solution 1.340 g/mL}$$

Thus, the centrifuge tube will contain the initial volume of plasma, the calculated volume of concentrated density solution 1.340 g/mL, and the initial density solution up to a final volume of 20 mL. For instance, taking 15 mL as an initial volume of VLDL- and IDL-depleted plasma in each tube, the final volume of density solution 1.006 g/mL needed was:

15 mL initial plasma volume + 2.705 mL of density solution 1.340 g/mL + volume of initial density solution = (up to a maximal of) 20 mL;

→ volume of initial density solution = 20 mL - (15 mL + 2.705 mL) = 2.295 mL of density solution 1.019 g/mL (initial density of plasma)

After centrifuging floating LDL were collected, pooled and stored at 4°C until use.

For kinetic studies, human lipoprotein-depleted (as a source of cholesteryl transfer protein, CETP) was obtained by removing the HDL from the previous non-HDL-depleted plasma, i.e., VLDL, IDL and LDL. Thus, the HDL fraction was isolated from the non-HDL-depleted plasma using the same procedure as that described for the isolation of previous lipoprotein fractions but considering the floating density of HDL.

After removal of floating non-HDL, i.e., VLDL, IDL and LDL, the HDL were next isolated. To that effect the final density of the non-HDL-depleted plasma was readjusted to a final density of 1.210 g/mL. Before proceeding, the volume of non-HDL-depleted plasma was readjusted to the original initial volume of plasma with the density solution 1.063 g/mL.

Non-HDL-depleted plasma was distributed in as many tubes as necessary to warrant that the sum of plasma in each tube and added solution density did not exceed the maximal working volume determined by the capacity of this type of centrifuge tube (i.e., 20 mL).

Calculations were as follows (per one tube):

$$\text{g KBr} = \frac{V * (fd - id)}{1 - (0.312 * fd)} = \frac{20 * (1.210 - 1.063)}{1 - (0.312 * 1.210)} = \frac{2.94}{0.6225} = 4.723 \text{ g KBr}$$

Once calculated the needed quantity in g of KBr, these were added to the non-HDL-depleted plasma in each of the tubes where the volume was distributed considering initial volume of the plasma pool. As previously described, the quantity in g of KBr was added using the concentrated density solution 1.340 g/mL:

$$\frac{4.723 \text{ g} * 117.9 \text{ mL}}{57.4 \text{g}} = 9.701 \text{ mL of density solution } 1.340 \text{ g/mL}$$

Thus, the centrifuge tube will contain the initial volume of plasma, the calculated volume of concentrated density solution 1.340 g/mL, and the initial density solution up to a final volume of 20 mL. For instance, taking 10 mL as an initial volume of non-HDL-depleted plasma in each tube, the final volume of density solution 1.063 g/mL needed was:

10 mL initial plasma volume + 9.701 mL of density solution 1.340 g/mL + volume of initial density solution = (up to a maximal of) 20 mL

→ volume of initial density solution = 20 mL - (10 mL + 9.701 mL) = 0.299 mL of density solution 1.063 g/mL (initial density of non-HDL-depleted plasma)

After centrifuging floating HDL were collected and discarded, whereas lipoprotein-depleted plasma was collected, keeping the final volume to a minimum hence obtaining a 5-fold concentrate of this fraction. Concentrated lipoprotein-depleted plasma was then pooled and dialyzed at 4°C against 8 L of Tris-HCl buffer, containing Tris-HCl 10 mM, NaCl 0.15 M, EDTA 1 mM, sodium azide 0.5 g/L, pH 7.4 in a tank for 24 h (with three changes of dialysis buffer) and stored at -80°C until use for labeling mouse non-HDL.

The composition of the lipoprotein subfractions were analyzed for lipids, including total cholesterol, free cholesterol, phospholipids and triglycerides, and proteins (total protein content) using commercial methods as described above. The protein levels in isolated lipoprotein fractions were determined using the bicinchoninic acid assay (cat#23225; Thermo Fisher Scientific, Waltham, Massachusetts), according to manufacturer's instructions.

3.2.4 ApoE-deficient mice phenotyping

Principle

Homozygous ApoE-deficient mice show a marked elevation in total plasma cholesterol levels that are unaffected by age or gender [309]. Mice phenotyping was assessed by quantification of plasma levels of cholesterol at 2-month-old mice. The differentiation of homozygous were established at cholesterol levels greater than 6 mM at mice fed with a chow diet [310].

Procedure

1. Draw 100 μ L of blood from the tail vein, via tail tip cut and dispose it in an EDTA containing micro tube (Ref. 41.504.005- SARSTEDT).
2. Centrifuge blood tubes to obtain plasma at 10,000 rpm at 4°C for 10 min.
3. Quantify cholesterol levels in COBAS c501 autoanalyzer.

3.2.5 Nicotinamide and N-methylnicotinamide determination in plasma

This determination was externalized to Centre for Omic Sciences, metabolomics platform in Reus. LC-MS (liquid chromatography-mass spectrometry) involves separating mixtures in accordance with their physical and chemical properties, then identifying the components within each peak and detecting based on their mass spectrum.

Metabolite extraction

To 25 μ L of mouse plasma 300 μ L of cold acetonitrile:methanol:water (5:4:1, v:v:v) containing an internal standard (IS) (d_4 -Nicotinamide to Nicotinamide and N-methylnicotinamide) was added. After vortexing samples were rested 30 min in ice and centrifuged (14,500 rpm at 4 °C for 10 min).

LC-MS analysis

Plasma extracts were analyzed by ultra-high-performance liquid chromatography system coupled to a 6490 triple quadrupole mass spectrometer (Agilent Technologies) with electrospray ion source (LC-ESI-QqQ) working in positive mode. 1 μ L of plasma extract was injected to liquid chromatographic system. For the chromatographic separation of the metabolites an InfinityLab Poroshell 120 HILIC-Z column (2.7 μ m, 2.1 \times 100 mm, Agilent) and a gradient mobile phase consisting of a solution of 50 mM ammonium acetate with 5 μ M acid medronic (InfinityLab deactivator additive, Agilent) as additive (Phase A) and acetonitrile (Phase B) were used. The gradient was the following: isocratic for 1.5 min at 98% B, from 1.5 to 4 min decreased to 55% B, until 4.5 min the percentage of B raised to 98% and finally column equilibrated at 98% B until 6.5 min. The flow of the method was 0.5 ml/min. The mass spectrometer parameters were: drying and sheath gas temperatures 290°C and 400°C, respectively; source and sheath gas flows 20 and 12 L/min, respectively; nebulizer flow 60 psi; capillary voltage 2,500 V; nozzle voltage 500 V; and iFunnel HRF and LRF 110 and 80V, respectively. QqQ worked in MRM mode using the transitions that can be seen in the Table 2.

Metabolite	RT (min)	1st Transition (CE (V))	2nd Transition (CE (V))
N-Me-Nicotinamide	0.76	137 → 80 (24)	137 → 108 (16)
d ₄ -Nicotinamide (IS)	0.91	127 → 84 (24)	127 → 81 (28)
Nicotinamide	0.93	123 → 80 (20)	123 → 53 (32)

Table 2. Transitions used in QqQ shown by different metabolites.

▶ 3.3 Tissue analyses

3.3.1 Tissue collection

At the end of each experiment, 4h-fasted mice were sacrificed by cervical dislocation. For RNA and protein analysis, tissues and organs were collected, weighted and rapidly frozen in liquid nitrogen. For histological analysis, a piece of tissue, approximately 0.5 cm³, was either fixed with formalin for posterior paraffin processing or embedded **with optimal cutting temperature (OCT) compound to obtain cryosections.**

3.3.2 Histological analysis

For histological analysis of adipose tissues (eWAT, scWAT and BAT) and livers, these tissues were fixated in formalin. Once fixed, tissue were dehydrated, embedded in paraffin and sectioned by Service of Immunohistochemistry from IR-HSCP. Paraffin embedded sections (5-8 µm thick) were stained with hematoxylin/eosin. Following staining and mounting, tissue sections were observed under a light field microscope (Olympus BX51) and images of representative sections were captured for analysis.

3.3.2a Adipocytes, BAT and liver droplets quantification

The number of adipocytes and their mean diameter were determined in 5-8 µm-thick paraffin embedded sections by computer-assisted image analysis (ImageJ). For each sample, 10 different sections were analyzed and 20 adipocytes were measured in each. The area of cells was calculated circulating each adipocyte.

To confirm iBAT activation and liver droplets, biopsies were taken for histological evaluation (hematoxylin and eosin [H&E] staining) using 8-8 µm-thick paraffin embedded sections. Samples were viewed by light microscopy to determine the presence of multilocular droplets. Images were saved as TIFF files (8 bits) and were quantified using the ImageJ software for light intensity (range 0 to 256) [311].

CLS density was obtained by counting the total number of CLS in each section compared with the total number of adipocytes and was expressed as CLS number/10,000 adipocytes [312].

3.3.2b Analysis and quantification of arterial lesions

Early aortic lesion areas were studied in three groups of male mice, 2-month-old mice were challenged a western type diet (TD.88137; Harlan Teklad) for 4 weeks at the same time they were receiving different doses of NAM or NA, as appropriate.

At the end of the experiment, mice were euthanized and their hearts flushed with saline, embedded in OCT, and snap-frozen in dry ice. The inferior vena cava was cut to allow the perfusate to exit. Frozen sections of 5-8 μm thickness were taken in the region of the proximal aorta starting from the end of the aortic sinus, and for 300 μm distally, according to the technique of Paigen et al. [313].

Sections were stained with Oil Red O (ORO) and counterstained with hematoxylin. Quantitative analysis of lipid-stained lesions was performed on sections starting at the end of the aortic sinus. The lipid-stained lesions were measured by digitizing morphometry and reported as area (μm^2 per lesion per mouse).

For monocyte/macrophage Marker F4/80 immunostaining, 5 μm thickness cryosections were taken from the region of the proximal aorta starting at the end of the aortic sinus.

3.3.2c ORO Staining

Principle

This staining procedure was used to reveal the extent of lipid accumulation and vascular lesion in proximal aorta of ApoE-deficient mice. The “variant 1” of the Lillie and Ashburn technique was used [314].

ORO preparation:

1. Dissolve 0.5 g of ORO (Ref. O0625-25G- Sigma Aldrich) in 200 mL of isopropyl alcohol.
2. Warm the solution in a long-necked container (2 L volumetric flask) in a 56°C water bath for 1 h and then let it cool.
3. The working solution is prepared prior to use by adding four parts of distilled water to six parts of stock solution.
4. Mix and stand for 10 min.
5. Filter through a fine filter paper.

Procedure

1. Rinse frozen sections in distilled water.
2. Rinse in 60% isopropyl alcohol prepared with distilled water.
3. Stain in ORO variant for 10 min.
4. Wash briefly in 60% isopropyl alcohol.
5. Wash well in distilled water.
6. Stain the nuclei in hematoxylin (Ref. HHS32-1L- Sigma Aldrich) for 1 min.
7. Wash in running water.
8. Wash in distilled water.
9. Aquatex mounting (Ref. 1085620050, Sigma- Aldrich).

3.3.2d F4/80 Immunohistochemical staining

Principle

The monocyte/macrophage marker F4/80 may reveal the presence or subnormal accumulation of resident macrophages in selected tissues.

Procedure

1. Frozen sections were fixed 5 min with formaldehyde 4%.
2. Three washes with phosphate-buffered saline pH 7.4 (PBS) of 5 min each.
3. Quenching peroxidase (5 mL of 30% H₂O₂ in a final volume of 100 mL PBS [1x]) for 30 min.
4. Blocking for 30 min (Blocking solution = 10 mL PBS + 0.2 g Albumin + 0.5 mL normal goat serum).
5. Primary antibody: Goat anti-rat F4/80 antigen dissolved in blocking solution, 1:50 (v:v) dilution was incubated with the cryosection specimens for 1 h.
6. Three washes with PBS [1x] of 5 min each.
7. Secondary antibody: Goat anti-rat (Ref. 14-4801-81, Invitrogen) dissolved in blocking solution marked with HRP, 1:50 (v:v) dilution was incubated with the cryosection specimens for 1 h.
8. Three washes with PBS [1x] of 5 min each.
9. Revealed solution chromogen 3,3'-diaminobenzidine (DAB). Stop reaction at 20 sec with distilled water.
10. Aquatex mounting (Ref. 1085620050, Sigma- Aldrich).

3.3.3 Determination of fecal and liver triglycerides

Feces from individually housed mice, fed ad libitum and with free access to water, were collected over 2 days. Mice were euthanized and exsanguinated by cardiac puncture at the end of the study and livers removed after extensive perfusion with saline. Triglycerides were extracted with isopropyl alcohol-hexane (2:3; v:v) from 1 g of feces and 500-1000 mg of liver. After the addition of sodium sulfate (Na_2SO_4), the hexane phase was isolated, dried with nitrogen, reconstituted with 0.5% sodium cholate, and sonicated using an ultrasound bath (model 5510-MT, Branson Ultrasonics Corp., Danbury, CT, USA) for 10 min (50 Hz) prior to lipid measurements.

3.3.4 Determination of energy metabolites

Principle

Adenosin phosphate metabolites in adipose tissues were determined using a commercial ATP/ADP/AMP assay kit (Cat. A-125, from Buffalo University) according to the instructions of the manufacturer's instructions.

Procedure

1. Sample preparation: Make an extraction with trichloroacetic acid (TCA) precipitation using ~50 mg of tissue.
2. Dilute samples at 1:4
3. Enzyme dilution: Gently agitate ADP-CE and AMP-CE tubes before pipetting. ADP/AMP-CE mix (for SET I) is prepared fresh by adding 1 μL ADP-CE and 1 μL AMP-CE to 98 μL EDB in a microtube followed by gentle mixing. ADP-CE mix (for SET II) is prepared fresh by adding 1 μL ADP-CE to 99 μL EDB in a microtube. Keep both prepared mixes on ice during assay.
4. SET I (AMP + ADP + ATP): Mix 5 μL AMP-CB and 5 μL of the first sample in a microtube and let sit at room temperature for ~5 min. Then add 5 μL ADP/AMP-CE mix to the 10- μl mix and pipette up and down 3 times to initiate enzyme reaction at room temperature. Stop reaction after 30 sec

(or 60 sec if low RLU obtained) by adding 35 μL ice-cold 4 mM EDTA and vortexing. Place tube on ice.

5. SET II (ADP + ATP): Mix 5 μL ADP-CB and 5 μL of the first sample in a microtube and let sit at room temperature for ~ 5 min. Then add 5 μL ADP-CE mix to the 10- μL mix and pipette up and down 3 times to initiate enzyme reaction at room temperature. Stop reaction after 30 sec (or 60 sec if low RLU obtained) by adding 35 μL ice-cold 4 mM EDTA and vortexing. Place tube on ice.
6. SET III (ATP only): Mix 10 μL dH₂O, 5 μL of the first sample and 35 μL ice-cold 4 mM EDTA in a microtube. Mix contents by brief vortexing. Place tube on ice. Repeat SET I, II and III for the next sample and so on.
7. ATP standards: Mix 10 μL dH₂O, 5 μL of each ATP standard (1 - 100 μM) and 35 μL ice-cold 4 mM EDTA in a microtube. Mix contents by brief vortexing. Keep tubes on ice.
8. RLU measurement: Add 10 μL of each sample from SET I, II and III and ATP standards to a set of luminometer assay tubes or wells. Add 0.1 ml ATP Assay Solution to each tube/well and measure RLU immediately. Background RLU, which may need to be subtracted from all sample and ATP standard RLU, is obtained by measuring the RLU of 10 μL distilled water.

Generate a plot of ATP standard RLU vs. ATP standard concentrations. Apply sample RLU to the standard curve to obtain the ATP concentration. Multiply measurement results by the dilution factor where applicable.

- Sample AMP concentration = $[\text{ATP}]_{\text{SET I}} - [\text{ATP}]_{\text{SET II}}$
- Sample ADP concentration = $[\text{ATP}]_{\text{SET II}} - [\text{ATP}]_{\text{SET III}}$
- Sample ATP concentration = $[\text{ATP}]_{\text{SET III}}$

NAD/NADH levels were determined in adipose tissues using an NAD/NADH colorimetric determination kit (ref. ab65348 Abcam) according to the instructions of the manufacturer.

Sample Preparation

1. Harvest 50-100 mg tissue necessary for each assay
2. Homogenize the sample using a politron with 400 μ L of NADH/NAD Extraction Buffer.
3. Centrifuge 5 min at 4°C at top speed in a cold microcentrifuge to remove any insoluble material.
4. Collect supernatant (containing extracted NAD/NADH) into a new tube. Keep on ice.
5. Tissues may contain enzymes that consume NADH rapidly. Remove enzymes by filtering the samples through a 10 kD Spin Column (ab93349) before performing the assay. Add sample to the spin column, centrifuge at 10,000 *g* at 4°C for 40 min. Collect the filtrate.

Decomposition Step for NADH detection in samples:

Total NADt (total NAD & NADH): leave your sample as it is.

NADH: NAD⁺ needs to be decomposed before the reaction.

1. Aliquot 60 μ L of extracted samples into microcentrifuge tubes.
2. Heat samples to 60°C for 30 min in a water bath or heating block. Under these conditions, all NAD⁺ will be decomposed while the NADH will still be intact.
3. Cool samples on ice. Quickly spin the samples to remove precipitate if precipitation occurs.
4. Label samples as NAD decomposed samples.

5. Set up Reaction wells: Standard wells = 50 μL standard dilutions. Sample Background control wells = 10 μL samples (adjust volume to 50 μL /well with Extraction Buffer). NADt Sample wells = 1 - 50 μL samples (adjust volume to 50 μL /well with Extraction Buffer). NADH Sample wells = 50 μL decomposed samples.
6. Prepare 100 μL of Reaction Mix for each reaction.
7. Mix enough reagents for the number of assays (samples and controls) to be performed. Prepare a master mix of the Reaction Mix to ensure consistency.
8. Add 100 μL of Reaction Mix to each standard and sample well.
9. Add 100 μL of Background Reaction Mix to sample background control sample wells.
10. Incubate plate at room temperature for 5 min to convert NAD to NADH.
11. Add 10 μL of NADH Developer into each well and mix. Let the reaction cycle at room temperature for 1 h.
12. Read absorbance at a λ 450 nm in a Beckman spectrophotometer AD340 (Beckman).

3.3.5 Protein abundance and gene expression analyses

3.3.5a Western blot analysis

Mice tissues were immediately frozen in liquid nitrogen after extraction, then homogenized in 50 mM Tris buffer, pH 7.4, containing 150 mM NaCl, 1% Triton X-100, 10 mM EDTA and complete protease inhibitor cocktail (P8340-Sigma Aldrich). Once homogenized, tissue extracts were centrifuged at 13 000 g and 4°C for 5 min, and supernatants were collected. The protein concentration of the supernatant was evaluated by bicinchoninic acid technique (BCA protein assay

kit; Pierce Biotechnology Inc.). A protein sample (25 µg) diluted 1:10 (v:v) was loaded on SDS–polyacrylamide gels (Bio-Rad, Hercules, CA, USA).

Western blots were performed following standard procedures. After electrophoresis, gels (Ref. 161-0185, Bio-Rad) were electrotransferred onto membranes (Ref. 1704157, Bio-Rad), and the membranes were blocked with blocking solution (Ref. 170-6404, Bio-Rad) in Tris-HCl Buffered Saline supplemented with Tween-20 (TBS-T; TBS with 1% Tween-20) and incubated with primary antibodies following the commercial instructions. After three washes with TBS-T, membranes were incubated with the corresponding secondary antibody in blocking solution in TBS-T, and developed with Luminol revealing (Ref. 170-5061, Bio-Rad) for quantification with AxioVision Rel. 4.8 software.

Total and phosphorylated AMP-activated protein kinase (p-AMPK, Cell signaling; ref. 4188 rabbit 1:2000 (v:v) (62 kDa)), uncoupling proteins 1 (UCP-1; ref. ab10983 rabbit 1:5000 (v:v) (32 kDa) Abcam, MA, USA), as well as Complex III (COMPLEX III ThermoFisher cat-459140, mouse 1:2000 (v:v) (45-50 kDa)) and TIM 44 (TIM44, Ref. ab194829 rabbit 1:3000 (v:v) (45-51 kDa) Abcam, MA, USA) were detected with specific antibodies. HRP-linked anti-rabbit or HRP-linked secondary antibodies (DAKO Corporation, Hamburg, Germany were used at a 1:5000 dilution (v:v)).

3.3.5b Gene expression analysis

- Isolation of mRNA

Total RNA was extracted from tissue biopsies (i.e., liver, fat pads) (approximately 25 mg) and cellular extracts (from 1 million cells) using TRIzol® reagent (Invitrogen), according to the manufacturer's protocol, and purified using the RNeasy Plus Mini Kit (Qiagen, Valencia, CA, USA). RNA concentration was determined using a NanoDrop2000 bioanalyzer (Thermo Scientific). Integrity of the total RNA samples were also determined using the same bioanalyzer.

- *RNA quality control*

After purification, RNA concentration was determined by measuring UV absorption in a NanoDrop ND-2000 spectrophotometer. The optical density (OD) at λ 260 nm was used to determine the RNA concentration in the solution, considering that an A_{260} of 1.0 is equivalent to about 40 $\mu\text{g/mL}$ of RNA.

The ratio of absorbance at λ 260 nm and 280 nm was used to assess the purity of RNA. A ratio of ~ 2.0 is generally accepted as “pure” for RNA. If the ratio is appreciably lower, it may indicate the presence of protein, phenol or other contaminants that absorb strongly at or near 280 nm. We accepted samples with a A_{260}/A_{280} ratio ≥ 1.8 .

- *Reverse Transcription*

To measure mRNA expression by qPCR, first RNA was reverse transcribed to complementary DNA (cDNA). cDNA synthesis is achieved by the action of reverse transcriptase, an enzyme able to create a single- stranded DNA from a RNA template in the presence of primers. We used oligo (dT) primers and a mixture of dNTPs purchased from Sigma Aldrich, M-MLV reverse transcriptase, RNase H Minus and Point Mutant purchased from Promega.

- *Quantitative real-time PCR analysis.*

- *Taqman approach*

To measure gene expression levels, we used quantitative polymerase chain reaction (qPCR) to amplify cDNA products reverse transcribed from mRNA. We used a relative quantification method, in which internal reference genes are used to determine fold-differences in the expression of the target gene. The internal reference is a housekeeping gene. The reference gene used in this study was *Beta actin* because we have previously determined that its expression is constant across the different experimental conditions we have used in this work.

The cDNAs were subjected to real-time PCR amplification using Taqman Master Mix (Applied Biosystems). Thermal cycling conditions included 10 min at 95°C before the onset of the PCR cycles, which consisted of 40 cycles at 95°C for 15 s and 65°C for 1 min. Specific mouse Taqman probes (Applied Biosystems) (Table 3.3) were used to analyze gene expression in mouse tissues. Real-time PCR assays were performed on a C1000 Thermal Cycler coupled to a CFX96 Real-Time System (Bio-Rad Laboratories SA, Life Science Group). All analyses were performed in duplicate. As an internal control, gene expression was normalized to the mouse β -actin gene using the Mouse β -actin (Mm00607939_s1) TaqMan gene expression assay (Applied Biosystems). Relative expression of the analysed genes was calculated according to the manufacturer's instructions. The relative mRNA expression levels were calculated using the $\Delta\Delta C_t$ method. Briefly, the analysed gene expression was normalized to β -actin in samples from different experimental groups, using the following formula: the mean value of $2^{\Delta C_t^{\text{Gene of interest}} - \Delta C_t^{\text{Gene of interest}}}$ (β -actin) for at least five different animals were considered 100% for each analyzed gene and the same values for treated mice tissues were referred to those values as previously described.

Gene	Protein	Reference
<i>Abca1</i>	ATP-binding cassette, sub-family A, member 1	Mm00442646_m1
<i>Abcg1</i>	ATP-binding cassette, sub-family G, member 1	Mm00437390_m1
<i>Abcg5</i>	ATP-binding cassette, sub-family G, member 5	Mm00446241_m1
<i>Abcg8</i>	ATP-binding cassette, sub-family G, member 8	Mm00445970_m1
<i>Abcg8</i>	ATP-binding cassette, sub-family G, member 8	Mm00445980_m1
<i>Apoa1</i>	Apolipoprotein A-I	Mm00437569_m1
<i>Cd36</i>	Cluster of Differentiation 36	Mm01135198_m1

<i>Cd68</i>	CD68 antigen	Mm03047340_m1
<i>Cox4i1</i>	Cytochrome C oxidase Subunit 4i1	Mm01250094_m1
<i>Cpt1a</i>	Carnitine palmitoyltransferase 1a, liver	Mm00550438_m1
<i>Cybb</i>	Cytochrome b-245, beta polypeptide	Mm01287743_m1
<i>Cyp7a1</i>	Cytochrome P450, family 7, subfamily a, polypeptide 1	Mm00484152_m1
<i>Cyp7b1</i>	Cytochrome P450, family 7, subfamily b, polypeptide 1	Mm00484157_m1
<i>Fgf21</i>	Fibroblast growth factor 21	Mm00840165_g1
<i>Hmgcr</i>	3-hydroxy-3-methylglutaryl-Coenzyme A reductase	Mm01282499_m1
<i>Hmox1</i>	Heme oxygenase (decycling) 1	Mm00516005_m1
<i>Il10</i>	Interleukin 10	Mm01288386_m1
<i>Il6</i>	Interleukin 6	Mm00446190_m1
<i>Klb</i>	klotho beta	Mm00473122_m1
<i>Lrp1</i>	LDL receptor-related protein 1	Mm00464608_m1
<i>Mfn2</i>	Mitofusin 2	Mm00500120_m1
<i>Nampt</i>	Nicotinamide phosphoribosyltransferase	Mm00451938_m1
<i>Nmrk1</i>	Nicotinamide riboside kinase 1	Mm00521050_m1
<i>Nnmt</i>	Nicotinamide N-methyltransferase	Mm00447994_m1
<i>Nr1h2</i>	Nuclear receptor subfamily 1, group H, member 2 (LXR beta)	Mm00437265_g1

<i>Nr1h3</i>	Nuclear receptor subfamily 1, group H, member 3 (LXR alpha)	Mm00443451_m1
<i>Ppara</i>	Peroxisome proliferator activated receptor alpha	Mm00440939_m1
<i>Pparg</i>	Peroxisome proliferator activated receptor gamma	Mm00440940_m1
<i>Ppargc1</i>	Peroxisome proliferative activated receptor, gamma, coactivator 1 alpha	Mm01208835_m1
<i>Sat1</i>	Spermidine/spermine N1-acetyl transferase 1	Mm00485911_g1
<i>Scarb1</i>	Scavenger receptor class B member 1 (SR-BI)	Mm00450236_m1
<i>Sirt1</i>	Sirtuin 1	Mm00490758_m1
<i>Sod2</i>	Superoxide dismutase 2, mitochondrial (MnSOD)	Mm01313000_m1
<i>Tnf</i>	Tumor necrosis factor	Mm99999068_m1
<i>Ucp-1</i>	Uncoupling protein 1	Mm01244861_m1
<i>Ucp-2</i>	Uncoupling protein 2	Mm00627599_m1
<i>Vldlr</i>	VLDL receptor	Mm00443298_m1

Table 3. List of specific Taqman probes used for gene expression analysis.

- *SYBR green approach*

Aortas were homogenized with Precellys® Evolution connected to a Cryolys cooling unit (Bertin Technologies). Total RNA was extracted using TRI reagent solution (Sigma-Aldrich) following the manufacturer's recommendations. RNA concentration was determined using a NanoDrop2000 (Thermo Scientific). cDNA synthesis was performed from 1 µg total RNA of each sample by using oligo(dT)15 primer, M-MLV reverse transcriptase RNase H Minus, Point Mutant and dNTPs from Promega. Real time quantitative PCR (qPCR) analysis was

performed in technical triplicates using the Power SYBR Green Reagent Kit (Applied Biosystems). Real-time monitoring of PCR amplification was performed using the CFX384TM Real-Time System (Bio-Rad). The oligonucleotide sequences for the primer pairs used are described in Table 3.4. Data were expressed as relative mRNA levels normalized to ribosomal L14 expression.

	5' Primer	3' Primer
<i>Abca1</i>	GCGAGGGCTCATCGACAT	GAAGCGGTTCTCCCCAAAC
<i>Abcg1</i>	TCACCCAGTTCTGCATCCTCTT	GCAGATGTGTCAGGACCGAGT
<i>Abcg5</i>	CTGCTCGCCTACGTGCTACACG TCC	CTATACCAAGCAGCACAAAGTGTAGAAATT CTC
<i>Abcg8</i>	TGCTCATCTCCCTCCACCAGCC TC	GCCTCAGCTTTCCACAGAAAGTCATCAA
<i>Adgre1</i>	CTTTGGCTATGGGCTTCCAGTC	GCAAGGAGGACAGAGTTTATCGTG
<i>Hmox1</i>	GCCGAGAATGCTGAGTTCATG	TGGTACAAGGAAGCCATCACC
<i>Il-10</i>	AGCCTTATCGGAAATGATCCAG T	GGCCTTGTAGACACCTTGGT
<i>Nr1h3</i>	CCTTCCTCAAGGACTTCAGTTA CAA	CATGGCTCTGGAGAACTCAAAGAT
<i>Nr1h2</i>	CATTGCGACTCCAGGACAAGA	CCCAGATCTCGGACAGCAAG
<i>Tnfa</i>	CCAGACCCTCACACTCAGATC	CACTTGGTGGTTTGCTACGAC

Table 4. List of primers sequences used for gene expression analysis.

▶ 3.4 Functional tests

3.4.1 Glucose tolerance test

Principle

Glucose tolerance tests were performed by administering an intraperitoneal injection of glucose (2 mg/g of body mass) after a 4-hour fast. Plasma glucose levels were determined at $t = 0$ (baseline), 15, 60, 120, and 180 min. Blood glucose was measured with Accu-Chek glucometer (Roche Diagnostics) using blood from the tail vein. The area under the concentration curve (AUC) was calculated by the linear trapezoidal method to compare glucose tolerance among groups.

Procedure

1. Animals were fasted for 4 hours before the test by taking the food away early in the morning.
2. Next, one drop of blood from the tail, via tail tip cut was transferred directly onto a glucose indicator strip. Basal blood glucose was measured immediately using the Accu-Chek glucometer (baseline).
3. Then, mice were given an intraperitoneal injection of sterile D-glucose (2 g/kg, dissolved in saline solution) with a 25G needle.
4. Additional blood samples were taken at 15, 30, 60, 120, and 180 min post-injection to measure blood glucose.
5. Between each time point, mouse was returned to its cage and monitored continuously.
6. The glucose response to GTT was also calculated as the area under the curve for each mouse using GraphPad Prism Software.

3.4.2 Insulin sensitivity test

Principle

Insulin sensitivity tests were performed by administering an intraperitoneal injection of insulin (Sigma- Aldrich, 0.9 U/kg of body mass) after a 4-h fast. Plasma glucose levels were determined at $t = 0$ (baseline), 15, 60, 120, and 180 min. Blood glucose was measured with Accu-Chek glucometer (Roche Diagnostics) using blood from the tail vein. The area under the concentration curve (AUC) was calculated by the linear trapezoidal method to compare glucose tolerance among groups.

Procedure

1. Mice were fasted for 4 hours by taking away food early in the morning.
2. Next, one drop of blood from the tail, via tail tip cut was transferred directly onto a glucose indicator strip. Basal blood glucose was measured immediately using the Accu-Chek glucometer (baseline).
3. Then, mice were given an intraperitoneal injection of sterile insulin (0.9 U/kg, dissolved in saline solution) with a 25G needle.
4. Additional blood samples were taken at 15, 30, 60, 120, and 180 min post-injection to measure blood glucose.
5. Between each time point, mouse was returned to its cage and monitored continuously.
6. The glucose response to ITT was also calculated as the area under the curve for each mouse using GraphPad Prism Software.

3.4.3 Susceptibility to lipoprotein oxidation

Principle

An increasing body of evidence suggests that oxidative modification of LDL plays an important role in the development of atherosclerosis in humans and animal models. Many studies have been carried out to establish the role of Cu^{2+} in the oxidation of LDL *ex vivo*. The standardized measurement of LDL oxidative susceptibility could thus be useful to assess the impact of antioxidant treatments.

Procedure

Isolated lipoproteins were dialyzed in phosphate-saline buffer (PBS [1x]) by gel filtration on PD-10 columns (Sephadex G-25™ M, cat#17-0851-01; GE Healthcare). Oxidation was initiated by adding 2.5 μM copper (II) sulfate (CuSO_4) to human LDL (0.1 mmol/L phospholipids).

Oxidized LDL (oxLDL) was obtained by incubating PBS-dialyzed LDL (0.1 mmol/L phospholipids) with 2.5 μM CuSO_4 for 18 h at 37°C. The formation of conjugated dienes was measured by incubating PBS-dialyzed LDL (0.1 mmol/L phospholipids) with 2.5 μM CuSO_4 and in the absence or presence of increasingly higher concentration of NAM (i.e., 0.1%, 0.5%, and 1%). Conjugated diene kinetics were obtained by continuously monitoring the absorbance at λ 234 nm in an ultraviolet Synergy HT microplate reader (Synergy, BioTek) at 37°C for 6 h. The lag phase was calculated from the intersection point between the maximal slope of the curve and initial absorbance, as previously described [315]. The oxidation reaction proceeded in the absence or presence of increasingly higher concentration of NAM (i.e., 0.1%, 0.5%, and 1%) and was terminated by the addition of 0.5 mM EDTA and 2 μM BHT.

The antioxidant capacity of each NAM concentration was the ability to prolong the lag phase and was expressed as the increment versus Ctrl-vehicle mice. The longer the 'lag phase', the higher the antioxidant capacity of NAM. Similarly, the

lower the maximal velocity of oxidation shown by either LDL or non-HDL, the higher their resistance to oxidation in the presence of NAM.

1. Typically, this analysis started from a sample of 600 μL non-HDL obtained by ultracentrifugation.
2. Due to the process of obtaining the non-HDLs, the samples have a high salt content. To remove the salt (KBr + EDTA), non-HDL were dialyzed against PBS [1x] using PD10 columns. Thus, 0.5 mL of the non-HDL were loaded to a PD10 column, which was previously and extensively equilibrated with 25 mL of PBS [1x]. Once the sample volume has been absorbed, it was pushed with 2.5 mL of PBS [1x], discarded this volume, and the final non-HDL eluates were eventually collected by adding 0.8 mL of PBS [1x].
3. The lipid content of the dialyzed lipoprotein fraction was determined in a COBAS autoanalyzer to ascertain the concentration of phospholipids.

Monitoring of oxidation kinetics

- Non-HDL were added at a final concentration of 0.1 mM phospholipids in a final volume of 0.2 mL in duplicate, considering that in one of them we also add 0.1 mM of phospholipids of control LDL control and in the others only the non-HDL.
- Next, PBS [1x] was added up to a final volume of 0.2 mL in each well. Apart from the samples, some wells contained control human LDL alone to assess full oxidation. Finally, we added freshly prepared CuSO_4 , so that it was at a final concentration of 1.25 μM of CuSO_4 in each well (250 μL of a stock concentration of 1 mM originally prepared in 10 mL distilled water). The absorbance was read at a λ 230 nm at 37°C for 4 h (kinetics mode) in a Synergy spectrophotometer (Biotek).

▶ 3.5 *In vivo* kinetic studies

3.5.1 *In vivo* non-HDL turnover

Principle

Assessment of non-HDL kinetics was pursued to dissect the mechanism involved in altered plasma levels of non-HDL observed in ApoE-deficient mice treated with NAM. To that effect, non-HDL were isolated and radiolabeled with [³H]-cholesteryl oleoyl ether (Perkin Elmer) was employed to study the uptake and distribution of non-HDL in plasma and different compartments of mice [316].

Procedure

Plasma lipoprotein resources

1. Obtention of plasma non-HDL from ApoE-deficient mice was pursued as previously described (section 3.2.4). Non-HDL were isolated by ultracentrifugation from freshly isolated pools of plasma from 5-6 mice as previously described (section 3.2.3). This lipoprotein fraction was kept in desntity solution until its use for radiolabeling within 2 weeks.

2. Mouse HDL isolated from male, wildtype (on a genetic background C57BL/6J) mouse plasma (5 mL) were obtained as previously described (section 3.2.3) and dialyzed against 8 L of dialysis buffer (i.e., Tris-HCl buffer, containing Tris-HCl 10 mM, NaCl 0.15 M, EDTA 1 mM, sodium azide 0.5 g/L, pH 7.4) at 4°C for 24 h. This step was repeated twice.

3. Human lipoprotein-depleted plasma concentrate (section 3.2.3) was dialyzed as previously described.

Incorporation of [³H]-cholesteryl oleoyl ether to non-HDL

This process is composed of two main parts. The incorporation of [³H]-cholesteryl oleoyl ether to HDL ([³H]-HDL) is first needed as it will be used as a [³H]-cholesteryl oleoyl ether donor to non-HDL in a reaction catalyzed by human CETP (from lipoprotein-depleted plasma concentrate).

Obtaining [³H]- HDL

1. In a glass tube, cholesteryl oleoyl ether (20 μ Ci, 20 μ L) was mixed with 80 μ L of hydroxytoluene butylate (BHT) solution (from a solution containing 5.5 mg of BHT in a final volume of 25 mL of chloroform), and 1.8 mg of egg lecithin.
2. The mixture was dried under a nitrogen stream in a fume hood.
3. Eight mL of dialysis buffer was added and vigorously mixed by vortexing for 2 min.
4. Next, this mixture was sonicated in a Braun Sonicator on an ice bath for 10 min.
5. Once sonicated, the mixture was mixed with the dialyzed mouse HDL (7 mL), and the lipoprotein-depleted concentrate (10 mL) in the presence of 1mM (final concentration) of 5,5-dithiobis(2-nitrobenzoic acid (lecithin:cholesterol acyltransferase inhibitor), and incubated in a 37°C bath for 24 h.
6. After the 24-h incubation, the mixture (at a density 1.006 g/mL) was centrifuged at 100,000 g at 4°C for 20 h, to remove floating liposomes from the resulting supernatant.
7. Next, the mixture density (1.006 g/mL) was adjusted at 1.063 g/mL as previously described and centrifuged at 100,000 g at 4°C for 20 h, to remove remaining floating liposomes from the resulting supernatant.

7. Next, the mixture density (1.063 g/mL) was adjusted at 1.210 g/mL as previously described and centrifuged at 100,000 g at 4°C for 48 h. [³H]-HDL from the resulting supernatant was obtained into the minimum volume. This procedure was repeated as many times as needed dialyze the whole HDL suspension.

8. Finally, this fraction was incorporated into dialysis buffer using a PD-10 desalting column, eluted by gravity. PD-10 columns were first equilibrated with 25 mL of dialysis buffer before adding 2.5 mL of non-HDL. Elute with 3.5 mL of dialysis buffer and collect by gravity the non-HDL-containing eluate into a separate tube. This procedure was repeated one more time. The non-HDL suspensions were pooled and the concentration of cholesterol determined in a COBAS autoanalyzer. Desalted [³H]-HDL were pooled and the concentration of cholesterol determined in a COBAS autoanalyzer. Desalted [³H]-HDL suspension contained 2 mM of cholesterol, 20·10⁶ cpm/mL, specific activity 10·10⁶ cpm/μmol.

Radiolabeling of mouse [³H]-non-HDL

1. Plasma non-HDL from ApoE-deficient mice were incorporated to dialysis buffer using a PD-10 desalting column, eluted by gravity. PD-10 columns were first equilibrated with 25 mL of dialysis buffer before adding 2.5 mL of non-HDL. It consisted of eluting non-HDL with 3.5 mL of dialysis buffer and collecting by gravity the non-HDL-containing eluate into a separate tube. This procedure was repeated one more time. The non-HDL suspensions were pooled and the concentration of cholesterol determined in a COBAS autoanalyzer. The suspension was filtered through a non-sterile filter with 0.2 μm diameter pores to avoid aggregated non-HDL. Desalted [³H]-non-HDL suspension contained 20 mM of cholesterol.

2. Next, desalted [³H]-non-HDL suspension (7 mL) was incubated with desalted [³H]-HDL (7 mL) (10:1, mmol:mmol) in the presence of 14 mL of desalted lipoprotein-depleted plasma concentrate, and incubated at 37°C for 24 h.

3. After the 24-h incubation, the mixture (at a density 1.006 g/mL) was adjusted at 1.063 g/mL as previously described and centrifuged at 100,000 *g* at 4°C for 20 h, to capture the floating [³H]-non-HDL.

4. [³H]-non-HDL were then incorporated to dialysis buffer using a PD-10 desalting column, eluted by gravity. PD-10 columns were first equilibrated with 25 mL of dialysis buffer before adding 2.5 mL of non-HDL. It consisted of eluting non-HDL with 3.5 mL of dialysis buffer and collecting by gravity the non-HDL-containing eluate into a separate tube. This procedure was repeated one more time. The non-HDL suspensions were pooled and the concentration of cholesterol determined in a COBAS autoanalyzer. The suspension was filtered through a non-sterile filter with 0.2 μm diameter pores to avoid aggregated non-HDL. Desalted [³H]-non-HDL suspension contained 0.75 mM of cholesterol 0.7·10⁵ cpm/mL, specific activity 0.9·10⁵ cpm/μmol.

In vivo kinetics of [³H]-non-HDL

Mice were fasted for 4 h.

Autologous [³H]-cholesteryl oleoyl ether-labeled non-HDL lipoproteins (containing 1 × 10⁵ cpm in 0.1 mL of 0.9% NaCl) obtained from KOE mice were isolated (as shown in section 3.2.2) and intravenously injected into each mouse. Labeled cholesterol was <5% of the total mass of plasma cholesterol.

Serum was collected into tubes at 2 min (initial point), and after 3 h, 6 h, and 9 h after injection, under isoflurane anesthesia. Blood was collected through a small incision at the end of the tail and radioactivity levels in 25 μL of serum was monitored by liquid scintillation counting.

Serum decay curves for the tracer were normalized to radioactivity were expressed taking the initial 2-min timepoint as 100% of activity after tracer injection.

At the end of the experiment, livers were collected and subjected to lipid extraction. Liver [³H]-tracer was expressed as percentage of injected dose was also determined. The lipid extraction of the different tissues / organs is performed as indicated in section 3.3.4.

The area under the curve from the curves drawn by plasma radioactivity levels measured for each individual. Fractional catabolic rates (FCR) were calculated from the area under the serum disappearance curves fitted to a nonlinear, two-phase exponential decay model. The non-HDL FCR values were used to calculate the non-HDL cholesterol (non-HDL-C) secretion rate using the formula [(pool size × FCR)/g]. To that effect, serum volume was estimated to be 4% of body weight.

3.5.2 Distribution of intragastrically-administered [³H]-cholesterol in mice

Principle

Administration of [³H]-cholesterol dissolved in olive oil to mice by oral fat gavage was pursued as an alternative approach to non-HDL kinetics analysis in evaluating the effect of NAM treatment on 'dietary cholesterol' kinetics and tissue distribution *in vivo*.

Procedure

1. Mice were fasted for 4 h
2. Take a blood sample of mice, as time 0.
3. Mice were given an oral fat gavage (OFG) consisting of 20 μCi [³H]-labeled cholesterol ([1α,2α(n)-³H]-cholesterol, Perkin Elmer) in 200 μL of virgin olive oil.

4. Plasma cholesterol levels were monitored at 3 and 6 h after oral administration, through a small incision at the end of the tail. Food was replaced.
5. Mice were bled by cardiac puncture at 24 h, after previous anesthesia with isoflurane.
6. The radioactivity in total plasma and the non-HDL fraction, and liver were determined by scintillation counting using a β counter (Perkin Elmer).
7. Data was expressed as percentage of activity vs. administered dose or in relation to the average value of the control group in plasma (at different times indicated) or tissue/organs at the end of the study, as appropriate.
8. The area under the curve from the curves drawn by plasma radioactivity levels measured for each individual.
9. The lipid extraction of the different tissues / organs is performed as indicated in section 3.4.3.

3.5.3 Assessment of oxygen consumption in mouse by indirect calorimetry

Indirect calorimeter is a tool to monitor resting energy metabolism through the measurement of oxygen (O₂) consumption and carbon dioxide (CO₂) production. From the measurement of VO₂ and VCO₂, the respiratory exchange ratio (RER) can be calculated to assess energy fuel utilization and energy expenditure [317, 318]. Previously, indirect calorimeter has been widely used in metabolic disease research in mice to reveal the potential roles of specific genes or treatments in regulating energy metabolism [319, 320]. This analysis was externalized to Parc Científic de Barcelona and conducted by Dr. David Sebastián.

Energy expenditure were assessed using Micro-Oxymax multiple sensor (Columbus Instruments). Mice (n=5-6 per group) kept on HFD were housed individually in Oxymax chambers and kept on a 12:12-h light–dark cycle (with lights on from 6 am to 6 pm) and room temperature of 22-24°C). Animals had free access to food and water during both dark and light cycles. Constant airflow (0.5 L/min) was drawn through each chamber. After 1 day of acclimation, O₂ consumption, CO₂ production, RQ, heat and ambulation parameters were recorded during 72 h, using software provided by Columbus Instruments. Gas exchange measurements were made every 20 min with room air composed of 20.5% O₂ and 0.05% CO₂.

3.5.4 Magnetic resonance imaging (MRI) analysis

For the in vivo magnetic resonance imaging (MRI) studies mice (n=16) were used, of which 5 were untreated, 6 NAM LD-treated mice, and 5 NAM HD-treated mice. MRI studies were performed at the at the joint nuclear magnetic resonance facility of the Universitat Autònoma de Barcelona and Centro de Investigación Biomédica en Red—Bioingeniería, Biomateriales y Nanomedicina (CIBER-BBN) (Cerdanyola del Vallès, Spain) in a 7T Bruker BioSpec 70/30 USR (Bruker BioSpin GmbH, Ettlingen, Germany) system equipped with a mini-imaging gradient set (400 mT/m) and using a 72 mm inner diameter quadrature 1H volume coil with. MR data were acquired and processed on a Linux computer using Paravision 5.1 software (Bruker BioSpin GmbH, Ettlingen, Germany).

Before the MR study, the animals were first induced with Nembutal (70 mg/kg) in a single intra-peritoneal injection. A catheter was then inserted in the intraperitoneal cavity to administer a maintenance dose of anesthesia (20 mg/kg every 45 minutes or as needed). The animals were then placed in a supine position inside the coila birdcage 1H coil with a 35 mm inner diameter. Bodyre temperature and respiration rate wereas then monitored using MR-compatible temperature probes. At the end of the study, animals were euthanized through an overdose of pentobarbital. At the time of dissection the WAT areas were readily recognizable by gross inspection of whole-body fat depots.

For fat enhancement imaging, T1-weighted images were acquired using a respiratory gated spin echo sequence (repetition time (TR)/echo time (TE) = 600 ms/10.5 ms) acquiring 23 coronal sections with field of view = 10×5 cm², matrix size = 512×256 and slice thickness of 1 mm with a 0.1 mm gap between slices.

In order to quantify fat volume, bright pixels with signal intensity above 30% of the maximum intensity, were considered to correspond to abdominal and/or subcutaneous fat and were computed in all mouse slices. Total mouse fat pixels were then multiplied by its corresponding pixel volume to obtain the whole body fat volume for each mouse.

Whole Body Fat fraction magnetic resonance spectroscopy (MRS) measurements were performed using a pulse-acquisition sequence (number of points (NP) = 4096, spectral width (SW) = 9014 Hz). Spectra were calibrated to water signal (4.7 ppm) and the area under the fat (FP, at 1.3 and 0.95 ppm) and water (WP at 4.7 ppm) peaks was quantified in fixed frequency intervals (lipids: 0.5 – 1.8 ppm, water: 3.1 – 6.2 ppm). Fat fraction (FF) was estimated for each mouse from the fat-to-water peak ratios according to $FF = FP / (FP + WP)$ [321].

Fat content in liver tissue was quantified by localized 1H-NMR spectroscopy using a point resolved spectroscopy (PRESS) sequence. Non-water-suppressed spectra were obtained from a 3 x 3 x 3 mm³ voxel localized within the liver (TE = 12 ms, TR = 5s, number of scans = 16, NP = 4096, SW = 4006 Hz). Liver spectra were processed as described above.

3.5.5 Palmitate β -oxidation measurement in isolated mitochondria

Principle

The conversion of acid-insoluble [¹⁴C]palmitoyl-CoA to acid soluble [¹⁴C]acetyl-CoA was measured in isolated mitochondria as described [322]. This analysis was made at Núria Roglans' lab.

Reagents

[1-¹⁴C]palmitoyl-CoA, 60 Ci/mol, 20 μCi/mL

Perchloric acid, 6 g/100 mL

Procedure

This assay method may be applied to mitochondria by omitting triton X-100 and including final concentrations of 0.25 M sucrose and 1 mM carnitine in the assay, and using freshly isolated organelles diluted with 0.25 M sucrose.

1. BAT biopsies (100-150 mg) were extracted and homogenized in 1 mL of buffer containing 0.25 M sucrose; 50 mM KH₂PO₄, pH 7.4; 150 mM NaCl; 30 mM EDTA; 1 mM dithiothreitol, on ice using a potter. Homogenates were next centrifuged at 700 g at 4°C for 10 min.

2. Enough volume of ice-cold mixture of reagents was prepared for analysis. The amount of each component per an individual assay was: 472 μL of Tris-HCL buffer, 50 mM, pH 8.0; 5 μL of NAD, 20 mM; 1.5 μL of dithiothreitol, 0.33 M; 2.5 μL of bovine serum albumin (fraction V), 1.5 g/100mL; 2.5 μL of Triton X-100, 2 g/100mL; 5 μL of CoA, 10 mM; 5 μL of FAD, 1 mM; 1 μL of unlabeled palmitoyl-CoA, 5 mM; 0.5 μL of [1-¹⁴C]palmitoyl-CoA [322].

3. Duplicated 100-μL aliquots of this mixture were taken for liquid scintillation counting. The measured counts per minute (cpm) were divided by the 1 nmol of total palmitoyl-CoA present in the aliquot to obtain the specific activity, which was generally about 3,400 cpm/nmol.

4. For the assay, aliquots of 495 μL of the reaction mixture were placed in 1.5-mL plastic microcentrifuge (Eppendorf type) tubes in an ice-water bath;

5. 5-μL samples of enzymes were added to the tubes and incubated at 37°C for 10 min.

6. After 11 min of incubation, the tubes were returned to the ice bath and 250 μL of ice-cold perchloric acid was added to each tube.
7. The tubes were then vortexed, left on ice for 1 h, and spun for 2 min in a microcentrifuge.
8. The radioactivity in 500 μL of the supernatant was determined by liquid scintillation counting. Two control tubes without enzyme source were similarly treated to determine the acid-soluble radioactivity present in the substrate. This typically represented less than 5% of the total cpm.
9. For calculation, the mean cpm in the control tubes were subtracted from the acid-soluble fraction of each sample. The difference was multiplied by 1.5 (to correct to the total supernatant volume), divided by the specific activity and by 10 min.
10. The resulting rate was expressed as nanomols of palmitoyl-CoA per min that had undergone at least one cycle of β -oxidation per mg of tissue.

▶ 3.6 *In vitro* studies

3.6.1 NAM-mediated prevention of lipopolysaccharide(LPS)-induced inflammation

Principle

Mouse macrophages J774A.1 stimulated with lipopolysaccharide (LPS) (from *E.coli* O111:B4; ref. L-4391-1MG, Sigma Aldrich) were incubated with different concentrations of NAM to test its potential possible anti-inflammatory activity. Anti-inflammatory activity was revealed by analyzing the relative mRNA levels of *Tnfa* in cell extracts by real time RT-qPCR.

Procedure

1. J774A.1 macrophages (ATCC® TIB-67™) were cultured in 6-well flat-bottom cell culture plates at 1×10^6 cells/well in growth medium containing RPMI 1640 medium supplemented with 2 mM glutamine, 100 U/L of penicillin, 100 μ L of streptomycin, 5% fetal bovine serum at 37°C in an atmosphere of 5% CO₂.
2. Cultured macrophages were stimulated with 100 ng/mL of LPS for 24h.
3. After 24h, the medium was removed, and fresh growth medium was added in the absence (untreated) or presence of different final concentrations of NAM, ranging from 1-10 mM, for 24 h. In each assay, each experimental condition was assayed in duplicate.
4. After 24 h of exposition culture the cells and supernatants were collected and frozen at -80°C until use.
5. Cells were processed for mRNA extraction to pursue gene expression analysis by real time qPCR. This experiment was repeated up to 5 times.

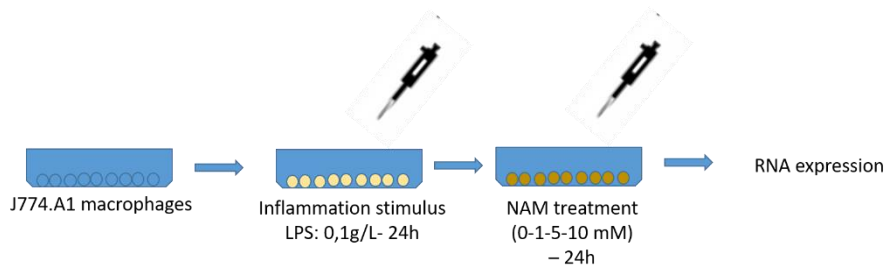


Figure 18. Effect of NAM on the production of TNF α by LPS-stimulated macrophages.

Cells stimulated with LPS (100 ng/ml) were exposed to NAM in the culture medium for 24 h and then the content of TNF α in the medium was measured by real time qPCR.

► 3.7 Statistical analysis

The data are presented as means \pm SEM. Statistical analyses were performed using GraphPad Prism software (GPAD, version 5.0, San Diego, CA, USA). The effects of NAM or NA administration on gross and plasma and tissue chemical parameters, histological traits, kinetic studies, or gene expression levels were determined using either a nonparametric Kruskal-Wallis test followed by the Dunn multiple comparison test or a parametric one-way ANOVA followed by the Newman-Keuls multiple comparison test, as appropriate. The relationships between hepatic gene expression and hepatic triglyceride levels or between weight gain and food intake were determined by calculating Pearson's correlation coefficients. Differences between groups were considered statistically significant when the P value was <0.05 .

• 4. RESULTS

4.1 Evaluating vitamin B₃ forms tolerance

4.1.1 Choosing the best dose

On a pilot experiment we first sought to determine the impact of vitamin B₃ forms in a range between 0.1% to 1.0%, on different gross parameters, including body and liver weight (Figure 19) in non-obese mice fed a regular diet.

At increasingly higher doses, both NAM and NA were well dissolved in drinking water and well tolerated by mice, as revealed by no appreciable changes in water consumption among groups (average of 4 mice/cage; untreated: 2.50 mL/day, NAM 0.1%: 2.75 mL/day, NAM 0.5%: 2.70 mL/day, NAM 1.0%: 3.00 mL/day, NA 0.1%: 3.00 mL/day, NA 0.5%: 2.75 mL/day, NA 1.0%: 3.00 mL/day).

The average intake of NAM and NA, through drinking water at 1.0% concentration, was approximately 0.8 g/kg/day.

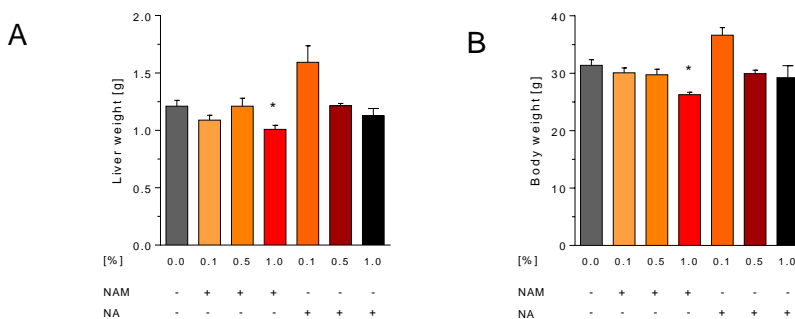


Figure 19. Effect of vitamin B₃ forms on body and liver weight.

(A) Body weight and (B) liver weight of 3 month-old mice, treated with NAM-NA for 1 month (n = 8 mice per group). Data are expressed as the mean \pm SD. Differences between the mean values were assessed by the nonparametric a Kruskal Wallis followed by Dunn's posttest or ANOVA followed a Newman-Keuls posttest, as appropriate. *Indicates statistical significance between untreated and treated mice. Specifically, *P<0.05 vs. untreated group. Abbreviations used: NAM, nicotinamide; NA, nicotinic acid.

The impact of each vitamin B₃ form on body weight of mice in the range of doses below 1.0% was rather negligible. However, body weight was significantly reduced at the maximal dose of NAM (1.0%) (Figure 19). In contrast, NA administration did not produce any changes in weight prevention.

Interestingly, the food intake in mice treated with either NAM or NA determined at the maximal dose (Untreated: 3.69 g (0.27); NAM 1%: 3.92 g (0.41); NA 1%: 3.78 g (0.38)) did not differ from that of untreated mice.

Liver weight changes paralleled those of body weight (Figure 19). The liver weight reduction observed in NAM treated mice was proportional to that of body weight. Of note, the liver-to-body ratio did not differ among groups (all groups displayed a close to 0.04 ratio) thereby suggesting absence of hepatic dysfunction in vitamin B₃ forms-treated mice. Consistently with this view, there was a significant reduction (-9.8%, P<0.05) in the plasma AST levels in mice treated with NAM 1.0%. Conversely, the administration of NA at 1.0% resulted in a significant increase (1.7-fold, P<0.05) in plasma ALT levels as compared to untreated mice (Table 5).

	Untreated	NAM 0.1%	NAM 0.5%	NAM 1.0%	NA 0.1%	NA 0.5%	NA 1.0%	P
AST [U/L]	89.83 (7.87)	93.00 (2.65)	88.29 (5.09)	81.13 (9.75)*	89.63 (7.01)	83.17 (7.94)	88.38 (15.04)	<0.05
ALT [U/L]	23.60 (11.65)	26.67 (5.78)	27.14 (8.99)	27.93 (14.9)	27.63 (7.44)	28.00 (6.32)	39.17 (12.06)*	<0.05

Table 5. . Effect of vitamin B3 forms on hepatic transaminases in mice fed a RD.

Results are expressed as the means (standard deviation) (n=8 mice per group). All analyses were made at 3 month-old mice, treated with NAM-NA for the last month. The biochemical measurement was made by commercial kits adapted to a COBAS auto analyzer. Differences between the mean values were assessed by the nonparametric a Kruskal Wallis followed by Dunn's posttest or ANOVA followed a Newman-Keuls posttest, as appropriate; differences were considered significant when P<0.05. Specifically, *P<0.05 vs. untreated group. Abbreviations used: FFA, free fatty acids; NAM, nicotinamide; NA, nicotinic acid

The intake of either NAM or NA did not influence the plasma levels of glucose and main circulating lipids (i.e., cholesterol, free fatty acids, and triglycerides) under fasting conditions at 1 mo. of the beginning of administration (Table 6). In contrast, only the administration of the highest dose (1.0%) of NA produced a raise in plasma levels of glucose. Moreover, a significant reduction in the plasma levels of total cholesterol was found at the two highest doses of NA assayed as compared with untreated mice, which would be consistent with its lipid-lowering effects [323].

	Glucose [mg/dL]	Triglycerides [mM]	FFA [mM]	Total cholesterol [mM]
Untreated	122.30 (25.70)	0.68 (0.23)	1.27 (0.20)	3.26 (0.50)
NAM 0.1	104.80 (15.41)	0.61 (0.27)	1.34 (0.17)	3.36 (0.25)
NAM 0.5	122.80 (22.53)	0.94 (0.31)	1.23 (0.08)	3.26 (0.38)
NAM 1.0	115.1 (19.79)	0.75 (0.14)	1.15 (0.17)	3.60 (0.35)
NA 0.1	140.1 (28.39)	0.87 (0.08)	1.50 (0.11)	3.67 (0.35)
NA 0.5	97.14 (14.19)	0.59 (0.11)	1.12 (0.21)	2.78 (0.37)*
NA 1.0	159.3 (22.70)*	0.78 (0.11)	1.46 (0.37)	2.51 (0.13)*
p	<0.001	0.15	0.78	<0.001

Table 6. Effect of vitamin B3 forms on plasma biochemical parameters in mice fed a RD. Results are expressed as the means (SD) (n=4-6 mice per group). All analyses were made at 3 month-old mice, treated with NAM-NA for 1 month. The biochemical measurement was made by commercial kits adapted to a COBAS auto analyzer. Differences between the mean values were assessed by the nonparametric a Kruskal Wallis followed by Dunn's posttest or ANOVA followed a Newman-Keuls posttest, as appropriate; differences were considered significant when P<0.05. Specifically, *P<0.05 vs. untreated group. Abbreviations used: FFA, free fatty acids; NAM, nicotinamide; NA, nicotinic acid

The effect of NAM was also tested at doses higher than 1.0% (Table 7). In these cases, water consumption by mice was significantly decreased (NAM 2.5%: 35%, $P<0.05$; NAM 5.0%: 34%, $P<0.05$) suggesting that concentrations higher than 1.0% NAM affected palatability (Table 7). Importantly, food intake was significantly lower (22%, $P<0.05$) in the mice receiving the maximal dose assayed of NAM (i.e. 5.0%). In both higher doses (2.5-5.0%) a dose-dependent weight loss was observed (Figure 20). The body weight gain of mice receiving NAM 2.5% and 5.0% was significantly reduced (NAM 2.5%: -0.5g, $P<0.05$; NAM 5.0%: -2.0g, $P<0.05$) vs. initial weight compared with untreated mice (untreated: +3.25g). Also, plasma levels of creatinine was elevated (~30%, $P<0.05$) in the mice group receiving NAM 5.0% compared with untreated mice (Table 7). Due to affected palatability and non-physiological results, the higher doses test was aborted before planning, at 2 months of treatment.

	Untreated	NAM 2.5%	NAM 5.0%	p
<i>Gross parameters</i>				
Diet intake [g/day]	3.76 (0.33)	3.55 (0.37)	2.96 (0.61)*	<0.001
Water intake [g/day]	4.08 (0.57)	2.67 (0.55)*	2.70 (1.93)*	<0.05
<i>Plasma biochemistry</i>				
Glucose [mM]	11.70 (0.80)	10.15 (2.46)	13.62 (2.07)	0.41
Creatinine [μ M]	25.24 (1.53)	27.38 (3.11)	32.07 (4.17)*	<0.05
AST [U/L]	64.60 (4.88)	83.75 (33.73)	70.00 (22.63)	0.18
ALT [U/L]	24.40 (4.72)	40.50 (54.59)	26.00 (12.66)	0.66

Table 7. Effect of vitamin B3 forms on plasma biochemical parameters in mice fed a RD.

Mice were 4 month-old treated with different doses of NAM for 2 consecutive months. Results are expressed as the means (standard deviation) ($n=4-5$ mice per group). All analyses were made at four months of age. The biochemical measurement was made by commercial kits adapted to a COBAS auto analyzer. Differences between the mean values were assessed by the nonparametric a Kruskal Wallis followed by Dunn's posttest or ANOVA followed a Newman-Keuls posttest, as appropriate; differences were considered significant when $P<0.05$. Specifically,

*P<0.05 vs. untreated group. Abbreviations used: NAM, nicotinamide; AST, Aspartate aminotransferase; ALT, Alanine aminotransferase

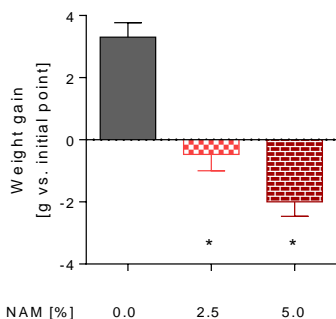


Figure 20. Effect of vitamin B3 forms on body weight gain.

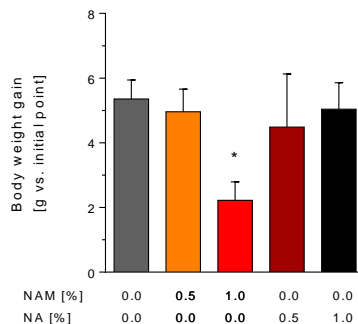
Body weight of 4 month-old mice, treated with NAM for 2 consecutive months. (n = 4-5 mice per group). Differences between the mean values were assessed by the nonparametric a Kruskal Wallis followed by Dunn's posttest or ANOVA followed a Newman-Keuls posttest, as appropriate. *Indicates statistical significance between untreated and treated mice. Specifically, *P<0.05 vs. untreated group. Abbreviations used: NAM, nicotinamide.

Based on this data, in following studies we established as 1% the safest dose of both vitamin B₃ forms and assessed their effect on gross parameters and plasma biochemistry.

Interestingly, the prevention in the body weight gain observed at 1% NAM dose shown at short-term (i.e., 1 mo.) (Figure 19), was maintained in a long-term analysis (i.e., 3 mo.) (Figure 21).

Figure 21. Effect of vitamin B3 forms on body weight gain.

Body weight of 5 month-old mice, treated with NAM-NA for 3 consecutive months (n = 4-6 mice per group). Differences between the mean values were assessed by the nonparametric a Kruskal Wallis followed by Dunn's posttest or ANOVA followed a Newman-Keuls posttest, as appropriate.*Indicates statistical significance between untreated and treated mice. Specifically, *P<0.05 vs. untreated group. Abbreviations used: NAM, nicotinamide; NA, nicotinic acid.



► 4.2 Impact of vitamin B₃ forms on body weight and adiposity in non-obese mice fed a regular diet (RD)

After determining the safe dose to use, we first aim to validate preliminary results, replicating the previous pilots experiment in order to analyze the effects on body weight of vitamin B₃ forms administration in non-obese mice fed a RD. The next 8 figures and 5 tables, indicate the results obtained in this first set of experiments.

4.2.1 Gross parameters and systemic phenotype

At 2 month-old of age, mice were challenged to treatment with either NAM or NA, and body weight was followed up for 3 consecutive months after the beginning of treatments. As observed in Figure 22 and Table 8, NAM supplementation significantly reduced body weight gain in mice.

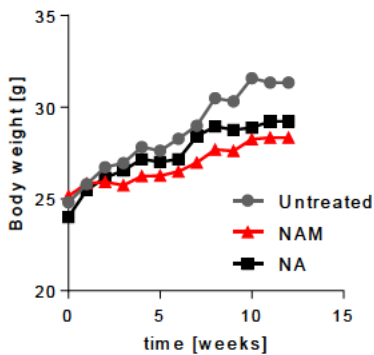


Figure 22. Body weight follow-up in mice fed a RD. Body weight of 5 month-old mice, treated with NAM-NA for 3 consecutive months. (n= 8 mice per group). Abbreviations used: NAM, nicotinamide; NA, nicotinic acid.

	Untreated	NAM	NA	p
<i>Gross parameters</i>				
Final body weight [g]	29.58 (1.54)	26.70 (1.45)*	27.88 (1.51)	<0.05
Body weight gain [g]	4.76 (1.55)	1.45 (1.49) *	3.86 (1.61) †	<0.05
Fat Pad [g]	1.73 (0.25)	1.11 (0.19)*	1.24 (0.22)*	<0.001
Lean Weight [g]	27.85 (1.43)	25.59 (0.73)*	26.64 (1.36)	<0.05
Liver weight [g]	1.53 (0.14)	1.11 (0.26)*	1.24 (0.14)*	<0.05
Liver-to-body weight ratio	0.05 (0.00)	0.04 (0.00)	0.04 (0.00)*	<0.05
Diet intake [g/day]	3.65 (0.39)	3.61 (0.55)	3.99 (0.80)	0.62
Water intake [g/day]	5.47 (0.59)	6.04 (1.21)	5.72 (2.18)	0.76
Calculated dose [g/kg/day]	-	2.43 (1.27)	2.15 (1.25)	
Calculated feed efficiency [mg per consumed kcal]	164.2 (75.9)	75.7 (41.4)*	137.9 (61.3)	<0.05

Table 8. Effect of vitamin B3 forms on gross parameters in mice fed a RD

Results are expressed as the means (standard deviation) (n=8 mice per group). All analyses were made at 5 month-old mice, treated with NAM-NA for 3 consecutive months. The dose of either NAM or NA effectively consumed by the mice was calculated by considering the amount of water consumption and the concentration of both vitamin B₃ forms in tap water. Food intake was measured at the end of the study as described in the Materials and Methods section. Differences between the mean values were assessed by the nonparametric a Kruskal Wallis followed by Dunn's posttest or ANOVA followed a Newman-Keuls posttest, as appropriate; differences were considered significant when P<0.05. Specifically, * P<0.05 vs. untreated group; or † P<0.05 vs. NAM-treated mice. Abbreviations used: NAM, nicotinamide; NA, nicotinic acid.

As shown in Table 8, the group of mice treated with NAM during 3 months significantly gained 30% less body weight ($P < 0.05$) respect to untreated mice. In contrast, the body weight in NA-treated mice did not differ from the untreated mice and was significantly higher (30%, $p < 0.05$) than that of NAM-treated mice (Table 8).

Reduction in the body weight found in mice receiving NAM were accompanied by a concomitant decrease in their fat pad (NAM: 36%, $P < 0.05$), and to a lesser extent also lean weight (8%, $P < 0.05$).

Intriguingly, although NA treatment did not produce change in total body weight, it did reduce fat (28%, $P < 0.05$) and liver weight (18%, $P < 0.05$) compared with untreated mice.

These findings were not associated with alterations in the pattern of food intake in the mice groups treated with the two vitamin B₃ forms, thus suggesting that a significant portion of ingested calories (kcal) were not eventually being accumulated as fat in NAM-treated mice. Feed efficiency (body weight change per kcal of food eaten) was determined before body weights diverged, in order to eliminate confounding measures by body weight differences. Our data revealed that feed efficiency was reduced around 50% in NAM-treated mice (Table 8) compared with untreated mice. No differences were observed in feed efficiency between NA-treated mice and untreated mice.

Consistently with our previous studies, no changes in water consumption were observed in the mice groups receiving either NAM or NA.

Plasma levels of leptin were significantly reduced in NAM-treated mice and were close-to-significance in NA-treated mice (NAM: 70%, $p < 0.05$; NA: 68%, $p = 0.05$)

(Table 9). Leptin concentration only showed a trend to be correlated with total body weight (Pearson $r = 0.3572$, $P = 0.14$) (Figure 23, panel A) but correlated directly with adiposity (Pearson $r = 0.7283$, $P < 0.05$) (Figure 23, panel B). Plasma levels of adiponectin were elevated in NAM-treated mice (60%, $p < 0.05$) (Table 9) compared with untreated mice, whereas no differences were found in NA-treated mice compared with untreated mice. Adiponectin concentration inversely correlated significantly with body weight (Pearson $r = -0.5400$, $P < 0.05$) and adiposity (Pearson $r = -0.5051$, $P < 0.05$) (Figure 23, panel C and D).

Some authors, have discussed the importance of adiponectin:leptin ratio as a marker of dysfunctional adipose tissue [324] as it is reported to be decreased in obese subjects. Our results showed a significant increase (3-fold, $P < 0.05$) of this ratio in NAM-treated mice compared with untreated mice. However, no significant changes were found in the case of NA-treated mice compared with untreated mice.

	Untreated	NAM	NA	p
Leptin [ng/mL]	14256 (8742)	4108 (1774)*	4588 (1974)	<0.05
Adiponectin [ng/mL]	59.70 (10.14)	98.40 (36.87)*	67.52 (13.13)	<0.05
Ratio adiponectin: leptin	0.00 (0.00)	0.03 (0.01)*	0.02 (0.00)	<0.05

Table 9. Effect of vitamin B3 forms on critical hormones involved in adiposity in mice fed a RD.

Results are expressed as the means (standard deviation) (n=8 mice per group). All analyses were made at 5 month-old mice, treated with NAM-NA for 3 consecutive months. Food intake was measured at the end of the study as described in the Materials and Methods section. Differences between the mean values were assessed by the nonparametric a Kruskal Wallis followed by Dunn's posttest or ANOVA followed a Newman-Keuls posttest, as appropriate; differences were considered significant when $P < 0.05$. Specifically, * $P < 0.05$ vs. untreated group; or † $P < 0.05$ vs. NAM-treated mice. Abbreviations used: NAM, nicotinamide; NA, nicotinic acid.

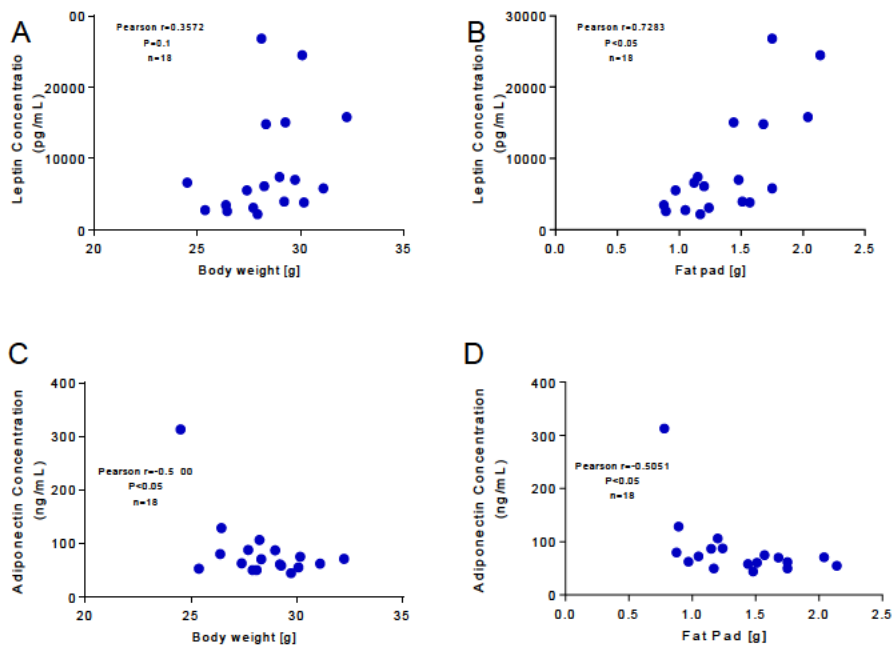


Figure 23. Relation between body weight and adiposity with adipokines related with obesity.

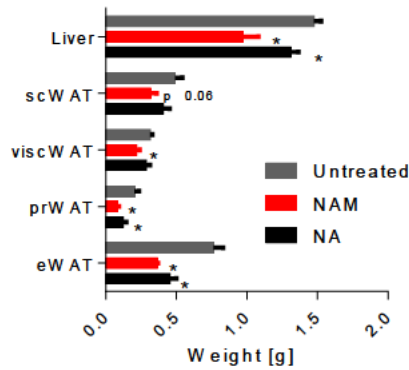
Direct correlation between leptin concentration and (A) body weight, (B) fat pad. Inverse correlation between adiponectin concentration and (C) body weight and (D) fat pad. Body weight and fat pads of 5 month-old mice, treated with NAM-NA for 3 consecutive months. (n = 6 mice per group). A parametric Pearson test was used to analyze whether these parameters were correlated.

In order to dissect the magnitude of changes produced by the treatment of mice with either NAM or NA, we analyzed body and tissue weights, including the liver and regional fat pads, in all groups of mice at necropsy (Figure 24). Our data revealed a significant reduction in different regional fat pads.

Visceral WAT (viscWAT), epididymal WAT (eWAT), perirenal WAT (prWAT) are significantly decreased in NAM-treated mice compared with untreated mice, whereas subcutaneous WAT (scWAT) just show a close-to-significant trend to be diminished. On the other hand, the treatment with NA led to significant changes only in prWAT and eWAT (Figure 24)

Figure 24. Effect of vitamin B3 forms on gross parameters in mice fed a RD.

Tissue weight of 5 month-old mice, treated with NAM-NA for 3 consecutive months (n= 8 mice per group). *Indicates statistical significance between untreated and treated mice. Specifically, *P<0.05 vs. untreated group. Abbreviations used: eWAT, epididymal white adipose tissue; prWAT, peri-renal white adipose tissue; viscWAT, visceral white adipose tissue; scWAT, subcutaneous white adipose tissue; NAM, nicotinamide; NA, nicotinic acid.



There was a direct correlation between fat pad and body weight (Pearson r= 0.8311, p<0.05) (Figure 25).

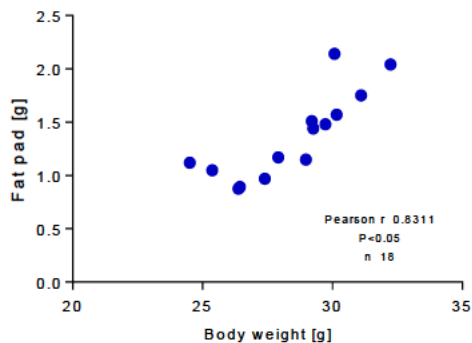


Figure 25. Relationship between total body and fat pad weights.

Total body were correlated with fat pad weights. Mice were 5 month-old and treated with NAM for 3 consecutive months. A parametric Pearson test was used to analyze whether these parameters were correlated.

Histological sections of eWAT and scWAT (Figure 26) revealed no apparent differences among experimental groups.

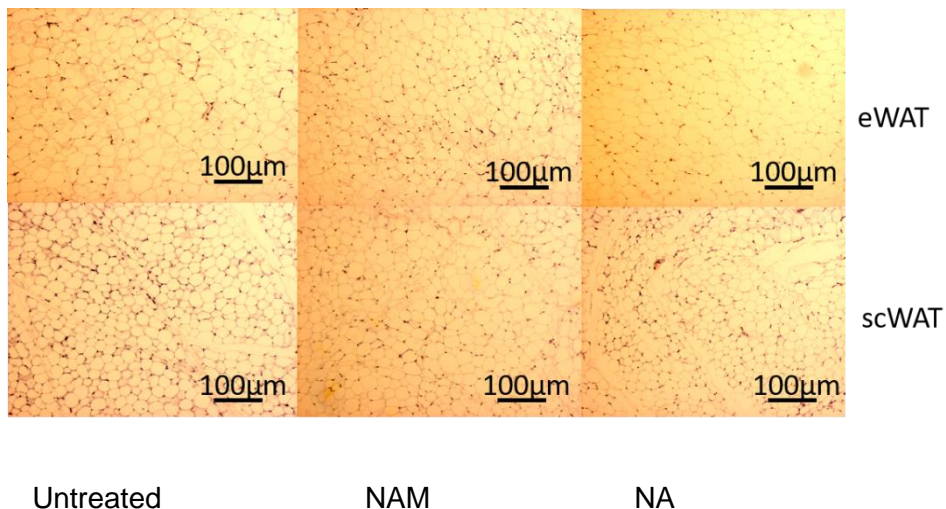


Figure 26. Effect of vitamin B3 forms on fat cell size from eWAT and scWAT in mice fed a RD.

Histological sections of epididymal and subcutaneous WAT stained with hematoxylin/ eosin from mice fed a RD \pm NAM at 5 month-old mice, treated with NAM-NA for 3 consecutive months. Abbreviations used: NAM, nicotinamide; NA, nicotinic acid; eWAT, epididymal white adipose tissue; scWAT, subcutaneous white adipose tissue.

4.2.1a Biochemical parameters

Plasmatic biochemistry was also evaluated in these same set of animals, indicating that even though cholesterol levels did not differ among groups, triglycerides and FFA were significantly lower in NAM-treated mice compared with untreated mice (Table 10). Interestingly, plasma FFA were directly related to body weight (Spearman $r = 0.8000$, $P < 0.05$) and adiposity (Spearman $r = 0.8500$, $P < 0.05$) (Figure 27). In contrast, plasma levels of FFA remained unchanged in NA-treated mice compared with untreated mice, even though plasma triglycerides were also significantly lower compared with untreated mice. Although, cholesterol levels in plasma did not differ among groups, HDL cholesterol were significantly lower (30%, $P < 0.05$) in mice receiving NA compared with untreated mice.

	Untreated	NAM	NA	P
Triglycerides [mM]	0.81 (1.19)	0.54 (0.17)*	0.48 (0.17)*	<0.05
FFA [mM]	1.46 (0.15)	1.14 (0.15)*	1.32 (0.20)	<0.05
Total cholesterol [mM]	3.46 (0.50)	2.91 (0.91)	2.74 (0.38)	0.07
HDL cholesterol [mM]	3.00 (0.35)	2.44 (0.82)	2.09 (0.35)*	<0.05
Non-HDL cholesterol [mM]	0.55 (0.20)	0.47 (0.13)	0.66 (0.23)	0.27

Table 10. Effect of vitamin B3 forms on plasma biochemical parameters in mice fed a RD. Results are expressed as the means (standard deviation) (n=8 mice per group). All analyses were made at 5 month-old mice, treated with NAM-NA for 3 consecutive months. Fasting plasma levels of the HDL fractions were determined in the plasma supernatants after precipitating with phosphotungstic acid (Roche); the non-HDL fraction was calculated by subtracting the HDL moiety to the total plasma. The biochemical measurement was made by commercial kits adapted to a COBAS autoanalyzer. Differences between the mean values were assessed by the nonparametric a Kruskal Wallis followed by Dunn's posttest or ANOVA followed a Newman-Keuls posttest, as appropriate; differences were considered significant when $P < 0.05$. Specifically, * $P < 0.05$ vs. untreated group; or † $P < 0.05$ vs. NAM-treated mice. Abbreviations used: FFA, free fatty acids; HDL, high-density lipoprotein; NAM, nicotinamide; NA, nicotinic acid

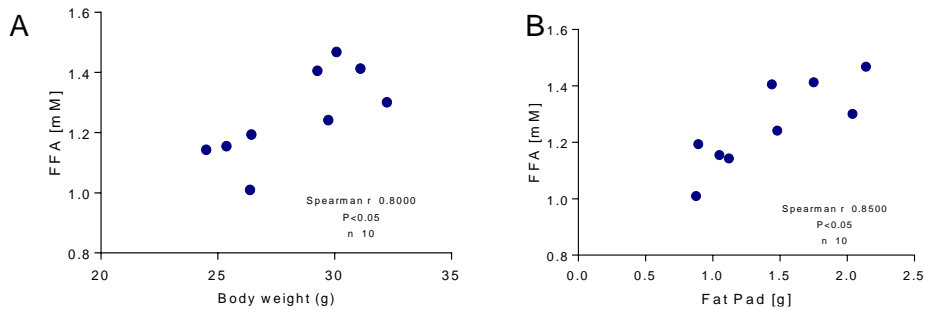


Figure 27. Relationship between total body and fat pad weights and plasma levels of FFA. Total body and fat pad weights were correlated with circulating FFA. Only mice treated with NAM and untreated were considered. Mice were 5 month-old mice, treated with NAM-NA for 3 consecutive months. A non-parametric Spearman test was used to analyze whether these parameters were correlated. Abbreviations used: FFA, fatty acids.

Both renal and hepatic parameters shown in Table 11 did not differ among groups, suggesting that none of the treatments caused clear hepatic or renal damage.

Fecal analysis showed no changes in fat (triglycerides) release in NAM- treated mice (Untreated: 0.73 (0.24) $\mu\text{mol/g}$, NAM: 0.86 (0.44) $\mu\text{mol/g}$, NA: 0.54 (0.09) $\mu\text{mol/g}$), thereby suggesting that triglyceride from food was not differentially drained into feces in treated mice.

	Untreated	NAM	NA	P
Creatinine [μM]	23.48 (1.67)	22.26 (2.03)	24.46 (2.83)	0.22
AST [U/L]	85.50 (26.02)	126.00 (44.81)	176.5 (12.80)	0.13
ALT [U/L]	20.00 (6.46)	27.14 (17.46)	35.88 (32.65)	0.36
Triglycerides [$\mu\text{mol/g}$ liver]	1.30 (1.81)	1.81 (1.69)	0.77 (0.56)	0.17

Table 11. . Effect of vitamin B3 forms on hepatic and renal parameters in mice fed a RD.

Results are expressed as the means (standard deviation) (n=8 mice per group). All analyses were made at 5 month-old mice, treated with NAM-NA for 3 consecutive months. The biochemical measurement was made from lipid extracts by commercial kits adapted to a COBAS auto analyzer. The data is expressed in relation to g of liver and feces. Differences between the mean values were assessed by the nonparametric a Kruskal Wallis followed by Dunn's posttest or ANOVA followed a Newman-Keuls posttest, as appropriate; differences were considered significant when $P < 0.05$. Specifically, * $P < 0.05$ vs. untreated group; or † $P < 0.05$ vs. NAM-treated mice. Abbreviations used: AST, Aspartate aminotransferase; ALT, Alanine aminotransferase; BUN, blood urea nitrogen; NAM, nicotinamide; NA, nicotinic acid.

4.2.1b Glucose homeostasis

Plasma biochemical analyses did not reveal changes in basal levels of glucose and insulin (Table 12).

	Untreated	NAM	NA	p
Glucose [mM]	10.34 (3.14)	10.86 (2.45)	11.49 (1.39)	0.64
Insulin [$\mu\text{g/L}$]	1.69 (0.36)	1.21 (0.12)	1.22 (0.25)	0.11

Table 12. Effect of vitamin B3 forms on glucose homeostasis in mice fed a RD.

Results are expressed as the means (SD) (n=8 mice per group). All analyses were made at 5 month-old mice, treated with NAM-NA for 3 consecutive months. The biochemical measurement was made by commercial kits adapted to a COBAS autoanalyzer. Differences between the mean values were assessed by the nonparametric a Kruskal Wallis followed by Dunn's posttest or ANOVA followed a Newman-Keuls posttest, as appropriate; differences were considered significant when $P < 0.05$. Specifically, * $P < 0.05$ vs. untreated group; or † $P < 0.05$ vs. NAM-treated mice. Abbreviations used: NAM, nicotinamide; NA, nicotinic acid

To assess if glucose homeostasis was altered in treated mice compared with untreated, we also performed a GTT on 5 month-old mice (a week before the end of the 3rd month of treatments). As shown in Figure 28, the vitamin B₃ forms-treated mice groups cleared blood glucose to the same extent as the untreated group, suggesting that peripheral glucose disposal was not altered by treatments with different vitamin B₃ forms.

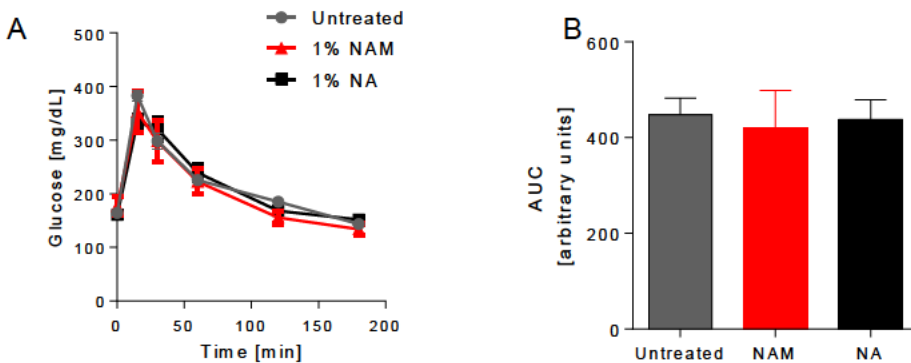


Figure 28. Functional analysis of glucose metabolism in mice on a RD: GTT.

(A) GTT was performed on 5-h fasted mice. Blood glucose levels were measured at 0, 15, 30, 60, 120 and 180 min after an intraperitoneal injection (2g/kg). (B) Area under curve of GGT associated curves. (n=8 mice per group). Mice were 5 month-old, and the test was made one week before the 3rd month of HFD and NA-NAM treatment. Differences between the mean values were assessed by the nonparametric a Kruskal Wallis followed by Dunn's posttest or ANOVA followed a Newman-Keuls posttest, as appropriate; differences were considered significant when $P < 0.05$. Specifically, * $P < 0.05$ vs. untreated group; or † $P < 0.05$ vs. NAM-treated mice. Abbreviations used: AUC, Area under the curve; NAM, nicotinamide; NA, nicotinic acid.

Results depicted in Figure 29 demonstrated that supplementation with vitamin B₃ forms, did not produce any effect on the insulin-stimulated glucose uptake, suggesting that insulin sensitivity was not altered in the treated mice as compared with untreated mice.

Taken together, our results rather showed that glucose homeostasis was not altered in mice fed with a RD regardless the treatment with each vitamin B₃ forms.

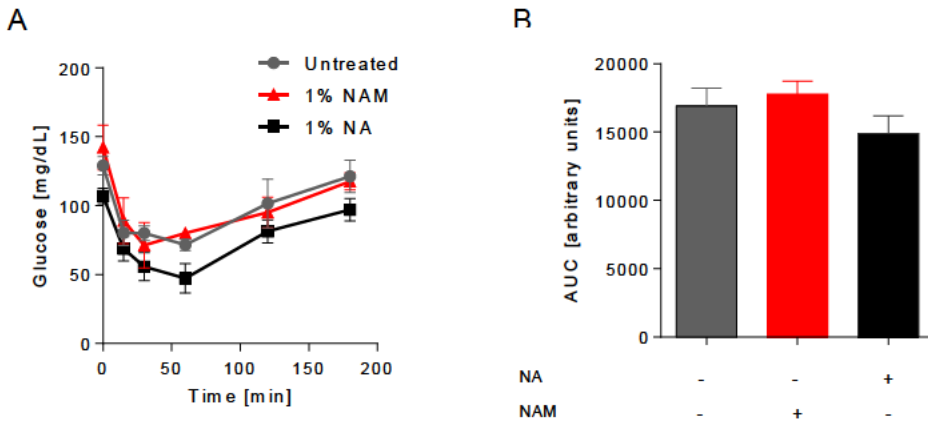


Figure 29. Functional analysis of glucose metabolism in mice on a RD: insulin sensitivity. (A) ITT was performed on 5h- fasted mice. Blood glucose levels were measured at 0, 15, 30, 60, 120 and 180 minutes after an intraperitoneal injection (0.9U/ kg). (B) Area under curve of ITT associated curves. (n=8 mice per group). Mice were 5 month-old, and the test was made one week before the 3rd month of HFD and NA-NAM treatment. Differences between the mean values were assessed by the nonparametric a Kruskal Wallis followed by Dunn's posttest or ANOVA followed a Newman-Keuls posttest, as appropriate; differences were considered significant when $P < 0.05$. Specifically, * $P < 0.05$ vs. untreated group; or † $P < 0.05$ vs. NAM-treated mice. Abbreviations used: NAM, nicotinamide; NA, nicotinic acid.

► 4.3 Impact of vitamin B3 forms on body weight and adiposity in a mouse model of diet-induced obesity (DIO)

Next, we wanted to reproduce the results obtained in non-obese mice, in a model of induced obesity, analyzing the effects on body weight of vitamin B₃ forms administration in DIO mice. The next 8 figures and 5 tables, indicate the results obtained in this second set of experiments.

4.3.1 Gross parameters and systemic phenotype

In a new batch of animals, mice at 2 months of age were challenged to a HFD and initiated the treatment with either NAM or NA, as appropriate, for 3 consecutive months. Consistent with previous data, and compared with untreated mice, only the group of mice treated with NAM prevented weight gain (69%, $P < 0.05$) (Table 13). Similar to our previous observations in treated mice fed a RD, the impact of NAM on body weight change was mainly due to a decrease in fat pad as compared with that of untreated mice. The percentage of fat pad compared to body weight, was significantly decreased in NAM-treated mice compared to untreated mice. There were no changes in NA-treated mice compared to untreated mice (Untreated: ~10%, NAM: ~6.6%, NA: ~8.2%). Notably, the latter was not associated with an alteration in either food or water intake.

As previously described (section 4.2.1), feed efficiency (body weight change per kcal of food eaten) was reduced more than 85% ($P < 0.05$) in NAM-treated mice compared with untreated mice (Table 13).

The liver weight was significantly decreased (20%, $P < 0.05$) in the mice receiving either NAM or NA respect to control mice (Table 13). The liver-to-body weight ratio did not differ between NAM-treated and untreated mice; however it was

significantly reduced in NA-treated mice compared with both NAM-treated and untreated mice.

	Untreated	NAM	NA	P
Final body weight [g]	34.36 (3.83)	27.73 (1.91)*	31.59 (2.48)†	<0.05
Body weight gain [g]	11.10 (3.34)	3.55 (2.00)*	6.31 (1.80)*†	<0.05
Fat Pad [g]	3.46 (1.23)	1.84 (1.01)*	2.58 (1.00)	<0.05
Lean weight [g]	30.23 (2.70)	26.58 (1.47)*	28.48 (1.63)	<0.05
Liver weight [g]	1.70 (0.21)	1.42 (0.13)*	1.41 (0.21)*	<0.05
Liver-to-body weight ratio	0.05 (0.00)	0.05 (0.00)	0.04 (0.00)*†	<0.05
Diet intake [g/day]	2.52 (0.80)	2.80 (0.10)	3.12 (0.46)	0.64
Water intake [g/day]	3.81 (0.69)	4.04 (1.14)	3.25 (1.16)	0.29
Calculated dose [g/kg/day]	-	1.28 (0.33)	1.14 (0.41)	
Calculated feed efficiency [mg per consumed kcal]	210.60 (14.6)	28.80 (1.18)*	181.20 (18.0)†	<0.05

Table 13. Effect of vitamin B3 forms on gross parameters in DIO mice.

Results are expressed as the means (standard deviation) (n=8-12 mice per group). All analyses were made at 5 month-old mice, fed with a HFD and treated with NAM-NA for 3 consecutive months. Food intake was measured at the end of the study as described in the Materials and Methods section. Differences between the mean values were assessed by the nonparametric a Kruskal Wallis followed by Dunn's posttest or ANOVA followed a Newman-Keuls posttest, as appropriate; differences were considered significant when P<0.05. Specifically, * P<0.05 vs. untreated group; or † P<0.05 vs. NAM-treated mice. Abbreviations used: HFD, high-fat diet; NAM, nicotinamide; NA, nicotinic acid.

Fecal excretion of triglycerides did not differ among groups (untreated: 2.46 (0.74) $\mu\text{mol/g}$; NAM: 3.36 (1.14) $\mu\text{mol/g}$; NA: 5.16 (0.98) $\mu\text{mol/g}$) suggesting that the loss of a representative energy substrate did not explain weight gain prevention in the NAM-treated mice.

Consistent with previous data (Table 13), prevention of body weight gain was mainly attributed to changes in the adipose tissue in NAM-treated mice compared with untreated mice (Figure 30, panels A and B). Body and tissue weights, including the liver and regional fat pads (Figure 30, panel B) revealed a reduction (scWAT: 35%, $P=0.06$; eWAT: 52%, $P<0.05$, prWAT: 35%, $P=0.08$, viscWAT: 30%, $P<0.05$) in different regional fat pads only in NAM-treated mice compared with untreated mice. Of note, the liver weight was also found reduced in mice treated with any of the two vitamin B₃ forms (NAM: 16.4%, $P<0.05$; NA: 17%, $P<0.05$).

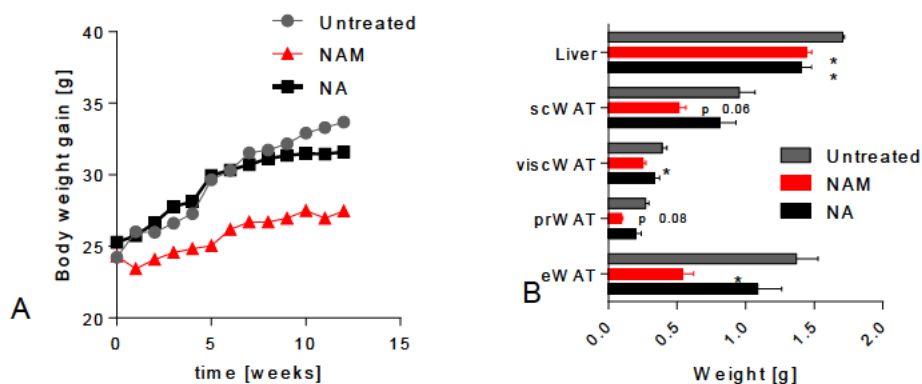


Figure 30. Effect of vitamin B3 forms on DIO mice.

Gross parameters in DIO mice (A) Body weight and (B) tissue weight of 5 month-old mice, fed with a HFD and treated with NAM-NA for 3 consecutive months. (n= 8 mice per group). Differences between the mean values were assessed by the nonparametric a Kruskal Wallis followed by Dunn's posttest or ANOVA followed a Newman-Keuls posttest, as appropriate; differences were considered significant when $P<0.05$. Specifically, * $P<0.05$ vs. untreated group; or † $P<0.05$ vs. NAM-treated mice. Abbreviations used: eWAT, epididymal white adipose tissue; HFD, high-fat diet; prWAT, peri-renal white adipose tissue; viscWAT, visceral white adipose tissue; scWAT, subcutaneous white adipose tissue; NAM, nicotinamide; NA, nicotinic acid.

Plasma levels of leptin were significantly reduced in both NAM and NA-treated mice (Table 14) (NAM: ~80%, $p < 0.05$; NA: 78%, $p < 0.05$). Leptin concentration correlated directly with total body weight (Pearson $r = 0.8265$, $p < 0.05$) (Figure 31, panel A) and adiposity (Pearson $r = 0.8241$, $P < 0.05$) (Figure 31, panel B). Plasma levels of adiponectin were elevated in NAM-treated mice (Table 14) (~40%, $p < 0.05$) compared with untreated mice and with NA-treated mice (25%, $p < 0.05$), whereas no differences were found in NA-treated mice compared with untreated mice. Adiponectin concentration inversely correlated significantly with body weight (Pearson $r = -0.5684$, $P < 0.05$) and adiposity (Pearson $r = -0.6039$, $P < 0.05$) (Figure 31, panel C and D).

In accordance to results found in mice fed with a RD, NAM also displayed a significant increase in adiponectin:leptin ratio compared to untreated mice (Table 14).

	Untreated	NAM	NA	p
Leptin [ng/mL]	30809 (16913)	6448 (5569)*	6540 (4311)*	<0.05
Adiponectin [ng/mL]	75.96 (11.13)	105.4 (15.80)*	78.77 (14.8)†	<0.05
Ratio adiponectin:leptin	0.00 (0.00)	0.03 (0.01)*	0.02 (0.02)	<0.05

Table 14. Effect of vitamin B3 forms on critical hormones involved in adiposity in DIO mice.

Results are expressed as the means (standard deviation) (n=8 mice per group). All analyses were made at 5 month-old mice, fed with a HFD and treated with NAM-NA for 3 consecutive months. Food intake was measured at the end of the study as described in the Materials and Methods section. Differences between the mean values were assessed by the nonparametric a Kruskal Wallis followed by Dunn's posttest or ANOVA followed a Newman-Keuls posttest, as appropriate; differences were considered significant when $P < 0.05$. Specifically, * $P < 0.05$ vs. untreated group; or † $P < 0.05$ vs. NAM-treated mice. Abbreviations used: NAM, nicotinamide; NA, nicotinic acid.

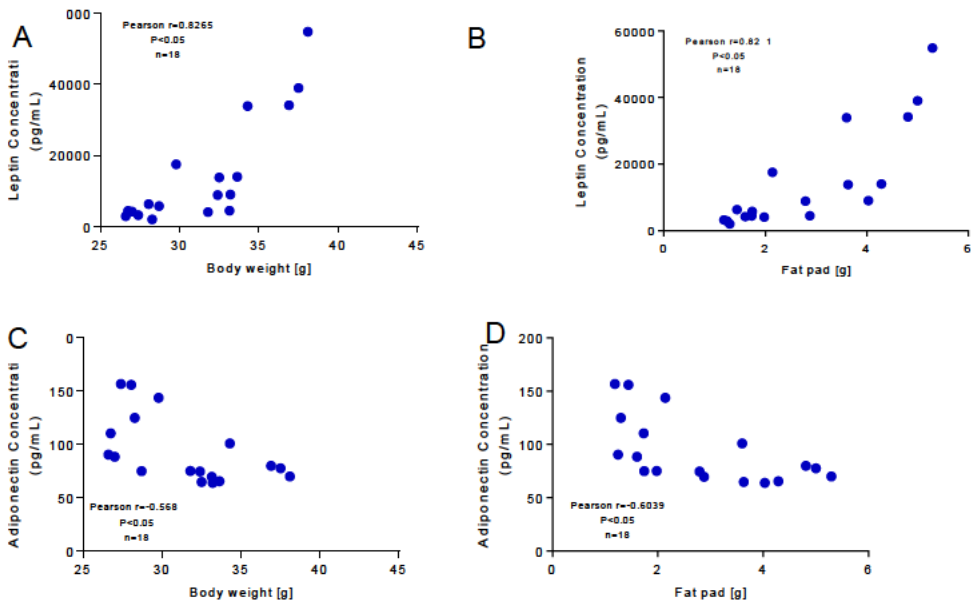


Figure 31. Relation between body weight and adiposity with adipokines involved in obesity in DIO mice.

Direct correlation between leptin concentration and (A) body weight, (B) fat pad. Inverse correlation between adiponectin concentration and (C) body weight and (D) fat pad. Body weight and fat pads of 5 month-old mice, fed with a HFD and treated with NAM-NA for 3 consecutive months. (n = 6 mice per group). A parametric Pearson test was used to analyze whether these parameters were correlated.

Subcutaneous and epididymal fat pads (i.e., scWAT and eWAT) were also histologically examined (Figure 32). Hematoxylin-eosin analysis revealed that the size of adipocytes of eWAT from NAM-treated mice was significantly smaller (adipocytes area (μm^2); Untreated group: 48231 ± 14032 ; NAM group: 19554 ± 6082)(-53%, $P < 0.05$) compared with untreated mice.

Adiposity is frequently associated with chronic inflammation [325]. The gene expression of selected inflammation markers (i.e. *Cd68*, *Ucp2*) were found significantly down-regulated (*Cd68*: 0.4-fold, $P < 0.05$; *Ucp2*: 0.5-fold, $P < 0.05$) in eWAT from NAM-treated mice compared with untreated mice (Figure 33). In contrast, no histological or molecular changes were observed in mice treated with NA in either eWAT or scWAT, as compared with untreated mice.

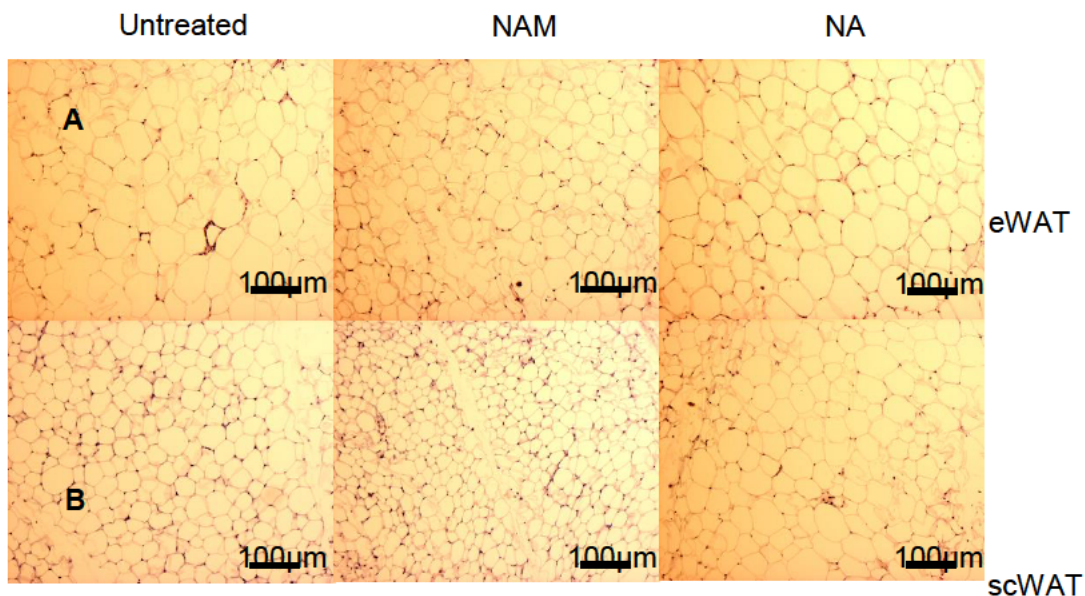


Figure 32. Histological images of epididymal and subcutaneous WAT in DIO mice. Representative histological sections of (A) epididymal WAT and (B) subcutaneous WAT stained with hematoxylin/eosin from 5 month-old mice, fed with a HFD and treated with NAM-NA for 3 consecutive months. Abbreviations used: NAM, nicotinamide; NA, nicotinic acid.

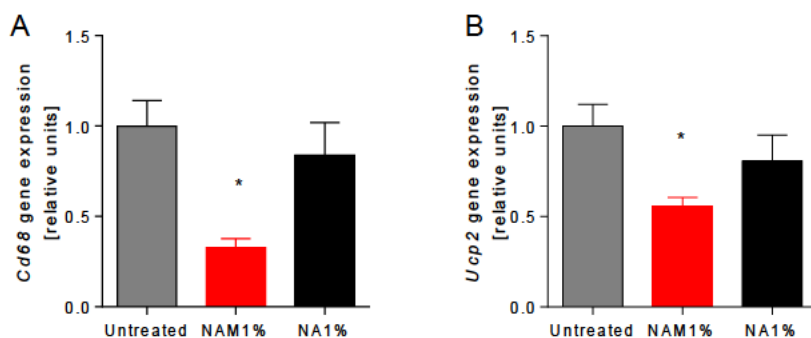


Figure 33. Gene expression of molecular targets involved in inflammatory processes in eWAT in DIO mice.

(A) Down-regulation of *Cd68* in NAM- treated mice. (B) Down-regulation of *Ucp2* in NAM- treated mice. Results are expressed as the means (standard deviation) (n=6-10 mice per group). All analyses were made at 5 month-old mice, fed with a HFD and treated with NAM-NA for 3 consecutive months. Differences between the mean values were assessed by the nonparametric a Kruskal Wallis followed by Dunn's posttest or ANOVA followed a Newman-Keuls posttest, as appropriate; differences were considered significant with $P < 0.05$. Specifically, * $P < 0.05$ vs. untreated group; or † $P < 0.05$ vs. NAM-treated mice. Abbreviations used NAM LD, nicotinamide low dose; NAM HD, nicotinamide high dose.

4.3.1a Biochemical and molecular parameters

Plasma triglycerides did not differ among groups. FFA showed a close-to-significant trend to be diminished in NAM-treated mice compared to untreated mice. Also, plasma levels of cholesterol were significantly lower (18%, $P < 0.05$) in NA-treated mice compared with untreated mice, which was mainly associated with a significant decrease (48%, $P < 0.05$) in the non-HDL fraction and, to a less extent, in the HDL (12%, $P < 0.05$) in these mice (Table 15). There were no changes in the lipid profile of NAM-treated mice respect to untreated mice.

	Untreated	NAM	NA	P
Triglycerides [mM]	0.56 (0.09)	0.52 (0.08)	0.39 (0.04)	0.38
FFA [mM]	1.92 (0.77)	0.66 (0.33)	1.62 (1.19)	0.13
Total cholesterol [mM]	3.85 (0.07)	4.09 (0.16)	3.15 (0.28)* †	<0.05
HDL cholesterol [mM]	3.14 (0.08)	3.27 (0.11)	2.76 (0.22)* †	<0.05
Non HDL cholesterol [mM]	0.73 (0.19)	0.81 (0.20)	0.38 (0.14)†	<0.05

Table 15. Effect of vitamin B3 forms on biochemical parameters in DIO mice.

Results are expressed as the means (standard deviation) (n=8-12 mice per group). All analyses were made at 5 month-old mice, fed with a HFD and treated with NAM-NA for 3 consecutive months. Fasting plasma levels of the HDL fractions were determined in the plasma supernatants after precipitating with phosphotungstic acid (Roche); the non-HDL fraction was calculated by subtracting the HDL moiety to the total plasma. The biochemical measurement was made by commercial kits adapted to a COBAS self-analyzer robot. Differences between the mean values were assessed by the nonparametric a Kruskal Wallis followed by Dunn's posttest or ANOVA followed a Newman-Keuls posttest, as appropriate; differences were considered significant when $P < 0.05$. Specifically, * $P < 0.05$ vs. untreated group; or † $P < 0.05$ vs. NAM-treated mice. Abbreviations used: FFA, free fatty acids; HDL, high-density lipoprotein; HFD, high-fat diet; NAM, nicotinamide; NA, nicotinic acid.

Even though, FFA did not change significantly, it did show a direct correlation with body weight and adiposity (Figure 34, panel A and B).

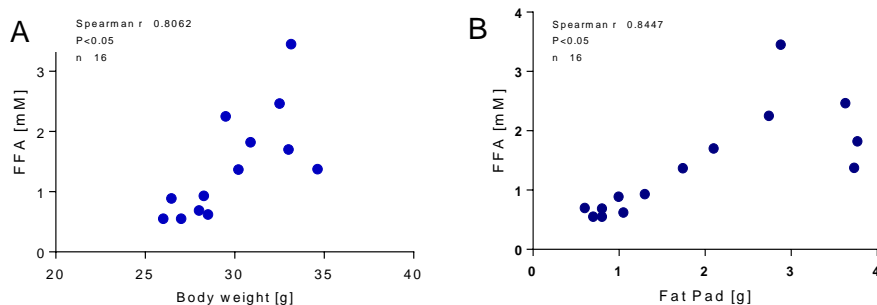


Figure 34. Relationship between total body and fat pad weights and plasma levels of FFA in DIO mice.

Total body and fat pad weights were correlated with circulating FFA. Mice were 5 month-old mice, fed with a HFD and treated with NAM for 3 consecutive months. A non-parametric Spearman test was used to analyze whether these parameters were correlated. Abbreviations used: FFA, free fatty acids.

Mice treated with the different vitamin B₃ forms did not show significant changes in the plasma levels of hepatic and renal-related parameters compared with untreated mice (Table 16). Indeed, plasma levels of hepatic transaminases and hepatic content of triglycerides were similar in all experimental groups. Also creatinine levels did not differ among groups.

	Untreated	NAM	NA	P
Creatinine [μ M]	21.87 (0.38)	20.95 (0.47)	21.43 (0.56)	0.57
AST [U/L]	420 (228)	201 (61)	166 (74)	0.27
ALT [U/L]	68 (43)	32 (7)	32 (8)	0.25
Liver triglycerides [μ mol/g]	5.6 (1.5)	4.1 (2.6)	6.99 (1.9)	0.53

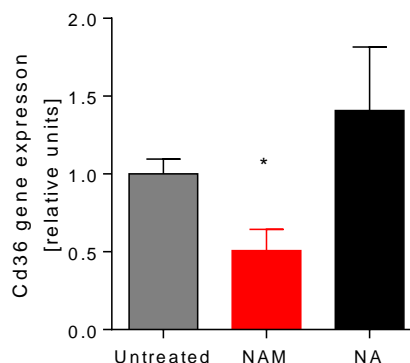
Table 16. . Effect of vitamin B3 forms on hepatic and renal parameters in DIO mice.

Results are expressed as the means (standard deviation) (n=8-12 mice per group). All analyses were made at 5 month-old mice, fed with a HFD and treated with NAM-NA for 3 consecutive months. The biochemical measurement was made from lipid extracts by commercial kits adapted to a COBAS self-analyzer robot. The data is expressed in relation to g of liver and feces. Differences between the mean values were assessed by the nonparametric a Kruskal Wallis followed by Dunn's posttest or ANOVA followed a Newman-Keuls posttest, as appropriate; differences were considered significant when $P < 0.05$. Specifically, * $P < 0.05$ vs. untreated group; or † $P < 0.05$ vs. NAM-treated mice. Abbreviations used: AST, Aspartate aminotransferase; ALT, Alanine aminotransferase; HFD, high-fat diet; NAM, nicotinamide; NA, nicotinic acid.

Hepatic gene expression of Cd36, which is regarded as a marker of obesity-related fatty liver in morbidly obese patients and experimental models of obesity [326] was significantly decreased in NAM-treated mice (50%, $P < 0.05$) compared with that of untreated mice. Of note, the relative expression of this gene was not significantly changed in the livers of NA-treated mice. (Figure 35)

Figure 35. Gene expression of Cd36 in liver in DIO mice.

Results are expressed as the means (standard deviation) (n=6-10 mice per group). All analyses were made at 5 month-old mice, fed with a HFD and treated with NAM-NA for 3 consecutive months. Differences between the mean values were assessed by the nonparametric a Kruskal Wallis followed by Dunn's posttest or ANOVA followed a Newman-Keuls posttest, as appropriate; differences were considered significant when $P < 0.05$. Specifically, * $P < 0.05$ vs. untreated group; or † $P < 0.05$ vs. NAM-treated mice.



4.3.1b Glucose homeostasis

Plasma levels of glucose and insulin did not differ among groups (Table 17).

	Untreated	NAM	NA	P
Glucose [mM]	12.10 (1.19)	15.66 (0.33)	15.01 (1.10)	0.06
Insulin [$\mu\text{g/L}$]	1.63 (0.79)	1.65 (0.73)	1.45 (0.39)	0.75

Table 17. Effect of vitamin B3 forms on glucose homeostasis in DIO mice.

Results are expressed as the means (SD) (n=8 mice per group). All analyses were made at 5 month-old mice, fed with a HFD and treated with NAM-NA for 3 consecutive months. The biochemical measurement was made by commercial kits adapted to a COBAS autoanalyzer. Differences between the mean values were assessed by the nonparametric a Kruskal Wallis followed by Dunn's posttest or ANOVA followed a Newman-Keuls posttest, as appropriate; differences were considered significant when $P < 0.05$. Specifically, * $P < 0.05$ vs. untreated group; or † $P < 0.05$ vs. NAM-treated mice. Abbreviations used: NAM, nicotinamide; NA, nicotinic acid.

Functional analyses of glucose metabolism were also analyzed in these mice (Figures 36 and 37). GTT analysis did not reveal changes in either glucose disposal (Figure 36) or insulin sensitivity (Figure 37) among groups. It was also included the group of untreated mice fed with RD to compare the altered glucose homeostasis expected in mice fed with a HFD.

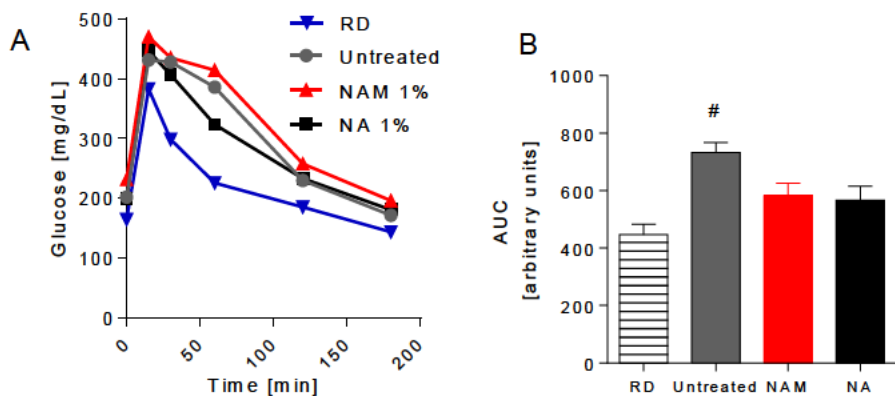


Figure 36. Functional analysis of glucose metabolism in DIO mice: GTT.

(A) GTT was performed on 5h- fasted mice. Blood glucose levels were measured at 0, 15, 30, 60, 120 and 180 minutes after an intraperitoneal injection (2g/kg). (B) Area under curve of GGT associated curves. (n=8 mice per group). Mice were 5 month-old, and the test was made one week before the 3rd month of HFD and NA-NAM treatment. Differences between the mean values were assessed by the nonparametric a Kruskal Wallis followed by Dunn's posttest or ANOVA followed a Newman-Keuls posttest, as appropriate; differences were considered significant when $P < 0.05$. Specifically, * $P < 0.05$ vs. untreated group; † $P < 0.05$ vs. NAM-treated mice; or #† $P < 0.05$ vs. RD group. Abbreviations used: NAM, nicotinamide; NA, nicotinic acid; RD, regular diet.

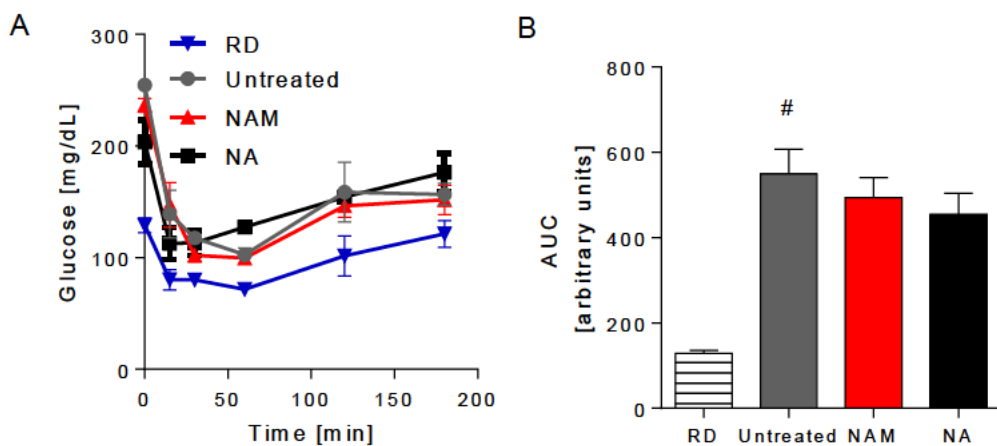


Figure 37. Functional analysis of glucose metabolism in DIO mice: insulin sensitivity.

(A) ITT was performed on 5h- fasted mice. Blood glucose levels were measured at 0, 15, 30, 60, 120 and 180 minutes after an intraperitoneal injection (0.9U/ kg). (B) Area under curve of IST associated curves. (n=8 mice per group). Mice were 5 month-old, and the test was made one week before the 3rd month of HFD and NA-NAM treatment. Differences between the mean values were assessed by the nonparametric a Kruskal Wallis followed by Dunn's posttest or ANOVA followed a Newman-Keuls posttest, as appropriate; differences were considered significant when $P < 0.05$. Specifically, * $P < 0.05$ vs. untreated group; † $P < 0.05$ vs. NAM-treated mice; or #† $P < 0.05$ vs. RD group. Abbreviations used: NAM, nicotinamide; NA, nicotinic acid; RD, regular diet.

▶ 4.4 Impact of different doses of NAM on body weight and adiposity in DIO mice

So far, our results indicated that the weight gain prevention directly associated with less adiposity accumulation, seems specific to NAM treatment. So, this third chapter is focused in the effects of two doses of NAM (and not NA) in the phenotype of DIO mice. This subdivision includes 31 figures and 7 tables.

4.4.1 Gross parameters and systemic phenotype

In this set of experiments, a new batch of mice were treated with different doses of NAM (i.e., NAM high dose, NAM HD: 1%, NAM low dose, NAM LD: 0.25%) (See methods section). Water intake was similar among mice groups (Table 18). The calculated dose of NAM intake was higher in the NAM-HD treated mice (25%, $P < 0.005$) compared with NAM LD-treated mice. As shown in Table 18 and Figure 38- panel A, body weight was significantly reduced (25%, $P < 0.05$) in NAM HD-treated mice compared with untreated mice, mainly as a result of a significant decrease in adiposity (Figure 38, panel B). Of note, the lowest dose of NAM only reached non-significant trends in body weight compared with untreated mice (Table 18). Again, the percentage of fat pad compared to total body weight was significantly reduced in the highest dose of NAM compared to untreated mice (Untreated: ~12%, NAM-LD: ~8%, NAM-HD: ~4%). Interestingly, the mice that received the highest dose of NAM also showed a slight, but significant reduction in the lean weight.

As previously shown (section 4.2.1), the effect of NAM on the body weight and adiposity was not associated with changes in food intake (Table 18).

As previously described (sections 4.1.1 and 4.2.1), feed efficiency (body weight change per kcal of food eaten) showed a significant reduction (more than 85%, $P<0.05$) in NAM HD-treated mice compared with untreated mice (Table 18). Of note, feed efficiency calculations also revealed a significant reduction (30%, $P<0.05$) of NAM LD-treated mice compared with untreated mice (Table 18).

	Untreated	NAM LD	NAM HD	p
Body weight [g]	37.72 (1.39)	31.08 (1.79)	28.42 (1.15)*	<0.0001
Final weight gain [g]	11.40 (2.17)	7.32 (0.75)	3.48 (1.01)*	<0.0001
Fat Pad [g]	4.55 (1.55)	2.55 (0.50)	1.31 (0.19)*	<0.0001
Lean Weight [g]	31.17 (1.26)	28.54 (1.36)	27.11 (1.14)*	<0.05
Liver weight [g]	1.21 (0.26)	1.08 (0.28)	1.06 (0.22)	0.63
Liver-to-body weight ratio	0.03 (0.00)	0.03 (0.00)	0.04 (0.00)	0.78
Diet intake [g/day]	2.74 (0.63)	2.92 (0.22)	2.99 (0.56)	0.64
Water intake [g/day]	4.95 (1.58)	4.17 (0.77)	4.39 (1.26)	0.67
Calculated dose [g/kg/day]	-	0.32 (0.08)	1.40 (0.26)	
Calculated feed efficiency [mg per consumed kcal]	260.40 (24.10)	183.70 (19.80)*	38.2 (12.62)*†	<0.05

Table 18. Effects of different doses of NAM in DIO mice.

Results are expressed as the means (standard deviation) ($n=5-6$ mice per group). All analyses were made at 5 month-old mice, fed with a HFD and treated with NAM for 3 consecutive months. Food intake was measured at the end of the study as described in the Materials and Methods section. Differences between the mean values were assessed by the nonparametric a Kruskal Wallis followed by Dunn's posttest or ANOVA followed a Newman-Keuls posttest, as appropriate; differences were considered significant when $P<0.05$. Specifically, * $P<0.05$ vs. untreated group; or † $P<0.05$ vs. NAM LD-treated mice. Abbreviations used: NAM LD, nicotinamide low dose; NAM HD, nicotinamide high dose.

The effect of NAM administration on body and different tissue weights, including the liver and regional fat pads, was further dissected (Figure 38). Our data showed a significant reduction (scWAT: 74%, $P < 0.05$; eWAT: 75%, $P < 0.05$, prWAT: 72%, $P < 0.05$, viscWAT: 52%, $P < 0.05$) in different regional fat pads only in NAM HD-treated mice respect to untreated. Also, regional fat pads of NAM LD- treated mice showed a significant reduction (prWAT: 52%, $P < 0.05$; viscWAT: 52%, $P < 0.05$) while other fat pads only reached a close-to- significant trend to be reduced (scWAT: 0.54-fold, $P = 0.05$; eWAT, 0.58-fold, $P = 0.05$) in mice treated with lowest dose of NAM as compared with untreated mice (Figure 38, panel B). These data confirmed data from previous serial trials, nevertheless the difference in liver weight was not replicated in this experiment (Figure 38, panel B). However, like in previous ones, the liver-to-body ratio did not differ among groups (Table 18).

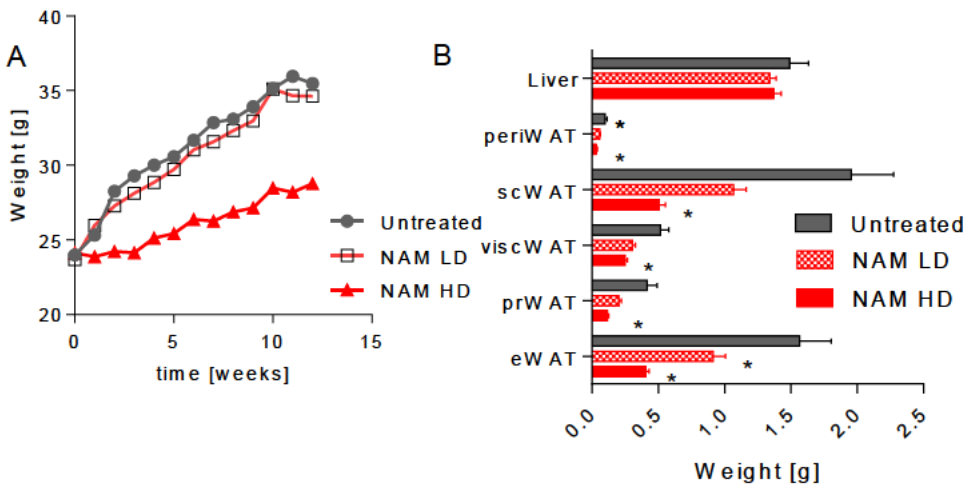


Figure 38. Effect of different doses on NAM on gross parameters in DIO mice. (A) Body weight and (B) tissue weight of 5 month-old mice, fed with a HFD and treated with NAM for 3 consecutive months. (n= 5-6 mice per group). Differences between the mean values were assessed by the nonparametric a Kruskal Wallis followed by Dunn's posttest or ANOVA followed a Newman-Keuls posttest, as appropriate. *Indicates statistical significance between untreated and treated mice. Specifically, * $P < 0.05$ vs. untreated group. Abbreviations used: eWAT, epididymal white adipose tissue; prWAT, peri-renal white adipose tissue; viscWAT, visceral white adipose tissue; scWAT, subcutaneous white adipose tissue; periWAT, pericardial white adipose tissue; NAM LD, nicotinamide low dose; NAM HD, nicotinamide high dose.

The correlation between fat pad and body weight was highly significant (Pearson $r = 0.9522$, $p < 0.05$) (Figure 39).

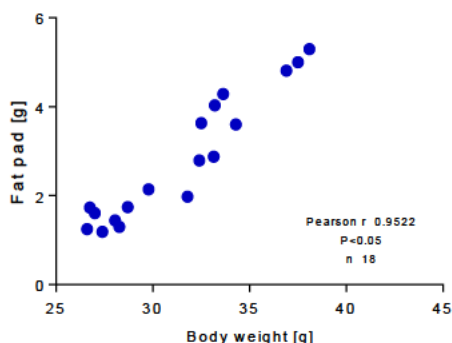


Figure 39. Relationship between total body and fat pad weights in DIO mice.

Total body were correlated with fat pad weights. Mice were 5 month-old mice, fed with a HFD and treated with NAM for 3 consecutive months. A parametric Pearson test.

4.4.1a MRI analysis

A series of magnetic resonance imaging (MRI) analysis were made to confirm reduced accumulation of fat and to further analyze regional adipose tissue distribution within the body of alive mice using an independent approach (Figures 40 and 41). As observed in Figure 40, MRI analysis revealed that estimated body weight size (0.7-fold, $P < 0.05$) (Figure 41, panel A) and adiposity accumulated in NAM HD-treated mice (0.47-fold, $P < 0.05$) (Figure 41, panel B) was much lower than that of untreated mice. Conversely, no differences in the above mentioned parameters were observed between NAM LD-treated mice and untreated mice. In accordance with previous data collected at necropsy, lean weight was also- through slightly- significantly reduced in NAM HD-treated mice compared with untreated mice (~ 0.8 -fold, $P < 0.05$) (Figure 41, panel C). Additionally, MRI analysis also revealed that the liver was less fatty (0.3-fold, $P < 0.05$) than that of untreated mice (Figure 41, panel D).

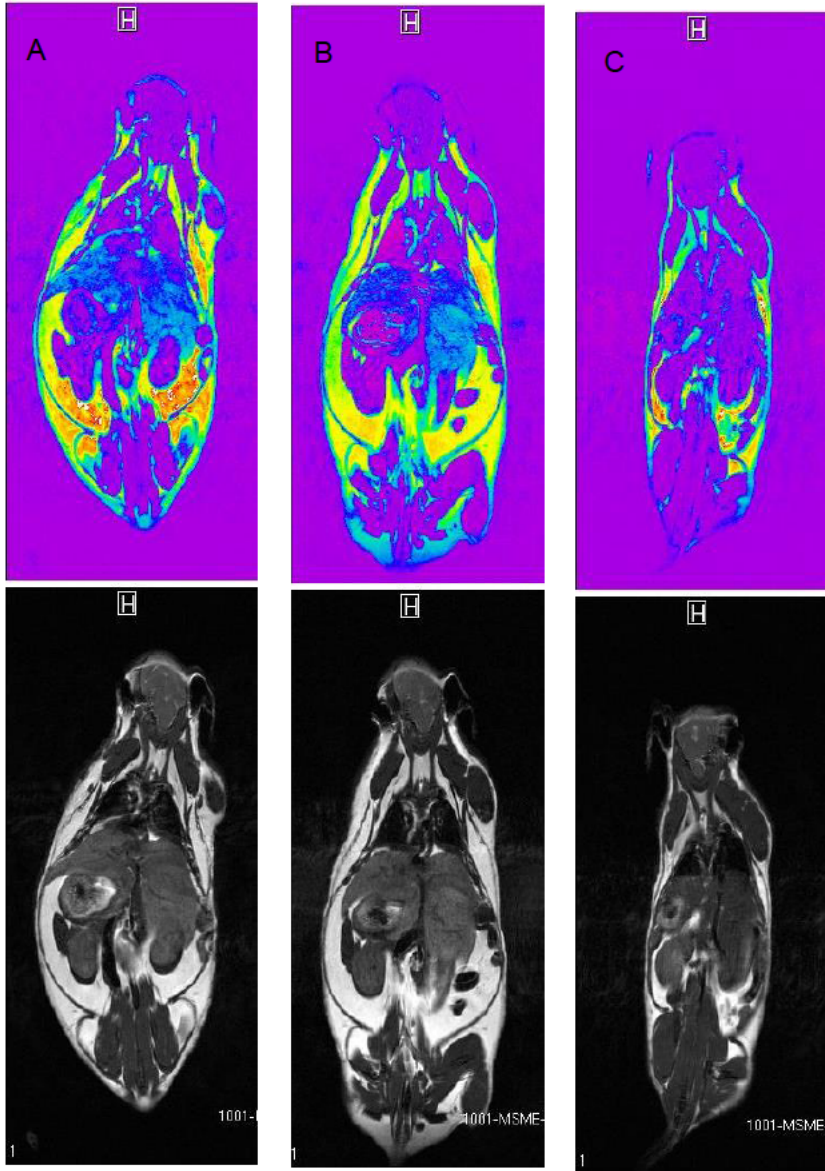


Figure 40. Representative T1W used to measure total fat pad in DIO mice and treated with different doses of NAM for 3 consecutive months.

(A) MRI of representative untreated mice (B) MRI of representative mice treated with NAM LD (C) MRI of representative mice treated with NAM HD. Mice were 5 month-old. Abbreviations used: NAM LD, nicotinamide low dose; NAM HD, nicotinamide high dose.

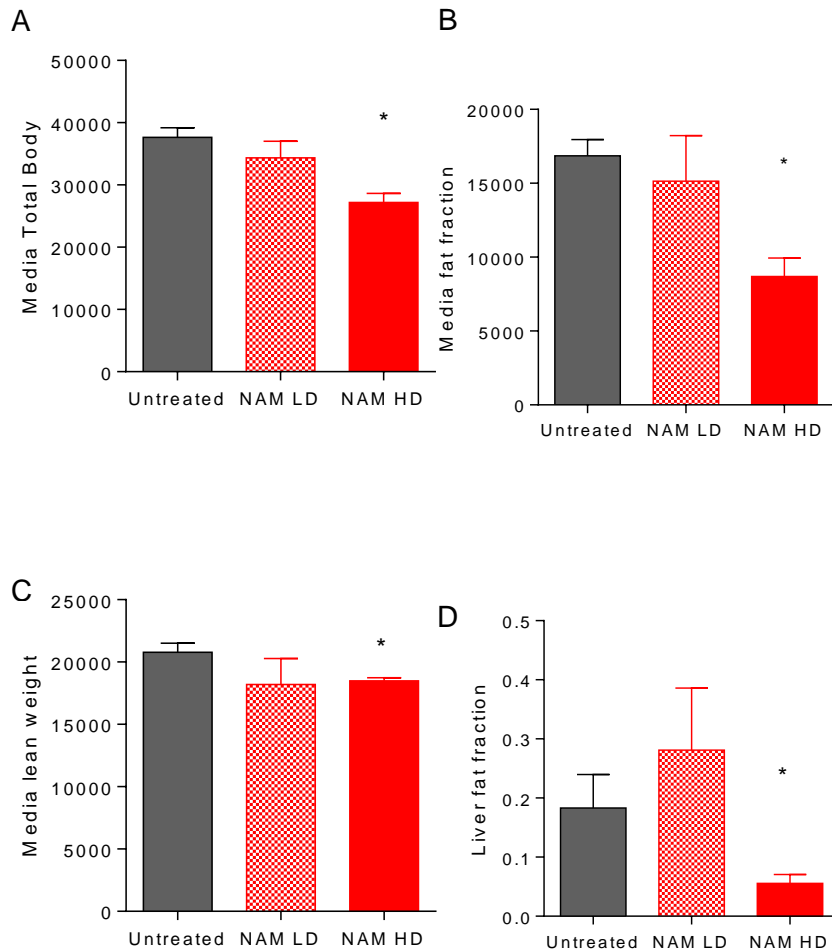


Figure 41. . Box-plot representing relative values or ROIs showing total fat pad and liver fat in DIO mice and treated with different doses of NAM for 3 consecutive months.

Differences between the mean values were assessed by the nonparametric a Kruskal Wallis followed by Dunn's posttest or ANOVA followed a Newman-Keuls posttest, as appropriate. *Indicates statistical significance between untreated and treated mice. Specifically, *P<0.05 vs. untreated group. Data is presented as mean \pm SEM. (A) Total body fraction of mice (B) Fat fraction (C) Lean weight. (D) Liver fat fraction. Mice were 5 month-old. Abbreviations used: NAM LD, nicotinamide low dose; NAM HD, nicotinamide high dose.

The liver fat fraction directly correlated to both, fat depot (Spearman $r = 0.9301$, $P < 0.05$) and body weight (Spearman $r = 0.7552$, $P < 0.05$) fractions (Figure 42).

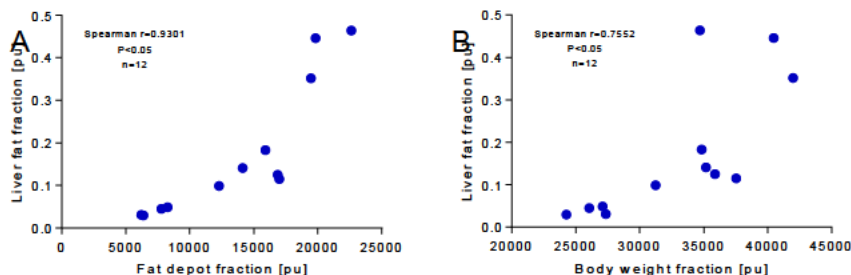


Figure 42. Relationship between total body and fat pad weights with liver fat fraction in DIO mice.

Liver fat fraction was correlated with (A) Fat depot fraction and (B) Total body fat fraction. Mice were 5 month-old, fed with a HFD and treated with NAM for 3 consecutive months. A non-parametric Spearman test was used to analyze whether these parameters were correlated. Abbreviations used: pu, pixels unit.

4.4.1b Biochemical parameters

Plasma levels of NAM and its methylated derivative, me-NAM, were both consistently elevated in NAM treated groups (NAM LD: 6.5-fold, $P < 0.05$; NAM HD: 18-fold, $P < 0.05$) compared with untreated mice (Figure 43) showing a dose dependent shape which was concomitant to the administered dose, respectively.

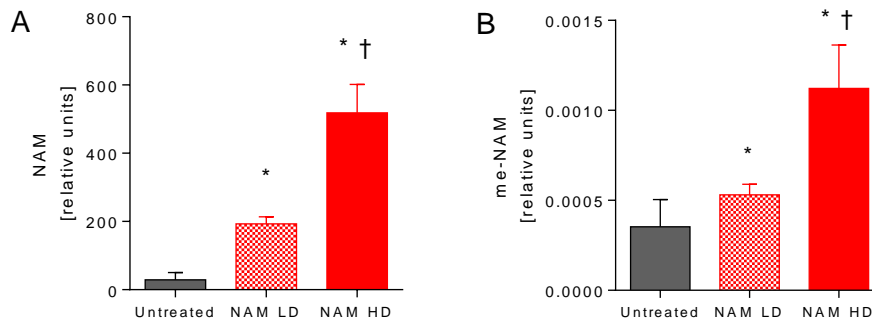


Figure 43. NAM and its methylated form (me- NAM) displayed a dose-dependent shape in plasma in DIO mice.

(A) NAM concentration (relative units) in plasma (B) me- NAM concentration (relative units) in plasma. (n= 5-6 mice per group). Mice were 5 month-old, fed with a HFD and treated with NAM for 3 consecutive months. Differences between the mean values were assessed by the nonparametric a Kruskal Wallis followed by Dunn's posttest or ANOVA followed a Newman-Keuls posttest, as appropriate. *Indicates statistical significance, *P<0.05 vs. untreated group or † P<0.05 vs. NAM-treated mice. Abbreviations used: NAM LD, nicotinamide low dose; NAM HD, nicotinamide high dose.

Plasma biochemistry did not reveal any significant changes in most of the parameters among groups, but a significant reduction was observed in the plasma levels of FFA, which were significantly decreased in NAM-treated groups (NAM LD: 20%, P<0.05; NAM HD: 40%, P<0.05) compared with untreated mice (Table 19). Importantly, plasma levels of FFA were directly related to body weight (Spearman $r = 0.6386$, P<0.05) and adiposity (Spearman $r = 0.5827$, P<0.05) (Figure 44).

	Untreated	NAM LD	NAM HD	p
Glucose [mM]	13.18 (1.85)	12.92 (2.16)	15.19 (1.47)	0.13
Triglycerides [mM]	0.83 (0.31)	1.01 (0.40)	1.44 (0.57)	0.22
FFA [mM]	0.85 (0.11)	0.67 (0.05)*	0.54 (0.10)*	<0.05
Total cholesterol [mM]	3.97 (1.07)	3.71 (0.53)	3.88 (0.10)	0.82
HDL cholesterol [mM]	2.66 (0.48)	2.44 (0.47)	2.77 (0.47)	0.65
Non-HDL cholesterol [mM]	1.30 (0.66)	1.10 (0.57)	1.30 (0.18)	0.77

Table 19. Effect NAM on plasma biochemical parameters in DIO mice.

Results are expressed as the means (standard deviation) (n=5-6 mice per group). All analyses were made at 5 month-old mice, fed with a HFD and treated with NAM for 3 consecutive months. Fasting plasma levels of the HDL fractions were determined in the plasma supernatants after precipitating with phosphotungstic acid (Roche); the non-HDL fraction was calculated by subtracting the HDL moiety to the total plasma. The biochemical measurement was made by commercial kits adapted to a COBAS auto- analyzer. Differences between the mean values were assessed by the nonparametric a Kruskal Wallis followed by Dunn's posttest or ANOVA followed a Newman-Keuls posttest, as appropriate; differences were considered significant when $P < 0.05$. Specifically, * $P < 0.05$ vs. untreated group; or † $P < 0.05$ vs. NAM-treated mice. Abbreviations used: FFA, free fatty acids; HDL, high-density lipoprotein; NAM LD, nicotinamide low dose; NAM HD, nicotinamide high dose.

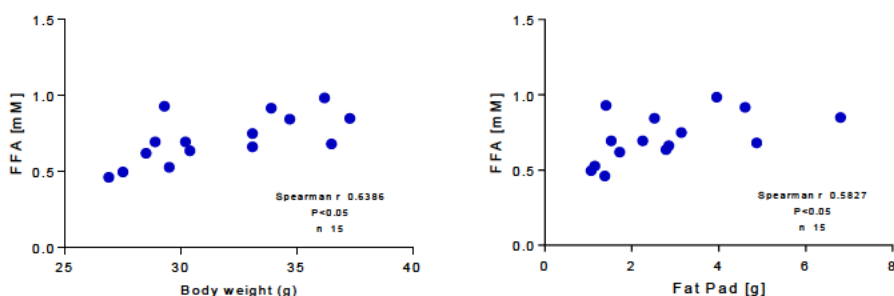


Figure 44. Relationship between total body and fat pad weights and plasma levels of FFA in DIO mice.

Total body and fat pad weights were correlated with circulating FFA. Mice were 5 month-old and treated with NAM for 3 consecutive months. A non-parametric Spearman test was used to analyze whether these parameters were correlated. Abbreviations used: FFA, free fatty acids.

There were no differences in any of the hepatic and renal parameters among groups (Table 20), indicating that any of the NAM doses used caused neither hepatic nor renal damage.

	Untreated	NAM LD	NAM HD	P
Creatinine [mM]	0.03 (0.00)	0.03 (0.00)	0.03 (0.00)	0.23
BUN [μ M]	7.58 (2.00)	6.94 (1.60)	8.69 (1.93)	0.23
AST [U/L]	152.8 (61.04)	173.1 (66.15)	124.6 (58.06)	0.56
ALT [U/L]	59.18 (46.07)	39.17 (17.77)	21.98 (6.49)	0.27
Liver triglycerides [μ mol/liver]	14.12 (6.06)	12.90 (1.13)	10.25 (6.52)	0.14
Liver triglycerides [μ mol/g]	5.44 (1.98)	2.06 (0.66)	3.23 (2.69)	0.11

Table 20. Effect of NAM on hepatic and renal parameters in DIO mice.

Results are expressed as the means (standard deviation) (n=5-6 mice per group). All analyses were made at 5 month-old mice, fed with a HFD and treated with NAM for 3 consecutive months. The biochemical measurement was made from lipid extracts by commercial kits adapted to a COBAS self-analyzer robot. The data is expressed in relation to g of liver. Differences between the mean values were assessed by the nonparametric a Kruskal Wallis followed by Dunn's posttest or ANOVA followed a Newman-Keuls posttest, as appropriate; differences were considered significant when P<0.05. Specifically, *P<0.05 vs. untreated group; or † P<0.05 vs. NAM-treated mice. Abbreviations used: AST, Aspartate aminotransferase; ALT, Alanine aminotransferase; NAM LD, nicotinamide low dose; NAM HD, nicotinamide high dose.

In contrast with our previous data (section 4.1.2 and 4.2.1), liver weight was not found significantly reduced in mice treated with NAM HD compared with untreated mice. As in previous experiments, the liver-to-body weight ratio was unchanged neither among groups (Table 20). However, the hepatic triglyceride content only showed a trend to be reduced (30%, P=0.14) in NAM HD-treated mice compared with that of untreated mice.

4.4.1c Histologic and molecular analysis on fatty liver

Hepatic histological analysis of livers from NAM HD-treated mice also suggested an improvement of the steatosis of mice in HFD, compared to untreated mice (Figure 45).

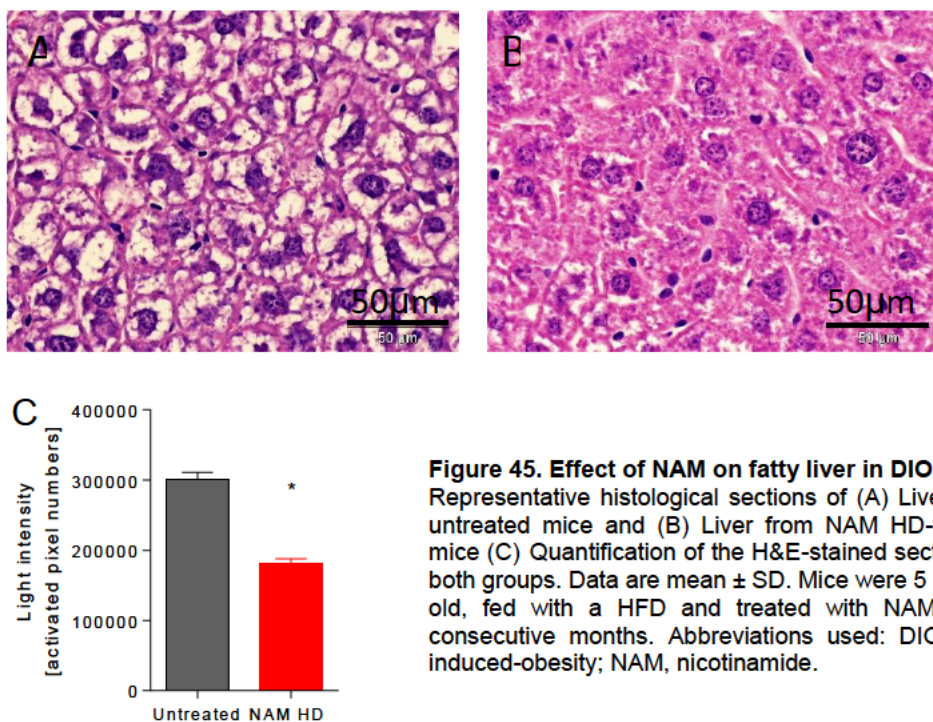


Figure 45. Effect of NAM on fatty liver in DIO mice. Representative histological sections of (A) Liver from untreated mice and (B) Liver from NAM HD-treated mice (C) Quantification of the H&E-stained sections in both groups. Data are mean \pm SD. Mice were 5 month-old, fed with a HFD and treated with NAM for 3 consecutive months. Abbreviations used: DIO, diet-induced-obesity; NAM, nicotinamide.

Consistent with this view, and as previously demonstrated in WAT, two gene markers of macrophage infiltration (i.e., *Cd68* and *Ucp2*) were also found significantly reduced in the liver (*Cd68* and *Ucp2* 40%, $P < 0.05$) in NAM HD-treated mice compared with untreated mice (Table 21).

	Untreated	NAM LD	NAM HD	P
Liver				
<i>Cd68</i>	1.00 (0.13)	1.05 (0.14)	0.59 (0.11)*	<0.05
<i>Ucp2</i>	1.00 (0.24)	nd	0.56 (0.11)*	<0.05

Table 21. Gene expression of molecular targets involved in macrophages infiltration and inflammation in DIO mice

Mice were 5 month-old, fed with a HFD and treated with NAM for 3 consecutive months. Differences between the mean values were assessed by the nonparametric a Kruskal Wallis followed by Dunn's posttest or ANOVA followed a Newman-Keuls posttest, as appropriate. Differences were considered significant when $P < 0.05$. Specifically, * $P < 0.05$ vs. untreated group. Data are expressed as mean \pm SEM ($n = 5-6$ group). Abbreviations used NAM LD, nicotinamide low dose; NAM HD, nicotinamide high dose.

Hepatic gene expression of *Cd36* was also significantly down regulated in NAM HD-treated mice (50%, $P < 0.05$) (Figure 46, panel A), as in previous experiments, compared with untreated mice. Circulating *Fgf21*, which is increased in human fatty liver [327], was significantly reduced (-6 fold, $P < 0.05$) in NAM HD-treated (Figure 46, panel B) compared with untreated mice. The liver is the main source of plasma *Fgf21* [328]. Our data showed that *Fgf21* gene expression was concomitantly down-regulated (Figure 46, panel C), even though to a lower extent, in the livers of mice treated with the highest dose of NAM.

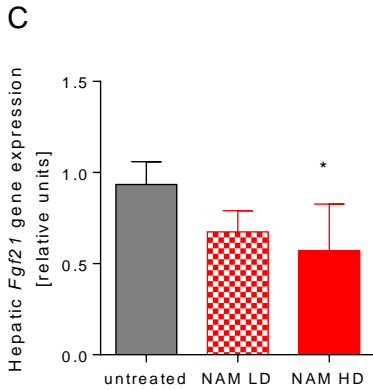
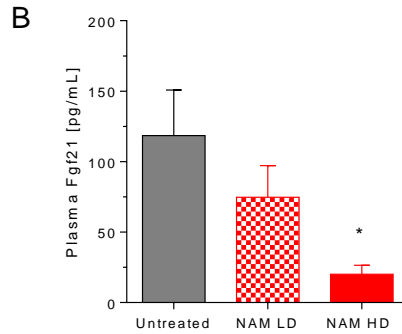
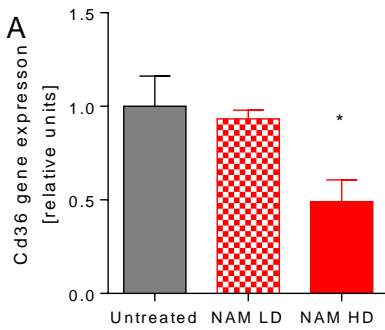


Figure 46. Impact of NAM over fatty liver-related markers in DIO mice.

(A) Hepatic mRNA *Cd36* (B) Circulating Fgf21 (C) Hepatic mRNA *Fgf21*. Mice were 5 month-old, fed with a HFD and treated with NAM for 3 consecutive months. Data are expressed as mean \pm SEM (n= 5-6 group). Differences between the mean values were assessed by the nonparametric a Kruskal Wallis followed by Dunn's posttest or ANOVA followed a Newman-Keuls posttest, as appropriate; differences were considered significant when $P < 0.05$. Specifically, * $P < 0.05$ vs. untreated group. Abbreviations used NAM LD, nicotinamide low dose; NAM HD, nicotinamide high dose.

It was observed a down-regulation of *Nnmt* in the liver in mice receiving the highest dose of NAM. However, the mRNA levels of *Nnmt* in the livers of mice treated with the lowest dose of NAM did not differ from that of untreated mice (Table 22). In contrast, the relative content in mRNA levels of *Nnmt* were significantly up-regulated in eWAT (2.2-fold, $P < 0.05$) and scWAT (2.8-fold, $P < 0.05$). Conversely, the relative content in mRNA levels of the two other genes involved in NAM metabolism (i.e. *Nampt* and *Nmrk1*) did not differ among groups.

	Untreated	NAM LD	NAM HD	P
Liver				
<i>Nnmt</i>	1.00 (0.54)	1.08 (0.17)	0.55 (0.11)*	<0.05
<i>Nampt</i>	1.00 (0.37)	1.39 (0.79)	1.27 (0.64)	0.63
<i>Nmrk1</i>	1.00 (0.68)	2.40 (1.41)	1.80 (0.42)	0.11
eWAT				
<i>Nnmt</i>	1.00 (0.32)	1.25 (0.37)	2.16 (1.18)*	<0.05
<i>Nampt</i>	1.00 (0.52)	1.26 (0.45)	1.60 (0.72)	0.46
<i>Nmrk1</i>	1.00 (0.47)	1.14 (0.37)	0.90 (0.35)	0.77
scWAT				
<i>Nnmt</i>	1.00 (0.56)	0.98 (0.71)	2.81 (1.53)*	<0.05
<i>Nampt</i>	1.00 (0.74)	1.18 (0.93)	1.65 (1.15)	0.23
<i>Nmrk1</i>	1.00 (0.65)	0.89 (0.43)	1.52 (0.85)	0.28

Table 22. Gene expression of molecular targets involved in NAM metabolism in liver and adipose tissue in DIO mice.

Mice were 5 month-old, fed with a HFD and treated with NAM for 3 consecutive months. Differences between the mean values were assessed by the nonparametric a Kruskal Wallis followed by Dunn's posttest or ANOVA followed a Newman-Keuls posttest, as appropriate. *Indicates statistical significance, *P<0.05 vs. untreated group. Data are expressed as mean \pm SD (n= 5-6 group). Abbreviations used NAM LD, nicotinamide low dose; NAM HD, nicotinamide high dose.

The down-regulation of *Nnmt* in the liver showed a significant inverse correlation with the plasmatic levels of NAM (Spearman: -0.5290, p<0.05) and a trend with me-NAM levels (Spearman: -0.4321, P=0.10) (Figure 47)

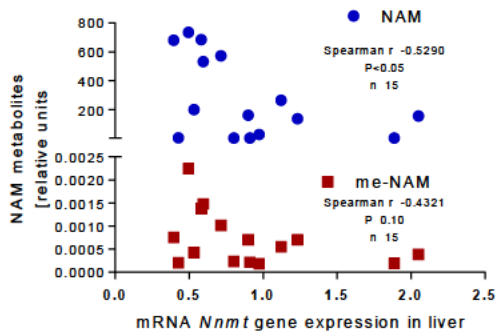


Figure 47. Gene expression of molecular targets involved in NAM metabolism in liver and adipose tissue in DIO mice.

Mice were 5 month-old, fed with a HFD and treated with NAM for 3 consecutive months. A non-parametric Spearman test was used to analyze whether these parameters were correlated.

4.4.1d Glucose homeostasis

Glucose intolerance and insulin resistance are common metabolic alterations of obesity [3]. Thus, we tested whether they were improved in the treated mice. Analysis did not reveal changes in either glucose disposal (Figure 48) or insulin sensitivity (Figure 49) among groups. This finding was consistent with previous data (section 4.2.2c) but contrasted with the reduction in the plasma levels of FFA of mice treated with NAM (Table 19).

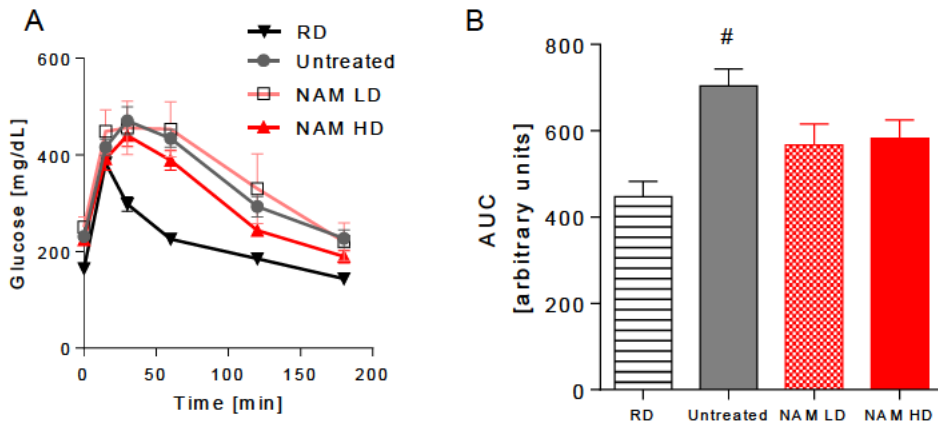


Figure 48. Effect of different doses of NAM on functional analysis of glucose metabolism in DIO mice: glucose tolerance test.

(A) GTT was performed on 5h- fasted mice. Blood glucose levels were measured at 0, 15, 30, 60, 120 and 180 minutes after an intraperitoneal injection (2g/kg). (B) Area under curve of GGT associated curves. (n=5-6 mice per group). Mice were 5 month-old, fed with a HFD and treated with NAM for 3 consecutive months. Differences between the mean values were assessed by the nonparametric a Kruskal Wallis followed by Dunn's posttest or ANOVA followed a Newman-Keuls posttest, as appropriate; differences were considered significant when $P < 0.05$. Specifically, * $P < 0.05$ vs. untreated group; † $P < 0.05$ vs. NAM-treated mice; or #† $P < 0.05$ vs. RD group. Abbreviations used: NAM LD, nicotinamide low dose; NAM HD, nicotinamide high dose; RD, regular diet.

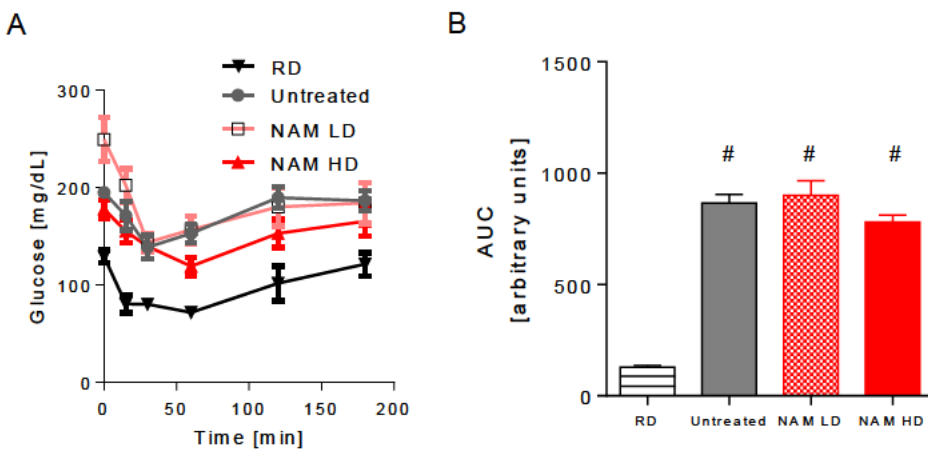


Figure 49. Effect of different doses of NAM on functional analysis of glucose metabolism in DIO mice: insulin sensitivity

(A) ITT was performed on 5h- fasted mice. Blood glucose levels were measured at 0, 15, 30, 60, 120 and 180 minutes after an intraperitoneal injection (0.9U/ kg). (B) Area under curve of IST associated curves. (n=5-6 mice per group). Mice were 5 month-old, fed with a HFD and treated with NAM for 3 consecutive months. Differences between the mean values were assessed by the nonparametric a Kruskal Wallis followed by Dunn's posttest or ANOVA followed a Newman-Keuls posttest, as appropriate; differences were considered significant when $P < 0.05$. Specifically, * $P < 0.05$ vs. untreated group; † $P < 0.05$ vs. NAM-treated mice; or #† $P < 0.05$ vs. RD group. Abbreviations used: NAM LD, nicotinamide low dose; NAM HD, nicotinamide high dose; RD, regular diet.

4.4.2 Energy metabolism

4.4.2a Global energy expenditure by indirect calorimetry analysis

There was an increase in whole-body O₂ consumption in NAM HD-treated mice compared with untreated mice (Figure 50, panel A and B). RER (CO₂ production/O₂ uptake) is commonly used to indirectly determine the relative contribution of carbohydrate and lipids to overall energy expenditure [329]. As shown in panels C and D of Figure 50, O₂ consumption was significantly increased during the light (1.2-fold, P<0.05) and dark period (1.2-fold, P<0.05) in NAM HD-treated mice. Consistently, both RER and energy expenditure (Ancova corrected, see methods) (Figure 50, panels E and F) were also elevated in this group. Both O₂ consumption and RER were also significantly elevated (O₂ consumption: 1.11-fold, P<0.05; RER: 1.03-fold, P<0.05) in NAM LD-treated mice only during the dark period (i.e., night).

Glucose oxidation fluxes showed a trend to be increased in NAM LD-treated mice in both diurnal and nocturnal phases. Ancova corrected glucose oxidation confirmed a close to significant trend (P=0.13) to be higher in NAM LD-treated mice (Figure 51) compared with untreated mice. The induction of glucose oxidation was significantly greater in NAM HD-treated mice compared with untreated mice. In contrast, changes in lipid oxidation in NAM-treated mice did not differ among mice groups (Figure 52).

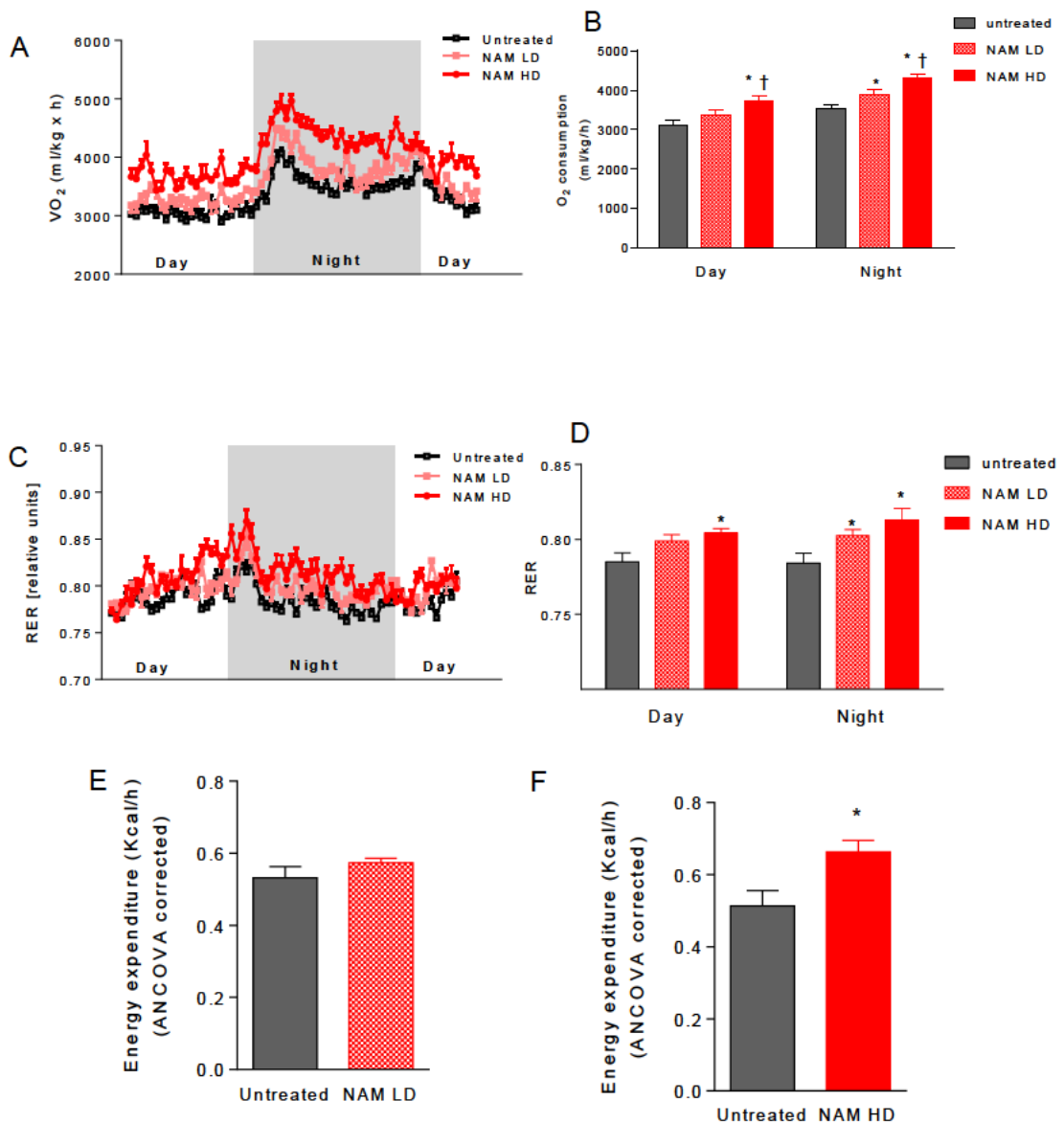


Figure 50. Analysis of energy expenditure of DIO mice measured in metabolic cages.

(A) Oxygen consumption through day and night of mice groups represented as mean \pm SD (B) Total oxygen consumption represented by bars as mean \pm SD (C) RER through day and night of mice groups represented as mean \pm SD (D) Total RER represented by bars as mean \pm SD (E) Energy expenditure of untreated and NAM LD- treated mice, corrected by body weight by ANCOVA posttest (F) Energy expenditure of untreated and NAM HD- treated mice, corrected by body weight by ANCOVA posttest. ANCOVA correction made for each group based on body weight: NAM LD: 33.396g; NAM HD: 32.53g. Mice were 5 month-old, fed with a HFD and treated with NAM for 3 consecutive months. (n=5-6 mice per group). Differences between the mean values were assessed by the nonparametric a Kruskal Wallis followed by Dunn's posttest or ANOVA followed a Newman-Keuls posttest, as appropriate. Differences were considered significant when $P < 0.05$. Specifically, * $P < 0.05$ vs. untreated group. Abbreviations used: VO_2 ; oxygen uptake; RER, respiratory exchange ratio; NAM LD, nicotinamide low dose; NAM HD, nicotinamide high dose.

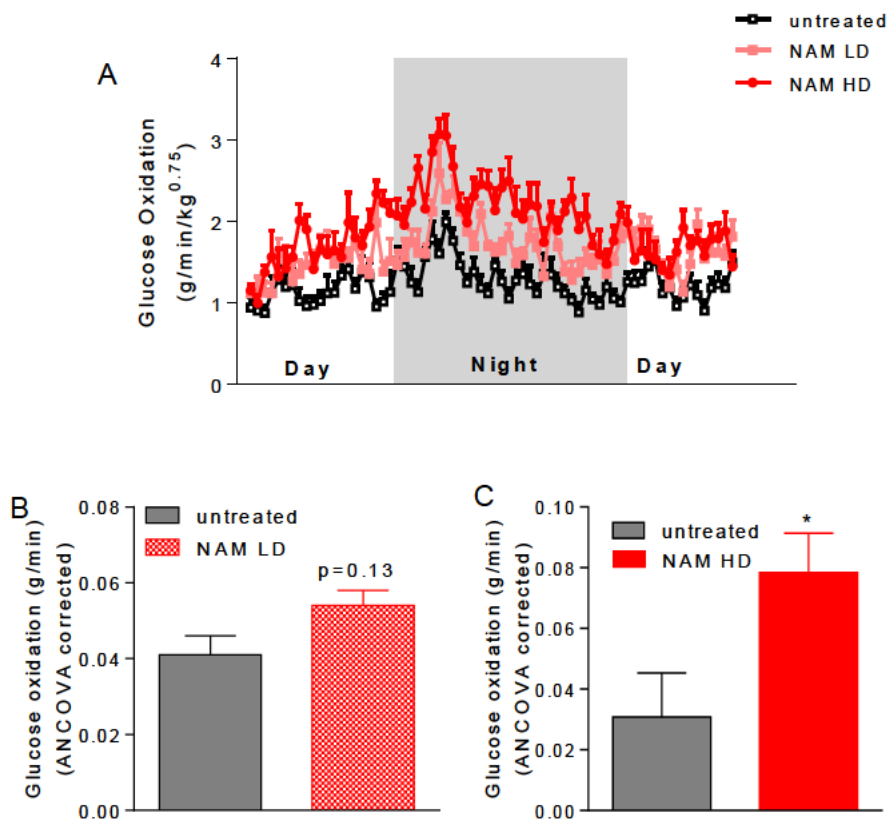


Figure 51. Analysis of glucose oxidation measured in metabolic cages of DIO mice.

(A) Glucose oxidation through day and night of mice groups represented as mean \pm SD. (B) Total glucose oxidation represented by bars of untreated and NAM LD- treated mice, corrected by body weight by ANCOVA posttest. (C) Total glucose oxidation represented by bars of untreated and NAM HD- treated mice, corrected by body weight by ANCOVA posttest. ANCOVA correction made for each group based on body weight: NAM LD: 33.396g; NAM HD: 32.53g. Mice were 5 month-old, fed with a HFD and treated with NAM for 3 consecutive months. (n=5-6 mice per group). Differences between the mean values were assessed by the nonparametric a Kruskal Wallis followed by Dunn's posttest or ANOVA followed a Newman-Keuls posttest, as appropriate. Differences were considered significant when $P < 0.05$. Specifically, $*P < 0.05$ vs. untreated group. Abbreviations used NAM LD, nicotinamide low dose; NAM HD, nicotinamide high dose.

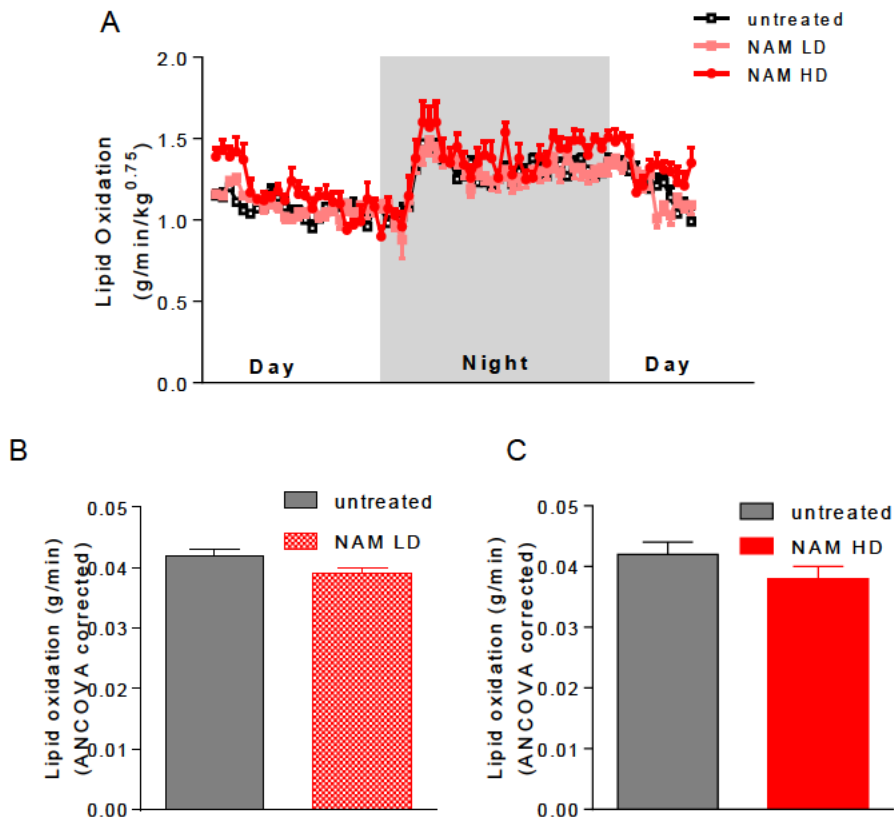


Figure 52. Analysis of lipid oxidation measured in metabolic cages of DIO mice.

(A) Lipid oxidation through day and night of mice groups represented as mean \pm SD (B) Total lipid oxidation represented by bars of untreated and NAM LD- treated mice, corrected by body weight by ANCOVA posttest. (C) Total lipid oxidation represented by bars of untreated and NAM HD- treated mice, corrected by body weight by ANCOVA posttest. ANCOVA correction made for each group based on body weight: NAM LD: 33.396g; NAM HD: 32.53g. Mice were 5 month-old, fed with a HFD and treated with NAM for 3 consecutive months. (n=5-6 mice per group). Differences between the mean values were assessed by the nonparametric a Kruskal Wallis followed by Dunn's posttest or ANOVA followed a Newman-Keuls posttest, as appropriate. Differences were considered significant when $P < 0.05$. Specifically, * $P < 0.05$ vs. untreated group. Abbreviations used NAM LD, nicotinamide low dose; NAM HD, nicotinamide high dose.

In our study, RER was inversely related to body weight (Figure 53, panel A) and adiposity (Figure 53, panel B).

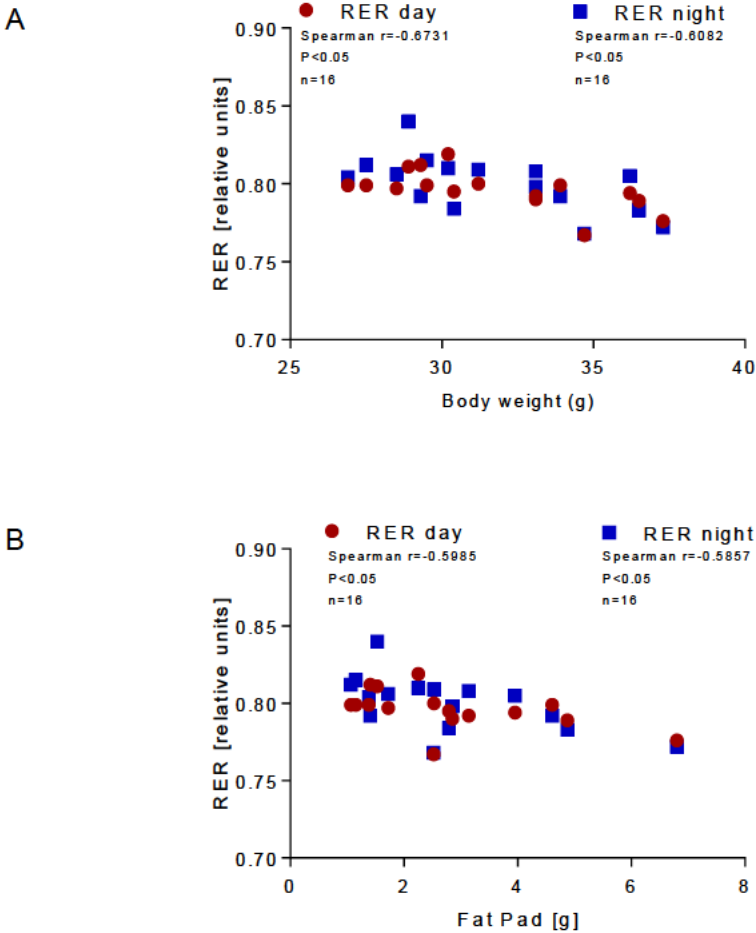


Figure 53. Relationship between total body and fat pad weights with RER in DIO mice.

(A) Inverse correlation between total body weight and both RER during day and night. (B) Inverse correlation between fat pad and both RER during day and night. Mice were 5 month-old and treated with NAM for 3 consecutive months. (n= 5-6 mice per group). A non-parametric Spearman test was used to analyze the relationship between parameters. Abbreviations used: RER, respiratory exchange ratio.

4.4.2b Energy metabolites in scWAT

As NAM is a precursor for the synthesis of NAD⁺, and its phosphorylated derivative NADP⁺, we aimed at determine NAD⁺ and NADH levels in the adipose tissue where the impact of treatment was more elevated (i.e., scWAT). The content in total NAD and the NAD⁺/NADH ratio were higher in scWAT of NAM HD-treated mice (1.5-fold, P<0.05) compared with untreated mice, suggesting increased bioavailability of NAD (Figure 54).

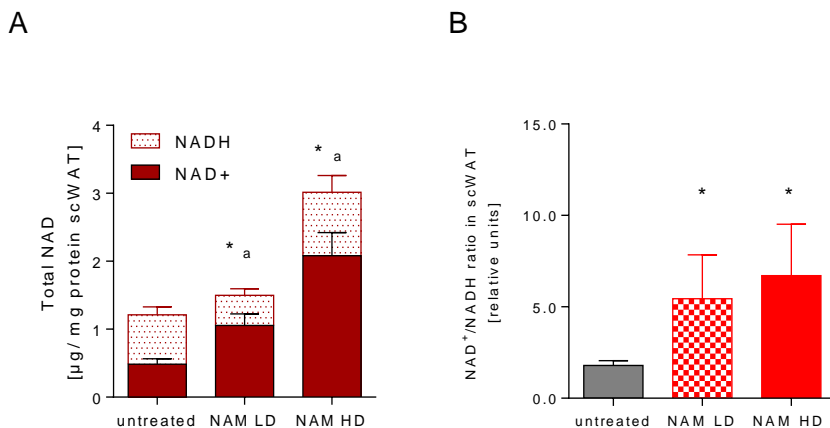


Figure 54. Analysis of NADt, NAD⁺, NADH and NAD⁺/NADH in scWAT in DIO mice.

(A) NAD total concentration in scWAT (B) NAD⁺/NADH ratio in scWAT. (n=5-8 mice per group). Mice were 5 month-old, fed with a HFD and treated with NAM for 3 consecutive months. Differences between the mean values were assessed by the nonparametric a Kruskal Wallis followed by Dunn's posttest or ANOVA followed a Newman-Keuls posttest, as appropriate. *Indicates statistical significance of total NAD, *P<0.05 vs. untreated group; (a) Indicates statistical significance of NAD⁺, *P<0.05 vs. untreated group. Abbreviations used NAM LD, nicotinamide low dose; NAM HD, nicotinamide high dose.

Given that Nampt is a key enzyme in the conversion of NAM to NMN in the generation of NAD⁺, the mRNA expression of *Nampt* was measured in scWAT (Table 22). Even though mRNA levels of *Nampt* were not significant up-regulated of NAM-treated mice compared to untreated mice, it showed a marginal significant direct correlation with NAD⁺ content (Spearman r= 0.5804,

p=0.05) in this tissue and also, with total NAD (Spearman $r = 0.5944$, $p < 0.05$) (Figure 55)

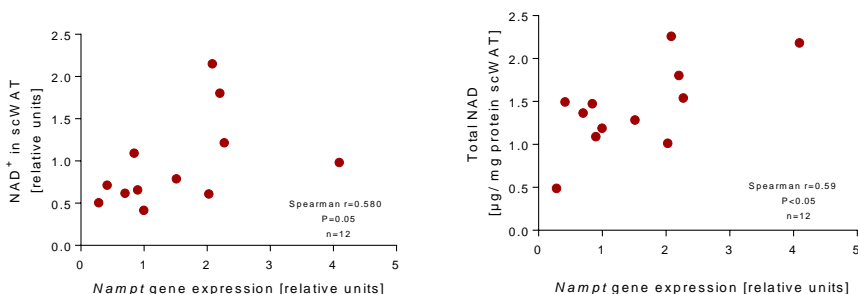


Figure 55. Relationship between NAD⁺ and NAD^t and *Nampt* mRNA in scWAT in DIO mice. Mice were 5 months-old and treated with NAM for 3 consecutive months. A non-parametric Spearman test was used to analyze whether these parameters were correlated.

Adipose tissue content in [ATP+ADP+AMP] was also evaluated in this same tissue to ascertain if the increased bioavailability of NAD⁺ did result in elevations of ATP (Figure 56). Of note, the levels of AMP and [ATP+ADP+AMP] were elevated in NAM HD-treated mice compared to untreated mice (Figure 56, panel A). The NAM LD-treated groups did not show changes in any of these metabolites. In contrast, the calculated AMP/ATP ratio in this fat pad did reach significance among groups (Figure 56, panel B).

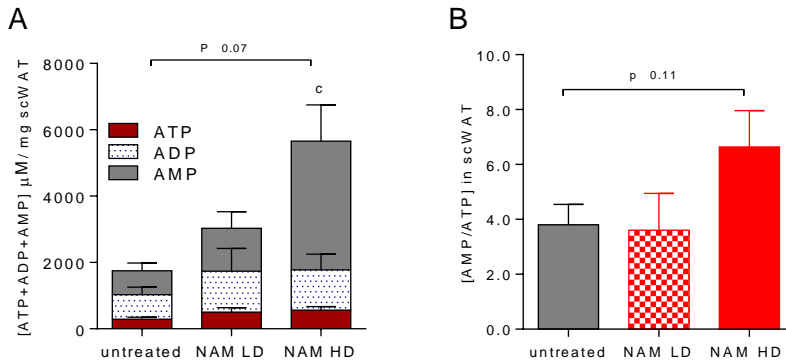


Figure 56. Analysis of [ATP+ ADP+ AMP] and AMP/ATP ratio in scWAT in DIO mice.

(A) ATP, ADP, AMP total concentration in scWAT (B) AMP/ATP ratio in ScWAT. (n=5-8 mice per group). Mice were 5 month-old, fed with a HFD and treated with NAM for 3 consecutive months. Differences between the mean values were assessed by the nonparametric a Kruskal Wallis followed by Dunn's posttest or ANOVA followed a Newman-Keuls posttest, as appropriate. *Indicates statistical significance of [ATP+ADP+AMP], *P<0.05 vs. untreated group (c) Indicates statistical significance of AMP levels, P<0.05 vs. untreated group. Abbreviations used NAM LD, nicotinamide low dose; NAM HD, nicotinamide high dose.

Interestingly, levels of [ATP+ADP+AMP] displayed a direct correlation ($r=0.5180$, $P<0.05$) with $NAD^+/NADH$ content in scWAT (Figure 57).

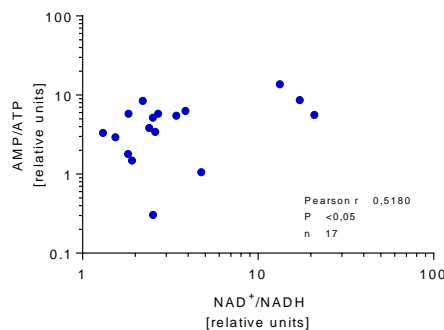


Figure 57. Relationship between [ATP+ADP+AMP] and [NAD+/ NADH] ratio in scWAT in DIO mice.

Mice were 5 months-old and treated with NAM for 3 consecutive months. A parametric Pearson test was used to analyze whether these parameters were correlated.

The AMP-activated protein kinase (AMPK) cascade is activated by an increase in the AMP/ATP ratio within the cell. Even though a significant change was not displayed in the AMP/ATP ratio in the analyzed tissues, AMP did reveal higher levels in NAM HD-treated mice in scWAT. AMPK is regulated allosterically by AMP and by reversible phosphorylation. The protein abundance of phosphorylated AMPK was measured by western blot, showing an increased protein levels in NAM HD-treated mice (2.2-fold, $P < 0.05$) compared with untreated mice. (Figure 58, panel A and B). Phosphorylated AMPK protein abundance correlated with RER (Figure 58, panel C).

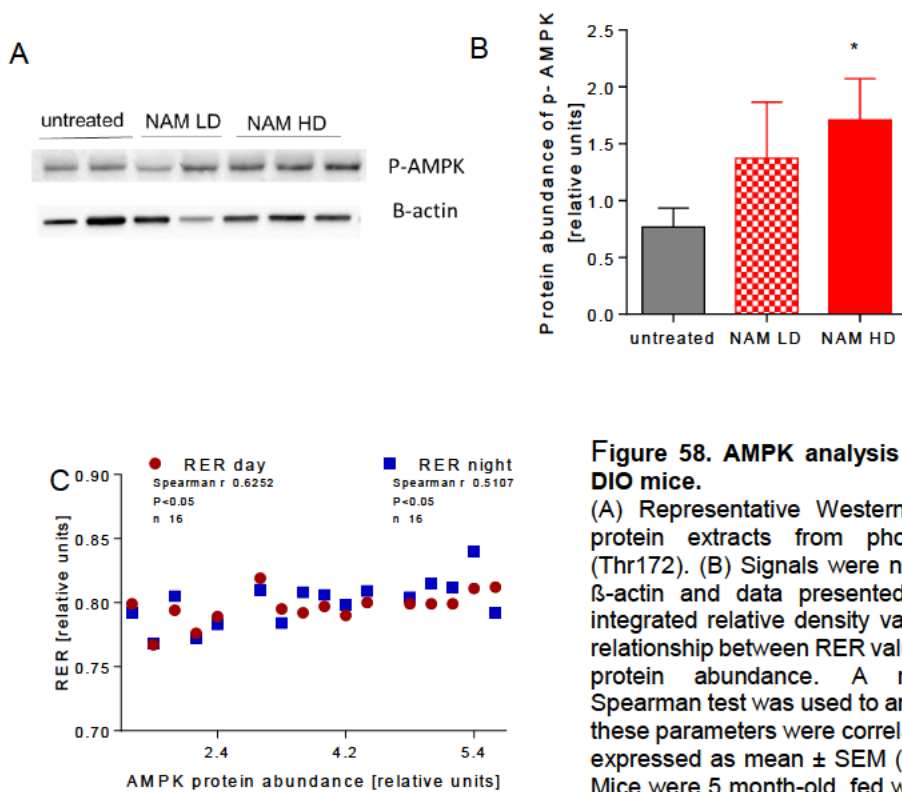


Figure 58. AMPK analysis in scWAT of DIO mice.

(A) Representative Western blot of total protein extracts from phospho-AMPK (Thr172). (B) Signals were normalized with β -actin and data presented as mean of integrated relative density value. (C) Direct relationship between RER values and AMPK protein abundance. A non-parametric Spearman test was used to analyze whether these parameters were correlated. Data are expressed as mean \pm SEM (n= 5-6 group). Mice were 5 month-old, fed with a HFD and treated with NAM for 3 consecutive months.

Differences between the mean values were assessed by the nonparametric a Kruskal Wallis followed by Dunn's posttest or ANOVA followed a Newman-Keuls posttest, as appropriate. Differences were considered significant when $P < 0.05$. Specifically, * $P < 0.05$ vs. untreated group. Abbreviations used NAM LD, nicotinamide low dose; NAM HD, nicotinamide high dose.

However, the increase in tissue content of the active form of AMPK only showed a tendency to be directly related to those of AMP (Figure 59, panel A) and the concentration of AMP / ATP (Figure 59, panel B).

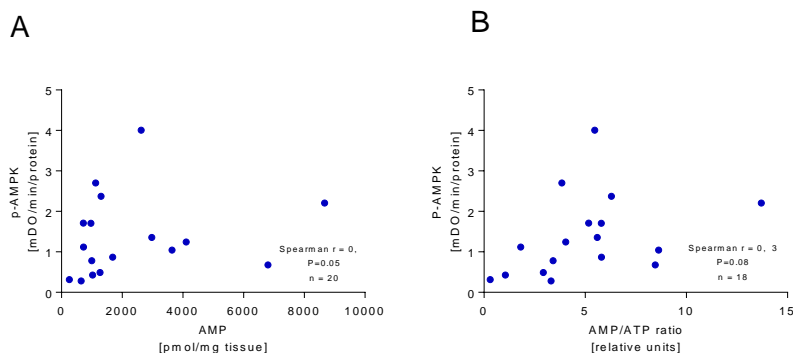


Figure 59. AMPK activity and its relationship with adenosine phosphate in subcutaneous white adipose tissue.

A) Correlation of phosphorylated AMPK concentrations with AMP concentrations; C) Correlation of AMPK concentrations with the AMP / ATP ratio. Mice were 5 months-old and treated with NAM for 3 consecutive months. A parametric Pearson test was used to analyze whether these parameters were correlated.

4.4.2c Mitochondrial activity and mass surrogates in iBAT

β -oxidation of fatty acids could be elevated in NAM-treated mice, as suggested by elevation in NAD and AMP in adipose tissues. This was shown to be the case in mitochondria isolated from iBAT (~ 2 fold, $P < 0.05$) of NAM HD-treated mice (Figure 60).

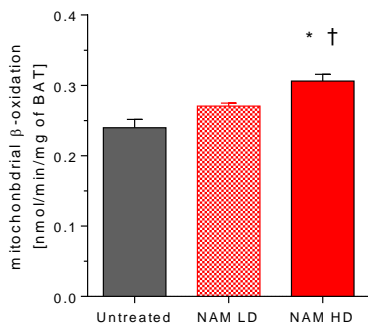


Figure 60. Analysis of mitochondrial activity in BAT of DIO mice.

Mitochondrial β -oxidation in BAT. Data are expressed as mean \pm SEM ($n = 5-6$ group). Mice were 5 month-old, fed with a HFD and treated with NAM for 3 consecutive months. Differences between the mean values were assessed by the nonparametric a Kruskal Wallis followed by Dunn's posttest or ANOVA followed a Newman-Keuls posttest, as appropriate. Differences were considered significant when $P < 0.05$. Specifically, * $P < 0.05$ vs. untreated group; † $P < 0.05$ vs. NAM LD-treated mice. Abbreviations used NAM LD, nicotinamide low dose; NAM HD, nicotinamide high dose.

To ascertain if the observed increase in mitochondrial activity was due to a greater number of mitochondria in iBAT or if it was due to increased mitochondrial efficiency, the mitochondrial mass in this tissue was determined by quantifying the relative abundance of Complex III. This is a protein present in the mitochondria of all animals, and plays a critical role in ATP generation of ATP (oxidative phosphorylation) [330]. TIM44, which as well is an essential component of the presequence translocase-associated motor (PAM) complex and is required for the translocation of transit peptide-containing proteins from the inner membrane into the mitochondrial matrix in an ATP-dependent manner [331], was also quantified (Figure 61)

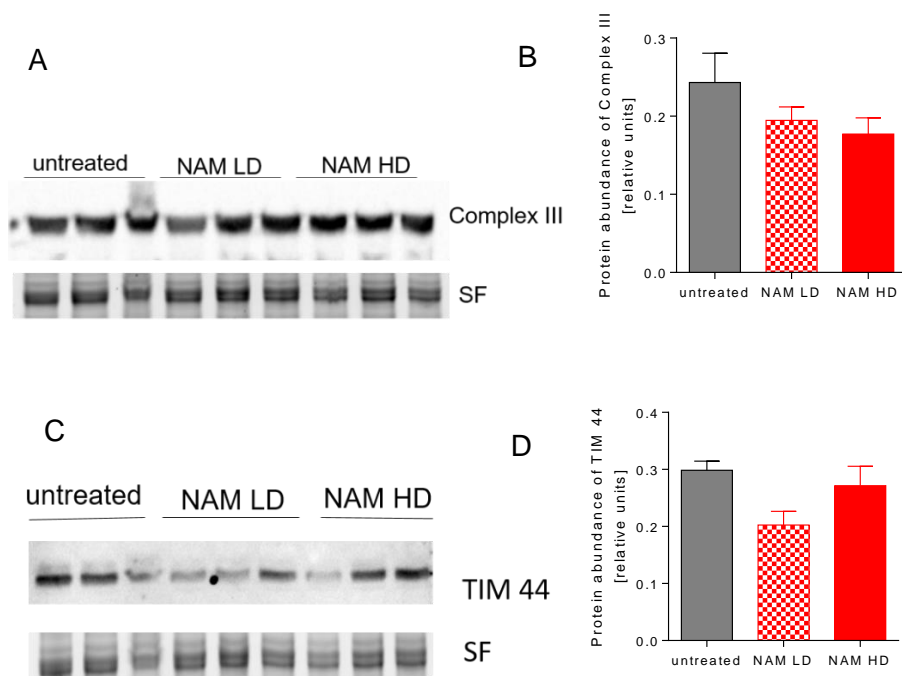


Figure 61. Western blot analysis of Complex III and TIM44 protein in iBAT of DIO mice.

(A) Representative Western blot of total protein extracts from Complex III. (B) Signals were normalized to stain free (SF) gels and data presented as mean of integrated relative density value. Data are expressed as mean \pm SEM (n= 5-6 group). (C) Representative Western blot of total protein extracts from TIM44. (D) Signals were normalized to stain free (SF) gels and data presented as mean of integrated relative density value. Data are expressed as mean \pm SEM (n= 5-6 group). Mice were 5 month-old, fed with a HFD and treated with NAM for 3 consecutive months. Differences between the mean values were assessed by the nonparametric a Kruskal Wallis followed by Dunn's posttest or ANOVA followed a Newman-Keuls posttest, as appropriate. Differences were considered significant when $P < 0.05$. Specifically, * $P < 0.05$ vs. untreated group. Abbreviations used NAM LD, nicotinamide low dose; NAM HD, nicotinamide high dose.

The relative content in both Complex III and TIM44 in iBAT did not show differences among groups (Figure 61) evidencing no changes in the mitochondrial mass among groups and thereby suggesting that increased mitochondrial β -oxidation was due to an increased mitochondrial activity.

4.4.3 Molecular and plasticity analysis on adipose tissue

4.4.3a Browning

An analysis of microscopy preparations of adipose tissue revealed the presence of small-sized adipocytes in mice treated with NAM HD. Of note, such small-sized adipocytes containing not a single (i.e., unilocular) but multiple, smaller lipid vesicles (i.e., multilocular) in their cytosol were commonly observed only in adipose tissue from mice treated with NAM HD (Figure 62). The number of clusters of small-sized adipocytes containing multiple lipid vesicles were increasingly present in white adipose tissue from NAM HD-treated mice in clusters showing a brown-like phenotype. These data revealed that NAM treatment might be inducing the conversion of adipocytes from white adipose tissue into adipocytes showing a cell morphology close to that of brown adipose tissue. The process leading to an increase in the accumulation of adipocytes with cellular morphologic characteristics similar to brown adipose tissue in a white adipose tissue, is commonly defined as “browning” [65]. This cellular phenotype is frequently associated with increased thermogenesis [332].

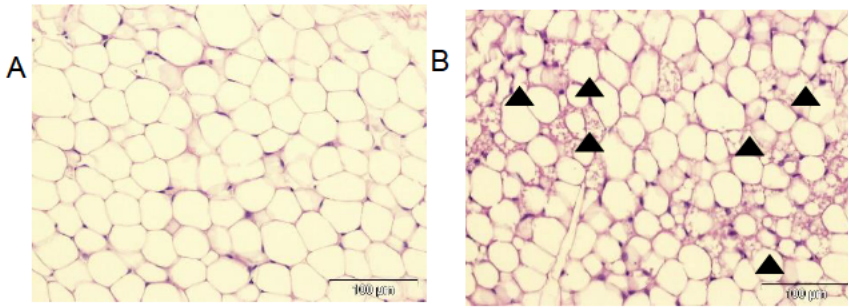


Figure 62. Effect NAM over browning on scWAT in DIO mice.

Representative histological sections of scWAT stained with hematoxylin/ eosin from mice fed a HFD. (A) Representative scWAT from an untreated mice. (B) Representative scWAT from a NAM HD-treated mice. Mice were 5 month-old, fed with a HFD and treated with NAM for 3 consecutive months.(n=5-6 mice per group).

Histologic analysis of iBAT stained with H&E showed that brown adipocytes in iBAT from NAM HD-treated mice had much less accumulation of large lipid vesicles than those in iBAT from untreated mice (Figure 63).

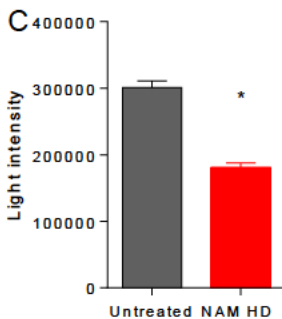
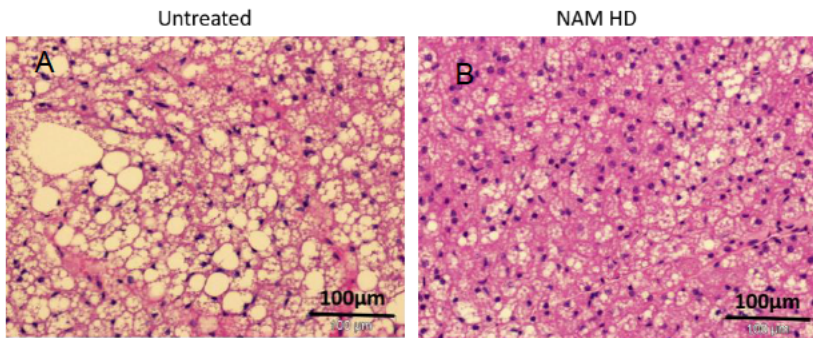


Figure 63. Effect NAM on iBAT in DIO mice.

Representative histological sections of BAT stained with hematoxylin/ eosin from DIO mice (A) Untreated mice, 40x. (B) NAM HD-treated mice, 40X. (C) Quantification of the H&E-stained sections in both groups. Data are mean \pm SD. Mice were 5 month-old, fed with a HFD and treated with NAM for 3 consecutive months.

Consistently, both the relative gene expression and protein abundance analysis of *Ucp1*, which is considered a marker of brown adipose tissue [333] by both real time RT-PCR and western blot analysis, respectively revealed significant elevations of this target in scWAT from NAM HD-treated mice (mRNA: 10-fold, $P < 0.05$; protein: 2.5-fold, $P < 0.05$) compared with untreated mice (Figure 64, panel A, B and C). Importantly, *Ucp1* concentration correlated significantly with RER (Figure 64, panel D).

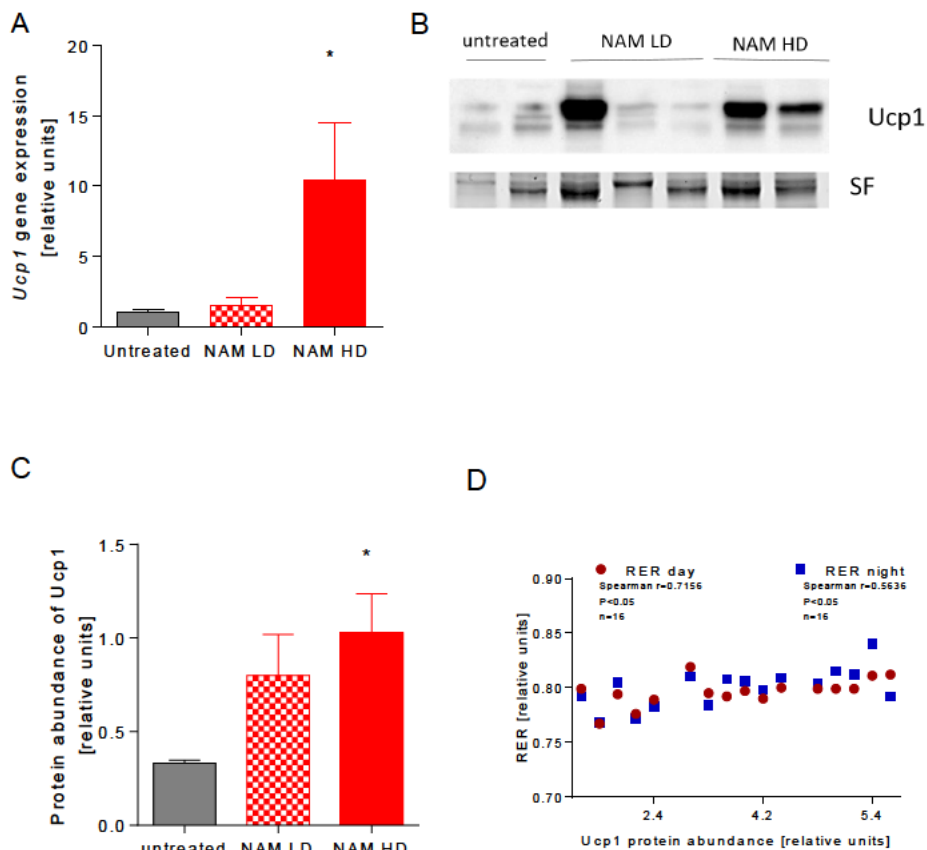


Figure 64. Analysis of *Ucp1* protein in scWAT of DIO mice.

(A) Gene expression of *Ucp1* in scWAT. (B) Representative Western blot of total protein extracts from *Ucp1* with antibody Anti-*Ucp1*. (C) Signals were normalized to stain free (SF) gels and data presented as mean of integrated relative density value. (D) Direct relationship between RER values and *Ucp1* protein abundance. Data are expressed as mean \pm SEM ($n = 5-6$ group). Mice were 5 month-old, fed with a HFD and treated with NAM for 3 consecutive months. Differences between the mean values were assessed by the nonparametric a Kruskal Wallis followed by Dunn's posttest or ANOVA followed a Newman-Keuls posttest, as appropriate. Differences were considered significant when $P < 0.05$. Specifically, * $P < 0.05$ vs. untreated group. Abbreviations used NAM LD, nicotinamide low dose; NAM HD, nicotinamide high dose.

Ucp1 protein abundance was also measured by western blot in iBAT, revealing no differences among groups (Figure 65), in accordance to mRNA levels of *Ucp1* (Table 23). However, the total protein abundance of Ucp1 corresponding total iBAT was calculated, and showed a significant increase in NAM HD-treated mice in comparison with untreated mice.

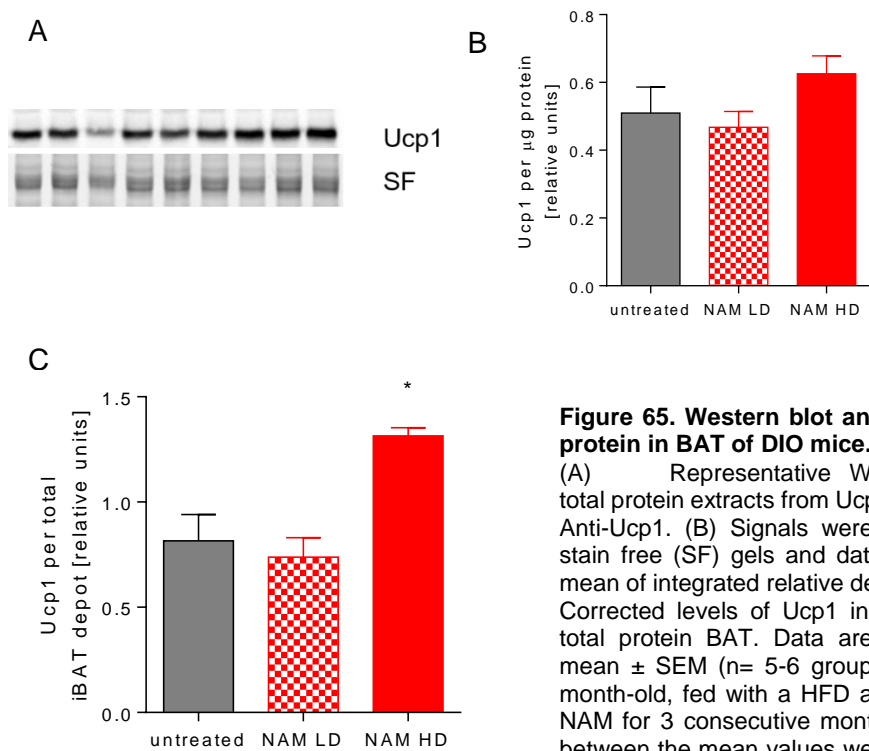


Figure 65. Western blot analysis of Ucp1 protein in BAT of DIO mice.

(A) Representative Western blot of total protein extracts from Ucp1 with antibody Anti-Ucp1. (B) Signals were normalized to stain free (SF) gels and data presented as mean of integrated relative density value. (C) Corrected levels of Ucp1 in accordance to total protein BAT. Data are expressed as mean ± SEM (n= 5-6 group). Mice were 5 month-old, fed with a HFD and treated with NAM for 3 consecutive months. Differences between the mean values were assessed by the nonparametric a Kruskal Wallis followed

by Dunn's posttest or ANOVA followed a Newman-Keuls posttest, as appropriate. Differences were considered significant when $P < 0.05$. Specifically, $*P < 0.05$ vs. untreated group. Abbreviations used NAM LD, nicotinamide low dose; NAM HD, nicotinamide high dose.

Gene expression analysis of scWAT also showed elevations in the mRNA levels of molecular targets involved in energy homeostasis (Table 23 and Figure 66). Relative gene expression of *Pgc1a/b* and *Sat* were significantly up-regulated in scWAT of NAM HD-treated mice (*Pgc1a*: 3-fold, $P < 0.05$, *Ppargc1b*: 2.5-fold, $P < 0.05$, *Sat*: 1.6-fold, $P < 0.05$) compared with that of untreated mice, whereas the mRNA levels of *Cpt1b* just showed a close-to-significant elevation. Importantly, the mRNA levels of *Mfn2* were up-regulated in scWAT of mice receiving a NAM HD, suggesting enhanced mitochondrial biogenesis in this tissue.

	Untreated	NAM LD	NAM HD	P
scWAT				
<i>Ucp1</i>	1.00 (0.45)	1.54 (1.22)	10.46 (8.98)	<0.05
<i>Pparg</i>	1.00 (0.74)	1.15 (0.94)	2.06 (0.97)	0.09
<i>Pgc1a</i>	1.00 (0.80)	2.63 (2.46)	3.03 (1.88)*	<0.05
<i>Ppargc1b</i>	1.00 (0.75)	1.46 (0.83)	2.52 (1.14)*	<0.05
<i>Cpt1a</i>	1.00 (0.77)	1.30 (1.03)	1.29 (0.73)	0.74
<i>Cpt1b</i>	1.00 (1.14)	1.74 (1.42)	2.63 (1.78)	0.07
<i>Mfn2</i>	1.00 (0.37)	3.68 (4.68)	4.29 (3.11)*	<0.05
<i>Sat</i>	1.00 (0.33)	1.08 (0.39)	1.57 (0.60)*	<0.05
BAT				
<i>Ucp1</i>	1.00 (0.33)	1.04 (0.47)	0.75 (0.32)	0.29

<i>Pparg</i>	1.00 (0.43)	1.66 (0.52)	1.26 (0.50)	0.26
<i>Pprgc1b</i>	1.00 (0.66)	1.16 (0.27)	0.81 (0.45)	0.48
<i>Cpt1b</i>	1.00 (0.35)	0.90 (0.49)	1.23 (0.24)	0.31
<i>Cox4</i>	1.00 (0.41)	1.20 (0.18)	0.84 (0.29)	0.17
<i>Mfn2</i>	1.00 (0.65)	1.39 (0.57)	0.99 (0.75)	0.58
<i>Sat</i>	1.00 (0.44)	1.32 (0.26)	1.06 (0.49)	0.36

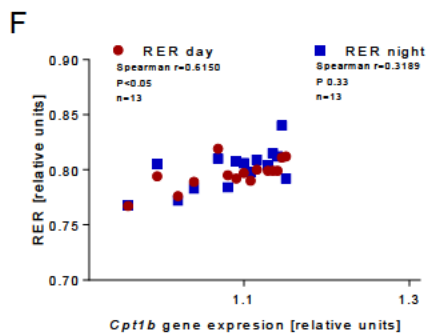
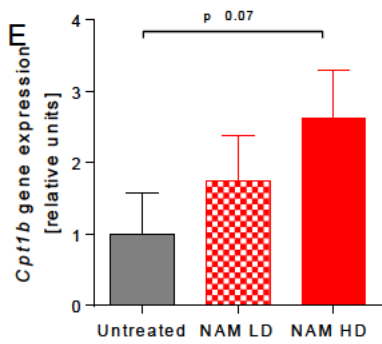
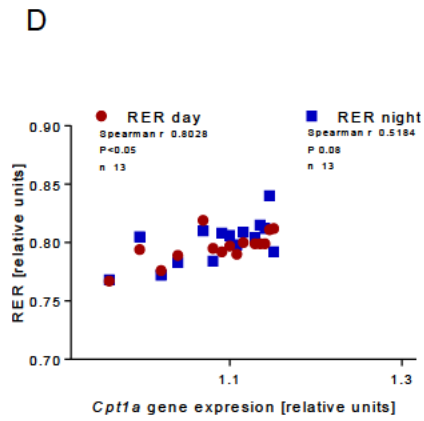
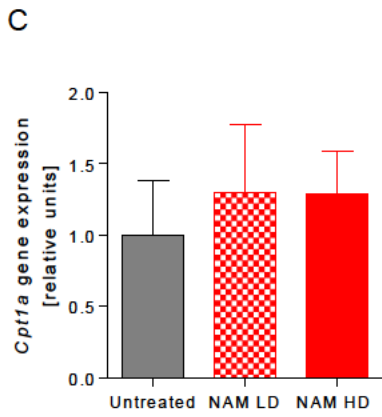
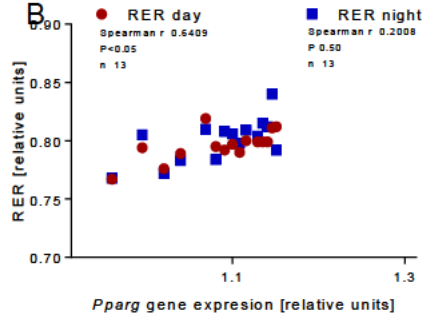
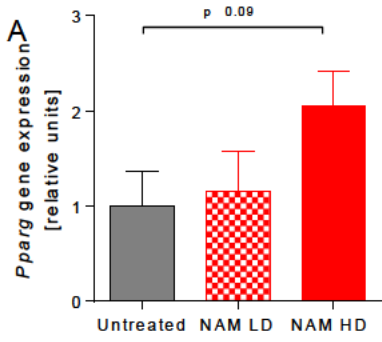
Table 23. Gene expression of molecular targets involved in energy homeostasis and browning of scWAT and iBAT in DIO mice.

Differences between the mean values were assessed by the nonparametric a Kruskal Wallis followed by Dunn's posttest or ANOVA followed a Newman-Keuls posttest, as appropriate. Mice were 5 month-old, fed with a HFD and treated with NAM for 3 consecutive months. Differences were considered significant when $P < 0.05$. Specifically, $*P < 0.05$ vs. untreated group. Data are expressed as mean (SD) (n= 5-6 group). Abbreviations used NAM LD, nicotinamide low dose; NAM HD, nicotinamide high dose.

The relationship between gene expression and RER was calculated in all gene targets, regardless if they were significantly changed or not. Only those showing significant correlation were shown.

Interestingly, RER showed a direct relationship with the gene expression of *Pparg*, *Cpt1a*, *Cpt1b*, and *Mfn2*, targets involved in browning and mitochondrial biogenesis (Figure 66).

On the other hand, the gene expression in iBAT of *Ucp1*, *Pparg*, *Pgc1a*, *Pprgc1b*, as well as *Cpt1b*, *Cox4*, *Mfn2* and *Sat*, did not differ among groups (Table 23).



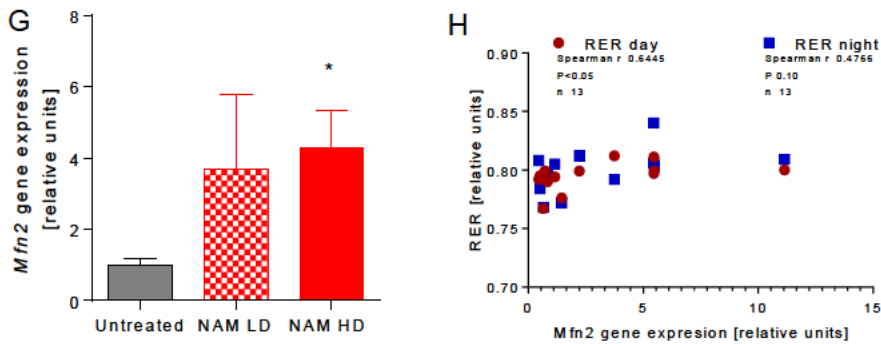


Figure 66. Relationship mRNA levels of browning and mitochondrial targets with RER in scWAT of DIO mice.

(A) Gene expression of *Pparg* in scWAT. (B) mRNA *Pparg* directly correlated with RER, but only during day. (C) Gene expression of *Cpt1a* in scWAT. (D) mRNA *Pparg* directly correlated with RER, but only during day and close-to-significant during night. (E) Gene expression of *Cpt1b* in scWAT. (F) mRNA *Cpt1b* directly correlated with RER, but only during day. (G) Gene expression of *Mfn2* in scWAT. (H) mRNA *Mfn2* directly correlated with RER during day and night periods. Mice were 5-month-old and treated with NAM for 3 consecutive months. A non-parametric Spearman test was used to analyze whether these parameters were correlated. Abbreviations used: RER, respiratory exchange ratio; *Mfn2*, gene that encodes mitofusin 2.

4.4.3b Obesity-related inflammation

The obese phenotype is generally accompanied by an increased inflammation in white adipose tissue [312]. Histological analysis of eWAT revealed the presence of characteristic crown-like structures (CLS) in untreated mice fed a HFD (Figure 67). Of note, the number of these structures was significantly diminished in eWAT from NAM HD-treated mice (Figure 67) (300 ± 30 CLS/10000 adipocytes in untreated mice in contrast with 45 ± 8 CLS/10000 adipocytes of NAM-HD-treated mice ($n=5$ fields/5 mice per group)) ($\sim 85\%$, $P<0.05$). Consistent with this view, two gene markers of macrophage infiltration were found significantly reduced in eWAT (*Cd68*: $\sim 40\%$, $P<0.05$, *Ucp2*: $\sim 45\%$, $P<0.05$) in NAM HD-treated mice compared with untreated mice (Table 24). Of note, *Il10* was significantly up-regulated (2.7-fold, $P<0.05$) in eWAT from NAM HD-treated mice compared with untreated mice. A close-to-significant trend was found in the case of *Tnfa*. Overall, these data might be revealing an anti-inflammatory effect by NAM in WAT of treated mice.

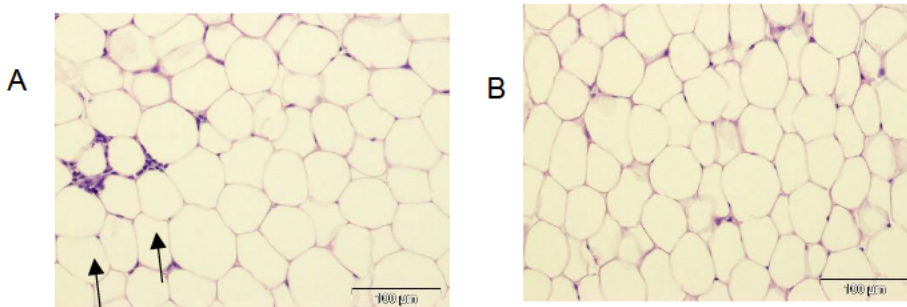


Figure 67. Effect NAM over crown-like structures (CLS) on eWAT in DIO mice. Representative histological sections of eWAT stained with hematoxylin/eosin from mice fed a HFD. (A) Representative eWAT from an untreated mice. (B) Representative eWAT from NAM HD-treated mice. Mice were 5 month-old, fed with a HFD and treated with NAM for 3 consecutive months.

	Untreated	NAM LD	NAM HD	P
eWAT				
<i>Tnfa</i>	1.00 (0.19)	0.83 (0.47)	0.78 (0.44)	0.12
<i>Cd68</i>	1.00 (0.46)	1.12 (0.34)†	0.58 (0.09)*	<0.05
<i>Ucp2</i>	1.00 (0.24)	nd.	0.56 (0.11)*	<0.05
<i>Il10</i>	1.00 (0.32)	1.23 (0.78)	2.73 (0.83)*	<0.05

Table 24. Gene expression of molecular targets involved in macrophages infiltration and inflammation in DIO mice.

Differences between the mean values were assessed by the nonparametric a Kruskal Wallis followed by Dunn's posttest or ANOVA followed a Newman-Keuls posttest, as appropriate. Mice were 5 month-old, fed with a HFD and treated with NAM for 3 consecutive months. Differences were considered significant when $P < 0.05$. Specifically, * $P < 0.05$ vs. untreated group. Data are expressed as mean \pm SEM (n= 5-6 group). Abbreviations used NAM LD, nicotinamide low dose; NAM HD, nicotinamide high dose.

In order to dissect further the effect of NAM over inflammatory phenotype produced by obesity, plasma levels of pro- and anti-inflammatory cytokines were measured. A close-to-significant increase in the anti-inflammatory IL-10 (Figure 68, panel A) was found. Similarly, plasma levels of pro-inflammatory *Tnfa*, IL-6 and IL-4 showed a trend, though not significant, to be higher in NAM-treated mice compared with untreated mice (Figure 68, panel B, C and D).

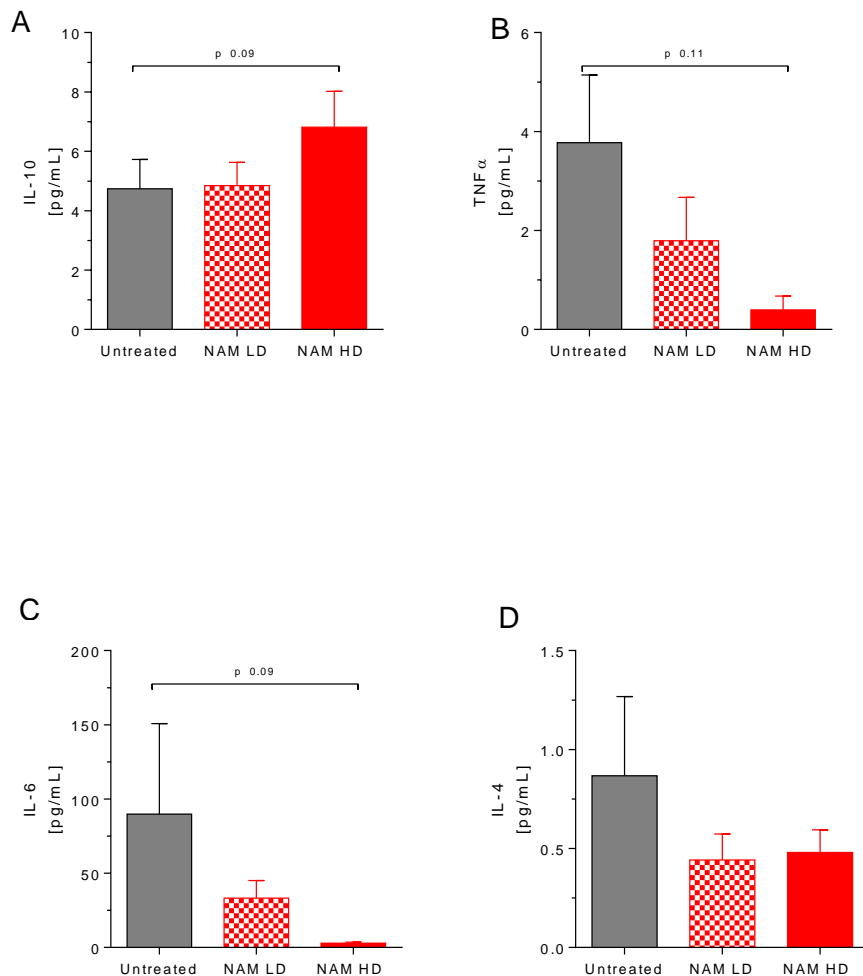


Figure 68. Evaluation of plasma cytokines associated with inflammation in DIO mice.

Plasma levels of (A) IL-10, (B) Tnfa, (C) IL-6 and (D) IL-4. Data are expressed as mean \pm SEM (n= 5-6 group). Mice were 5 month-old, fed with a HFD and treated with NAM for 3 consecutive months. Differences between the mean values were assessed by the nonparametric a Kruskal Wallis followed by Dunn's posttest or ANOVA followed a Newman-Keuls posttest, as appropriate. Differences were considered significant when $P < 0.05$. Abbreviations used NAM LD, nicotinamide low dose; NAM HD, nicotinamide high dose.

▶ 4.5 Effect of NAM-treated ApoE-deficient mice on chronic inflammation: Atherosclerosis

Previous published data indicated a favorable effect by NAM in the amelioration of systemic and adipose-tissue inflammation. In this order, in our last set of experiments, we wanted to demonstrate the effect on inflammation of NAM in ApoE-deficient mice. This chapter includes 13 figures and 7 tables.

4.5.1 Inflammation analysis *in vitro*

Compelling evidence suggests that NAM may have an anti-inflammatory effect in cultured macrophages [290], which is a cell type frequently associated with vascular inflammation. To directly replicate these results, we incubated J774A.1 macrophages with different NAM doses, and found a dose-response effect, when we evaluated the gene expression of a representative pro-inflammatory marker, i.e., *Tnfa* (Figure 69).

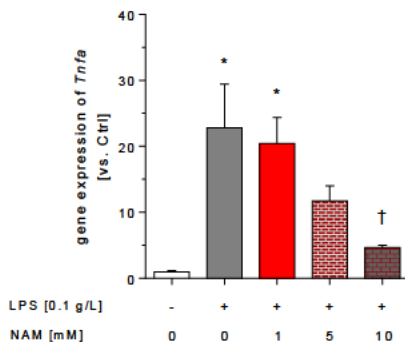


Figure 69. Gene expression of an inflammation target in an *in vitro* assay. J774A.1 macrophages incubated for 24h with doses of NAM. Data are expressed as mean \pm SEM (n= 5-6 group). Abbreviations used NAM, nicotinamide; LPS, Lipopolysaccharide.

In the following sections, the impact of different doses of NAM were checked to directly assess their impact on the development of atherosclerosis in Apo E-deficient mice. Similar to the studies made with DIO mice, a 25% of the highest dose (NAM LD) was used to also dissect the potential effect of lower doses of NAM on atherosclerosis.

4.5.2 Gross parameters and systemic phenotype

The impact of NAM on body weight changes were monitored weekly. Even though, the term of treatment in this case was shorter (1 month), the results obtained were similar to DIO mice (treated for 3 months) and the data reported in the previous section with the same mouse genotype, NAM administration prevented body weight gain (Figure 70, panel A). At necropsy, this finding was mainly attributed to the fact that NAM-treated mice, at the highest dose, accumulated less adiposity than untreated mice (Figure 70). The lower dose of NAM was not effective in preventing weight gain or adiposity as the highest dose (Figure 70, panel A and B). No significant changes were observed in the liver weight among groups (Figure 70, panel B). Overall, our data revealed a significant reduction only in different regional fat pads.

Interestingly, and compared with untreated mice, the treatment of mice with NAM HD also led to a reduction in the lean weight in these mice (Table 25). This result was consistent with previous data showing the same effect of NAM HD in the lean weight in DIO mice (section 4.2.3a). The liver weight and liver-to-body weight ratio did not differ among groups (Table 25).

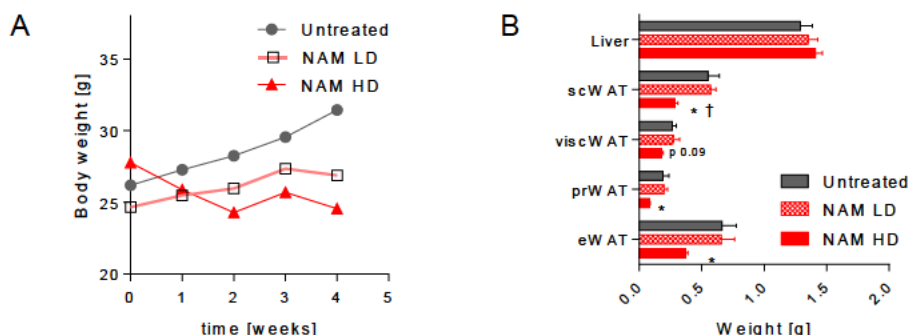


Figure 70. Effect of vitamin B3 forms on gross parameters in ApoE-deficient mice.

(A) Body weight and (B) tissue weight of 3 month-old mice, challenged with a HFD and treated with NAM-NA for 1 month. (n= 8 mice per group). Differences between the mean values were assessed by the nonparametric a Kruskal Wallis followed by Dunn's posttest or ANOVA followed a Newman-Keuls posttest, as appropriate. Differences were considered significant when $P < 0.05$. Specifically, * $P < 0.05$ vs. untreated group. Abbreviations used: eWAT, epididymal white adipose tissue; prWAT, peri-renal white adipose tissue; viscWAT, visceral white adipose tissue; scWAT, subcutaneous white adipose tissue; NAM, nicotinamide.

	Untreated	NAM LD	NAM HD	p
<i>Gross parameters</i>				
Body weight [g]	29.59 (1.72)	30.35 (1.21)	26.58 (1.46)	< 0.05
Final weight gain [g]	4.27 (1.26)	2.55 (0.79)†	-2.06 (3.20)*	<0.05
Fat Pad [g]	1.57 (0.53)	1.70 (0.45)†	0.92 (0.06)*	<0.05
Lean Weight [g]	28.02 (1.24)	28.65 (0.83)†	25.67 (1.44)*	<0.05
Liver weight [g]	1.31 (0.18)	1.35 (0.16)	1.41 (0.14)	0.57
Liver-to-body weight ratio	0.04 (0.00)	0.04 (0.00)	0.04 (0.00)	0.06
Diet intake [g/day]	3.00 (0.79)	2.85 (0.19)	2.78 (0.23)	0.54
Water intake [g/day]	3.82 (0.75)	4.51 (0.86)	4.37 (0.97)	0.11
Calculated dose [g/kg/day]	-	0.48 (0.12)	1.62 (0.25)	

Table 25. Effect of NAM on gross parameters in ApoE-deficient mice.

Results are expressed as the means (SD) (n=8-12 mice per group). All analyses were made at three months of age. Mice were 3 month-old, fed with a HFD and treated with NAM for 1 month. Food intake was measured at the end of the study as described in the Materials and Methods section. Differences between the mean values were assessed by the nonparametric a Kruskal Wallis followed by Dunn's posttest or ANOVA followed a Newman-Keuls posttest, as appropriate; differences were considered significant when P<0.05. Specifically, * P<0.05 vs. untreated group; or † P<0.05 vs. NAM-treated mice. Abbreviations used: NAM LD, nicotinamide low dose; NAM HD; nicotinamide high dose.

4.5.2a Biochemical parameters

Compared with untreated mice, NAM levels were significantly elevated (55-fold, $P < 0.05$) in NAM-treated groups, displaying a dose-dependent shape (Figure 71, panel A). Consistently, me-NAM was also elevated in NAM HD-treated mice (3.5-fold, $P < 0.05$) compared with untreated mice (Figure 71, panel B).

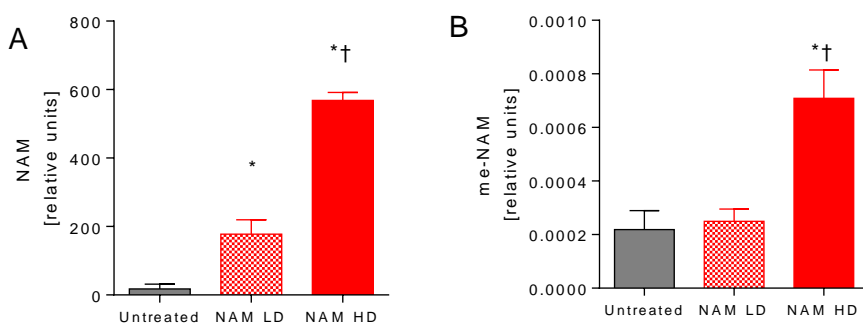


Figure 71. NAM and its methylated form (me-NAM) displayed a dose-dependent shape in plasma in ApoE-deficient mice.

(A) NAM concentration (relative units) in plasma (B) me-NAM concentration (relative units) in plasma. ($n = 5-6$ mice per group). Mice were 3 month-old, fed with a HFD and treated with NAM for 1 month. Differences between the mean values were assessed by the nonparametric a Kruskal Wallis followed by Dunn's posttest or ANOVA followed a Newman-Keuls posttest, as appropriate. Differences were considered significant when $P < 0.05$. Specifically, * $P < 0.05$ vs. untreated group or † $P < 0.05$ vs. NAM-treated mice. Abbreviations used: NAM LD, nicotinamide low dose; NAM HD, nicotinamide high dose.

NAM treatment unexpectedly increased total cholesterol levels (1.8-fold, $P < 0.05$) exclusively due to elevations in the non-HDL fraction (Table 26). Consistently, total triglycerides levels were also moderately elevated in NAM HD-treated mice (Table 26). Of note, plasma cholesterol levels were also found elevated (1.5-fold, $P < 0.05$), in the mice receiving a low dose of NAM. HDL-cholesterol levels did not differ among groups.

Plasma glucose levels were not changed in NAM-treated mice, regardless the dose, compared with untreated mice.

	untreated	NAM LD	NAM HD	P
Glucose [mM]	12.85 (2.74)	10.69 (1.62)	10.52 (3.32)	0.12
Insulin [μ g/L]	0.69 (0.09)	<i>nd</i>	0.66 (0.06)	0.34
Triglycerides [mM]	1.19 (0.77)	1.80 (0.59)*	1.65 (0.53)*	<0.05
Total cholesterol [mM]	38.74 (5.02)	47.11 (6.84)	71.25 (13.39)*	<0.05
HDL cholesterol [mM]	0.38 (0.17)	0.36 (0.05)	0.35 (0.23)	0.91
Non-HDL cholesterol [mM]	38.36 (7.38)	46.75 (6.85)	70.90 (6.88)*	<0.05

Table 26. Effect of NAM on plasma biochemical parameters in ApoE-deficient mice.

Results are expressed as the means (SD) (n=8 mice per group). All analyses were made at 3 month-old mice, fed with a HFD and treated with NAM for 1 month. Fasting plasma levels of the HDL fractions were determined in the plasma supernatants after precipitating with phosphotungstic acid (Roche); the non-HDL fraction was calculated by subtracting the HDL moiety to the total plasma. The biochemical measurement was made by commercial kits adapted to a COBAS autoanalyzer. Differences between the mean values were assessed by the nonparametric a Kruskal Wallis followed by Dunn's posttest or ANOVA followed a Newman-Keuls posttest, as appropriate; differences were considered significant when $P < 0.05$. Specifically, * $P < 0.05$ vs. untreated group; or † $P < 0.05$ vs. NAM-treated mice. Abbreviations used: HDL, high-density lipoprotein; NAM LD, nicotinamide low dose; NAM HD; nicotinamide high dose.

4.5.2b Non-HDL metabolism

The analysis of plasma non-HDL particles did not reveal changes in their composition among groups of mice (Table 27).

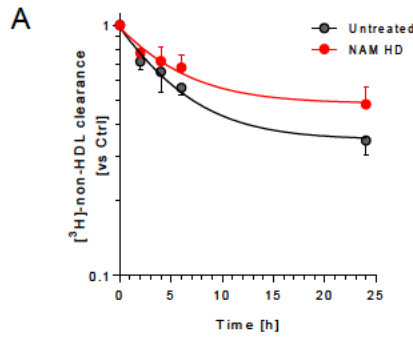
	Free cholesterol [%]	Esterified cholesterol [%]	Triglyceride [%]	Phospholipid [%]	Protein [%]
Untreated	19.9	47.3	2.4	22.0	8.4
NAM LD	20.4	49.4	2.5	20.6	7.1
NAM HD	22.4	46.2	2.2	21.9	7.4

Table 27. Effect of NAM on the relative composition of non-HDL particles of ApoE-deficient mice.

Values shown are relative values for each components of non-HDL isolated by ultracentrifugation from fasting plasma of NAM-treated and untreated mice. A single pool composed of three mice per condition was used. Abbreviations used: NAM LD, nicotinamide low dose; NAM HD; nicotinamide high dose.

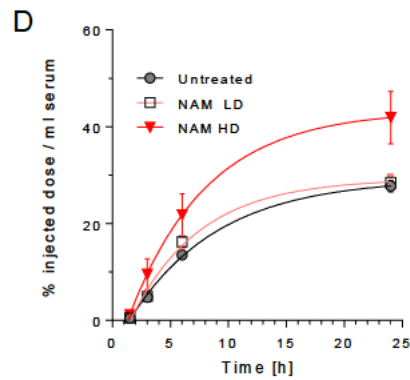
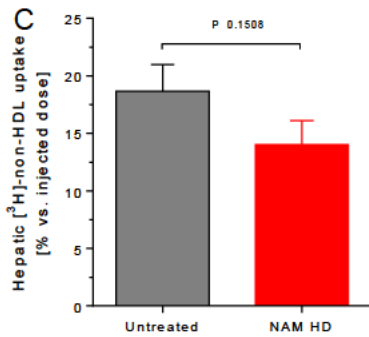
Kinetic analysis of non-HDL revealed that their clearance was significantly delayed in mice treated with NAM HD (FCR: 16%, $P < 0.05$) compared with untreated mice (Figure 72, panel A and B). As non-HDL is mainly cleared by the liver was also analyzed the relative amount of radiotracer in the livers of i.v. injected mice. Of note, the relative content in [^3H]-tracer showed a trend, though not significant, to be decreased in the livers of NAM-treated mice compared with untreated mice (Figure 72, panel C). This finding was further confirmed in an independent experimental whereby mice were oral gavaged with [^3H]-cholesterol and its distribution into plasma and liver analyzed. Relative levels of radiotracer in plasma further suggested that circulating non-HDL cholesterol clearance might be defective in NAM-treated mice (Figure 72, panel D and E). Consistent with this observation, the relative levels of radiotracer in the livers, were significantly reduced in NAM-treated mice compared with those of untreated mice (Figure 72, panel F). The latter was not associated with changes in the

gene expression of hepatic lipoprotein receptors (Table 28), mainly involved in the clearance of non-HDL, possibly indicating the participation of post transcriptional mechanisms in particular, NAM mediated effects on non HDL particles.



B

	untreated	NAM HD	p
FCR [h⁻¹]	0.080 ± 0.003	0.067 ± 0.003	<0.05
Synthesis rate [μmol non-HDL-C x g⁻¹ x h⁻¹]	0.108 ± 0.005	0.096 ± 0.005	0.10



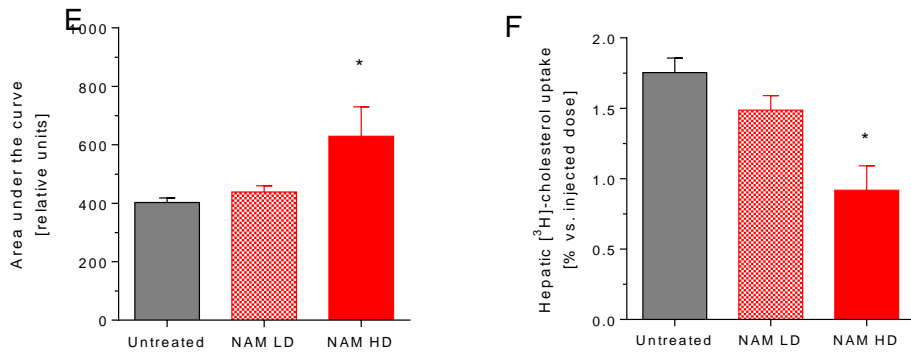


Figure 72. Effect of NAM on metabolic fate of non-HDL lipoproteins in plasma in ApoE-deficient mice.

Panels (A), (B) and (C). In vivo kinetics of [³H]-cholesterol oleoyl ether non-HDL in plasma (A-B) and liver (C). Autologous [³H]-cholesterol oleoyl ether non-HDL were injected intravenously into fasted mice. The amounts of radioactivity remaining in the plasma (expressed as the average percentage \pm SEM, n= 5-6 mice) were indicated at the indicated times after injection. (B) Fractional catabolic rate (FCR) and synthetic rates of the different mouse groups. Panels (D) and (E). Oral fat gavage (OFG) assays in NAM-treated and untreated mice. (D) An olive oil-based emulsion containing radiolabeled [³H]-cholesterol was prepared and oral gavaged into KOE mice. Radiolabeled [³H]-cholesterol was, respectively, measured in plasma ((D) Area under the curve of results expressed in graph (E)) and in the liver (F) after a single bolus of 200 μ L of radiolabeled olive oil-based emulsion (20 μ Ci per mouse) at the times indicated. Results are expressed as the average percentage vs. injected dose \pm SEM of individual animals (n=5 mice at each time point). * P <0.05 compared with the untreated group. Inset: area under the curve of [³H]-cholesterol non-HDL after the OFG of the different mouse groups. Each data represents the mean \pm SEM of 5 mice. Mice were 3 month-old, fed with a HFD and treated with NAM for 1 month

	Untreated	NAM LD	NAM HD	P
<i>Ldlr</i>	1.0 ± 0.3	1.3 ± 0.6	1.2 ± 0.3	0.76
<i>Lrp1</i>	1.0 ± 0.3	1.7 ± 0.4	1.3 ± 0.4	0.46
<i>Lrpap1</i>	1.0 ± 0.1	1.3 ± 0.4	1.1 ± 0.1	0.67
<i>Vldlr</i>	1.0 ± 0.3	0.9 ± 0.5	1.3 ± 0.6	0.91
<i>Scarb1</i>	1.0 ± 0.2	0.7 ± 0.1	1.2 ± 0.1 †	0.77

Table 28. Hepatic gene expression profile of molecular targets involved in non-HDL clearance in ApoE-deficient mice.

Results are expressed as the means ± standard deviation (n=5 mice per group). The signal of Ctrl mice was set at a normalized value of 1 arbitrary unit. Mice were 3 month-old, fed with a HFD and treated with NAM for 1 month. Differences between the mean values were assessed by the nonparametric a Kruskal Wallis followed by Dunn's posttest or ANOVA followed a Newman-Keuls posttest, as appropriate; differences were considered significant when P<0.05. Specifically, * P<0.05 vs. untreated group; or † P<0.05 vs. low-dose, NAM-treated mice. Abbreviations used: Un, untreated mice; Lo, low-dose, NAM-treated mice; Hi, high-dose, NAM-treated mice.

4.5.2c Anti-oxidative function of lipoproteins

Oxidative stress is regarded as one of the driving mechanisms involved in the development of aortic atherosclerosis. The susceptibility to oxidation of non-HDL particles, as measured by conjugated diens formation, was delayed in NAM HD-treated mice. (Figure 73, panels A and B). However, the NAM-mediated protection against oxidation of non-HDL was not observed in lipoproteins isolated from NAM LD-treated mice.

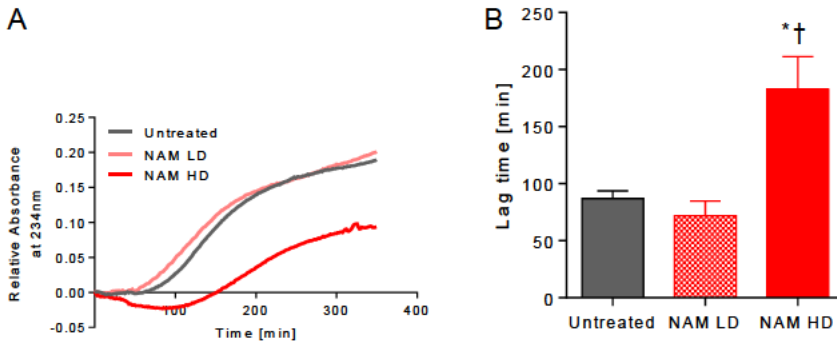


Figure 73. Atheroprotective property of non-HDL particles of ApoE-deficient mice.

(A) Oxidation curves of non- HDL particles of Apo E deficient mice. (B) Lag time of oxidation curves. Mice were 3 month-old, fed with a HFD and treated with NAM for 1 month. (n= 3-4 plasma pools/group). Differences between the mean values were assessed by the nonparametric a Kruskal Wallis followed by Dunn's posttest or ANOVA followed a Newman-Keuls posttest, as appropriate. Differences were considered significant when $P < 0.05$. Specifically, * $P < 0.05$ vs. untreated group. Abbreviations used: NAM, nicotinamide; NA, nicotinic acid.

To assess if there was a direct antioxidant effect of NAM over non-HDL particles, human LDL were incubated with three concentrations of NAM (i.e., 0.1-1.0-2.0 mM) NAM protected these lipoproteins from oxidation at 1.0 mM concentration (Figure 74). In the graph, the maximum velocity was calculated (V_{max}) revealing an improvement showing a dose- response to oxidation (LDL alone: 0.71 mOD/min; LDL+ NAM 0.10mM: 0.71 mOD/min; LDL+ NAM 1.0mM: 0.55 mOD/min; LDL+ NAM 2.mM: 0.28 mOD/min).

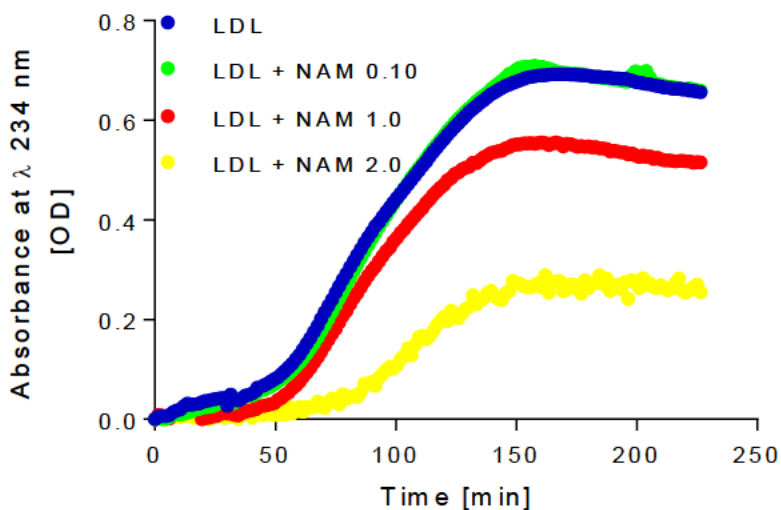


Figure 74. Antioxidant activity of LDL particles of human plasma incubated with different concentrations of NAM

Oxidation curves of human LDL, incubated at NAM concentration 0.10 mM and 1.0 mM. This experiment was replicated twice with similar outcome.

The analysis of relative mRNA levels of gene markers of oxidative stress and inflammation revealed a potentially favorable induction in the relative gene expression of the anti-oxidant *Hmox1* in the liver of NAM HD-treated mice (Table 29).

	Untreated	NAM LD	NAM HD	P
Liver				
<i>Hmox1</i>	1.00 (0.25)	1.15 (0.52)	2.17 (0.94)*	<0.05
<i>Sod2</i>	1.00 (0.31)	0.74 (0.10)	1.22 (0.39)	0.18
<i>Cybb</i>	1.00 (0.26)	0.92 (0.24)	1.15 (0.69)	0.94
eWAT				
<i>Hmox1</i>	1.00 (0.39)	0.76 (0.25)	0.96 (0.04)	0.44
<i>Sod2</i>	1.00 (0.19)	5.73 (2.06)*	4.56 (5.92)*	<0.05
<i>Cybb</i>	1.00 (0.36)	1.63 (0.81)	1.48 (0.55)	0.09
<i>Cd68</i>	1.00 (0.37)	1.36 (0.51)	1.31 (0.93)	0.40
<i>Il10</i>	1.00 (0.66)	4.19 (4.51)	4.25 (3.62)	0.06
Aorta				
<i>Hmox1</i>	1.00 (0.21)	1.51 (0.73)	0.85 (0.27)	0.37
<i>Sod2</i>	1.00 (0.45)	1.17 (0.67)	0.83 (0.92)	0.58
<i>Cybb</i>	1.00 (0.62)	2.67 (1.32)	4.53 (1.64)	0.10
<i>Il10</i>	1.00 (0.81)	0.74 (0.38)	2.95 (2.22)*	<0.05

Table 29. Gene expression of molecular targets involved in oxidation and inflammatory properties in liver, eWAT and aorta of ApoE-deficient mice

Mice were 3 month-old, fed with a HFD and treated with NAM for 1 month. Differences between the mean values were assessed by the nonparametric a Kruskal Wallis followed by Dunn's posttest or ANOVA followed a Newman-Keuls posttest, as appropriate. Differences were considered significant when $P < 0.05$. Specifically, * $P < 0.05$ vs. untreated group. Data are expressed as mean (SD) ($n = 5-6$ group). Abbreviations used NAM LD, nicotinamide low dose; NAM HD, nicotinamide high dose.

On the other hand, the relative mRNA levels of the antioxidant *Sod2* was significantly upregulated in the eWAT of NAM LD-treated mice (~6-fold, $P < 0.05$) and NAM HD-treated mice (~5-fold, $P < 0.05$) compared with untreated mice. Importantly, *I110* relative mRNA levels was elevated in the aorta of NAM HD-treated mice compared with untreated mice.

The relative content of hepatic mRNA of molecular determinants of NAM metabolism revealed a significant down-regulation in *Nnmt* only in those mice receiving the highest dose of NAM (Table 30). The gene expression analysis of other molecular targets involved in NAM metabolism were not changed in NAM-treated mice compared with untreated mice.

	Untreated	NAM LD	NAM HD	P
<i>Nnmt</i>	1.00 (0.77)	0.57 (0.16)	0.48 (0.27)*	<0.05
<i>Nampt</i>	1.00 (0.37)	0.84 (0.30)	1.47 (0.80)	0.05
<i>Nmrk1</i>	1.00 (0.53)	0.87 (0.29)	1.20 (0.91)	0.54

Table 30. Gene expression of hepatic molecular targets involved in NAM metabolism of ApoE-deficient mice.

Data are expressed as mean (SD) (n= 5-6 group). Mice were 3 month-old, fed with a HFD and treated with NAM for 1 month. Differences between the mean values were assessed by the nonparametric a Kruskal Wallis followed by Dunn’s posttest or ANOVA followed a Newman-Keuls posttest, as appropriate. Differences were considered significant when $P < 0.05$. Specifically, * $P < 0.05$ vs. untreated group Abbreviations used NAM LD, nicotinamide low dose; NAM HD, nicotinamide high dose.

4.5.2d Histologic and molecular analysis on fatty liver

Consistent with liver weight and liver-to-body weight ratio previously shown in Table 25, none of NAM doses exerted negative effects on plasma indicators of hepatic function (Table 31). Treatment with NAM at highest dose presented with lower liver triglycerides (63%, $P < 0.05$) compared to untreated ones. Plasma levels of ALT were significantly decreased in NAM-treated mice compared with those of untreated mice, whereas no changes were observed in the plasma levels of AST. Morphologic analysis of livers also suggested an improvement in hepatic steatosis in the NAM HD-treated groups (Figure 75).

No changes in kidney function between groups of mice were detected by creatinine measurement.

	Untreated	NAM LD	NAM HD	P
Creatinine [mM]	0.02 (0.01)	0.01 (0.01)	0.01 (0.01)	0.17
AST [U/L]	104.40 (70.65)	107.75 (10.97)	101.50 (58.97)	0.30
ALT [U/L]	21.50 (13.44)	14.50 (1.73)*	15.30 (6.33)*	<0.05
Triglycerides [$\mu\text{mol/liver}$]	28.59 (12.49)	28.47 (5.21)†	10.73 (5.65)*	<0.05

Table 31. Effect of NAM on hepatic and renal parameters in ApoE-deficient mice.

Results are expressed as the means (SD) ($n=8$ mice per group). All analyses were made at 3 month-old mice, fed with a HFD and treated with NAM for 1 month. The biochemical measurement was made from lipid extracts by commercial kits adapted to a COBAS auto analyzer. The data is expressed in relation to g of liver. Differences between the mean values were assessed by the nonparametric a Kruskal Wallis followed by Dunn's posttest or ANOVA followed a Newman-Keuls posttest, as appropriate; differences were considered significant when $P < 0.05$. Specifically, * $P < 0.05$ vs. untreated group; or † $P < 0.05$ vs. NAM-treated mice. Abbreviations used: AST, Aspartate aminotransferase; ALT, Alanine aminotransferase; NAM, nicotinamide; NA, nicotinic acid.

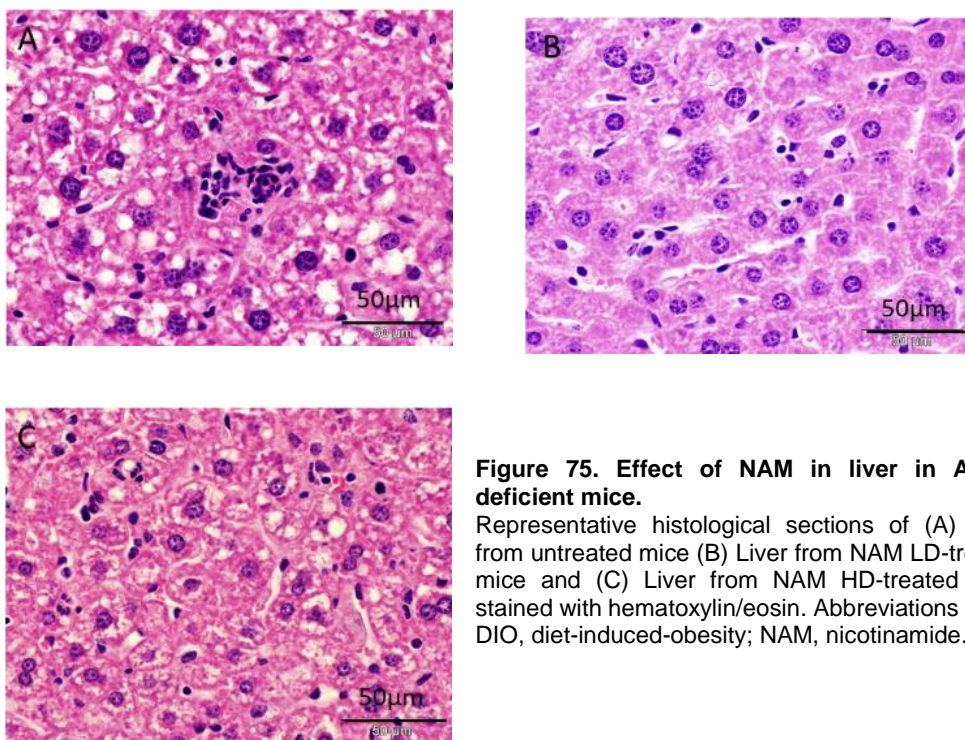


Figure 75. Effect of NAM in liver in ApoE-deficient mice.

Representative histological sections of (A) Liver from untreated mice (B) Liver from NAM LD-treated mice and (C) Liver from NAM HD-treated mice stained with hematoxylin/eosin. Abbreviations used: DIO, diet-induced-obesity; NAM, nicotinamide.

4.5.3 Atherosclerosis development

We next evaluated the impact if any of NAM on this phenotype in ApoE-deficient mice, a mouse model of massive atherosclerosis, as this disease is directly involved in the development of cardiovascular disease, and is sustained by a chronic inflammation mechanism.

Histologic analysis of aortic lesions revealed that NAM-treated mice presented a significantly lower atherosclerotic areas (NAM LD: 0.42-fold, $P < 0.05$; NAM HD: 0.35-fold, $P < 0.05$) than untreated mice, regardless the dose used (Figure 76).

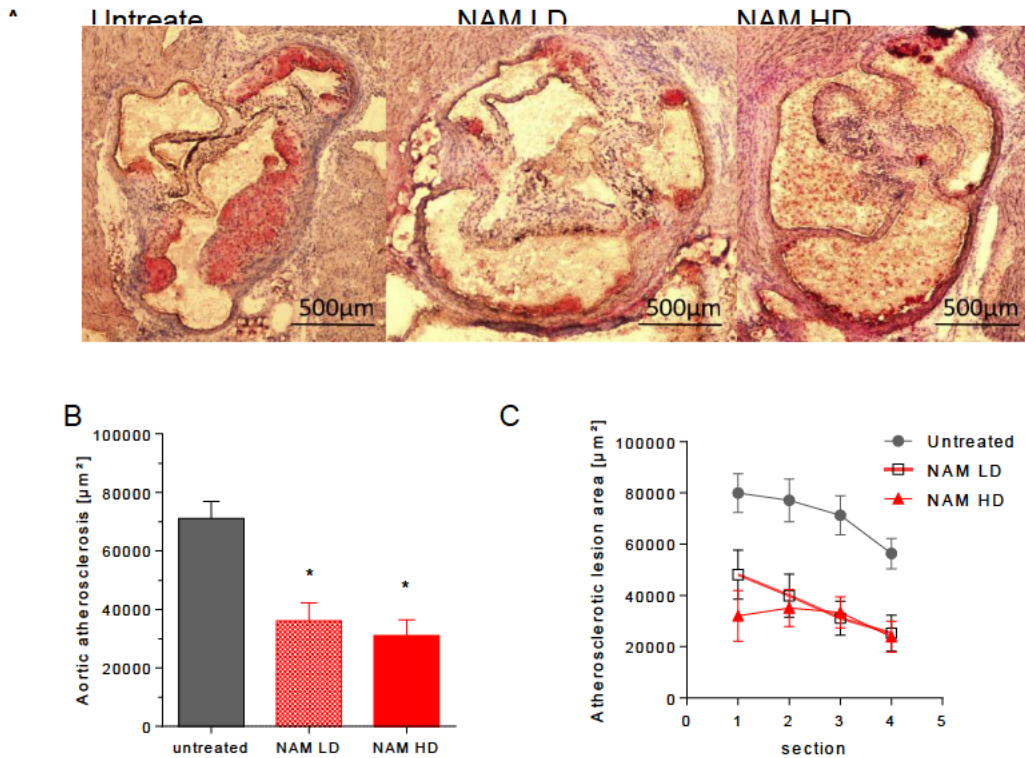


Figure 76. Representative images of proximal aorta of ApoE-deficient mice treated with different doses of NAM for 1 month.

(A) Images of a representative mouse from untreated and NAM stained with Oil Red O. (B) Area of atherosclerotic lesion quantified from 8-10 mice per group. (C) Development of atherosclerotic lesions throughout the aortic sinus of ApoE-deficient mice, the mean of 4 different points, 20 μm apart from each other. The image insets are representative lesions at the 12-week time-point when mice were fed diet. Mice were 3 month-old, fed with a HFD and treated with NAM for 1 month. Differences between the mean values were assessed by the nonparametric a Kruskal Wallis followed by Dunn's posttest or ANOVA followed a Newman-Keuls posttest, as appropriate. Differences were considered significant when $P < 0.05$. Specifically, $*P < 0.05$ vs. untreated group. Abbreviations used: NAM LD, nicotinamide low dose; NAM, nicotinamide high dose.

The atherosclerotic plaque found in proximal aortas, correlated inversely with NAM concentration in plasma (Pearson $r = -0.4043$, $p < 0.05$) (Figure 77)

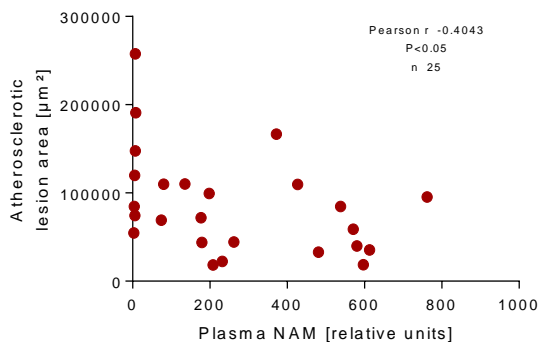


Figure 77. Relationship between circulating plasma NAM levels and atherosclerosis in ApoE-deficient mice.

Inverse correlation between atherosclerotic lesion area and plasmatic NAM concentration. A parametric Pearson test was used to analyze whether these parameters were correlated.

This results were confirmed with female mice, endorsing the data obtained is independent of sex in this animal model (results not shown).

4.5.4 Systemic inflammation markers

Plasma levels of pro- and anti-inflammatory cytokines showed a significant increase in the anti-inflammatory IL-10 (NAM HD: ~6-fold, $P < 0.05$) in NAM HD-treated mice compared with untreated mice (Figure 78, panel A). Similarly, plasma levels of IL-4 showed a trend, though not significant, to be higher in NAM-treated mice compared with untreated mice (Figure 78, panel B) and Tnfa did not show differences among groups (Figure 78, panel C). Cytokines analysis also revealed a close-to-significant trend to be decreased in the plasma levels of IL-6 (Figure 78, panel D). Of note, the reduction in atherosclerotic lesion area

was inversely associated with changes in plasma levels of IL-10 (Figure 78, panel E).

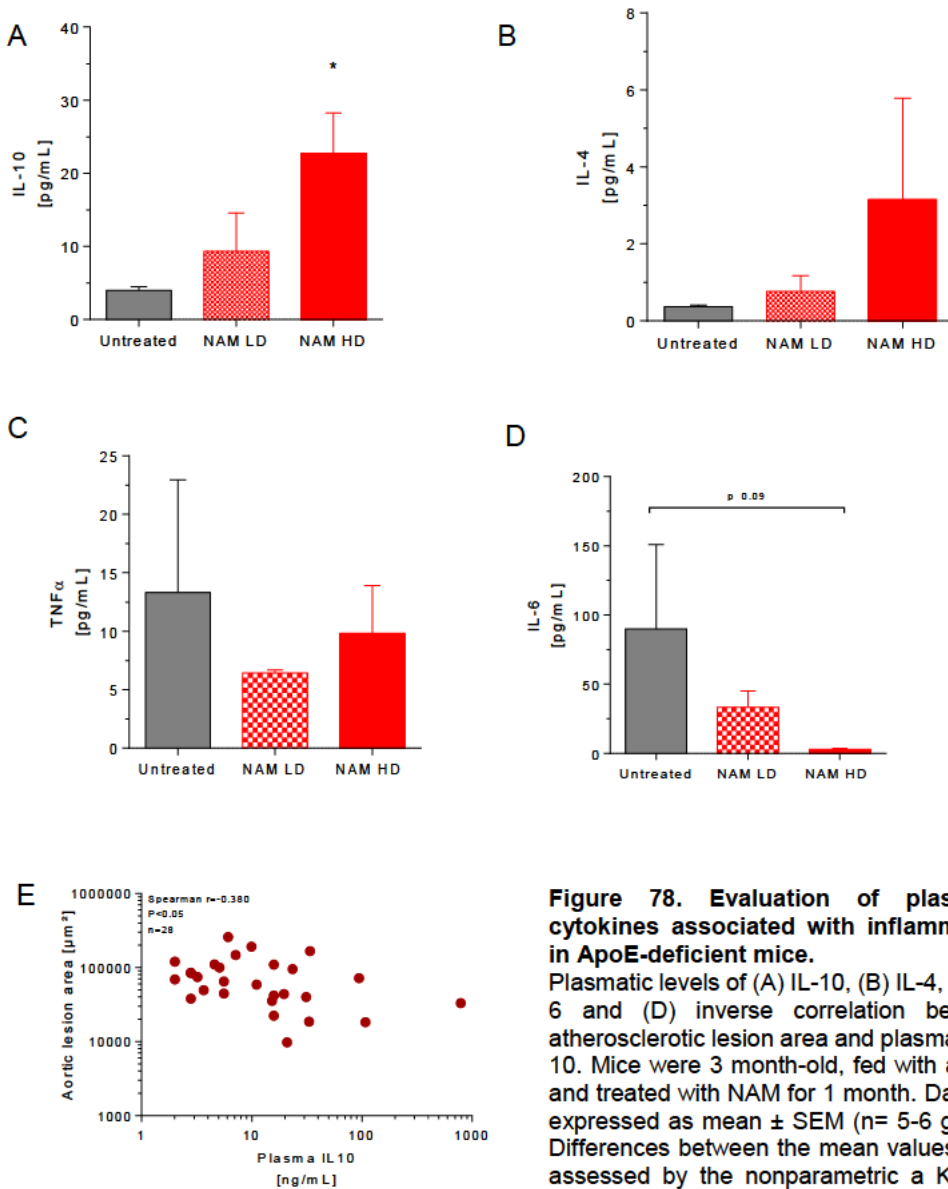


Figure 78. Evaluation of plasmatic cytokines associated with inflammation in ApoE-deficient mice.

Plasmatic levels of (A) IL-10, (B) IL-4, (C) IL-6 and (D) inverse correlation between atherosclerotic lesion area and plasmatic IL-10. Mice were 3 month-old, fed with a HFD and treated with NAM for 1 month. Data are expressed as mean \pm SEM (n= 5-6 group). Differences between the mean values were assessed by the nonparametric a Kruskal Wallis followed by Dunn's posttest or

ANOVA followed a Newman-Keuls posttest, as appropriate. Differences were considered significant when $P < 0.05$. Specifically, $*P < 0.05$ vs. untreated group A non-parametric Spearman test was used to analyze whether these parameters were correlated. Abbreviations used NAM LD, nicotinamide low dose; NAM HD, nicotinamide high dose.

Gene expression analysis revealed a significant elevation in the relative mRNA levels of *Ii10* in aorta of NAM-treated mice compared with that of untreated mice (Fig 79, panel A). *Tnfa* was also measured, revealing no differences among groups (Fig 79, panel B).

Adgre1 gene expression, which encodes the F4/80 phenotype, was measured in thoracoabdominal aortas. No differences were found in this target, likely indicating that the favorable induction in *IL-10* was independent of the number of macrophages present in this tissue (Fig 79, panel C). Interestingly, the relative mRNA levels of *Ii10* were inversely related to aortic atherosclerosis (Fig 79, panel D).

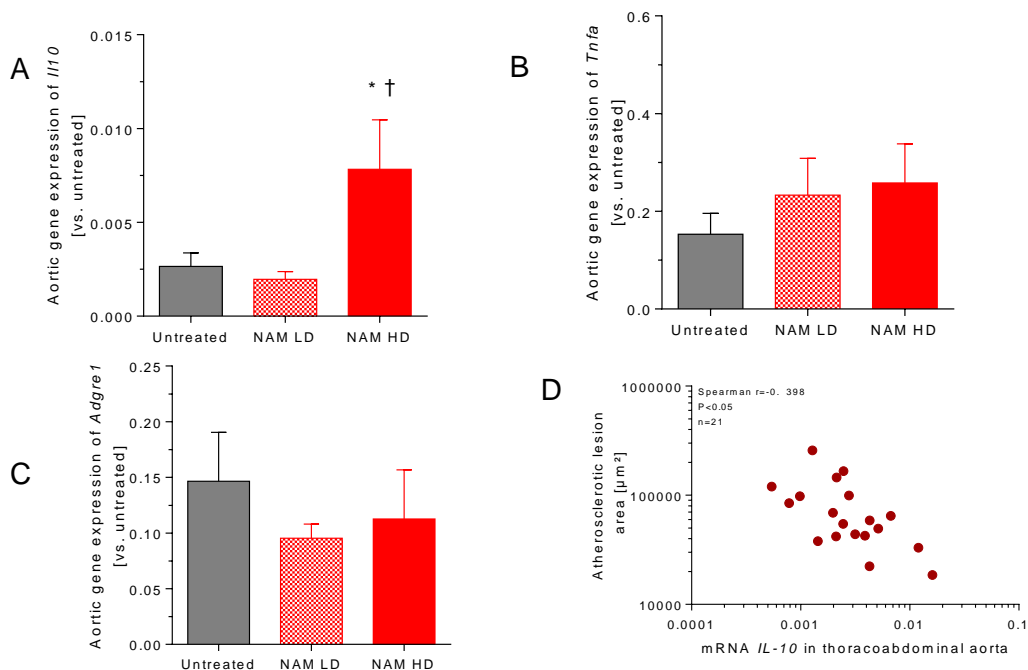


Figure 79. Gene expression in thoracoabdominal aorta determined by real-time PCR analysis in ApoE-deficient mice.

(A) mRNA levels of *Ii10* (B) mRNA levels of *Tnfa* (C) mRNA levels of *Adgre1* encodes the gene F4/80 (D) Inverse correlation between mRNA *Ii10* in thoracoabdominal aorta and atherosclerotic lesion. Mice were 3 month-old, fed with a HFD and treated with NAM for 1 month. Data are expressed as mean \pm SEM (n= 8-12 per group). Differences between the mean values were assessed by the nonparametric a Kruskal Wallis followed by Dunn's posttest or ANOVA followed a Newman-Keuls posttest, as appropriate. Differences were considered significant when $P < 0.05$. Specifically, * $P < 0.05$ vs. untreated group Abbreviations used NAM LD, nicotinamide low dose; NAM HD, nicotinamide high dose.

Immunohistochemical analysis did not show differences on the F4/80 content (Fig 80), thereby confirming that NAM treatment did not influence macrophage infiltration in the proximal aorta.

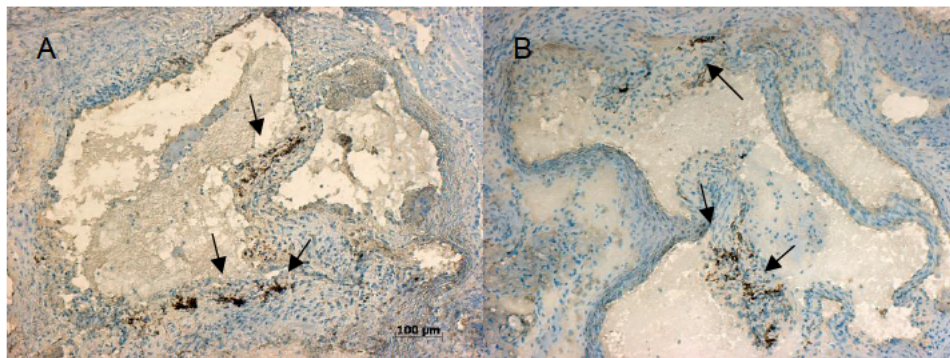


Figure 80. Representative IHQ of F4/80 in thoracoabdominal aortas of ApoE-deficient mice treated and non-treated with NAM.

Images of IHQ of F4/80 of a representative mouse from (A) untreated and (B) NAM-treated mice. n= 2/group. Mice were 3 month-old, fed with a HFD and treated with NAM for 1 month

In thoracoabdominal aorta, other molecular targets, were also measured, including LXR, and some others under LXR regulation. Our data indicates that NAM HD-treated mice promoted *Nr1h2* (encoding for LXRb) (2-fold, $P < 0.05$) without changing *Nr1h3* (encoding for LXRa) (Figure 81). *Abca1* was up-regulated in NAM LD-treated mice (2.1-fold, $P < 0.05$) and in NAM HD-treated mice (2.9-fold, $P < 0.05$), as well *Abcg1* increased in NAM HD-treated mice (3.3-fold, $P < 0.05$). There was a non-significant tendency to increase *Abcg5* (1.5-fold, $P = 0.10$) whereas *Abcg8* was not detected in this tissue (Figure 481).

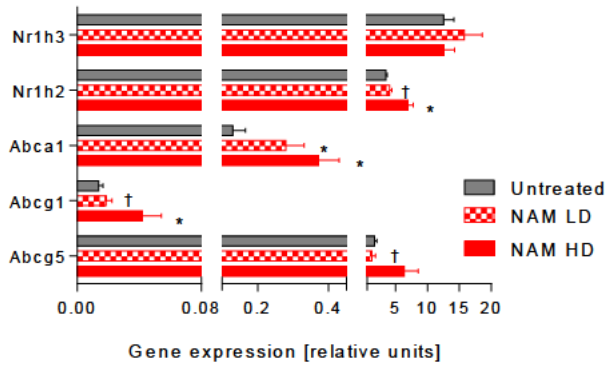


Figure 81. Gene expression of molecular targets regulated by LXR in the thoracoabdominal aorta of ApoE-deficient mice.

Data are expressed as mean \pm SEM (n= 7-10 per group). Mice were 3 month-old, fed with a HFD and treated with NAM for 1 month. Differences between the mean values were assessed by the nonparametric a Kruskal Wallis followed by Dunn's posttest or ANOVA followed a Newman-Keuls posttest, as appropriate. Differences were considered significant when $P < 0.05$. Specifically, * $P < 0.05$ vs. untreated group or † $P < 0.05$ vs. NAM-treated mice. Abbreviations used NAM LD, nicotinamide low dose; NAM HD, nicotinamide high dose.

• 5. DISCUSSION

▶ 5.1 Determination of oral dose of NAM to mice

The term vitamin B₃ comprises the two main water-soluble forms NA and NAM. Both vitamin forms are very stable either in solution or pelleted [334]. Additionally, both are well-absorbed when taken orally. In this work, vitamin supplementation was accomplished by providing the mice with drinking water containing NAM or NA at concentrations equal or lower than 1% (g/mL). These molecules were completely dissolved in the drinking water and given first to mice to establish a safety range of NAM concentrations. NAM is generally unpalatable when taken in solution and therefore is usually given in capsules or in tablet form [335]. In our study, no differences in water consumption were observed among groups at the different doses assayed. The same was observed for its acid partner, NA. Short-term administration at the assayed NAM concentrations in drinking water brought out an effect on the body weight of mice treated at the highest dose of NAM. Food consumption did not differ in mice receiving NAM as seen in other series of experiments in this work.

NAM and NA have been used at elevated doses in the intended use for treatment of a variety of disorders [335]. The pharmacokinetics of NAM is strongly dependent on dose, species, sex and route of treatment [335] and its safety has been assessed in different toxicity studies [336, 337]. In general, NAM intake has been found to have low toxicity in both short- and long-term studies [246, 270]. In relation to the impact of NAM on body weight, in previous studies, long-term, parenteral (i.e., intraperitoneal) rats receiving doses of NAM up to 0.6 g/kg/day were reported to have lower weight gain [272]. This effect was mainly explained by food intake suppression. No effect on the body weight or food intake was found in rats made obese with a HFD [231]. Of note, in the latter

study, dosed NAM was lower (maximal dose assayed at 0.1 g/kg/day) and thus, at least partly, this might explain the lack of effect of NAM in treated rats.

As daily parenteral administration of NAM may exert potential metabolic distress or toxic effects, most studies evaluated the impact on phenotype by supplying NAM to the drinking water or diet on a preventive mode.

In our study, NAM was supplied in drinking water from the beginning of the study. NAM intake was not concomitantly associated with undesirable effects in mice at the highest concentration tested (1%) (0.8 g/kg/day). Indeed, it did not produce signs of hepato- or renotoxicity in treated mice, as revealed by the plasma liver enzymes or creatinine, respectively. Liver weights in NAM-treated mice were concomitantly and proportionally diminished in parallel to the body weight reduction, as revealed by the liver-to-body weight ratio. Moreover, NAM treatment did not influence insulin function, as revealed by the functional analysis of glucose metabolism.

A three months administration of 1% NAM in drinking water significantly prevented body weight gain to a similar extent in either mice fed a RD or made obese with a HFD (RD cohort: 30.5%, Table 4; DIO cohort: 69%, Table 9), being this mainly attributed to a marked decrease in fat pad accumulation. Importantly, such body weight prevention was not due to differences in food intake among groups. Intriguingly, this effect was not previously reported using mice with a different background (i.e., NOD mice) receiving the same dose either in chow diet [246, 338] or drinking water [246]. In contrast, weight gain was found reduced in rats treated with NAM supplied in the diet [338-340]. Particularly, a marked inhibition of weight gain has also been reported in rats fed with NAM at a concentration of 0.4% [338] and up to 1% [339] supplied in the diet. Consistent

with this view, rats dosed with ~0.215 and 1 g/kg/day of NAM supplied in the diet showed significant reductions in both the body weight [340], being this phenotype partly explained by a decreased food intake. Of note, high-dose, NAM-treated rats displayed a mild liver enlargement as well as in some liver enzymes. However, the administration of NAM to other species (i.e., rabbits and guinea-pigs) does not exert such kind of influence on body weight [341]. Taken together, these data show that the effect of NAM on the body weight is rather controversial and may be species-specific.

In previous studies, the oral dose of NAM was established at 1.0% to evaluate the anti-diabetic properties of this form of vitamin B₃ [335]. The impact of higher doses than 1% was also evaluated in mice (i.e., 2.5% and 5%, Table 3). Our study also revealed that weight gain prevention was much more exacerbated when the mice were treated with doses of NAM higher than 1%. However, in this case, it was attributed to a decreased food intake at least in the case of mice receiving the maximal dose (5%) of NAM. Moreover, water intake was found decreased in the mice receiving both high doses of NAM, suggesting that at these concentrations of NAM would make drinking water apparently unpalatable.

Notably, although circulating levels of liver enzymes did not differ among groups, plasma levels of creatinine were significantly elevated in the mice receiving the maximal dose of NAM, thereby suggesting renal dysfunction at this concentration. Given the unfavorable impact of NAM treatment on water consumption and the extremely negative body weight loss observed the treatment was discontinued before the end of the three months previously established.

In agreement with previous reports [339, 342], NA administration did not produce such preventive effect in weight gain in mice, which suggested a NAM-specific

effect on this phenotype. As previously reported in independent studies [303, 343, 344], NA administration promoted a significant decrease in total plasma levels of cholesterol compared with untreated mice. Similar reductions in circulating cholesterol levels has also been observed in Rhesus monkeys receiving repeated subcutaneous injections of NA (0.15 g/kg/day) [345], with this finding being partly explained by a decrease in the hepatic synthesis of cholesterol. Moreover, NA-treated mice also showed a significant, though moderate, elevation in the plasma levels of glucose. This finding would be consistent with those previously reported in mice receiving a dose even lower (0.03 g/kg/day) than that used in the present study [346]. Hyperglycemia was explained by a NA-induced insulin resistance in treated mice and attributed to islet function deterioration. However, the moderate hyperglycemia first observed in mice treated with NA (0.8 g/kg/day) was not repeated in subsequent experiments. This could partly be explained by differences in the time of food deprivation of mice prior glycemic analysis used between this first batch of mice (overnight fast) and the others (4-h fast). Data on systemic levels of glucose were significantly lower, and less dispersed, after an overnight fast, than when mice were studied after just a 4-h fast.

In our studies, with NAM oral administration, we were able to determine the plasmatic concentrations of NAM and also its methylated derivative, me-NAM, both of them consistently elevated in treated groups accordingly to the administrated dose. Oral administration of me-NAM, have been previously reported to improve the metabolic profile in DIO mice, but showing no changes in body weight [347], this would suggest, that metabolic effects observed in our mice could be a synergy of both increased molecules, but the active metabolite causing the prevention of body weight gain should be NAM.

► 5.2 Anti-obesity mechanisms of NAM

Despite the wealth of data in rodents and humans showing the efficacy of NAD intermediates on adipose tissue energy metabolism [194], the mechanisms accounting for the broad spectrum of health benefits of such interventions are still poorly understood. Like other NAD⁺ intermediates (i.e., NMN and NR), NAM also suppressed body weight gain. NAM-mediated prevention of body weight gain was mainly explained by decreased adiposity. This phenotype was not accompanied by changes in food intake, but rather increased whole-body energy expenditure in NAM-treated mice. NAM treatment was thus revealed as a determinant of adipose morphology and function.

Our data further unveiled changes in the plasticity and modulation of the thermogenic and mitochondrial activity of body adipose tissue, particularly in scWAT. Indeed, in this depot, NAM administration prevented HFD-induced adipocyte hypertrophy, and increased the number of clusters with brown/beige adipocytes. Consistently, *Ucp1* gene expression and protein abundance, a known marker of brown adipocyte [46], was significantly up-regulated (gene expression: 10-fold, $P < 0.05$; protein abundance: 2.5-fold, $P < 0.05$) in this tissue. Additionally, these whole-body changes were associated by elevations in the adipose (scWAT) content of total NAD, mainly due to the NAD⁺ form, and significant elevations in the tissue content of AMP. Remarkably, AMP/ATP ratio elevations in scWAT from treated mice were directly related to increased abundance of the phosphorylated (active) form of AMPK (P-AMPK), a key energy sensor involved in the regulation of the whole-body metabolism.

► 5.3 Effect of NAM on adipose “browning”

Differentiation into brown-like adipocytes is generally referred to as ‘browning’ [348]. Histological, molecular and biochemical data collected in scWAT from treated mice were consistent with a NAM-induced browning of this tissue. NAM-induced activation of brown-like cells, as revealed by the up-regulation of *Ucp1*, was markedly improved in scWAT of DIO mice. Potentially, *Ucp1* up-regulation in scWAT could be one of the causes of the enhanced energy expenditure shown by NAM HD-treated mice. In contrast to adipocytes from WAT, brown-like adipocytes express *Ucp1* and harbor high levels of mitochondria and multilocular lipid droplets [349]. In agreement with this finding, the relative mRNA levels of gene targets of mitochondrial abundance (i.e., *Cpt1b*) and biogenesis (i.e., *Mfn2*) showed a marginally significant elevation in scWAT. Of note, other molecular targets commonly involved in the browning process (i.e., *Pgc1a*, *Pparg*) [350] were significantly up-regulated or showed a trend to be induced in the subcutaneous fat depot of treated mice receiving the highest dose of NAM. In line with this view, the increased proliferation of brown-like adipocyte clusters embedded in scWAT, supported an enhanced browning in this tissue.

Thermogenesis is the main function of BAT, especially in rodents [351]. BAT is enriched in mitochondria that use *Ucp1*-mediated uncoupling to convert significant amounts of chemical energy to dissipate as heat [352]. Our data did not reveal changes in the relative gene expression or protein abundance of *Ucp1* in this tissue. Nevertheless, *Ucp1* corrected by the total protein amount in the iBAT deposit, was indeed increased in NAM-treated mice, suggesting that NAM increases iBAT hypertrophic activity rather than the “relative” levels of *Ucp1*. Histological examination showed that brown adipocytes from BAT of mice treated with NAM were much less loaded with lipids than the untreated mice, suggesting that this tissue was more active. Consistently, mitochondria in iBAT were metabolically more active in treated mice than in untreated mice, as

revealed by the enhanced β -oxidation of fatty acids, albeit in the absence of differences in the gene expression of mitochondrial biogenesis markers in this tissue, suggesting NAM is boosting mitochondrial activity and not increasing mitochondria quantity.

Circulating adipokines (adiponectin and leptin) are adipose tissue surrogates of fat distribution and adipose tissue function [353]. Moreover, both may thus either directly or indirectly influence adipose phenotype. Remarkably, adipose tissue is a target of adiponectin. The favorable impact of NAM on adiponectin levels has previously been reported in treated rats fed an HFD [231]. However, in this study, NAM-mediated elevations in circulating adiponectin were not accompanied by concomitant reductions in body weight gain [231]. In our study, systemic levels of adiponectin were increased in NAM-treated mice compared with untreated mice, in parallel to prevention in weight gain and total fat depot.

The potential contribution of adiponectin to browning was not deeply explored in our study, but it could be a critical role in promoting this phenotype in NAM-treated mice. Indeed, adiponectin-deficient mice are resistant to scWAT browning during cold adaptation [354], thereby suggesting that this adipokine influences thermogenesis and energy expenditure in mice. However, another study adds some controversy to this concept, by showing that adiponectin was rather anti-thermogenic and reduced energy expenditure in mice [355]. Of note, in this last study, adiponectin-mediated inhibition of *Ucp1* expression was pursued via down-regulating β 3 adrenergic receptor expression in brown adipocytes, and was independent on adiponectin receptor signaling.

In response to β -adrenergic stimulation (mostly β_3) by the adenylate cyclase, intracellular cyclic (c)AMP are elevated. cAMP is another endogenous signal involved in brown fat thermogenesis and *Ucp1* gene transcription [350]. NAM does not directly influence adenylate cyclase activity [356], but excess NAM has been suggested to inhibit methylation-mediated meta(nor)epinephrine degradation [357]. The sympathetic nervous system is the primary effector of thermogenesis [358]. Even though meta(nor)epinephrines were not eventually determined in this work; it cannot be ruled out that they might be potentiating β -adrenergic signaling in response to elevated levels of NAM.

Inadequate accumulation of ceramides in WAT, which is an intracellular marker of metabolic stress, is induced by excess fat accumulation [359]. Interestingly, adipocyte-specific inhibition of ceramide synthesis has recently been reported to induce scWAT browning in mice [360].

Moreover, the administration of β -adrenergic agonists to mice, which induce adipose browning [82, 84, 361], selectively reduces ceramides in adipose tissue [360]. In this work, we could not yet determine ceramide content in scWAT.

Importantly, proliferation of M2 macrophages is a key feature related to WAT browning [354, 360]. In agreement with this view, the gene expression of *Il10*, an anti-inflammatory target, was up-regulated, whereas that of *Cd68*, a target of macrophage infiltration, was down-regulated in eWAT from NAM-treated mice compared with untreated mice, suggesting an alleviation in chronic inflammation in treated mice. As adiponectin promotes the polarization of macrophages toward the anti-inflammatory M2 phenotype in WAT [362] and counteracts obesity-induced macrophage infiltration and inflammation [363], a potential role of adiponectin in the observed browning of NAM-treated mice can be suggested.

Among other functions, leptin plays an important role in modulating food intake [364]. Plasma levels of leptin were decreased in NAM-treated mice compared with untreated mice, being this finding in line with the fat pad reduction observed in these mice. Conversely, elevations of plasma leptin have been reported to act on the appetite-suppressing proopiomelanocortin (POMC) neurons to promote WAT browning and reduce adiposity [365]. In addition to the immediate effects of leptin on food intake, and energy expenditure, by eliciting BAT activity, it has also been reported that this adipokine in combination with elevations in postprandial insulin may act to promote sustained overt WAT browning and increased energy expenditure [365]. Our data, however, might rather suggest that leptin signaling might not be significantly influencing WAT browning in our NAM-treated mice, as they present decreased leptin levels. Decreased levels of leptin could be explained by a reduced fat only in treated mice fed a RD, but not in DIO mice.

The impact of NA on leptin expression in adipose tissue found is rather controversial in the literature. For instance, similar results have been yielded in hypercholesterolemic rabbits treated with NA, being mainly explained by a significant decrease in leptin mRNA expression in adipose tissue and cultured primary adipocytes [366]. In contrast, both NA and acipimox, a long-acting NA analog, enhanced leptin release from adipocytes isolated from rats [367]. However, in our study, decreased plasma levels of this adipokine were not accompanied by changes in food intake in NA-treated mice.

► 5.4 Contribution of NAM-mediated NAD⁺ boost to adipose phenotype

Given that NAD⁺ biosynthesis is largely reduced in obese mice and NAD⁺ bioavailability is compromised by HFD [194], strategies leading to increasing adipose tissue NAD⁺ could be a target for treating obesity. In the last years two other NAD⁺ precursors (NR, NMN) have been reported to increase NAD⁺ bioavailability in tissues, primarily in the liver, skeletal muscle and BAT, but not in WAT [215, 217]. In contrast to these two other NAD⁺ intermediates, our data revealed that NAM administration in mice promoted a dose-dependent increase of NAD⁺ in scWAT. NAD⁺ is consumed by NAD⁺-dependent deacetyltransferases (Sirtuins) and has gained interest as a critical regulator of multiple cell signaling pathways, including those involved in energy metabolism [187]. Nampt determines NAM bioavailability in tissues. The relative mRNA levels of this enzyme did not differ in WAT among groups. Although it does not necessarily represent the protein function, the activity of this enzyme would be expected to be elevated in the presence of enhanced bioavailability of NAM.

Intriguingly, adipose tissue NAD⁺ elevations were accompanied by a rise of adenosine phosphates in scWAT, mainly AMP levels. Conceivably, increased AMP in scWAT could activate AMPK which in turn activates Pgc1a via direct phosphorylation and facilitates Sirt1-dependent Pgc1a deacetylation [210, 368]. Additionally, LKB1 which phosphorylates AMPK is also a target of Sirt1 [369]. Conceivably Sirt1-mediated activation of these targets in scWAT might also contribute to AMPK activation in treated mice.

Pgc1a activation may also drive the transcription of the Ucp1 gene and contribute to browning of WAT [370]. Pgc1a activation leads to increased oxidative metabolism and mitochondrial biogenesis in skeletal muscle [370], and conceivably also in other tissues, including WAT. Supporting to this, up-regulation of *Pgc1a* in adipose tissues increases mitochondrial biogenesis and protects from HFD-induced obesity in mice [371, 372]. Considering that AMPK

is a cellular energy-sensor which is mainly activated when AMP is elevated, it could be plausible that oxidative capacity rather than energy uncoupling would be primed in WAT following chronic AMPK activation. Supporting this, AMPK activation has been described to protect against diet-induced-obesity via Ucp1-independent uncoupling of ATP production [373]. Overall, our data might suggest that fat depot gain decreases might be accounted for a combination of both mechanisms in scWAT of NAM-treated mice. Global decrease in adiposity in NAM-treated mice was accompanied by increased levels of NAD⁺ and AMP levels, and a direct correlation between NAD⁺/NADH and AMP/ATP in scWAT, suggesting that energy demand could be augmented in this tissue.

► 5.5 Effect of NAM on other mechanisms of energy expenditure

Polyamine flux has a major role in energy homeostasis [197, 374, 375]. Genetic knockout of *Sat* results in increased diet-induced obesity and transgenic *Sat* overexpression causes leanness owing to increased energy expenditure [374, 375]. As NAM increased hepatic and adipose *Sat* mRNA levels, this may be leading a reaction to polyamine flux increasing energy expenditure in treated mice. Both *Odc* and *Sat* activation drives polyamine flux, which consumes the metabolic substrate, acetyl-CoA, for polyamine acetylation [375]. Our data could suggest that increased bioavailability of NAM could regulate polyamine flux.

As NAM treatment enhances oxygen consumption, and this depends on polyamine flux [197], it is fair to make the assumption that NAM could be a regulator of adiposity by directly altering NAD, polyamine flux, and perhaps, Sirt1 signaling. NAM leads to metabolic substrate consumption or loss from adipocytes coupled with increased energy expenditure.

▶ 5.6 NAM on homeostasis and metabolism of glucose

NAM-induced weight prevention was not accompanied by favorable elevations in insulin sensitivity and function. Our data is inconsistent with previous data showing an improved glucose tolerance in rats treated with NAM [231]. Adiponectin is a widely recognized insulin sensitizer, and reduced adiponectin levels are linked to insulin resistance [376]. Consistently, the improved glucose metabolism observed in rats treated with the highest dose of NAM could concomitantly be related to elevated adiponectin levels [231].

Our data showed that NAM supplementation did not improve glucose disposal or insulin resistance in DIO mice. This finding contrasted with previous observations by others in an independent study [377], whereby glucose homeostasis was improved in NAM-treated DIO mice [377]. In the latter study, metabolomic analysis suggested that NAM supplementation might favor liver glucose catabolism *in vivo*. It was mainly revealed by relative reductions in the hepatic levels of glucose and glucose 1-phosphate, and elevations in citrate, intermediate in the tricarboxylic cycle, in NAM-treated DIO mice compared with untreated DIO mice. Concomitantly, NAM supplementation to HepG2 cells in the presence of lipids (mimicking HFD) increased glucose uptake and increased glucose uptake, enhanced degradation of glycogen stores, and oxygen consumption rate compared with untreated cells [377]. Consistently with these observations, we did observe a significant elevation of glucose oxidation in NAM HD-treated mice as revealed by *in vivo* analysis. However, the direct analysis of NAM on hepatic glucose metabolism in our DIO mice could not be addressed in the present study.

► 5.7 NAM on fatty liver

Our data revealed an improvement in fatty liver condition in induced-obesity mice treated with NAM as shown by reduced lipid content determined by biochemical, histologically and MRI approaches. This was directly related to reduction of body fat. In this regard, *Cd36*, a known fatty liver-related marker [326], was favorably down-regulated in treated mice. Consistent with this observation, NAM supplementation to DIO mice has been also accompanied by a significant amelioration of fatty liver and inflammation in an independent study [377].

Fibroblast growth factor (Fgf)21, which increases in human with fatty liver and decreases in response to improvement in steatosis and steatohepatitis [327], was found to be reduced in NAM-treated mice. Moreover, this phenotype was accompanied by a reduction in gene markers of macrophages infiltration in this tissue, suggesting a potential role by NAM to prevent inflammation along with lipid accumulation.

NAM is methylated to me-NAM in a reaction catalyzed by Nnmt. S-adenosyl methionine (SAM) is a major methyl group donor mainly involved in this process. In addition to me-NAM, SAM is also involved in the production of many other products, including polyamine [197]. Me-NAM produced by Nnmt has been reported to improve hepatic steatosis [347]. Our data showed that Nnmt expression was reduced in the livers of NAM-treated mice, albeit elevations of circulating me-NAM. The liver-specific knockdown of Nnmt protected the liver from hepatic steatosis [197], whereas its overexpression promoted fatty liver deterioration [378]. There is also published data indicating that elevated levels of me-NAM in the liver, caused by the inhibition of aldehyde oxidase, enzyme responsible of me-NAM oxidation, leads to fatty liver amelioration [379].

Although this work has not evaluated yet metabolites such as SAM or me-NAM in the liver, we could theorize that elevations in plasma me-NAM due to increasing NAM bioavailability would promote Sirt's action in this tissue of treated mice.

▶ 5.8 NAM administration prevented vascular chronic inflammation and atherosclerosis in ApoE-deficient mice

5.8a Anti-inflammatory effect of NAM

The infiltration and activation of cells of the immune system is a characteristic finding in chronic inflammation processes, such as obesity [380] and atherosclerosis [381]. Our data showed that the administration with NAM produced a general amelioration of the inflammatory status in all studied mice. Importantly, this phenotype paralleled with weight gain prevention and reduced adiposity.

Advances in adipose biology have provided convincing evidence that adipose tissue secrete adipokines that influence metabolism in peripheral tissues [382]. Inflammation is often characterized by elevations in plasma concentrations of a number of pro-inflammatory (e.g., IL-6, TNFa) markers, expressed and released by adipose tissue [383]. The pro-inflammatory status in obesity is frequently accompanied by a decrease of anti-inflammatory cytokines, such as IL-10 [384] and adipokines, such as adiponectin [385]. Our current work reports that plasma concentrations of IL-10 were significantly elevated in ApoE-deficient mice treated with NAM. Of note, the relative mRNA levels of the anti-inflammatory *Il10* were significantly elevated in aorta. Likewise circulating levels of IL-10, relative mRNA levels of *Il10* were inversely related to atherosclerosis development in ApoE-deficient mice. Consistently, *Il10* was also found up-regulated in eWAT from both DIO and, showing a close to significant trend to be significant, ApoE-deficient mice. In humans, circulating levels of IL-10 did not change after moderate (diet-induced) weight loss [101], but were significantly raised after surgery-induced excess weight loss [99].

Our data would suggest that NAM might exert changes (mainly anti-inflammatory) in the effector state of immune cells in target tissues. In particular, the up-regulation of *I110* rather suggest the activation of M2 macrophages (anti-inflammatory) in both aorta and adipose tissue of NAM-treated ApoE-deficient mice [386]. However, mRNA levels of *Tnfa* in these same tissues only showed a non-significant trend to differ among groups of either DIO or ApoE-deficient mice. The latter contrasted with data [290] showing a favorable effect of NAM on *Tnfa* synthesis and secretion in vitro. As Tnf- α is mainly released by activated M1 macrophages [386], this finding might further suggest that NAM predominantly exert its anti-inflammatory effect mainly by up-regulating *I110* in macrophages.

The anti-inflammatory phenotype shown by NAM-treated mice was accompanied by a decrease in the accumulation of macrophages in both adipose tissue and liver of DIO mice, as shown by the relative gene expression of tissue marker of macrophage (i.e., *Cd68*). Consistent with this finding, the number of CLS, which commonly accumulate in fat depots from obese mice [94], were also diminished in eWAT from NAM-treated, compared with untreated mice. In accordance, *Cd68* was down-regulated concomitantly to fat reduction. However, no molecular evidence of differential accumulation of macrophages was shown, at least, in eWAT, where *Cd68* mRNA expression showed no changes or, in aortas where F4/80 marker did not revealed differences in macrophages infiltration of ApoE-deficient mice (its expression was not evaluated in the livers of ApoE-deficient mice). Conceivably, as the mice shared the same genetic background (i.e., C57BL/6J), differences in macrophage infiltration might be explained by differences in the time period they both were challenged on a HFD diet (3 mo. in the case of DIO mice vs. 1 mo. in ApoE-deficient mice).

Adiponectin influences macrophage function and inflammation in a diverse array of tissues, not only in adipose tissue [387]. In this regard, this adipokine has also been reported to be anti-atherogenic [388]. Although plasma levels of adiponectin were not determined in plasma of ApoE-deficient mice, its plasma levels were found elevated in DIO mice treated with the highest dose of NAM as compared with untreated mice.

Adiponectin induces the production of the anti-inflammatory IL-10 in human myeloid cells, including macrophages and leukocytes [389-391] and inhibits the release of pro-inflammatory cytokines [392, 393]. Collectively, these data suggest that adiponectin promotes the polarization of macrophages towards an M2 (i.e. anti-inflammatory) phenotype. Peritoneal [389], alveolar [392] and hepatic macrophages [362] all display M2 polarization under the influence of adiponectin. In the context of atherogenesis, aortic up-regulation of *Il10* would conceivably suggest a M2 phenotype polarization of macrophages in aortas of NAM-treated, ApoE-deficient mice. Consistently, adiponectin inhibits macrophage transformation into lipid-laden foam cells [394, 395]. Adiponectin also impairs the production of the pro-inflammatory cytokine IFN- γ in human macrophages [390]. However, in our work, the mRNA levels of this cytokine in aorta of ApoE-deficient mice did not differ among groups.

Inflammatory signalling has only recently been recognized as playing a role in the browning of WAT, emerging as a relevant component of the adipose alterations in obesity [385]. In agreement with this concept, chronic exposure to β -adrenergic agonists may not only induce adipose beiging [82, 84, 361], but, also inhibit the production of pro-inflammatory cytokines, such as Tnfa and IFN γ , and stimulate the production of anti-inflammatory cytokines, such as IL-10, IL-4, respectively [386]. In our study, the induction of beiging/browning by NAM in scWAT in treated mice might be thus proposed as another NAM-mediated anti-

inflammatory mechanism. Unfortunately, the gene expression of pro- and anti-inflammatory cytokines was determined in eWAT and the analysis is pending in scWAT. However, it would be expected that their expression pattern in response to NAM treatment would be quite like that found in eWAT.

Contrary to NAM, me-NAM does not change inflammatory cytokines profile in immune cells like macrophages [290], but has anti-thrombotic, anti-inflammatory, and vasorelaxation properties [296, 396], that protects the cardiovascular system. It has been suggested as a therapeutic factor for ameliorating the endothelial-dependent disorders such as atherosclerosis [397].

5.8b Anti-oxidant effect of NAM

The anti-inflammatory action by NAM may also involve antioxidant mechanisms. Indeed, NAM has been defined as an O[•] radical scavenger, and may also inhibit free radical (e.g., NO[•], O[•], HClO[•]) generation [398]. In agreement with this concept, NAM has been reported to protect against both protein oxidation and lipid peroxidation induced by reactive oxygen species [399]. In this regard, although plasma non-HDL accumulated in plasma of NAM HD-treated, ApoE-deficient mice, these lipoproteins were less prone to oxidation than those from untreated mice. Our data showed a direct effect of NAM in inhibiting lipid peroxidation, as illustrated by an *in vitro* protective effect against LDL oxidation. This direct antioxidant effect of NAM could conceivably contribute to prevent atherosclerosis prevention, despite the elevation of plasma non-HDL.

The antioxidant effect by NAM in vascular disease has not previously explored *in vivo* in detail. However, the administration of other dietary vitamin B3-related metabolites (i.e., NMN and NR) provided vascular protection against oxidative

stress [297, 298], and reversed arterial dysfunction [298]. As NMN and NR are NAD⁺ intermediaries, this effect was mainly attributed to the induction of the Sirt1 signaling in target tissues, involving the acetylation of the p65 NFκB subunit. Likewise, NAM is also a NAD⁺ precursor [219]. Therefore, its administration could also provide tissues with extra source of NAD⁺ to induce Sirt1 activity. In this regard, the NAD⁺ content in the liver and adipose tissues was significantly increased in NAM-treated mice compared with untreated mice. Additionally, NAM needs to be first converted into NMN by the action of Nampt to eventually generate NAD⁺. Consistently, tissue NAD⁺ elevations were directly related to the relative mRNA levels of *Nampt*, at least, in adipose tissue. Although we did not analyze the relative mRNA levels of *neither Nampt nor* NAD⁺ content in aortas of NAM-treated, ApoE-deficient mice, a similar result would be expected. Sirt1, by suppressing NFκB signaling, reduces the inflammatory response [400]. Our data suggests that NAM, by providing NAD⁺ to cells, might enhance deacetylation of cellular p65 protein.

NAM administration was accompanied by favorable elevations in the gene expression of *Hmox1* in the liver or *Sod2* in eWAT. Both are important determinants of cellular antioxidant status and their up-regulation would support the concept that NAM could stimulate an antioxidant response in different tissues. Consistently, NAM has been shown to reduce brain injury in neonatal rats, in part by reducing oxidative stress in an independent study [401]. Interestingly, our data further revealed tissue-specific mechanisms. For instance, neither of these genes (*Hmox1*, *Sod2*) were expressed differentially in aortas of NAM-treated, ApoE-deficient mice.

Both *Hmox1* and *Sod2* are directly controlled by the action of nuclear factor erythroid 2-related factor 2 (Nrf2). Nrf2 is a key oxidative stress response modifier that induces transcription of antioxidant genes through binding to the

antioxidant response element [402]. Although the connection between NAM and Nrf2 was not studied in this work, a potential, though controversial, crosstalk between Sirt1 and Keap1/Nrf2/ARE anti-oxidative pathway has recently been reported *in vitro* [403, 404]. In one of these studies, Sirt1 activation was shown to inhibit Nrf2-dependent gene transcription by virtue of the direct deacetylation of Nrf2. In contrast, NAM, an *in vitro* putative inhibitor of SIRT1, induced the Nrf2-dependent gene transcription [404]. Conversely, in an independent study, Sirt1 was reported to significantly enhance the activity of Keap1/Nrf2/ARE pathway by promoting transcriptional activity of Nrf2, elevating the protein abundance of Hmox1, a target gene of Nrf2, which eventually quenched intracellular ROS overproduction *in vitro* [403]. The first of these last studies worked under the premise that NAM acts as a potent inhibitor of Sirt1 *in vitro*. However, compelling evidences rather suggest that NAM may behave different *in vivo* [405]. For instance, NAM would provide cells with an extra source of NAD⁺ and fuel Sirt1 activity.

Although the differential deacetylation of Sirt1 targets was not directly evaluated in this work, we observed a commensurate elevation in the gene expression of LXR targets in aorta (*Abca1*: 2.9-fold, P<0.05; *Abcg1*: 3.3-fold, P<0.05; *Abcg5*: 1.5-fold, P=0.10) in NAM-treated mice compared to untreated mice. This data matches with previous results of our group where evidences that NAM promotes molecular targets regulated by LXR in other tissues (e.g., liver, small intestine) [406]. Indeed, Sirt1 positively regulates the nuclear receptor LXR [407]. Our data also showed that mRNA levels of *Nr1h2* were significantly increased in aortas from NAM-treated mice (*Nr1h2*: 2-fold, P<0.05) compared with untreated mice. LXRalpha regulates its own expression in human macrophages [408, 409], but not that of *Nr1h2* [408], indicating that autoregulation is restricted to the *Nr1h3* gene.

► 5.9 Limitations of the study

This study on the effect of NAM supplementation was conducted in male mice. This work provides quantifiable evidence that NAM may exerts beneficial effects on weight gain prevention by enhancing global energy expenditure, partly due to induced adaptive thermogenesis and energy consumption in WAT of treated mice; however, the contribution of other tissues also important in metabolic homeostasis in vivo, such as skeletal muscle, was not eventually evaluated. In addition, although mitochondrial fatty acid β -oxidation was increased in BAT of treated mice, hence indicating improved mitochondrial activity in that tissue, this mitochondrial function could not be evaluated in WAT during the development of this study. In this regard, the direct analysis of glucose oxidation in WAT and skeletal muscle using an isotopic approach was also pending. Furthermore, a deeper analysis on the effect of NAM over other determinants of energy metabolism status, including polyamine's metabolism or methyl group donors could also shed light on their potential contribution in energy metabolism of targets tissues. Finally, the impact of NAM on β -adrenergic response was not evaluated in the present study. The favorable contribution of meta(nor)epinephrines in adaptive thermogenesis of WAT is widely reported. Although the effect of NAM in modulating meta(nor)epinephrine production has not previously been reported, its direct analysis could also shed light on other potential mechanism of beiging/browning in WAT of treated mice.

NAM-treated mice had higher WAT content of NAD⁺. However, whether it enhanced mitochondrial oxidative metabolism in this tissue remained unclear. In addition, NAD⁺ is also a necessary coenzyme for Sirt1 activation; however, Sirt1 activity could not directly be assessed. Interestingly, several liver X receptor (Lxra) gene targets were up-regulated in different tissues. As Lxra is a known Sirt1 target, it could conceivably be proposed that Lxra signaling could be activated as result of Sirt1-dependent mechanisms; however, the direct analysis

of the relative abundance of deacetylated Lxra as well as other Sirt1 targets, such as Pgc1a or NfkB, in selected tissues was also pending.

Last, the experimental design used in this study was just to assess the preventive, not therapeutic effects of NAM on different phenotypes associated with adiposity and inflammation. Longitudinal evaluation of these phenotypes would have allowed a better assessment of the favorable contribution of NAM in their reversal upon treatment, i.e., once these phenotypes were established.

• 6. CONCLUSIONS

1. The range of NAM doses used (0.1-1.0%) in this study was considered safe as revealed by the absence of toxic effects. Circulating NAM-related metabolites were dose-dependently increased in NAM-treated mice.
2. The administration of NAM at 1% in drinking water most effectively prevented weight gain, mostly by reducing the fat pads of the different mouse models studied.
3. The beneficial effects of NAM administration were specific of NAM, as the obese phenotype was not prevented by the treatment with NA.
4. The mechanisms studied in NAM treated mice provided, in general, results consistent with the fat pad gain prevention observed in these mice, as summarized below:
 - a. Increase in adipose tissue NAD⁺/NADH ratio.
 - b. Increase in total adenosine metabolites, mainly AMP in in scWAT, together with a commensurate increase in activated AMPK.
 - c. While the gene expression of *Nampt* in scWAT did not significantly changed, it did correlate with the increased levels of NAD⁺ in this tissue.
 - d. BAT was metabolically more active, as revealed by increased mitochondrial activity. Also the increased total Ucp1 protein, suggested that thermogenesis could be elevated.

- e. Increase in energy expenditure, as determined by indirect calorimetry and revealed by enhanced oxygen consumption.
 - f. WAT browning, as evidenced by the presence of brown-like adipocytes and the up-regulation of *Ucp1* mRNA and protein in this tissue.
 - g. Lack of improvement in glucose disposal or insulin sensitivity.
 - h. Improvement of fatty liver, as revealed by decreased hepatic lipid content, down-regulation of *Cd36* and *Fgf21*, and reduced plasma levels of *Fgf21*.
5. NAM treatment reverted the pro-inflammatory status of DIO mice, as illustrated by favorable elevations in circulating IL-10 and gene expression of *Il10* in eWAT.
6. NAM administration prevented aortic lesions in ApoE-deficient mice. Mechanisms potentially involved in this phenotype included:
- a. Circulating IL-10 and aortic mRNA *Il10* levels were elevated in treated ApoE-deficient mice and significantly correlated with aortic lesions. The *Il10* up-regulation in aorta suggest a switch to anti-inflammatory M2 macrophages in this tissue.
 - b. Plasma non-HDL liver clearance was impaired in treated mice increasing the plasma concentration of these lipoproteins. Despite this, non-HDL isolated *in vitro* from plasma of treated mice were less prone to oxidation than those from untreated mice. Moreover, human LDL susceptibility to oxidation was directly prevented by NAM *in vitro*, thereby suggesting a direct anti-oxidant effect by this vitamin form. This mechanism could conceivably contribute to alleviate aortic inflammation in treated mice.

• 7. References

- [1] E.A. Finkelstein, O.A. Khavjou, H. Thompson, J.G. Trogdon, L. Pan, B. Sherry, W. Dietz, Obesity and severe obesity forecasts through 2030, *Am J Prev Med*, 42 (2012) 563-570.
- [2] Obesity and overweight, 2018, pp. World Health Organization.
- [3] S.M. Grundy, Metabolic complications of obesity, *Endocrine*, 13 (2000) 155-165.
- [4] A. Doria, M.E. Patti, C.R. Kahn, The emerging genetic architecture of type 2 diabetes, *Cell Metab*, 8 (2008) 186-200.
- [5] J.K. Sethi, A.J. Vidal-Puig, Adipose tissue development, structure and function, in: R.S. Ahima (Ed.) *Metabolic basis of obesity*, Springer Science+Business Media, LLC, Place Published, 2011, pp. 53-68.
- [6] K. Makki, P. Froguel, I. Wolowczuk, Adipose tissue in obesity-related inflammation and insulin resistance: cells, cytokines, and chemokines, *ISRN Inflamm*, 2013 (2013) 139239.
- [7] R. Jokinen, S. Pirnes-Karhu, K.H. Pietilainen, E. Pirinen, Adipose tissue NAD(+)-homeostasis, sirtuins and poly(ADP-ribose) polymerases -important players in mitochondrial metabolism and metabolic health, *Redox Biol*, 12 (2017) 246-263.
- [8] M. Abdelaal, C.W. le Roux, N.G. Docherty, Morbidity and mortality associated with obesity, *Ann Transl Med*, 5 (2017) 161.
- [9] M. Bluher, Adipose tissue dysfunction contributes to obesity related metabolic diseases, *Best Pract Res Clin Endocrinol Metab*, 27 (2013) 163-177.
- [10] C.M. Kusminski, P.E. Bickel, P.E. Scherer, Targeting adipose tissue in the treatment of obesity-associated diabetes, *Nat Rev Drug Discov*, 15 (2016) 639-660.
- [11] F.T. Yazdi, S.M. Clee, D. Meyre, Obesity genetics in mouse and human: back and forth, and back again, *PeerJ*, 3 (2015) e856.
- [12] R.D. Cox, C.D. Church, Mouse models and the interpretation of human GWAS in type 2 diabetes and obesity, *Dis Model Mech*, 4 (2011) 155-164.
- [13] T.A. Lutz, S.C. Woods, Overview of animal models of obesity, *Curr Protoc Pharmacol*, Chapter 5 (2012) Unit5 61.
- [14] J. Alexander, G.Q. Chang, J.T. Dourmashkin, S.F. Leibowitz, Distinct phenotypes of obesity-prone AKR/J, DBA2J and C57BL/6J mice compared to control strains, *Int J Obes (Lond)*, 30 (2006) 50-59.
- [15] D.B. West, C.N. Boozer, D.L. Moody, R.L. Atkinson, Dietary obesity in nine inbred mouse strains, *Am J Physiol*, 262 (1992) R1025-1032.
- [16] R.S. Surwit, C.M. Kuhn, C. Cochrane, J.A. McCubbin, M.N. Feinglos, Diet-induced type II diabetes in C57BL/6J mice, *Diabetes*, 37 (1988) 1163-1167.

- [17] A.A. Butler, L.P. Kozak, A recurring problem with the analysis of energy expenditure in genetic models expressing lean and obese phenotypes, *Diabetes*, 59 (2010) 323-329.
- [18] K.L. Ellacott, G.J. Morton, S.C. Woods, P. Tso, M.W. Schwartz, Assessment of feeding behavior in laboratory mice, *Cell Metab*, 12 (2010) 10-17.
- [19] K.J. Kaiyala, G.J. Morton, B.G. Leroux, K. Ogimoto, B. Wisse, M.W. Schwartz, Identification of body fat mass as a major determinant of metabolic rate in mice, *Diabetes*, 59 (2010) 1657-1666.
- [20] J.E. Ayala, V.T. Samuel, G.J. Morton, S. Obici, C.M. Croniger, G.I. Shulman, D.H. Wasserman, O.P. McGuinness, Standard operating procedures for describing and performing metabolic tests of glucose homeostasis in mice, *Dis Model Mech*, 3 (2010) 525-534.
- [21] Y.C. Tung, E. Ayuso, X. Shan, F. Bosch, S. O'Rahilly, A.P. Coll, G.S. Yeo, Hypothalamic-specific manipulation of *Fto*, the ortholog of the human obesity gene *FTO*, affects food intake in rats, *PLoS One*, 5 (2010) e8771.
- [22] S.M. Clee, A.D. Attie, The genetic landscape of type 2 diabetes in mice, *Endocr Rev*, 28 (2007) 48-83.
- [23] G.R. Hajer, T.W. van Haefen, F.L. Visseren, Adipose tissue dysfunction in obesity, diabetes, and vascular diseases, *Eur Heart J*, 29 (2008) 2959-2971.
- [24] M. Coelho, T. Oliveira, R. Fernandes, Biochemistry of adipose tissue: an endocrine organ, *Arch Med Sci*, 9 (2013) 191-200.
- [25] P. Trayhurn, C. Bing, I.S. Wood, Adipose tissue and adipokines--energy regulation from the human perspective, *J Nutr*, 136 (2006) 1935S-1939S.
- [26] S.S. Choe, J.Y. Huh, I.J. Hwang, J.I. Kim, J.B. Kim, Adipose Tissue Remodeling: Its Role in Energy Metabolism and Metabolic Disorders, *Front Endocrinol (Lausanne)*, 7 (2016) 30.
- [27] V. Pellegrinelli, S. Carobbio, A. Vidal-Puig, Adipose tissue plasticity: how fat depots respond differently to pathophysiological cues, *Diabetologia*, 59 (2016) 1075-1088.
- [28] S.P. Weisberg, D. McCann, M. Desai, M. Rosenbaum, R.L. Leibel, A.W. Ferrante, Jr., Obesity is associated with macrophage accumulation in adipose tissue, *J Clin Invest*, 112 (2003) 1796-1808.
- [29] M.F. Gregor, G.S. Hotamisligil, Inflammatory mechanisms in obesity, *Annu Rev Immunol*, 29 (2011) 415-445.
- [30] F. Biobaku, H. Ghanim, M. Batra, P. Dandona, Macronutrient Mediated Inflammation and Oxidative Stress: Relevance to Insulin Resistance, Obesity and Atherogenesis, *J Clin Endocrinol Metab*, (2019).
- [31] K. Ikeda, P. Maretich, S. Kajimura, The Common and Distinct Features of Brown and Beige Adipocytes, *Trends Endocrinol Metab*, 29 (2018) 191-200.
- [32] R.K. Zwick, C.F. Guerrero-Juarez, V. Horsley, M.V. Plikus, Anatomical, Physiological, and Functional Diversity of Adipose Tissue, *Cell Metab*, 27 (2018) 68-83.

- [33] F. Item, D. Konrad, Visceral fat and metabolic inflammation: the portal theory revisited, *Obes Rev*, 13 Suppl 2 (2012) 30-39.
- [34] S. Gesta, Y.H. Tseng, C.R. Kahn, Developmental origin of fat: tracking obesity to its source, *Cell*, 131 (2007) 242-256.
- [35] K.H. Kwok, K.S. Lam, A. Xu, Heterogeneity of white adipose tissue: molecular basis and clinical implications, *Exp Mol Med*, 48 (2016) e215.
- [36] S. Cinti, The adipose organ, *Prostaglandins Leukot Essent Fatty Acids*, 73 (2005) 9-15.
- [37] S. Sam, Differential effect of subcutaneous abdominal and visceral adipose tissue on cardiometabolic risk, *Horm Mol Biol Clin Investig*, 33 (2018).
- [38] A. Shuster, M. Patlas, J.H. Pinthus, M. Mourtzakis, The clinical importance of visceral adiposity: a critical review of methods for visceral adipose tissue analysis, *Br J Radiol*, 85 (2012) 1-10.
- [39] T.T. Tran, Y. Yamamoto, S. Gesta, C.R. Kahn, Beneficial effects of subcutaneous fat transplantation on metabolism, *Cell Metab*, 7 (2008) 410-420.
- [40] E.D. Rosen, B.M. Spiegelman, What we talk about when we talk about fat, *Cell*, 156 (2014) 20-44.
- [41] T. Tchkonina, T. Thomou, Y. Zhu, I. Karagiannides, C. Pothoulakis, M.D. Jensen, J.L. Kirkland, Mechanisms and metabolic implications of regional differences among fat depots, *Cell Metab*, 17 (2013) 644-656.
- [42] S. Cinti, Transdifferentiation properties of adipocytes in the adipose organ, *Am J Physiol Endocrinol Metab*, 297 (2009) E977-986.
- [43] L. Scheja, J. Heeren, Metabolic interplay between white, beige, brown adipocytes and the liver, *J Hepatol*, 64 (2016) 1176-1186.
- [44] A.M. Cypess, S. Lehman, G. Williams, I. Tal, D. Rodman, A.B. Goldfine, F.C. Kuo, E.L. Palmer, Y.H. Tseng, A. Doria, G.M. Kolodny, C.R. Kahn, Identification and importance of brown adipose tissue in adult humans, *N Engl J Med*, 360 (2009) 1509-1517.
- [45] D.O. Foster, M.L. Frydman, Nonshivering thermogenesis in the rat. II. Measurements of blood flow with microspheres point to brown adipose tissue as the dominant site of the calorogenesis induced by noradrenaline, *Can J Physiol Pharmacol*, 56 (1978) 110-122.
- [46] B. Cannon, J. Nedergaard, Brown adipose tissue: function and physiological significance, *Physiol Rev*, 84 (2004) 277-359.
- [47] A. Bartelt, O.T. Bruns, R. Reimer, H. Hohenberg, H. Ittrich, K. Peldschus, M.G. Kaul, U.I. Tromsdorf, H. Weller, C. Waurisch, A. Eychmuller, P.L. Gordts, F. Rinninger, K. Bruegelmann, B. Freund, P. Nielsen, M. Merkel, J. Heeren, Brown adipose tissue activity controls triglyceride clearance, *Nat Med*, 17 (2011) 200-205.

- [48] K.I. Stanford, R.J. Middelbeek, K.L. Townsend, D. An, E.B. Nygaard, K.M. Hitchcox, K.R. Markan, K. Nakano, M.F. Hirshman, Y.H. Tseng, L.J. Goodyear, Brown adipose tissue regulates glucose homeostasis and insulin sensitivity, *J Clin Invest*, 123 (2013) 215-223.
- [49] J. Heeren, H. Munzberg, Novel aspects of brown adipose tissue biology, *Endocrinol Metab Clin North Am*, 42 (2013) 89-107.
- [50] M. Watanabe, S.M. Houten, C. Matakai, M.A. Christoffolete, B.W. Kim, H. Sato, N. Messaddeq, J.W. Harney, O. Ezaki, T. Kodama, K. Schoonjans, A.C. Bianco, J. Auwerx, Bile acids induce energy expenditure by promoting intracellular thyroid hormone activation, *Nature*, 439 (2006) 484-489.
- [51] E.P. Broeders, E.B. Nascimento, B. Havekes, B. Brans, K.H. Roumans, A. Tailleux, G. Schaart, M. Kouach, J. Charton, B. Deprez, N.D. Bouvy, F. Mottaghy, B. Staels, W.D. van Marken Lichtenbelt, P. Schrauwen, The Bile Acid Chenodeoxycholic Acid Increases Human Brown Adipose Tissue Activity, *Cell Metab*, 22 (2015) 418-426.
- [52] M. Bordicchia, D. Liu, E.Z. Amri, G. Ailhaud, P. Dessi-Fulgheri, C. Zhang, N. Takahashi, R. Sarzani, S. Collins, Cardiac natriuretic peptides act via p38 MAPK to induce the brown fat thermogenic program in mouse and human adipocytes, *J Clin Invest*, 122 (2012) 1022-1036.
- [53] T. Gnad, S. Scheibler, I. von Kugelgen, C. Scheele, A. Kilic, A. Glode, L.S. Hoffmann, L. Reverte-Salisa, P. Horn, S. Mutlu, A. El-Tayeb, M. Kranz, W. Deuther-Conrad, P. Brust, M.E. Lidell, M.J. Betz, S. Enerback, J. Schrader, G.G. Yegutkin, C.E. Muller, A. Pfeifer, Adenosine activates brown adipose tissue and recruits beige adipocytes via A2A receptors, *Nature*, 516 (2014) 395-399.
- [54] W. Wang, P. Seale, Control of brown and beige fat development, *Nat Rev Mol Cell Biol*, 17 (2016) 691-702.
- [55] S. Kajimura, P. Seale, B.M. Spiegelman, Transcriptional control of brown fat development, *Cell Metab*, 11 (2010) 257-262.
- [56] A. Bartelt, J. Heeren, The holy grail of metabolic disease: brown adipose tissue, *Curr Opin Lipidol*, 23 (2012) 190-195.
- [57] M. Ghorbani, J. Himms-Hagen, Appearance of brown adipocytes in white adipose tissue during CL 316,243-induced reversal of obesity and diabetes in Zucker fa/fa rats, *Int J Obes Relat Metab Disord*, 21 (1997) 465-475.
- [58] J. Himms-Hagen, A. Melnyk, M.C. Zingaretti, E. Ceresi, G. Barbatelli, S. Cinti, Multilocular fat cells in WAT of CL-316243-treated rats derive directly from white adipocytes, *Am J Physiol Cell Physiol*, 279 (2000) C670-681.
- [59] J.G. Granneman, M. Burnazi, Z. Zhu, L.A. Schwamb, White adipose tissue contributes to UCP1-independent thermogenesis, *Am J Physiol Endocrinol Metab*, 285 (2003) E1230-1236.
- [60] K. Ikeda, Q. Kang, T. Yoneshiro, J.P. Camporez, H. Maki, M. Homma, K. Shinoda, Y. Chen, X. Lu, P. Maretich, K. Tajima, K.M. Ajuwon, T. Soga, S. Kajimura, UCP1-independent signaling involving SERCA2b-mediated calcium cycling regulates beige fat thermogenesis and systemic glucose homeostasis, *Nat Med*, 23 (2017) 1454-1465.

- [61] J. Ukropec, R.P. Anunciado, Y. Ravussin, M.W. Hulver, L.P. Kozak, UCP1-independent thermogenesis in white adipose tissue of cold-acclimated Ucp1^{-/-} mice, *J Biol Chem*, 281 (2006) 31894-31908.
- [62] P. Li, Z. Zhu, Y. Lu, J.G. Granneman, Metabolic and cellular plasticity in white adipose tissue II: role of peroxisome proliferator-activated receptor- α , *Am J Physiol Endocrinol Metab*, 289 (2005) E617-626.
- [63] E.K. Anderson, D.A. Gutierrez, A.H. Hasty, Adipose tissue recruitment of leukocytes, *Curr Opin Lipidol*, 21 (2010) 172-177.
- [64] V. Dam, T. Sikder, S. Santosa, From neutrophils to macrophages: differences in regional adipose tissue depots, *Obes Rev*, 17 (2016) 1-17.
- [65] Y.H. Lee, E.P. Mottillo, J.G. Granneman, Adipose tissue plasticity from WAT to BAT and in between, *Biochim Biophys Acta*, 1842 (2014) 358-369.
- [66] J.L. Halaas, K.S. Gajiwala, M. Maffei, S.L. Cohen, B.T. Chait, D. Rabinowitz, R.L. Lallone, S.K. Burley, J.M. Friedman, Weight-reducing effects of the plasma protein encoded by the obese gene, *Science*, 269 (1995) 543-546.
- [67] H. Xu, G.T. Barnes, Q. Yang, G. Tan, D. Yang, C.J. Chou, J. Sole, A. Nichols, J.S. Ross, L.A. Tartaglia, H. Chen, Chronic inflammation in fat plays a crucial role in the development of obesity-related insulin resistance, *J Clin Invest*, 112 (2003) 1821-1830.
- [68] S.K. Biswas, A. Mantovani, Orchestration of metabolism by macrophages, *Cell Metab*, 15 (2012) 432-437.
- [69] O. Osborn, J.M. Olefsky, The cellular and signaling networks linking the immune system and metabolism in disease, *Nat Med*, 18 (2012) 363-374.
- [70] S. Gordon, P.R. Taylor, Monocyte and macrophage heterogeneity, *Nat Rev Immunol*, 5 (2005) 953-964.
- [71] C.N. Lumeng, J.L. Bodzin, A.R. Saltiel, Obesity induces a phenotypic switch in adipose tissue macrophage polarization, *J Clin Invest*, 117 (2007) 175-184.
- [72] C.N. Lumeng, S.M. Deyoung, J.L. Bodzin, A.R. Saltiel, Increased inflammatory properties of adipose tissue macrophages recruited during diet-induced obesity, *Diabetes*, 56 (2007) 16-23.
- [73] J.I. Odegaard, A. Chawla, Alternative macrophage activation and metabolism, *Annu Rev Pathol*, 6 (2011) 275-297.
- [74] J.I. Odegaard, R.R. Ricardo-Gonzalez, M.H. Goforth, C.R. Morel, V. Subramanian, L. Mukundan, A. Red Eagle, D. Vats, F. Brombacher, A.W. Ferrante, A. Chawla, Macrophage-specific PPAR γ controls alternative activation and improves insulin resistance, *Nature*, 447 (2007) 1116-1120.
- [75] K.D. Nguyen, Y. Qiu, X. Cui, Y.P. Goh, J. Mwangi, T. David, L. Mukundan, F. Brombacher, R.M. Locksley, A. Chawla, Alternatively activated macrophages produce catecholamines to sustain adaptive thermogenesis, *Nature*, 480 (2011) 104-108.

- [76] H.L. Kammoun, M.J. Kraakman, M.A. Febbraio, Adipose tissue inflammation in glucose metabolism, *Rev Endocr Metab Disord*, 15 (2014) 31-44.
- [77] P.E. Scherer, The Multifaceted Roles of Adipose Tissue-Therapeutic Targets for Diabetes and Beyond: The 2015 Banting Lecture, *Diabetes*, 65 (2016) 1452-1461.
- [78] G. Fantuzzi, Adipose tissue, adipokines, and inflammation, *J Allergy Clin Immunol*, 115 (2005) 911-919; quiz 920.
- [79] A. De Pauw, S. Tejerina, M. Raes, J. Keijer, T. Arnould, Mitochondrial (dys)function in adipocyte (de)differentiation and systemic metabolic alterations, *Am J Pathol*, 175 (2009) 927-939.
- [80] P. Arner, K.L. Spalding, Fat cell turnover in humans, *Biochem Biophys Res Commun*, 396 (2010) 101-104.
- [81] K.L. Spalding, E. Arner, P.O. Westermark, S. Bernard, B.A. Buchholz, O. Bergmann, L. Blomqvist, J. Hoffstedt, E. Naslund, T. Britton, H. Concha, M. Hassan, M. Ryden, J. Frisen, P. Arner, Dynamics of fat cell turnover in humans, *Nature*, 453 (2008) 783-787.
- [82] B. Cousin, S. Cinti, M. Morrioni, S. Raimbault, D. Ricquier, L. Penicaud, L. Casteilla, Occurrence of brown adipocytes in rat white adipose tissue: molecular and morphological characterization, *J Cell Sci*, 103 (Pt 4) (1992) 931-942.
- [83] J.G. Granneman, P. Li, Z. Zhu, Y. Lu, Metabolic and cellular plasticity in white adipose tissue I: effects of beta3-adrenergic receptor activation, *Am J Physiol Endocrinol Metab*, 289 (2005) E608-616.
- [84] J. Himms-Hagen, J. Cui, E. Danforth, Jr., D.J. Taatjes, S.S. Lang, B.L. Waters, T.H. Claus, Effect of CL-316,243, a thermogenic beta 3-agonist, on energy balance and brown and white adipose tissues in rats, *Am J Physiol*, 266 (1994) R1371-1382.
- [85] C.M. Kusminski, S. Shetty, L. Orci, R.H. Unger, P.E. Scherer, Diabetes and apoptosis: lipotoxicity, *Apoptosis*, 14 (2009) 1484-1495.
- [86] K. Sun, C.M. Kusminski, P.E. Scherer, Adipose tissue remodeling and obesity, *J Clin Invest*, 121 (2011) 2094-2101.
- [87] J. Pienkowska, B. Brzeska, M. Kaszubowski, O. Kozak, A. Jankowska, E. Szurowska, MRI assessment of ectopic fat accumulation in pancreas, liver and skeletal muscle in patients with obesity, overweight and normal BMI in correlation with the presence of central obesity and metabolic syndrome, *Diabetes Metab Syndr Obes*, 12 (2019) 623-636.
- [88] I. Trouwborst, S.M. Bowser, G.H. Goossens, E.E. Blaak, Ectopic Fat Accumulation in Distinct Insulin Resistant Phenotypes; Targets for Personalized Nutritional Interventions, *Front Nutr*, 5 (2018) 77.
- [89] X. Yi, Y.H. Liu, X.F. Zhou, Y.J. Wang, J. Deng, J. Liu, H.B. He, Z.Q. Xu, The Influence of Abdominal and Ectopic Fat Accumulation on Carotid Intima-Media Thickness: A Chongqing Study, *J Stroke Cerebrovasc Dis*, 27 (2018) 1992-1997.

- [90] R.G. Singh, H.D. Yoon, S.D. Poppitt, L.D. Plank, M.S. Petrov, Ectopic fat accumulation in the pancreas and its biomarkers: A systematic review and meta-analysis, *Diabetes Metab Res Rev*, 33 (2017).
- [91] R.G. Singh, H.D. Yoon, L.M. Wu, J. Lu, L.D. Plank, M.S. Petrov, Ectopic fat accumulation in the pancreas and its clinical relevance: A systematic review, meta-analysis, and meta-regression, *Metabolism*, 69 (2017) 1-13.
- [92] B. Gustafson, Adipose tissue, inflammation and atherosclerosis, *J Atheroscler Thromb*, 17 (2010) 332-341.
- [93] R. Cencello, J. Tordjman, C. Poitou, G. Guilhem, J.L. Bouillot, D. Hugol, C. Coussieu, A. Basdevant, A. Bar Hen, P. Bedossa, M. Guerre-Millo, K. Clement, Increased infiltration of macrophages in omental adipose tissue is associated with marked hepatic lesions in morbid human obesity, *Diabetes*, 55 (2006) 1554-1561.
- [94] S. Cinti, G. Mitchell, G. Barbatelli, I. Murano, E. Ceresi, E. Faloia, S. Wang, M. Fortier, A.S. Greenberg, M.S. Obin, Adipocyte death defines macrophage localization and function in adipose tissue of obese mice and humans, *J Lipid Res*, 46 (2005) 2347-2355.
- [95] U. Kintscher, M. Hartge, K. Hess, A. Foryst-Ludwig, M. Clemenz, M. Wabitsch, P. Fischer-Posovszky, T.F. Barth, D. Dragan, T. Skurk, H. Hauner, M. Bluher, T. Unger, A.M. Wolf, U. Knippschild, V. Hombach, N. Marx, T-lymphocyte infiltration in visceral adipose tissue: a primary event in adipose tissue inflammation and the development of obesity-mediated insulin resistance, *Arterioscler Thromb Vasc Biol*, 28 (2008) 1304-1310.
- [96] V. Elgazar-Carmon, A. Rudich, N. Hadad, R. Levy, Neutrophils transiently infiltrate intra-abdominal fat early in the course of high-fat feeding, *J Lipid Res*, 49 (2008) 1894-1903.
- [97] A. Guilherme, J.V. Virbasius, V. Puri, M.P. Czech, Adipocyte dysfunctions linking obesity to insulin resistance and type 2 diabetes, *Nat Rev Mol Cell Biol*, 9 (2008) 367-377.
- [98] N. Stefan, M. Stumvoll, Adiponectin--its role in metabolism and beyond, *Horm Metab Res*, 34 (2002) 469-474.
- [99] E. Dalmás, C. Rouault, M. Abdenour, C. Rovere, S. Rizkalla, A. Bar-Hen, J.L. Nahon, J.L. Bouillot, M. Guerre-Millo, K. Clement, C. Poitou, Variations in circulating inflammatory factors are related to changes in calorie and carbohydrate intakes early in the course of surgery-induced weight reduction, *Am J Clin Nutr*, 94 (2011) 450-458.
- [100] K. Esposito, A. Pontillo, C. Di Palo, G. Giugliano, M. Masella, R. Marfella, D. Giugliano, Effect of weight loss and lifestyle changes on vascular inflammatory markers in obese women: a randomized trial, *JAMA*, 289 (2003) 1799-1804.
- [101] N. Tajik, S.A. Keshavarz, F. Masoudkabar, M. Djalali, H.H. Sadrzadeh-Yeganeh, M.R. Eshraghian, M. Chamary, Z. Ahmadvand, T. Yazdani, M.H. Javanbakht, Effect of diet-induced weight loss on inflammatory cytokines in obese women, *J Endocrinol Invest*, 36 (2013) 211-215.

- [102] B.H. Goodpaster, L.M. Sparks, Metabolic Flexibility in Health and Disease, *Cell Metab*, 25 (2017) 1027-1036.
- [103] P. Bostrom, J. Wu, M.P. Jedrychowski, A. Korde, L. Ye, J.C. Lo, K.A. Rasbach, E.A. Bostrom, J.H. Choi, J.Z. Long, S. Kajimura, M.C. Zingaretti, B.F. Vind, H. Tu, S. Cinti, K. Hojlund, S.P. Gygi, B.M. Spiegelman, A PGC1-alpha-dependent myokine that drives brown-fat-like development of white fat and thermogenesis, *Nature*, 481 (2012) 463-468.
- [104] J. Nedergaard, B. Cannon, The browning of white adipose tissue: some burning issues, *Cell Metab*, 20 (2014) 396-407.
- [105] K.I. Stanford, R.J. Middelbeek, L.J. Goodyear, Exercise Effects on White Adipose Tissue: Beiging and Metabolic Adaptations, *Diabetes*, 64 (2015) 2361-2368.
- [106] L. Reshef, Y. Olswang, H. Cassuto, B. Blum, C.M. Croniger, S.C. Kalhan, S.M. Tilghman, R.W. Hanson, Glyceroneogenesis and the triglyceride/fatty acid cycle, *J Biol Chem*, 278 (2003) 30413-30416.
- [107] X.X. Yu, D.A. Lewin, W. Forrest, S.H. Adams, Cold elicits the simultaneous induction of fatty acid synthesis and beta-oxidation in murine brown adipose tissue: prediction from differential gene expression and confirmation in vivo, *FASEB J*, 16 (2002) 155-168.
- [108] S.M. Grundy, J.I. Cleeman, S.R. Daniels, K.A. Donato, R.H. Eckel, B.A. Franklin, D.J. Gordon, R.M. Krauss, P.J. Savage, S.C. Smith, Jr., J.A. Spertus, F. Costa, Diagnosis and management of the metabolic syndrome: an American Heart Association/National Heart, Lung, and Blood Institute Scientific Statement, *Circulation*, 112 (2005) 2735-2752.
- [109] R.H. Eckel, S.M. Grundy, P.Z. Zimmet, The metabolic syndrome, *Lancet*, 365 (2005) 1415-1428.
- [110] S. Nielsen, Z. Guo, C.M. Johnson, D.D. Hensrud, M.D. Jensen, Splanchnic lipolysis in human obesity, *J Clin Invest*, 113 (2004) 1582-1588.
- [111] L.C. Groop, R.C. Bonadonna, S. DelPrato, K. Ratheiser, K. Zyck, E. Ferrannini, R.A. DeFronzo, Glucose and free fatty acid metabolism in non-insulin-dependent diabetes mellitus. Evidence for multiple sites of insulin resistance, *J Clin Invest*, 84 (1989) 205-213.
- [112] J.F. Horowitz, R. Mora-Rodriguez, L.O. Byerley, E.F. Coyle, Substrate metabolism when subjects are fed carbohydrate during exercise, *Am J Physiol*, 276 (1999) E828-835.
- [113] P.J. Campbell, M.G. Carlson, N. Nurjhan, Fat metabolism in human obesity, *Am J Physiol*, 266 (1994) E600-605.
- [114] S.E. McQuaid, L. Hodson, M.J. Neville, A.L. Dennis, J. Cheeseman, S.M. Humphreys, T. Ruge, M. Gilbert, B.A. Fielding, K.N. Frayn, F. Karpe, Downregulation of adipose tissue fatty acid trafficking in obesity: a driver for ectopic fat deposition?, *Diabetes*, 60 (2011) 47-55.

- [115] J. Girard, [Mechanisms of action of thiazolidinediones], *Diabetes Metab*, 27 (2001) 271-278.
- [116] D.M. Muoio, Metabolic inflexibility: when mitochondrial indecision leads to metabolic gridlock, *Cell*, 159 (2014) 1253-1262.
- [117] C.R. Bruce, A.J. Hoy, N. Turner, M.J. Watt, T.L. Allen, K. Carpenter, G.J. Cooney, M.A. Febbraio, E.W. Kraegen, Overexpression of carnitine palmitoyltransferase-1 in skeletal muscle is sufficient to enhance fatty acid oxidation and improve high-fat diet-induced insulin resistance, *Diabetes*, 58 (2009) 550-558.
- [118] T.R. Koves, J.R. Ussher, R.C. Noland, D. Slentz, M. Mosedale, O. Ilkayeva, J. Bain, R. Stevens, J.R. Dyck, C.B. Newgard, G.D. Lopaschuk, D.M. Muoio, Mitochondrial overload and incomplete fatty acid oxidation contribute to skeletal muscle insulin resistance, *Cell Metab*, 7 (2008) 45-56.
- [119] M. Cedikova, M. Kripnerova, J. Dvorakova, P. Pitule, M. Grundmanova, V. Babuska, D. Mullerova, J. Kuncova, Mitochondria in White, Brown, and Beige Adipocytes, *Stem Cells Int*, 2016 (2016) 6067349.
- [120] S. Boudina, T.E. Graham, Mitochondrial function/dysfunction in white adipose tissue, *Exp Physiol*, 99 (2014) 1168-1178.
- [121] M.K. Montgomery, N. Turner, Mitochondrial dysfunction and insulin resistance: an update, *Endocr Connect*, 4 (2015) R1-R15.
- [122] X. Yin, I.R. Lanza, J.M. Swain, M.G. Sarr, K.S. Nair, M.D. Jensen, Adipocyte mitochondrial function is reduced in human obesity independent of fat cell size, *J Clin Endocrinol Metab*, 99 (2014) E209-216.
- [123] N. Turner, L.K. Heilbronn, Is mitochondrial dysfunction a cause of insulin resistance?, *Trends Endocrinol Metab*, 19 (2008) 324-330.
- [124] K.J. Dunham-Snary, S.W. Ballinger, Mitochondrial genetics and obesity: evolutionary adaptation and contemporary disease susceptibility, *Free Radic Biol Med*, 65 (2013) 1229-1237.
- [125] D.J. Betteridge, What is oxidative stress?, *Metabolism*, 49 (2000) 3-8.
- [126] D.L. Johannsen, E. Ravussin, The role of mitochondria in health and disease, *Curr Opin Pharmacol*, 9 (2009) 780-786.
- [127] S. Furukawa, T. Fujita, M. Shimabukuro, M. Iwaki, Y. Yamada, Y. Nakajima, O. Nakayama, M. Makishima, M. Matsuda, I. Shimomura, Increased oxidative stress in obesity and its impact on metabolic syndrome, *J Clin Invest*, 114 (2004) 1752-1761.
- [128] C.H. Wang, C.C. Wang, H.C. Huang, Y.H. Wei, Mitochondrial dysfunction leads to impairment of insulin sensitivity and adiponectin secretion in adipocytes, *FEBS J*, 280 (2013) 1039-1050.
- [129] C.R. Kahn, Insulin resistance, insulin insensitivity, and insulin unresponsiveness: a necessary distinction, *Metabolism*, 27 (1978) 1893-1902.

- [130] F. Boyer, J.B. Vidot, A.G. Dubourg, P. Rondeau, M.F. Essop, E. Bourdon, Oxidative stress and adipocyte biology: focus on the role of AGEs, *Oxid Med Cell Longev*, 2015 (2015) 534873.
- [131] C.H. Wang, T.F. Tsai, Y.H. Wei, Role of mitochondrial dysfunction and dysregulation of Ca(2+) homeostasis in insulin insensitivity of mammalian cells, *Ann N Y Acad Sci*, 1350 (2015) 66-76.
- [132] S. Heinonen, J. Buzkova, M. Muniandy, R. Kaksonen, M. Ollikainen, K. Ismail, A. Hakkarainen, J. Lundbom, N. Lundbom, K. Vuolteenaho, E. Moilanen, J. Kaprio, A. Rissanen, A. Suomalainen, K.H. Pietilainen, Impaired Mitochondrial Biogenesis in Adipose Tissue in Acquired Obesity, *Diabetes*, 64 (2015) 3135-3145.
- [133] L.N. Sutherland, L.C. Capozzi, N.J. Turchinsky, R.C. Bell, D.C. Wright, Time course of high-fat diet-induced reductions in adipose tissue mitochondrial proteins: potential mechanisms and the relationship to glucose intolerance, *Am J Physiol Endocrinol Metab*, 295 (2008) E1076-1083.
- [134] S.D. Martin, S. Morrison, N. Konstantopoulos, S.L. McGee, Mitochondrial dysfunction has divergent, cell type-dependent effects on insulin action, *Mol Metab*, 3 (2014) 408-418.
- [135] A.J. Walley, A.I. Blakemore, P. Froguel, Genetics of obesity and the prediction of risk for health, *Hum Mol Genet*, 15 Spec No 2 (2006) R124-130.
- [136] G.C. Kujoth, P.C. Bradshaw, S. Haroon, T.A. Prolla, The role of mitochondrial DNA mutations in mammalian aging, *PLoS Genet*, 3 (2007) e24.
- [137] C.L. Gao, C. Zhu, Y.P. Zhao, X.H. Chen, C.B. Ji, C.M. Zhang, J.G. Zhu, Z.K. Xia, M.L. Tong, X.R. Guo, Mitochondrial dysfunction is induced by high levels of glucose and free fatty acids in 3T3-L1 adipocytes, *Mol Cell Endocrinol*, 320 (2010) 25-33.
- [138] M.P. Keller, A.D. Attie, Physiological insights gained from gene expression analysis in obesity and diabetes, *Annu Rev Nutr*, 30 (2010) 341-364.
- [139] P. Puigserver, Z. Wu, C.W. Park, R. Graves, M. Wright, B.M. Spiegelman, A cold-inducible coactivator of nuclear receptors linked to adaptive thermogenesis, *Cell*, 92 (1998) 829-839.
- [140] R. Pardo, N. Enguix, J. Lasheras, J.E. Feliu, A. Kralli, J.A. Villena, Rosiglitazone-induced mitochondrial biogenesis in white adipose tissue is independent of peroxisome proliferator-activated receptor gamma coactivator-1alpha, *PLoS One*, 6 (2011) e26989.
- [141] C. Tiraby, G. Tavernier, C. Lefort, D. Larrouy, F. Bouillaud, D. Ricquier, D. Langin, Acquirement of brown fat cell features by human white adipocytes, *J Biol Chem*, 278 (2003) 33370-33376.
- [142] R.K. Semple, V.C. Crowley, C.P. Sewter, M. Laudes, C. Christodoulides, R.V. Considine, A. Vidal-Puig, S. O'Rahilly, Expression of the thermogenic nuclear hormone receptor coactivator PGC-1alpha is reduced in the adipose tissue of morbidly obese subjects, *Int J Obes Relat Metab Disord*, 28 (2004) 176-179.

[143] A. Afshin, M.H. Forouzanfar, M.B. Reitsma, P. Sur, K. Estep, A. Lee, L. Marczak, A.H. Mokdad, M. Moradi-Lakeh, M. Naghavi, J.S. Salama, T. Vos, K.H. Abate, C. Abbafati, M.B. Ahmed, Z. Al-Aly, A. Alkerwi, R. Al-Raddadi, A.T. Amare, A. Amberbir, A.K. Amegah, E. Amini, S.M. Amrock, R.M. Anjana, J. Arnlov, H. Asayesh, A. Banerjee, A. Barac, E. Baye, D.A. Bennett, A.S. Beyene, S. Biadgilign, S. Biryukov, E. Bjertness, D.J. Boneya, I. Campos-Nonato, J.J. Carrero, P. Cecilio, K. Cercy, L.G. Ciobanu, L. Cornaby, S.A. Damtew, L. Dandona, R. Dandona, S.D. Dharmaratne, B.B. Duncan, B. Eshрати, A. Esteghamati, V.L. Feigin, J.C. Fernandes, T. Furst, T.T. Gebrehiwot, A. Gold, P.N. Gona, A. Goto, T.D. Habtewold, K.T. Hadush, N. Hafezi-Nejad, S.I. Hay, M. Horino, F. Islami, R. Kamal, A. Kasaeian, S.V. Katikireddi, A.P. Kengne, C.N. Kesavachandran, Y.S. Khader, Y.H. Khang, J. Khubchandani, D. Kim, Y.J. Kim, Y. Kinfu, S. Kosen, T. Ku, B.K. Defo, G.A. Kumar, H.J. Larson, M. Leinsalu, X. Liang, S.S. Lim, P. Liu, A.D. Lopez, R. Lozano, A. Majeed, R. Malekzadeh, D.C. Malta, M. Mazidi, C. McAlinden, S.T. McGarvey, D.T. Mengistu, G.A. Mensah, G.B.M. Mensink, H.B. Mezgebe, E.M. Mirrakhimov, U.O. Mueller, J.J. Noubiap, C.M. Obermeyer, F.A. Ogbo, M.O. Owolabi, G.C. Patton, F. Pourmalek, M. Qorbani, A. Rafay, R.K. Rai, C.L. Ranabhat, N. Reinig, S. Safiri, J.A. Salomon, J.R. Sanabria, I.S. Santos, B. Sartorius, M. Sawhney, J. Schmidhuber, A.E. Schutte, M.I. Schmidt, S.G. Sepanlou, M. Shamsizadeh, S. Sheikhabaehi, M.J. Shin, R. Shiri, I. Shiue, H.S. Roba, D.A.S. Silva, J.I. Silverberg, J.A. Singh, S. Stranges, S. Swaminathan, R. Tabares-Seisdedos, F. Tadese, B.A. Tedla, B.S. Tegegne, A.S. Terkawi, J.S. Thakur, M. Tonelli, R. Topor-Madry, S. Tyrovolas, K.N. Ukwaja, O.A. Uthman, M. Vaezghasemi, T. Vasankari, V.V. Vlassov, S.E. Vollset, E. Weiderpass, A. Werdecker, J. Wesana, R. Westerman, Y. Yano, N. Yonemoto, G. Yonga, Z. Zaidi, Z.M. Zenebe, B. Zipkin, C.J.L. Murray, Health Effects of Overweight and Obesity in 195 Countries over 25 Years, *N Engl J Med*, 377 (2017) 13-27.

[144] P. Balagopal, D. George, N. Patton, H. Yarandi, W.L. Roberts, E. Bayne, S. Gidding, Lifestyle-only intervention attenuates the inflammatory state associated with obesity: a randomized controlled study in adolescents, *J Pediatr*, 146 (2005) 342-348.

[145] J.G. Knudsen, M. Murholm, A.L. Carey, R.S. Bienso, A.L. Basse, T.L. Allen, J. Hidalgo, B.A. Kingwell, M.A. Febbraio, J.B. Hansen, H. Pilegaard, Role of IL-6 in exercise training- and cold-induced UCP1 expression in subcutaneous white adipose tissue, *PLoS One*, 9 (2014) e84910.

[146] S. Ringholm, J. Grunnet Knudsen, L. Leick, A. Lundgaard, M. Munk Nielsen, H. Pilegaard, PGC-1 α is required for exercise- and exercise training-induced UCP1 up-regulation in mouse white adipose tissue, *PLoS One*, 8 (2013) e64123.

[147] P. Aldiss, J. Betts, C. Sale, M. Pope, H. Budge, M.E. Symonds, Exercise-induced 'browning' of adipose tissues, *Metabolism*, 81 (2018) 63-70.

[148] L.N. Sutherland, M.R. Bomhof, L.C. Capozzi, S.A. Basaraba, D.C. Wright, Exercise and adrenaline increase PGC-1 α mRNA expression in rat adipose tissue, *J Physiol*, 587 (2009) 1607-1617.

[149] G. Rao, T.M. Powell-Wiley, I. Ancheta, K. Hairston, K. Kirley, S.A. Lear, K.E. North, L. Palaniappan, M.C. Rosal, Identification of Obesity and Cardiovascular Risk in

Ethnically and Racially Diverse Populations: A Scientific Statement From the American Heart Association, *Circulation*, 132 (2015) 457-472.

[150] P. Poirier, J. Martin, P. Marceau, S. Biron, S. Marceau, Impact of bariatric surgery on cardiac structure, function and clinical manifestations in morbid obesity, *Expert Rev Cardiovasc Ther*, 2 (2004) 193-201.

[151] N.K. Brownell, M. Rodriguez-Flores, E. Garcia-Garcia, S. Ordonez-Ortega, J. Oseguera-Moguel, C.A. Aguilar-Salinas, P. Poirier, Impact of Body Mass Index >50 on Cardiac Structural and Functional Characteristics and Surgical Outcomes After Bariatric Surgery, *Obes Surg*, 26 (2016) 2772-2778.

[152] M.E. Piche, P. Poirier, I. Lemieux, J.P. Despres, Overview of Epidemiology and Contribution of Obesity and Body Fat Distribution to Cardiovascular Disease: An Update, *Prog Cardiovasc Dis*, 61 (2018) 103-113.

[153] H.C. McGill, Jr., Fatty streaks in the coronary arteries and aorta, *Lab Invest*, 18 (1968) 560-564.

[154] J.C. Geer, H.C. McGill, Jr., W.B. Robertson, J.P. Strong, Histologic characteristics of coronary artery fatty streaks, *Lab Invest*, 18 (1968) 565-570.

[155] K. Skalen, M. Gustafsson, E.K. Rydberg, L.M. Hulten, O. Wiklund, T.L. Innerarity, J. Boren, Subendothelial retention of atherogenic lipoproteins in early atherosclerosis, *Nature*, 417 (2002) 750-754.

[156] M.L. Bots, A. Hofman, D.E. Grobbee, Increased common carotid intima-media thickness. Adaptive response or a reflection of atherosclerosis? Findings from the Rotterdam Study, *Stroke*, 28 (1997) 2442-2447.

[157] J.D. Spence, Ultrasound measurement of carotid plaque as a surrogate outcome for coronary artery disease, *Am J Cardiol*, 89 (2002) 10B-15B; discussion 15B-16B.

[158] G. Heiss, A.R. Sharrett, R. Barnes, L.E. Chambless, M. Szklo, C. Alzola, Carotid atherosclerosis measured by B-mode ultrasound in populations: associations with cardiovascular risk factors in the ARIC study, *Am J Epidemiol*, 134 (1991) 250-256.

[159] M. Ciccone, R. Vettor, N. Pannacciulli, A. Minenna, M. Bellacicco, P. Rizzon, R. Giorgino, G. De Pergola, Plasma leptin is independently associated with the intima-media thickness of the common carotid artery, *Int J Obes Relat Metab Disord*, 25 (2001) 805-810.

[160] M.L. Bots, A.W. Hoes, P.J. Koudstaal, A. Hofman, D.E. Grobbee, Common carotid intima-media thickness and risk of stroke and myocardial infarction: the Rotterdam Study, *Circulation*, 96 (1997) 1432-1437.

[161] D.H. O'Leary, J.F. Polak, R.A. Kronmal, T.A. Manolio, G.L. Burke, S.K. Wolfson, Jr., Carotid-artery intima and media thickness as a risk factor for myocardial infarction and stroke in older adults. Cardiovascular Health Study Collaborative Research Group, *N Engl J Med*, 340 (1999) 14-22.

- [162] P.A. Kern, M. Saghizadeh, J.M. Ong, R.J. Bosch, R. Deem, R.B. Simolo, The expression of tumor necrosis factor in human adipose tissue. Regulation by obesity, weight loss, and relationship to lipoprotein lipase, *J Clin Invest*, 95 (1995) 2111-2119.
- [163] G.S. Hotamisligil, P. Arner, J.F. Caro, R.L. Atkinson, B.M. Spiegelman, Increased adipose tissue expression of tumor necrosis factor- α in human obesity and insulin resistance, *J Clin Invest*, 95 (1995) 2409-2415.
- [164] B.L. Wajchenberg, Subcutaneous and visceral adipose tissue: their relation to the metabolic syndrome, *Endocr Rev*, 21 (2000) 697-738.
- [165] E.K. Oikonomou, C. Antoniades, Immunometabolic Regulation of Vascular Redox State: The Role of Adipose Tissue, *Antioxid Redox Signal*, 29 (2018) 313-336.
- [166] J.S. Yudkin, C.D. Stehouwer, J.J. Emeis, S.W. Coppack, C-reactive protein in healthy subjects: associations with obesity, insulin resistance, and endothelial dysfunction: a potential role for cytokines originating from adipose tissue?, *Arterioscler Thromb Vasc Biol*, 19 (1999) 972-978.
- [167] V. Mohamed-Ali, S. Goodrick, A. Rawesh, D.R. Katz, J.M. Miles, J.S. Yudkin, S. Klein, S.W. Coppack, Subcutaneous adipose tissue releases interleukin-6, but not tumor necrosis factor- α , in vivo, *J Clin Endocrinol Metab*, 82 (1997) 4196-4200.
- [168] P.M. Ridker, Novel risk factors and markers for coronary disease, *Adv Intern Med*, 45 (2000) 391-418.
- [169] M. Cigolini, G. Targher, I.A. Bergamo Andreis, M. Tonoli, G. Agostino, G. De Sandre, Visceral fat accumulation and its relation to plasma hemostatic factors in healthy men, *Arterioscler Thromb Vasc Biol*, 16 (1996) 368-374.
- [170] S. Yusuf, S. Hawken, S. Ounpuu, L. Bautista, M.G. Franzosi, P. Commerford, C.C. Lang, Z. Rumboldt, C.L. Onen, L. Lisheng, S. Tanomsup, P. Wangai, Jr., F. Razak, A.M. Sharma, S.S. Anand, Obesity and the risk of myocardial infarction in 27,000 participants from 52 countries: a case-control study, *Lancet*, 366 (2005) 1640-1649.
- [171] R.F. Kushner, Weight Loss Strategies for Treatment of Obesity: Lifestyle Management and Pharmacotherapy, *Prog Cardiovasc Dis*, 61 (2018) 246-252.
- [172] V. Yumuk, C. Tsigos, M. Fried, K. Schindler, L. Busetto, D. Micic, H. Toplak, European Guidelines for Obesity Management in Adults, *Obes Facts*, 8 (2015) 402-424.
- [173] E.E. Kershaw, J.S. Flier, Adipose tissue as an endocrine organ, *J Clin Endocrinol Metab*, 89 (2004) 2548-2556.
- [174] F.M. Fisher, S. Kleiner, N. Douris, E.C. Fox, R.J. Mepani, F. Verdeguer, J. Wu, A. Kharitonov, J.S. Flier, E. Maratos-Flier, B.M. Spiegelman, FGF21 regulates PGC-1 α and browning of white adipose tissues in adaptive thermogenesis, *Genes Dev*, 26 (2012) 271-281.
- [175] P. Lee, J.D. Linderman, S. Smith, R.J. Brychta, J. Wang, C. Idelson, R.M. Perron, C.D. Werner, G.Q. Phan, U.S. Kammula, E. Kebebew, K. Pacak, K.Y. Chen, F.S. Celi, Irisin

and FGF21 are cold-induced endocrine activators of brown fat function in humans, *Cell Metab*, 19 (2014) 302-309.

[176] S. Fang, J.M. Suh, S.M. Reilly, E. Yu, O. Osborn, D. Lackey, E. Yoshihara, A. Perino, S. Jacinto, Y. Lukasheva, A.R. Atkins, A. Khvat, B. Schnabl, R.T. Yu, D.A. Brenner, S. Coulter, C. Liddle, K. Schoonjans, J.M. Olefsky, A.R. Saltiel, M. Downes, R.M. Evans, Intestinal FXR agonism promotes adipose tissue browning and reduces obesity and insulin resistance, *Nat Med*, 21 (2015) 159-165.

[177] T.P. Combs, U.B. Pajvani, A.H. Berg, Y. Lin, L.A. Jelicks, M. Laplante, A.R. Nawrocki, M.W. Rajala, A.F. Parlow, L. Cheeseboro, Y.Y. Ding, R.G. Russell, D. Lindemann, A. Hartley, G.R. Baker, S. Obici, Y. Deshaies, M. Ludgate, L. Rossetti, P.E. Scherer, A transgenic mouse with a deletion in the collagenous domain of adiponectin displays elevated circulating adiponectin and improved insulin sensitivity, *Endocrinology*, 145 (2004) 367-383.

[178] M.M. Veniant, G. Sivits, J. Helmering, R. Komorowski, J. Lee, W. Fan, C. Moyer, D.J. Lloyd, Pharmacologic Effects of FGF21 Are Independent of the "Browning" of White Adipose Tissue, *Cell Metab*, 21 (2015) 731-738.

[179] R.J. Samms, D.P. Smith, C.C. Cheng, P.P. Antonellis, J.W. Perfield, 2nd, A. Kharitonov, R.E. Gimeno, A.C. Adams, Discrete Aspects of FGF21 In Vivo Pharmacology Do Not Require UCP1, *Cell Rep*, 11 (2015) 991-999.

[180] L. Wilson-Fritch, S. Nicoloso, M. Chouinard, M.A. Lazar, P.C. Chui, J. Leszyk, J. Straubhaar, M.P. Czech, S. Corvera, Mitochondrial remodeling in adipose tissue associated with obesity and treatment with rosiglitazone, *J Clin Invest*, 114 (2004) 1281-1289.

[181] L. Qiang, L. Wang, N. Kon, W. Zhao, S. Lee, Y. Zhang, M. Rosenbaum, Y. Zhao, W. Gu, S.R. Farmer, D. Accili, Brown remodeling of white adipose tissue by Sirt1-dependent deacetylation of Ppargamma, *Cell*, 150 (2012) 620-632.

[182] F. Picard, M. Kurtev, N. Chung, A. Topark-Ngarm, T. Senawong, R. Machado De Oliveira, M. Leid, M.W. McBurney, L. Guarente, Sirt1 promotes fat mobilization in white adipocytes by repressing PPAR-gamma, *Nature*, 429 (2004) 771-776.

[183] J.H. Choi, A.S. Banks, J.L. Estall, S. Kajimura, P. Bostrom, D. Laznik, J.L. Ruas, M.J. Chalmers, T.M. Kamenecka, M. Bluher, P.R. Griffin, B.M. Spiegelman, Anti-diabetic drugs inhibit obesity-linked phosphorylation of PPARgamma by Cdk5, *Nature*, 466 (2010) 451-456.

[184] W. Wahli, L. Michalik, PPARs at the crossroads of lipid signaling and inflammation, *Trends Endocrinol Metab*, 23 (2012) 351-363.

[185] A. Kauppinen, T. Suuronen, J. Ojala, K. Kaarniranta, A. Salminen, Antagonistic crosstalk between NF-kappaB and SIRT1 in the regulation of inflammation and metabolic disorders, *Cell Signal*, 25 (2013) 1939-1948.

[186] R. Mayoral, O. Osborn, J. McNelis, A.M. Johnson, D.Y. Oh, C.L. Izquierdo, H. Chung, P. Li, P.G. Traves, G. Bandyopadhyay, A.R. Pessentheiner, J.M. Ofrecio, J.R. Cook, L. Qiang, D. Accili, J.M. Olefsky, Adipocyte SIRT1 knockout promotes PPARgamma activity,

adipogenesis and insulin sensitivity in chronic-HFD and obesity, *Mol Metab*, 4 (2015) 378-391.

[187] C. Canto, K.J. Menzies, J. Auwerx, NAD(+) Metabolism and the Control of Energy Homeostasis: A Balancing Act between Mitochondria and the Nucleus, *Cell Metab*, 22 (2015) 31-53.

[188] G. Magni, A. Amici, M. Emanuelli, G. Orsomando, N. Raffaelli, S. Ruggieri, Enzymology of NAD⁺ homeostasis in man, *Cell Mol Life Sci*, 61 (2004) 19-34.

[189] R.H. Houtkooper, C. Canto, R.J. Wanders, J. Auwerx, The secret life of NAD⁺: an old metabolite controlling new metabolic signaling pathways, *Endocr Rev*, 31 (2010) 194-223.

[190] B. Schwer, E. Verdin, Conserved metabolic regulatory functions of sirtuins, *Cell Metab*, 7 (2008) 104-112.

[191] B.A. Gibson, W.L. Kraus, New insights into the molecular and cellular functions of poly(ADP-ribose) and PARPs, *Nat Rev Mol Cell Biol*, 13 (2012) 411-424.

[192] P. Belenky, K.L. Bogan, C. Brenner, NAD⁺ metabolism in health and disease, *Trends Biochem Sci*, 32 (2007) 12-19.

[193] H.C. Lee, Cyclic ADP-ribose and nicotinic acid adenine dinucleotide phosphate (NAADP) as messengers for calcium mobilization, *J Biol Chem*, 287 (2012) 31633-31640.

[194] J. Yoshino, J.A. Baur, S.I. Imai, NAD(+) Intermediates: The Biology and Therapeutic Potential of NMN and NR, *Cell Metab*, 27 (2018) 513-528.

[195] P. Bieganowski, C. Brenner, Discoveries of nicotinamide riboside as a nutrient and conserved NRK genes establish a Preiss-Handler independent route to NAD⁺ in fungi and humans, *Cell*, 117 (2004) 495-502.

[196] A.A. Sauve, NAD⁺ and vitamin B3: from metabolism to therapies, *J Pharmacol Exp Ther*, 324 (2008) 883-893.

[197] D. Kraus, Q. Yang, D. Kong, A.S. Banks, L. Zhang, J.T. Rodgers, E. Pirinen, T.C. Pulinilkunnil, F. Gong, Y.C. Wang, Y. Cen, A.A. Sauve, J.M. Asara, O.D. Peroni, B.P. Monia, S. Bhanot, L. Alhonen, P. Puigserver, B.B. Kahn, Nicotinamide N-methyltransferase knockdown protects against diet-induced obesity, *Nature*, 508 (2014) 258-262.

[198] R. Felici, A. Lapucci, M. Ramazzotti, A. Chiarugi, Insight into molecular and functional properties of NMNAT3 reveals new hints of NAD homeostasis within human mitochondria, *PLoS One*, 8 (2013) e76938.

[199] R. Weinshilboum, Methyltransferase pharmacogenetics, *Pharmacol Ther*, 43 (1989) 77-90.

[200] S. Aksoy, C.L. Szumlanski, R.M. Weinshilboum, Human liver nicotinamide N-methyltransferase. cDNA cloning, expression, and biochemical characterization, *J Biol Chem*, 269 (1994) 14835-14840.

- [201] R. Castro, I. Rivera, H.J. Blom, C. Jakobs, I. Tavares de Almeida, Homocysteine metabolism, hyperhomocysteinaemia and vascular disease: an overview, *J Inherit Metab Dis*, 29 (2006) 3-20.
- [202] M. Bartus, M. Lomnicka, R.B. Kostogrys, P. Kazmierczak, C. Watala, E.M. Slominska, R.T. Smolenski, P.M. Pisulewski, J. Adamus, J. Gebicki, S. Chlopicki, 1-Methylnicotinamide (MNA) prevents endothelial dysfunction in hypertriglyceridemic and diabetic rats, *Pharmacol Rep*, 60 (2008) 127-138.
- [203] S. Chlopicki, J. Swies, A. Mogielnicki, W. Buczek, M. Bartus, M. Lomnicka, J. Adamus, J. Gebicki, 1-Methylnicotinamide (MNA), a primary metabolite of nicotinamide, exerts anti-thrombotic activity mediated by a cyclooxygenase-2/prostacyclin pathway, *Br J Pharmacol*, 152 (2007) 230-239.
- [204] L. Mateuszuk, T.I. Khomich, E. Slominska, M. Gajda, L. Wojcik, M. Lomnicka, P. Gwozdz, S. Chlopicki, Activation of nicotinamide N-methyltransferase and increased formation of 1-methylnicotinamide (MNA) in atherosclerosis, *Pharmacol Rep*, 61 (2009) 76-85.
- [205] M. Sternak, T.I. Khomich, A. Jakubowski, M. Szafarz, W. Szczepanski, M. Bialas, M. Stojak, J. Szymura-Oleksiak, S. Chlopicki, Nicotinamide N-methyltransferase (NNMT) and 1-methylnicotinamide (MNA) in experimental hepatitis induced by concanavalin A in the mouse, *Pharmacol Rep*, 62 (2010) 483-493.
- [206] C. Watala, P. Kazmierczak, M. Dobaczewski, T. Przygodzki, M. Bartus, M. Lomnicka, E.M. Slominska, Z. Durackova, S. Chlopicki, Anti-diabetic effects of 1-methylnicotinamide (MNA) in streptozocin-induced diabetes in rats, *Pharmacol Rep*, 61 (2009) 86-98.
- [207] M. Fukaya, Y. Tamura, Y. Chiba, T. Tanioka, J. Mao, Y. Inoue, M. Yamada, C. Waeber, Y. Ido-Kitamura, T. Kitamura, M. Kaneki, Protective effects of a nicotinamide derivative, isonicotinamide, against streptozotocin-induced beta-cell damage and diabetes in mice, *Biochem Biophys Res Commun*, 442 (2013) 92-98.
- [208] S. Bijland, S.J. Mancini, I.P. Salt, Role of AMP-activated protein kinase in adipose tissue metabolism and inflammation, *Clin Sci (Lond)*, 124 (2013) 491-507.
- [209] E.M. Desjardins, G.R. Steinberg, Emerging Role of AMPK in Brown and Beige Adipose Tissue (BAT): Implications for Obesity, Insulin Resistance, and Type 2 Diabetes, *Curr Diab Rep*, 18 (2018) 80.
- [210] C. Canto, Z. Gerhart-Hines, J.N. Feige, M. Lagouge, L. Noriega, J.C. Milne, P.J. Elliott, P. Puigserver, J. Auwerx, AMPK regulates energy expenditure by modulating NAD⁺ metabolism and SIRT1 activity, *Nature*, 458 (2009) 1056-1060.
- [211] M.B. Schultz, D.A. Sinclair, Why NAD(+) Declines during Aging: It's Destroyed, *Cell Metab*, 23 (2016) 965-966.
- [212] Y.S. Elhassan, A.A. Philp, G.G. Lavery, Targeting NAD⁺ in Metabolic Disease: New Insights Into an Old Molecule, *J Endocr Soc*, 1 (2017) 816-835.
- [213] K.L. Stromsdorfer, S. Yamaguchi, M.J. Yoon, A.C. Moseley, M.P. Franczyk, S.C. Kelly, N. Qi, S. Imai, J. Yoshino, NAMPT-Mediated NAD(+) Biosynthesis in Adipocytes

- Regulates Adipose Tissue Function and Multi-organ Insulin Sensitivity in Mice, *Cell Rep*, 16 (2016) 1851-1860.
- [214] S. Yamaguchi, J. Yoshino, Adipose tissue NAD(+) biology in obesity and insulin resistance: From mechanism to therapy, *Bioessays*, 39 (2017).
- [215] C. Canto, R.H. Houtkooper, E. Pirinen, D.Y. Youn, M.H. Oosterveer, Y. Cen, P.J. Fernandez-Marcos, H. Yamamoto, P.A. Andreux, P. Cettour-Rose, K. Gademann, C. Rinsch, K. Schoonjans, A.A. Sauve, J. Auwerx, The NAD(+) precursor nicotinamide riboside enhances oxidative metabolism and protects against high-fat diet-induced obesity, *Cell Metab*, 15 (2012) 838-847.
- [216] K.F. Mills, S. Yoshida, L.R. Stein, A. Grozio, S. Kubota, Y. Sasaki, P. Redpath, M.E. Migaud, R.S. Apte, K. Uchida, J. Yoshino, S.I. Imai, Long-Term Administration of Nicotinamide Mononucleotide Mitigates Age-Associated Physiological Decline in Mice, *Cell Metab*, 24 (2016) 795-806.
- [217] J. Yoshino, K.F. Mills, M.J. Yoon, S. Imai, Nicotinamide mononucleotide, a key NAD(+) intermediate, treats the pathophysiology of diet- and age-induced diabetes in mice, *Cell Metab*, 14 (2011) 528-536.
- [218] C.R. Martens, B.A. Denman, M.R. Mazzo, M.L. Armstrong, N. Reisdorph, M.B. McQueen, M. Chonchol, D.R. Seals, Chronic nicotinamide riboside supplementation is well-tolerated and elevates NAD(+) in healthy middle-aged and older adults, *Nat Commun*, 9 (2018) 1286.
- [219] K.L. Bogan, C. Brenner, Nicotinic acid, nicotinamide, and nicotinamide riboside: a molecular evaluation of NAD+ precursor vitamins in human nutrition, *Annu Rev Nutr*, 28 (2008) 115-130.
- [220] J.C. Cresto, L.E. Fabiano de Bruno, G.F. Cao, C.F. Pastorale, N. Confalonieri, M. del Carmen Camberos, J.C. Basabe, The association of acetyl-L-carnitine and nicotinamide remits the experimental diabetes in mice by multiple low-dose streptozotocin, *Pancreas*, 33 (2006) 403-411.
- [221] S. Reddy, M. Young, S. Ginn, Immunoexpression of interleukin-1beta in pancreatic islets of NOD mice during cyclophosphamide-accelerated diabetes: co-localization in macrophages and endocrine cells and its attenuation with oral nicotinamide, *Histochem J*, 33 (2001) 317-327.
- [222] V. Piercy, C.D. Toseland, N.C. Turner, Acceleration of the development of diabetes in obese diabetic (db/db) mice by nicotinamide: a comparison with its antidiabetic effects in non-obese diabetic mice, *Metabolism*, 49 (2000) 1548-1554.
- [223] J.Y. Kim, J.K. Chi, E.J. Kim, S.Y. Park, Y.W. Kim, S.K. Lee, Inhibition of diabetes in non-obese diabetic mice by nicotinamide treatment for 5 weeks at the early age, *J Korean Med Sci*, 12 (1997) 293-297.
- [224] O. Bouix, M. Reynier, R. Guinrand-Hugret, A. Orsetti, Protective effect of gamma-hydroxybutyrate and nicotinamide on low-dose streptozotocin-induced diabetes in mice, *Horm Metab Res*, 27 (1995) 216-220.

- [225] O. Korsgren, A. Andersson, S. Sandler, Pretreatment of fetal porcine pancreas in culture with nicotinamide accelerates reversal of diabetes after transplantation to nude mice, *Surgery*, 113 (1993) 205-214.
- [226] T.N. Pyzhik, I.G. Obrosova, [Effects of nicotinamide and oxythiamine on the lipogenic parameters of the adipose tissue of mice with non-insulin-dependent type of experimental diabetes mellitus and hyperinsulinemia], *Vopr Pitan*, (1991) 49-51.
- [227] L.J. Fischer, J. Falany, R. Fisher, Characteristics of nicotinamide and N1-methylnicotinamide protection from alloxan diabetes in mice, *Toxicol Appl Pharmacol*, 70 (1983) 148-155.
- [228] K. Yamada, K. Nonaka, T. Hanafusa, A. Miyazaki, H. Toyoshima, S. Tarui, Preventive and therapeutic effects of large-dose nicotinamide injections on diabetes associated with insulinitis. An observation in nonobese diabetic (NOD) mice, *Diabetes*, 31 (1982) 749-753.
- [229] H. Tjalve, E. Wilander, The uptake in the pancreatic islets of nicotinamide, nicotinic acid and tryptophan and their ability to prevent streptozotocin diabetes in mice, *Acta Endocrinol (Copenh)*, 83 (1976) 357-364.
- [230] A. Jangra, A.K. Datusalia, S. Khandwe, S.S. Sharma, Amelioration of diabetes-induced neurobehavioral and neurochemical changes by melatonin and nicotinamide: implication of oxidative stress-PARP pathway, *Pharmacol Biochem Behav*, 114-115 (2013) 43-51.
- [231] S.J. Yang, J.M. Choi, L. Kim, S.E. Park, E.J. Rhee, W.Y. Lee, K.W. Oh, S.W. Park, C.Y. Park, Nicotinamide improves glucose metabolism and affects the hepatic NAD-sirtuin pathway in a rodent model of obesity and type 2 diabetes, *J Nutr Biochem*, 25 (2014) 66-72.
- [232] A. Lazarow, J. Liambies, A.J. Tausch, Protection against diabetes with nicotinamide, *J Lab Clin Med*, 36 (1950) 249-258.
- [233] H.J. Wade, Nicotinamide and diabetes mellitus, *Br Med J*, 1 (1947) 414.
- [234] F.J. Neuwahl, Nicotinamide and diabetes mellitus, *Br Med J*, 1 (1947) 614.
- [235] W. Gordon, Nicotinamide and diabetes mellitus, *Br Med J*, 1 (1947) 863.
- [236] W.E. Dulin, B.M. Wyse, Reversal of streptozotocin diabetes with nicotinamide, *Proc Soc Exp Biol Med*, 130 (1969) 992-994.
- [237] W. Stauffacher, I. Burr, A. Gutzeit, D. Beaven, J. Veleminsky, A.E. Renold, Streptozotocin diabetes: time course of irreversible B-cell damage; further observations on prevention by nicotinamide, *Proc Soc Exp Biol Med*, 133 (1970) 194-200.
- [238] P.S. Schein, N. Rakietyen, D.A. Cooney, R. Davis, M.L. Vernon, Streptozotocin diabetes in monkeys and dogs, and its prevention by nicotinamide, *Proc Soc Exp Biol Med*, 143 (1973) 514-518.

- [239] P. Masiello, E. Bergamini, Nicotinamide and streptozotocin diabetes in the rat. Factors influencing the effectiveness of the protection, *Experientia*, 33 (1977) 1246-1247.
- [240] S. Reddy, N.J. Bibby, R.B. Elliott, Early nicotinamide treatment in the NOD mouse: effects on diabetes and insulinitis suppression and autoantibody levels, *Diabetes Res*, 15 (1990) 95-102.
- [241] J. Pan, E.K. Chan, D. Cheta, V. Schranz, M.A. Charles, The effects of nicotinamide and glimepiride on diabetes prevention in BB rats, *Life Sci*, 57 (1995) 1525-1532.
- [242] S. Reddy, N.J. Bibby, D. Wu, C. Swinney, G. Barrow, R.B. Elliott, A combined casein-free-nicotinamide diet prevents diabetes in the NOD mouse with minimum insulinitis, *Diabetes Res Clin Pract*, 29 (1995) 83-92.
- [243] Y. Hu, Y. Wang, L. Wang, H. Zhang, B. Zhao, A. Zhang, Y. Li, Effects of nicotinamide on prevention and treatment of streptozotocin-induced diabetes mellitus in rats, *Chin Med J (Engl)*, 109 (1996) 819-822.
- [244] B.A. O'Brien, B.V. Harmon, D.P. Cameron, D.J. Allan, Nicotinamide prevents the development of diabetes in the cyclophosphamide-induced NOD mouse model by reducing beta-cell apoptosis, *J Pathol*, 191 (2000) 86-92.
- [245] S. Reddy, M. Karanam, E. Robinson, Prevention of cyclophosphamide-induced accelerated diabetes in the NOD mouse by nicotinamide or a soy protein-based infant formula, *Int J Exp Diabetes Res*, 1 (2001) 299-313.
- [246] R.B. Elliott, C.C. Pilcher, A. Stewart, D. Fergusson, M.A. McGregor, The use of nicotinamide in the prevention of type 1 diabetes, *Ann N Y Acad Sci*, 696 (1993) 333-341.
- [247] L. Hermitte, B. Vialettes, N. Atlef, M.J. Payan, N. Doll, A. Scheimann, P. Vague, High dose nicotinamide fails to prevent diabetes in BB rats, *Autoimmunity*, 5 (1989) 79-86.
- [248] S.S. Zhou, D. Li, W.P. Sun, M. Guo, Y.Z. Lun, Y.M. Zhou, F.C. Xiao, L.X. Jing, S.X. Sun, L.B. Zhang, N. Luo, F.N. Bian, W. Zou, L.B. Dong, Z.G. Zhao, S.F. Li, X.J. Gong, Z.G. Yu, C.B. Sun, C.L. Zheng, D.J. Jiang, Z.N. Li, Nicotinamide overload may play a role in the development of type 2 diabetes, *World J Gastroenterol*, 15 (2009) 5674-5684.
- [249] P.E. Beales, L.A. Burr, G.P. Webb, K.J. Mansfield, P. Pozzilli, Diet can influence the ability of nicotinamide to prevent diabetes in the non-obese diabetic mouse: a preliminary study, *Diabetes Metab Res Rev*, 15 (1999) 21-28.
- [250] **Scientific Committee on Food**, Opinion of the Scientific Committee on Food on the Tolerable Upper Intake Level of Nicotinic Acid and Nicotinamide (Niacin), Directorate C -Scientific Opinions; C2 - Management of Scientific committees II; scientific co-operation and networks, SCF/CS/NUT/UPPLEV/39 Final (2002) pp. 1-20.
- [251] P. Pozzilli, N. Visalli, A. Signore, M.G. Baroni, R. Buzzetti, M.G. Cavallo, M.L. Boccuni, D. Fava, C. Gagnoli, D. Andreani, et al., Double blind trial of nicotinamide in recent-onset IDDM (the IMDIAB III study), *Diabetologia*, 38 (1995) 848-852.

- [252] T.J. Wilkin, Insulin resistance and progression to type 1 diabetes in the European Nicotinamide Diabetes Intervention Trial (ENDIT): response to Bingley et al, *Diabetes Care*, 31 (2008) e29.
- [253] P.J. Bingley, J.L. Mahon, E.A. Gale, Insulin resistance and progression to type 1 diabetes in the European Nicotinamide Diabetes Intervention Trial (ENDIT), *Diabetes Care*, 31 (2008) 146-150.
- [254] E.A. Gale, P.J. Bingley, C.L. Emmett, T. Collier, European Nicotinamide Diabetes Intervention Trial (ENDIT): a randomised controlled trial of intervention before the onset of type 1 diabetes, *Lancet*, 363 (2004) 925-931.
- [255] D.A. Schatz, P.J. Bingley, Update on major trials for the prevention of type 1 diabetes mellitus: the American Diabetes Prevention Trial (DPT-1) and the European Nicotinamide Diabetes Intervention Trial (ENDIT), *J Pediatr Endocrinol Metab*, 14 Suppl 1 (2001) 619-622.
- [256] M. Chianelli, M.G. Parisella, N. Visalli, S.J. Mather, C. D'Alessandria, P. Pozzilli, A. Signore, Pancreatic scintigraphy with ^{99m}Tc-interleukin-2 at diagnosis of type 1 diabetes and after 1 year of nicotinamide therapy, *Diabetes Metab Res Rev*, 24 (2008) 115-122.
- [257] M. Hedman, J. Ludvigsson, M.K. Faresjo, Nicotinamide reduces high secretion of IFN-gamma in high-risk relatives even though it does not prevent type 1 diabetes, *J Interferon Cytokine Res*, 26 (2006) 207-213.
- [258] E. Cabrera-Rode, G. Molina, C. Arranz, M. Vera, P. Gonzalez, R. Suarez, M. Prieto, S. Padron, R. Leon, J. Tillan, I. Garcia, C. Tiberti, O.M. Rodriguez, A. Gutierrez, T. Fernandez, A. Govea, J. Hernandez, D. Chiong, E. Dominguez, U. Di Mario, O. Diaz-Diaz, O. Diaz-Horta, Effect of standard nicotinamide in the prevention of type 1 diabetes in first degree relatives of persons with type 1 diabetes, *Autoimmunity*, 39 (2006) 333-340.
- [259] A. Crino, R. Schiaffini, P. Ciampalini, M.C. Suraci, S. Manfrini, N. Visalli, M.C. Matteoli, P. Patera, R. Buzzetti, C. Guglielmi, S. Spera, F. Costanza, E. Fioriti, D. Pitocco, P. Pozzilli, A two year observational study of nicotinamide and intensive insulin therapy in patients with recent onset type 1 diabetes mellitus, *J Pediatr Endocrinol Metab*, 18 (2005) 749-754.
- [260] Intervening before the onset of Type 1 diabetes: baseline data from the European Nicotinamide Diabetes Intervention Trial (ENDIT), *Diabetologia*, 46 (2003) 339-346.
- [261] P.J. Bingley, E.A. Gale, Progression to type 1 diabetes in islet cell antibody-positive relatives in the European Nicotinamide Diabetes Intervention Trial: the role of additional immune, genetic and metabolic markers of risk, *Diabetologia*, 49 (2006) 881-890.
- [262] A.E. Long, A.T. Gooneratne, S. Rokni, A.J. Williams, P.J. Bingley, The role of autoantibodies to zinc transporter 8 in prediction of type 1 diabetes in relatives: lessons from the European Nicotinamide Diabetes Intervention Trial (ENDIT) cohort, *J Clin Endocrinol Metab*, 97 (2012) 632-637.

- [263] J.I. Reimers, C.M. Larsen, T.R. Mandrup-Poulsen, [European Nicotinamide Diabetes Intervention Trial (ENDIT)--secondary publication. A randomized, placebo-controlled trial of intervention before the onset of type 1 diabetes], *Ugeskr Laeger*, 167 (2005) 293-296.
- [264] A. Crino, R. Schiaffini, S. Manfrini, C. Mesturino, N. Visalli, G. Beretta Anguissola, C. Suraci, D. Pitocco, S. Spera, S. Corbi, M.C. Matteoli, I.P. Patera, M.L. Manca Bitti, C. Bizzarri, P. Pozzilli, A randomized trial of nicotinamide and vitamin E in children with recent onset type 1 diabetes (IMDIAB IX), *Eur J Endocrinol*, 150 (2004) 719-724.
- [265] D. Pitocco, A. Crino, E. Di Stasio, S. Manfrini, C. Guglielmi, S. Spera, G.B. Anguissola, N. Visalli, C. Suraci, M.C. Matteoli, I.P. Patera, M.G. Cavallo, C. Bizzarri, P. Pozzilli, The effects of calcitriol and nicotinamide on residual pancreatic beta-cell function in patients with recent-onset Type 1 diabetes (IMDIAB XI), *Diabet Med*, 23 (2006) 920-923.
- [266] I.C. Fernandez, M. Del Carmen Camberos, G.A. Passicot, L.C. Martucci, J.C. Cresto, Children at risk of diabetes type 1. Treatment with acetyl-L-carnitine plus nicotinamide - case reports, *J Pediatr Endocrinol Metab*, 26 (2013) 347-355.
- [267] J. Vidal, M. Fernandez-Balsells, G. Sesmilo, E. Aguilera, R. Casamitjana, R. Gomis, I. Conget, Effects of nicotinamide and intravenous insulin therapy in newly diagnosed type 1 diabetes, *Diabetes Care*, 23 (2000) 360-364.
- [268] N. Visalli, M.G. Cavallo, A. Signore, M.G. Baroni, R. Buzzetti, E. Fioriti, C. Mesturino, R. Fiori, L. Lucentini, M.C. Matteoli, A. Crino, S. Corbi, S. Spera, C. Teodonio, F. Paci, R. Amoretti, L. Pisano, C. Suraci, G. Multari, N. Sulli, M. Cervoni, G. De Mattia, M.R. Faldetta, B. Boscherini, P. Pozzilli, et al., A multi-centre randomized trial of two different doses of nicotinamide in patients with recent-onset type 1 diabetes (the IMDIAB VI), *Diabetes Metab Res Rev*, 15 (1999) 181-185.
- [269] R.B. Elliott, C.C. Pilcher, D.M. Fergusson, A.W. Stewart, A population based strategy to prevent insulin-dependent diabetes using nicotinamide, *J Pediatr Endocrinol Metab*, 9 (1996) 501-509.
- [270] F. Pociot, J.I. Reimers, H.U. Andersen, Nicotinamide--biological actions and therapeutic potential in diabetes prevention. IDIG Workshop, Copenhagen, Denmark, 4-5 December 1992, *Diabetologia*, 36 (1993) 574-576.
- [271] E.F. Lampeter, A. Klinghammer, W.A. Scherbaum, E. Heinze, B. Haastert, G. Giani, H. Kolb, The Deutsche Nicotinamide Intervention Study: an attempt to prevent type 1 diabetes. DENIS Group, *Diabetes*, 47 (1998) 980-984.
- [272] Y.A. Kang-Lee, R.W. McKee, S.M. Wright, M.E. Swendseid, D.J. Jenden, R.S. Jope, Metabolic effects of nicotinamide administration in rats, *J Nutr*, 113 (1983) 215-221.
- [273] M.J. Chapman, How does nicotinic acid modify the lipid profile?, *European Heart Journal Supplements*, 8 (2006) F54-F59.
- [274] M. Chhetry, I. Jialal, *Lipid Lowering Drug Therapy*, StatPearls, Place Published, 2019.

- [275] H.E. Bays, D.J. Rader, Does nicotinic acid (niacin) lower blood pressure?, *Int J Clin Pract*, 63 (2009) 151-159.
- [276] L. Ma, B.H. Lee, H. Clifton, S. Schaefer, J. Zheng, Nicotinic acid is a common regulator of heat-sensing TRPV1-4 ion channels, *Sci Rep*, 5 (2015) 8906.
- [277] B.M. O'Sullivan, W.F. Blakemore, Acute nicotinamide deficiency in pigs, *Vet Rec*, 103 (1978) 543-544.
- [278] L.P. Varma, Mental Symptoms in Pellagra and Nicotinic Acid Deficiency, *Ind Med Gaz*, 78 (1943) 543-546.
- [279] F.A. Mc, Dermatitis as a monosymptomatic manifestation of nicotinic acid deficiency, *Glasgow Med J*, 28 (1947) 103-115.
- [280] V.A. Valdes, P.O. Bolo, [Nicotinic acid deficiency without pellagra; radiological changes in colon due to deficiency], *Prensa Med Argent*, 40 (1953) 2622-2628.
- [281] A.R. Shalita, J.G. Smith, L.C. Parish, M.S. Sofman, D.K. Chalker, Topical nicotinamide compared with clindamycin gel in the treatment of inflammatory acne vulgaris, *Int J Dermatol*, 34 (1995) 434-437.
- [282] E. Emanuele, M. Bertona, K. Altabas, V. Altabas, G. Alessandrini, Anti-inflammatory effects of a topical preparation containing nicotinamide, retinol, and 7-dehydrocholesterol in patients with acne: a gene expression study, *Clin Cosmet Investig Dermatol*, 5 (2012) 33-37.
- [283] G. Fabbrocini, M. Cantelli, G. Monfrecola, Topical nicotinamide for seborrheic dermatitis: an open randomized study, *J Dermatolog Treat*, 25 (2014) 241-245.
- [284] S. Ashkani Esfahani, M. Khoshneviszadeh, M.R. Namazi, A. Noorafshan, B. Geramizadeh, E. Nadimi, S.T. Razavipour, Topical Nicotinamide Improves Tissue Regeneration in Excisional Full-Thickness Skin Wounds: A Stereological and Pathological Study, *Trauma Mon*, 20 (2015) e18193.
- [285] V.A. Snaidr, D.L. Damian, G.M. Halliday, Nicotinamide for photoprotection and skin cancer chemoprevention: A review of efficacy and safety, *Exp Dermatol*, 28 Suppl 1 (2019) 15-22.
- [286] G. Waetzig, D. Seegert, Pharmaceutical composition containing nicotinic acid, nicotinamide, and/or tryptophan for positively influencing the intestinal microbiota, in: C.r.i. AG (Ed.)DE, 2015.
- [287] R. Weiss, E. Schilling, A. Grahnert, V. Kolling, J. Dorow, U. Ceglarek, U. Sack, S. Hauschildt, Nicotinamide: a vitamin able to shift macrophage differentiation toward macrophages with restricted inflammatory features, *Innate Immun*, 21 (2015) 813-826.
- [288] Y. Hiromatsu, M. Sato, K. Tanaka, N. Ishisaka, J. Kamachi, K. Nonaka, Inhibitory effects of nicotinamide on intercellular adhesion molecule-1 expression on cultured human thyroid cells, *Immunology*, 80 (1993) 330-332.
- [289] Y. Hiromatsu, M. Sato, K. Yamada, K. Nonaka, Inhibitory effects of nicotinamide on recombinant human interferon-gamma-induced intercellular adhesion molecule-1

- (ICAM-1) and HLA-DR antigen expression on cultured human endothelial cells, *Immunol Lett*, 31 (1992) 35-39.
- [290] R. Biedron, M. Ciszek, M. Tokarczyk, M. Bobek, M. Kurnyta, E.M. Slominska, R.T. Smolenski, J. Marcinkiewicz, 1-Methylnicotinamide and nicotinamide: two related anti-inflammatory agents that differentially affect the functions of activated macrophages, *Arch Immunol Ther Exp (Warsz)*, 56 (2008) 127-134.
- [291] M. Fukuzawa, J. Satoh, G. Muto, Y. Muto, S. Nishimura, S. Miyaguchi, X.L. Qiang, T. Toyota, Inhibitory effect of nicotinamide on in vitro and in vivo production of tumor necrosis factor-alpha, *Immunol Lett*, 59 (1997) 7-11.
- [292] J.S. Ungerstedt, K. Heimersson, T. Soderstrom, M. Hansson, Nicotinamide inhibits endotoxin-induced monocyte tissue factor expression, *J Thromb Haemost*, 1 (2003) 2554-2560.
- [293] J.S. Ungerstedt, M. Blomback, T. Soderstrom, Nicotinamide is a potent inhibitor of proinflammatory cytokines, *Clin Exp Immunol*, 131 (2003) 48-52.
- [294] P.A. Grange, J. Raingeaud, V. Calvez, N. Dupin, Nicotinamide inhibits *Propionibacterium acnes*-induced IL-8 production in keratinocytes through the NF-kappaB and MAPK pathways, *J Dermatol Sci*, 56 (2009) 106-112.
- [295] M. Lappas, M. Permezel, The anti-inflammatory and antioxidative effects of nicotinamide, a vitamin B(3) derivative, are elicited by FoxO3 in human gestational tissues: implications for preterm birth, *J Nutr Biochem*, 22 (2011) 1195-1201.
- [296] L. Mateuszuk, A. Jasztal, E. Maslak, M. Gasior-Glogowska, M. Baranska, B. Sitek, R. Kostogryś, A. Zakrzewska, A. Kij, M. Walczak, S. Chlopicki, Antiatherosclerotic Effects of 1-Methylnicotinamide in Apolipoprotein E/Low-Density Lipoprotein Receptor-Deficient Mice: A Comparison with Nicotinic Acid, *J Pharmacol Exp Ther*, 356 (2016) 514-524.
- [297] H.Y. KM Hawrylyshyn, C O'Neil, A Watson, J Pickering, NICOTINAMIDE RIBOSIDE DELIVERY GENERATES NAD⁺ RESERVES TO PROTECT VASCULAR CELLS AGAINST OXIDATIVE DAMAGE, *Canadian Journal of Cardiology*, 31 (2015) S 226.
- [298] N.E. de Picciotto, L.B. Gano, L.C. Johnson, C.R. Martens, A.L. Sindler, K.F. Mills, S. Imai, D.R. Seals, Nicotinamide mononucleotide supplementation reverses vascular dysfunction and oxidative stress with aging in mice, *Aging Cell*, 15 (2016) 522-530.
- [299] E. Holzhauser, C. Albrecht, Q. Zhou, A. Buttler, M.R. Preusch, E. Blessing, H.A. Katus, F. Bea, Nicotinic acid has anti-atherogenic and anti-inflammatory properties on advanced atherosclerotic lesions independent of its lipid-modifying capabilities, *J Cardiovasc Pharmacol*, 57 (2011) 447-454.
- [300] P. Lipton, J.G. Michels, The Effects of Nicotinic Acid on Rabbit Hypercholesterolemia and Atherogenesis, *Geriatrics*, 71 (1965) 379-387.
- [301] M. Lukasova, C. Malaval, A. Gille, J. Kero, S. Offermanns, Nicotinic acid inhibits progression of atherosclerosis in mice through its receptor GPR109A expressed by immune cells, *J Clin Invest*, 121 (2011) 1163-1173.

- [302] V. Orbetsova, T. Iurukova, T. Kirov, [Regression of experimental cholesterol-induced atherosclerosis in rabbits after stopping the atherogenic diet and after treatment with nicotinic acid], *Eksp Med Morfol*, 24 (1985) 32-38.
- [303] A.M. Strack, E. Carballo-Jane, S.P. Wang, J. Xue, X. Ping, L.A. McNamara, A. Thankappan, O. Price, M. Wolff, T.J. Wu, D. Kawka, M. Mariano, C. Burton, C.H. Chang, J. Chen, J. Menke, S. Luell, E.I. Zycband, X. Tong, R. Raubertas, C.P. Sparrow, B. Hubbard, J. Woods, G. O'Neill, M.G. Waters, A. Sitlani, Nicotinic acid and DP1 blockade: studies in mouse models of atherosclerosis, *J Lipid Res*, 54 (2013) 177-188.
- [304] F. Teixeira, M.L. Beja, P. Serra e Silva, S. Cabrita, M.B. Franca, L. Almeida, M.T. Morgadinho, Experimental atherogenesis and vascular noradrenaline content in NZW rabbits and activity of a new nicotinic acid derivative (L 44-0), *J Lipid Mediat*, 3 (1991) 167-175.
- [305] R.H. Knopp, Evaluating niacin in its various forms, *Am J Cardiol*, 86 (2000) 51L-56L.
- [306] (!!! INVALID CITATION !!! [1, 2]).
- [307] R.J. Havel, H.A. Eder, J.H. Bragdon, The distribution and chemical composition of ultracentrifugally separated lipoproteins in human serum, *J Clin Invest*, 34 (1955) 1345-1353.
- [308] C.M. Radding, D. Steinberg, Studies on the synthesis and secretion of serum lipoproteins by rat liver slices, *J Clin Invest*, 39 (1960) 1560-1569.
- [309] J.A. Piedrahita, S.H. Zhang, J.R. Hageman, P.M. Oliver, N. Maeda, Generation of mice carrying a mutant apolipoprotein E gene inactivated by gene targeting in embryonic stem cells, *Proc Natl Acad Sci U S A*, 89 (1992) 4471-4475.
- [310] G.S. Getz, C.A. Reardon, ApoE knockout and knockin mice: the history of their contribution to the understanding of atherogenesis, *J Lipid Res*, 57 (2016) 758-766.
- [311] M.R. Mirbolooki, C.C. Constantinescu, M.L. Pan, J. Mukherjee, Quantitative assessment of brown adipose tissue metabolic activity and volume using ¹⁸F-FDG PET/CT and β -adrenergic receptor activation, *EJNMMI Res*, 1 (2011) 30.
- [312] I. Murano, G. Barbatelli, V. Parisani, C. Latini, G. Muzzonigro, M. Castellucci, S. Cinti, Dead adipocytes, detected as crown-like structures, are prevalent in visceral fat depots of genetically obese mice, *J Lipid Res*, 49 (2008) 1562-1568.
- [313] B. Paigen, A. Morrow, P.A. Holmes, D. Mitchell, R.A. Williams, Quantitative assessment of atherosclerotic lesions in mice, *Atherosclerosis*, 68 (1987) 231-240.
- [314] A.L. Lillie R, Supersaturated solutions of fat stains in dilute isopropanol for demonstration of acute fatty degeneration not shown by Herxheimer's technique, *Archives of Pathology*, 1943, pp. 432-440.
- [315] V. Ribas, J.L. Sanchez-Quesada, R. Anton, M. Camacho, J. Julve, J.C. Escola-Gil, L. Vila, J. Ordonez-Llanos, F. Blanco-Vaca, Human apolipoprotein A-II enrichment displaces paraoxonase from HDL and impairs its antioxidant properties: a new

- mechanism linking HDL protein composition and antiatherogenic potential, *Circ Res*, 95 (2004) 789-797.
- [316] D.J. Manual Kollareth, C.L. Chang, I.H. Hansen, R.J. Deckelbaum, Radiolabeled cholesteryl ethers: A need to analyze for biological stability before use, *Biochem Biophys Rep*, 13 (2018) 1-6.
- [317] P.C. Even, N.A. Nadkarni, Indirect calorimetry in laboratory mice and rats: principles, practical considerations, interpretation and perspectives, *Am J Physiol Regul Integr Comp Physiol*, 303 (2012) R459-476.
- [318] Y. Nie, T.P. Gavin, S. Kuang, Measurement of Resting Energy Metabolism in Mice Using Oxymax Open Circuit Indirect Calorimeter, *Bio Protoc*, 5 (2015).
- [319] B. Feng, P. Jiao, Y. Helou, Y. Li, Q. He, M.S. Walters, A. Salomon, H. Xu, Mitogen-activated protein kinase phosphatase 3 (MKP-3)-deficient mice are resistant to diet-induced obesity, *Diabetes*, 63 (2014) 2924-2934.
- [320] P. Bi, T. Shan, W. Liu, F. Yue, X. Yang, X.R. Liang, J. Wang, J. Li, N. Carlesso, X. Liu, S. Kuang, Inhibition of Notch signaling promotes browning of white adipose tissue and ameliorates obesity, *Nat Med*, 20 (2014) 911-918.
- [321] (!!! INVALID CITATION !!! [13, 14]).
- [322] P.B. Lazarow, Assay of peroxisomal beta-oxidation of fatty acids, *Methods Enzymol*, 72 (1981) 315-319.
- [323] N.B. Pike, A. Wise, Identification of a nicotinic acid receptor: is this the molecular target for the oldest lipid-lowering drug?, *Curr Opin Investig Drugs*, 5 (2004) 271-275.
- [324] M. Inoue, M. Yano, M. Yamakado, E. Maehata, S. Suzuki, Relationship between the adiponectin-leptin ratio and parameters of insulin resistance in subjects without hyperglycemia, *Metabolism*, 55 (2006) 1248-1254.
- [325] S. Milic, D. Lulic, D. Stimac, Non-alcoholic fatty liver disease and obesity: biochemical, metabolic and clinical presentations, *World J Gastroenterol*, 20 (2014) 9330-9337.
- [326] E. Pardina, R. Ferrer, J. Rossell, D. Ricart-Jane, K.A. Mendez-Lara, J.A. Baena-Fustegueras, A. Lecube, J. Julve, J. Peinado-Onsurbe, Hepatic CD36 downregulation parallels steatosis improvement in morbidly obese undergoing bariatric surgery, *Int J Obes (Lond)*, (2017).
- [327] L.R. Braun, M.N. Feldpausch, N. Czerwonka, M. Torriani, S.K. Grinspoon, T.L. Stanley, Fibroblast growth factor 21 decreases after liver fat reduction via growth hormone augmentation, *Growth Horm IGF Res*, 37 (2017) 1-6.
- [328] F.M. Fisher, E. Maratos-Flier, Understanding the Physiology of FGF21, *Annu Rev Physiol*, 78 (2016) 223-241.
- [329] D.C. Simonson, R.A. DeFronzo, Indirect calorimetry: methodological and interpretative problems, *Am J Physiol*, 258 (1990) E399-412.

- [330] N.S. Chandel, Mitochondrial complex III: an essential component of universal oxygen sensing machinery?, *Respir Physiol Neurobiol*, 174 (2010) 175-181.
- [331] D. Pan, C. Lindau, S. Lagies, N. Wiedemann, B. Kammerer, Metabolic profiling of isolated mitochondria and cytoplasm reveals compartment-specific metabolic responses, *Metabolomics*, 14 (2018) 59.
- [332] S. Rajan, A. Gupta, M. Beg, K. Shankar, A. Srivastava, S. Varshney, D. Kumar, A.N. Gaikwad, Adipocyte transdifferentiation and its molecular targets, *Differentiation*, 87 (2014) 183-192.
- [333] E. Castro, T.E.O. Silva, W.T. Festuccia, Critical review of beige adipocyte thermogenic activation and contribution to whole-body energy expenditure, *Horm Mol Biol Clin Investig*, 31 (2017).
- [334] European Food Safety Authority (EFSA) panel on additives and products or substances used in animal feed (FEEDAP); Scientific opinion on the safety and efficacy of niacin (nicotinic acid and nicotinamide) as a feed additive for all animal species based on a dossier submitted by VITAC EEIG, *EFSA journal*, 2012, pp. 2885 [2820 pp.].
- [335] M. Knip, I.F. Douek, W.P. Moore, H.A. Gillmor, A.E. McLean, P.J. Bingley, E.A. Gale, Safety of high-dose nicotinamide: a review, *Diabetologia*, 43 (2000) 1337-1345.
- [336] F.G. Brazda, R.A. Coulson, Toxicity of nicotinic acid and some of its derivatives, *Proc Soc Exp Biol Med*, 62 (1946) 19.
- [337] F. Bergmann, L. Wislicki, The pharmacological effects of massive doses of nicotinamide, *Br J Pharmacol Chemother*, 8 (1953) 49-53.
- [338] L.M. Horger, E.B. Gerheim, Effects of excess dietary methionine and niacinamide in the rat, *Proc Soc Exp Biol Med*, 97 (1958) 444-446.
- [339] P. Handler, W.J. Dann, The inhibition of rat growth by nicotinamide, *Journal of Biological Chemistry*, 146 (1942) 357-368.
- [340] BIBRA toxicology advice & consulting. Toxicity Profile for Niacinamide, Toxicity profiles, 1998.
- [341] P. Handler, The effect of excessive nicotinamide feeding on rabbits and guinea-pigs, *J Biol Chem*, 154 (1944) 203-206.
- [342] M. Lukasova, J. Hanson, S. Tunaru, S. Offermanns, Nicotinic acid (niacin): new lipid-independent mechanisms of action and therapeutic potentials, *Trends Pharmacol Sci*, 32 (2011) 700-707.
- [343] J.W. van der Hoorn, W. de Haan, J.F. Berbee, L.M. Havekes, J.W. Jukema, P.C. Rensen, H.M. Princen, Niacin increases HDL by reducing hepatic expression and plasma levels of cholesteryl ester transfer protein in APOE*3Leiden.CETP mice, *Arterioscler Thromb Vasc Biol*, 28 (2008) 2016-2022.
- [344] S. Kuhnast, M.C. Louwe, M.M. Heemskerk, E.J. Pieterman, J.B. van Klinken, S.A. van den Berg, J.W. Smit, L.M. Havekes, P.C. Rensen, J.W. van der Hoorn, H.M. Princen, J.W. Jukema, Niacin Reduces Atherosclerosis Development in APOE*3Leiden.CETP Mice Mainly by Reducing NonHDL-Cholesterol, *PLoS One*, 8 (2013) e66467.

- [345] A.A. Magide, N.B. Myant, Effect of nicotinic acid on cholesterol metabolism in monkeys, *Clin Sci Mol Med*, 46 (1974) 527-538.
- [346] L. Chen, W.Y. So, S.Y. Li, Q. Cheng, B.J. Boucher, P.S. Leung, Niacin-induced hyperglycemia is partially mediated via niacin receptor GPR109a in pancreatic islets, *Mol Cell Endocrinol*, 404 (2015) 56-66.
- [347] S. Hong, J.M. Moreno-Navarrete, X. Wei, Y. Kikukawa, I. Tzamelis, D. Prasad, Y. Lee, J.M. Asara, J.M. Fernandez-Real, E. Maratos-Flier, P. Pissios, Nicotinamide N-methyltransferase regulates hepatic nutrient metabolism through Sirt1 protein stabilization, *Nat Med*, 21 (2015) 887-894.
- [348] F. Villarroya, R. Cereijo, A. Gavaldà-Navarro, J. Villarroya, M. Giralt, Inflammation of brown/beige adipose tissues in obesity and metabolic disease, *J Intern Med*, 284 (2018) 492-504.
- [349] S. Cinti, Adipocyte differentiation and transdifferentiation: plasticity of the adipose organ, *J Endocrinol Invest*, 25 (2002) 823-835.
- [350] F. Villarroya, M. Peyrou, M. Giralt, Transcriptional regulation of the uncoupling protein-1 gene, *Biochimie*, 134 (2017) 86-92.
- [351] L.P. Kozak, R.A. Koza, R. Anunciado-Koza, Brown fat thermogenesis and body weight regulation in mice: relevance to humans, *Int J Obes (Lond)*, 34 Suppl 1 (2010) S23-27.
- [352] H.M. Feldmann, V. Golozoubova, B. Cannon, J. Nedergaard, UCP1 ablation induces obesity and abolishes diet-induced thermogenesis in mice exempt from thermal stress by living at thermoneutrality, *Cell Metab*, 9 (2009) 203-209.
- [353] M. Bluher, Clinical relevance of adipokines, *Diabetes Metab J*, 36 (2012) 317-327.
- [354] X. Hui, P. Gu, J. Zhang, T. Nie, Y. Pan, D. Wu, T. Feng, C. Zhong, Y. Wang, K.S. Lam, A. Xu, Adiponectin Enhances Cold-Induced Browning of Subcutaneous Adipose Tissue via Promoting M2 Macrophage Proliferation, *Cell Metab*, 22 (2015) 279-290.
- [355] L. Qiao, H. Yoo, C. Bosco, B. Lee, G.S. Feng, J. Schaack, N.W. Chi, J. Shao, Adiponectin reduces thermogenesis by inhibiting brown adipose tissue activation in mice, *Diabetologia*, 57 (2014) 1027-1036.
- [356] K. Aktories, G. Schultz, K.H. Jakobs, Regulation of adenylate cyclase activity in hamster adipocytes. Inhibition by prostaglandins, alpha-adrenergic agonists and nicotinic acid, *Naunyn Schmiedeberg's Arch Pharmacol*, 312 (1980) 167-173.
- [357] W.P. Sun, D. Li, Y.Z. Lun, X.J. Gong, S.X. Sun, M. Guo, L.X. Jing, L.B. Zhang, F.C. Xiao, S.S. Zhou, Excess nicotinamide inhibits methylation-mediated degradation of catecholamines in normotensives and hypertensives, *Hypertens Res*, 35 (2012) 180-185.
- [358] B.E. Levin, A.C. Sullivan, Regulation of thermogenesis in obesity, *Int J Obes*, 8 Suppl 1 (1984) 159-180.

- [359] A. Vegiopoulos, M. Rohm, S. Herzig, Adipose tissue: between the extremes, *EMBO J*, 36 (2017) 1999-2017.
- [360] B. Chaurasia, V.A. Kaddai, G.I. Lancaster, D.C. Henstridge, S. Sriram, D.L. Galam, V. Gopalan, K.N. Prakash, S.S. Velan, S. Bulchand, T.J. Tsong, M. Wang, M.M. Siddique, G. Yuguang, K. Sigmundsson, N.A. Mellet, J.M. Weir, P.J. Meikle, M.Y.M.S. Bin, A. Shabbir, J.A. Shayman, Y. Hirabayashi, S.T. Shiow, S. Sugii, S.A. Summers, Adipocyte Ceramides Regulate Subcutaneous Adipose Browning, Inflammation, and Metabolism, *Cell Metab*, 24 (2016) 820-834.
- [361] C. Guerra, R.A. Koza, H. Yamashita, K. Walsh, L.P. Kozak, Emergence of brown adipocytes in white fat in mice is under genetic control. Effects on body weight and adiposity, *J Clin Invest*, 102 (1998) 412-420.
- [362] P. Mandal, B.T. Pratt, M. Barnes, M.R. McMullen, L.E. Nagy, Molecular mechanism for adiponectin-dependent M2 macrophage polarization: link between the metabolic and innate immune activity of full-length adiponectin, *J Biol Chem*, 286 (2011) 13460-13469.
- [363] J.Y. Kim, E. van de Wall, M. Laplante, A. Azzara, M.E. Trujillo, S.M. Hofmann, T. Schraw, J.L. Durand, H. Li, G. Li, L.A. Jelicks, M.F. Mehler, D.Y. Hui, Y. Deshaies, G.I. Shulman, G.J. Schwartz, P.E. Scherer, Obesity-associated improvements in metabolic profile through expansion of adipose tissue, *J Clin Invest*, 117 (2007) 2621-2637.
- [364] Y. Zhou, L. Rui, Leptin signaling and leptin resistance, *Front Med*, 7 (2013) 207-222.
- [365] G.T. Dodd, S. Decherf, K. Loh, S.E. Simonds, F. Wiede, E. Balland, T.L. Merry, H. Munzberg, Z.Y. Zhang, B.B. Kahn, B.G. Neel, K.K. Bence, Z.B. Andrews, M.A. Cowley, T. Tiganis, Leptin and insulin act on POMC neurons to promote the browning of white fat, *Cell*, 160 (2015) 88-104.
- [366] J. Yang, S.P. Zhao, J. Li, S.Z. Dong, Effect of niacin on adipocyte leptin in hypercholesterolemic rabbits, *Cardiovasc Pathol*, 17 (2008) 219-225.
- [367] Y.L. Wang-Fisher, J. Han, W. Guo, Acipimox stimulates leptin production from isolated rat adipocytes, *J Endocrinol*, 174 (2002) 267-272.
- [368] S. Jager, C. Handschin, J. St-Pierre, B.M. Spiegelman, AMP-activated protein kinase (AMPK) action in skeletal muscle via direct phosphorylation of PGC-1alpha, *Proc Natl Acad Sci U S A*, 104 (2007) 12017-12022.
- [369] F. Lan, J.M. Cacicedo, N. Ruderman, Y. Ido, SIRT1 modulation of the acetylation status, cytosolic localization, and activity of LKB1. Possible role in AMP-activated protein kinase activation, *J Biol Chem*, 283 (2008) 27628-27635.
- [370] M.L. Bonet, P. Oliver, A. Palou, Pharmacological and nutritional agents promoting browning of white adipose tissue, *Biochim Biophys Acta*, 1831 (2013) 969-985.
- [371] L. Ye, S. Kleiner, J. Wu, R. Sah, R.K. Gupta, A.S. Banks, P. Cohen, M.J. Khandekar, P. Bostrom, R.J. Mepani, D. Laznik, T.M. Kamenecka, X. Song, W. Liedtke, V.K. Mootha, P. Puigserver, P.R. Griffin, D.E. Clapham, B.M. Spiegelman, TRPV4 is a regulator of

adipose oxidative metabolism, inflammation, and energy homeostasis, *Cell*, 151 (2012) 96-110.

[372] M. Yan, E. Audet-Walsh, S. Manteghi, C.R. Dufour, B. Walker, M. Baba, J. St-Pierre, V. Giguere, A. Pause, Chronic AMPK activation via loss of FLCN induces functional beige adipose tissue through PGC-1alpha/ERRalpha, *Genes Dev*, 30 (2016) 1034-1046.

[373] A.E. Pollard, L. Martins, P.J. Muckett, S. Khadayate, A. Bornot, M. Clausen, T. Admyre, M. Bjursell, R. Fiadeiro, L. Wilson, C. Whilding, V.N. Kotiadis, M.R. Duchon, D. Sutton, L. Penfold, A. Sardini, Y.M. Bohlooly, D.M. Smith, J.A. Read, M.A. Snowden, A. Woods, D. Carling, AMPK activation protects against diet induced obesity through Ucp1-independent thermogenesis in subcutaneous white adipose tissue, *Nat Metab*, 1 (2019) 340-349.

[374] E. Pirinen, T. Kuulasmaa, M. Pietila, S. Heikkinen, M. Tusa, P. Itkonen, S. Boman, J. Skommer, A. Virkamaki, E. Hohtola, M. Kettunen, S. Fatrai, E. Kansanen, S. Koota, K. Niiranen, J. Parkkinen, A.L. Levonen, S. Yla-Herttuala, J.K. Hiltunen, L. Alhonen, U. Smith, J. Janne, M. Laakso, Enhanced polyamine catabolism alters homeostatic control of white adipose tissue mass, energy expenditure, and glucose metabolism, *Mol Cell Biol*, 27 (2007) 4953-4967.

[375] J. Jell, S. Merali, M.L. Hensen, R. Mazurchuk, J.A. Spornyak, P. Diegelman, N.D. Kisiel, C. Barrero, K.K. Deeb, L. Alhonen, M.S. Patel, C.W. Porter, Genetically altered expression of spermidine/spermine N1-acetyltransferase affects fat metabolism in mice via acetyl-CoA, *J Biol Chem*, 282 (2007) 8404-8413.

[376] H. Ruan, L.Q. Dong, Adiponectin signaling and function in insulin target tissues, *J Mol Cell Biol*, 8 (2016) 101-109.

[377] S.J. Mitchell, M. Bernier, M.A. Aon, S. Cortassa, E.Y. Kim, E.F. Fang, H.H. Palacios, A. Ali, I. Navas-Enamorado, A. Di Francesco, T.A. Kaiser, T.B. Waltz, N. Zhang, J.L. Ellis, P.J. Elliott, D.W. Frederick, V.A. Bohr, M.S. Schmidt, C. Brenner, D.A. Sinclair, A.A. Sauve, J.A. Baur, R. de Cabo, Nicotinamide Improves Aspects of Healthspan, but Not Lifespan, in Mice, *Cell Metab*, 27 (2018) 667-676 e664.

[378] M. Komatsu, T. Kanda, H. Urai, A. Kurokochi, R. Kitahama, S. Shigaki, T. Ono, H. Yukioka, K. Hasegawa, H. Tokuyama, H. Kawabe, S. Wakino, H. Itoh, NNMT activation can contribute to the development of fatty liver disease by modulating the NAD (+) metabolism, *Sci Rep*, 8 (2018) 8637.

[379] K. Takeuchi, C. Yokouchi, H. Goto, K. Umehara, H. Yamada, Y. Ishii, Alleviation of fatty liver in a rat model by enhancing N(1)-methylnicotinamide bioavailability through aldehyde oxidase inhibition, *Biochem Biophys Res Commun*, 507 (2018) 203-210.

[380] N. Esser, S. Legrand-Poels, J. Piette, A.J. Scheen, N. Paquot, Inflammation as a link between obesity, metabolic syndrome and type 2 diabetes, *Diabetes Res Clin Pract*, 105 (2014) 141-150.

[381] D. Wolf, K. Ley, Immunity and Inflammation in Atherosclerosis, *Circ Res*, 124 (2019) 315-327.

- [382] P. Trayhurn, I.S. Wood, Signalling role of adipose tissue: adipokines and inflammation in obesity, *Biochem Soc Trans*, 33 (2005) 1078-1081.
- [383] P.D. Cani, J. Amar, M.A. Iglesias, M. Poggi, C. Knauf, D. Bastelica, A.M. Neyrinck, F. Fava, K.M. Tuohy, C. Chabo, A. Waget, E. Delmee, B. Cousin, T. Sulpice, B. Chamontin, J. Ferrieres, J.F. Tanti, G.R. Gibson, L. Casteilla, N.M. Delzenne, M.C. Alessi, R. Burcelin, Metabolic endotoxemia initiates obesity and insulin resistance, *Diabetes*, 56 (2007) 1761-1772.
- [384] F.S. Lira, J.C. Rosa, R.V. Dos Santos, D.P. Venancio, J. Carnier, L. Sanches Pde, C.M. do Nascimento, A. de Piano, L. Tock, S. Tufik, M.T. de Mello, A.R. Damaso, L.M. Oyama, Visceral fat decreased by long-term interdisciplinary lifestyle therapy correlated positively with interleukin-6 and tumor necrosis factor-alpha and negatively with adiponectin levels in obese adolescents, *Metabolism*, 60 (2011) 359-365.
- [385] D.M. Mosser, J.P. Edwards, Exploring the full spectrum of macrophage activation, *Nat Rev Immunol*, 8 (2008) 958-969.
- [386] I.J. Elenkov, G.P. Chrousos, Stress hormones, proinflammatory and antiinflammatory cytokines, and autoimmunity, *Ann N Y Acad Sci*, 966 (2002) 290-303.
- [387] A.T. Turer, P.E. Scherer, Adiponectin: mechanistic insights and clinical implications, *Diabetologia*, 55 (2012) 2319-2326.
- [388] T. Yamauchi, K. Hara, N. Kubota, Y. Terauchi, K. Tobe, P. Froguel, R. Nagai, T. Kadowaki, Dual roles of adiponectin/Acrp30 in vivo as an anti-diabetic and anti-atherogenic adipokine, *Curr Drug Targets Immune Endocr Metabol Disord*, 3 (2003) 243-254.
- [389] K. Ohashi, J.L. Parker, N. Ouchi, A. Higuchi, J.A. Vita, N. Gokce, A.A. Pedersen, C. Kalthoff, S. Tullin, A. Sams, R. Summer, K. Walsh, Adiponectin promotes macrophage polarization toward an anti-inflammatory phenotype, *J Biol Chem*, 285 (2010) 6153-6160.
- [390] A.M. Wolf, D. Wolf, H. Rumpold, B. Enrich, H. Tilg, Adiponectin induces the anti-inflammatory cytokines IL-10 and IL-1RA in human leukocytes, *Biochem Biophys Res Commun*, 323 (2004) 630-635.
- [391] M. Kumada, S. Kihara, N. Ouchi, H. Kobayashi, Y. Okamoto, K. Ohashi, K. Maeda, H. Nagaretani, K. Kishida, N. Maeda, A. Nagasawa, T. Funahashi, Y. Matsuzawa, Adiponectin specifically increased tissue inhibitor of metalloproteinase-1 through interleukin-10 expression in human macrophages, *Circulation*, 109 (2004) 2046-2049.
- [392] T. Yokota, K. Oritani, I. Takahashi, J. Ishikawa, A. Matsuyama, N. Ouchi, S. Kihara, T. Funahashi, A.J. Tenner, Y. Tomiyama, Y. Matsuzawa, Adiponectin, a new member of the family of soluble defense collagens, negatively regulates the growth of myelomonocytic progenitors and the functions of macrophages, *Blood*, 96 (2000) 1723-1732.
- [393] M.C. Wulster-Radcliffe, K.M. Ajuwon, J. Wang, J.A. Christian, M.E. Spurlock, Adiponectin differentially regulates cytokines in porcine macrophages, *Biochem Biophys Res Commun*, 316 (2004) 924-929.

- [394] L. Tian, N. Luo, R.L. Klein, B.H. Chung, W.T. Garvey, Y. Fu, Adiponectin reduces lipid accumulation in macrophage foam cells, *Atherosclerosis*, 202 (2009) 152-161.
- [395] N. Ouchi, S. Kihara, Y. Arita, M. Nishida, A. Matsuyama, Y. Okamoto, M. Ishigami, H. Kuriyama, K. Kishida, H. Nishizawa, K. Hotta, M. Muraguchi, Y. Ohmoto, S. Yamashita, T. Funahashi, Y. Matsuzawa, Adipocyte-derived plasma protein, adiponectin, suppresses lipid accumulation and class A scavenger receptor expression in human monocyte-derived macrophages, *Circulation*, 103 (2001) 1057-1063.
- [396] A. Bar, M. Olkowicz, U. Tyrankiewicz, E. Kus, K. Jasinski, R.T. Smolenski, T. Skorcka, S. Chlopicki, Functional and Biochemical Endothelial Profiling In Vivo in a Murine Model of Endothelial Dysfunction; Comparison of Effects of 1-Methylnicotinamide and Angiotensin-converting Enzyme Inhibitor, *Front Pharmacol*, 8 (2017) 183.
- [397] H.R. Nejabati, A. Mihanfar, M. Pezeshkian, A. Fattahi, Z. Latifi, N. Safaie, M. Valiloo, A.R. Jodati, M. Nouri, N1-methylnicotinamide (MNAM) as a guardian of cardiovascular system, *J Cell Physiol*, 233 (2018) 6386-6394.
- [398] S. Ogata, M. Takeuchi, S. Teradaira, N. Yamamoto, K. Iwata, K. Okumura, H. Taguchi, Radical scavenging activities of niacin-related compounds, *Biosci Biotechnol Biochem*, 66 (2002) 641-645.
- [399] J.P. Kamat, T.P. Devasagayam, Nicotinamide (vitamin B3) as an effective antioxidant against oxidative damage in rat brain mitochondria, *Redox Rep*, 4 (1999) 179-184.
- [400] H. Yang, W. Zhang, H. Pan, H.G. Feldser, E. Lainez, C. Miller, S. Leung, Z. Zhong, H. Zhao, S. Sweitzer, T. Considine, T. Riera, V. Suri, B. White, J.L. Ellis, G.P. Vlasuk, C. Loh, SIRT1 activators suppress inflammatory responses through promotion of p65 deacetylation and inhibition of NF-kappaB activity, *PLoS One*, 7 (2012) e46364.
- [401] Y. Feng, I.A. Paul, M.H. LeBlanc, Nicotinamide reduces hypoxic ischemic brain injury in the newborn rat, *Brain Res Bull*, 69 (2006) 117-122.
- [402] Q. Ma, Role of nrf2 in oxidative stress and toxicity, *Annu Rev Pharmacol Toxicol*, 53 (2013) 401-426.
- [403] K. Huang, X. Gao, W. Wei, The crosstalk between Sirt1 and Keap1/Nrf2/ARE anti-oxidative pathway forms a positive feedback loop to inhibit FN and TGF-beta1 expressions in rat glomerular mesangial cells, *Exp Cell Res*, 361 (2017) 63-72.
- [404] Y. Kawai, L. Garduno, M. Theodore, J. Yang, I.J. Arinze, Acetylation-deacetylation of the transcription factor Nrf2 (nuclear factor erythroid 2-related factor 2) regulates its transcriptional activity and nucleocytoplasmic localization, *J Biol Chem*, 286 (2011) 7629-7640.
- [405] E.S. Hwang, S.B. Song, Nicotinamide is an inhibitor of SIRT1 in vitro, but can be a stimulator in cells, *Cell Mol Life Sci*, 74 (2017) 3347-3362.
- [406] K.A. Mendez-Lara, D. Santos, N. Farre, M.N. Nan, V. Pallares, A. Perez-Perez, N. Alonso, J.C. Escola-Gil, F. Blanco-Vaca, J. Julve, Vitamin B3 impairs reverse cholesterol transport in Apolipoprotein E-deficient mice, *Clin Investig Arterioscler*, (2019).

[407] X. Li, S. Zhang, G. Blander, J.G. Tse, M. Krieger, L. Guarente, SIRT1 deacetylates and positively regulates the nuclear receptor LXR, *Mol Cell*, 28 (2007) 91-106.

[408] K.D. Whitney, M.A. Watson, B. Goodwin, C.M. Galardi, J.M. Maglich, J.G. Wilson, T.M. Willson, J.L. Collins, S.A. Kliewer, Liver X receptor (LXR) regulation of the LXRalpha gene in human macrophages, *J Biol Chem*, 276 (2001) 43509-43515.

[409] B.A. Laffitte, S.B. Joseph, R. Walczak, L. Pei, D.C. Wilpitz, J.L. Collins, P. Tontonoz, Autoregulation of the human liver X receptor alpha promoter, *Mol Cell Biol*, 21 (2001) 7558-7568.